

UNCLASSIFIED

AD NUMBER
AD867092
NEW LIMITATION CHANGE
TO Approved for public release, distribution unlimited
FROM Distribution authorized to U.S. Gov't. agencies only; Critical Technology; AUG 1969. Other requests shall be referred to Air Force Armament Laboratory, Attn: ATRA, Eglin AFB, FL 32542.
AUTHORITY
USADTC ltr, 5 Apr 1979

THIS PAGE IS UNCLASSIFIED

THIS REPORT HAS BEEN DECLASSIFIED
AND CLEARED FOR PUBLIC RELEASE
UNDER DOD DIRECTIVE 5200.20 AND
NO RESTRICTIONS ARE IMPOSED UPON
ITS USE OR DISCLOSURE.

DISTRIBUTION STATEMENT A

APPROVED FOR PUBLIC RELEASE,
DISTRIBUTION UNLIMITED.

AD 867092

AFATL-TR-69-109

An Investigation of the Dynamic Behavior of a Split-Skirt Bomb in Free Flight

Department of Aero-Space Engineering
University of Notre Dame

TECHNICAL REPORT AFATL-TR-69-109

AUGUST 1969

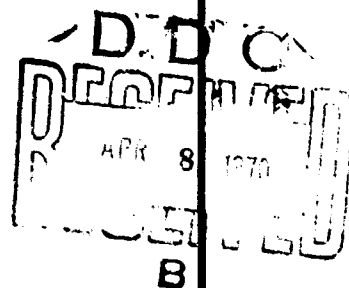
This document is subject to special export controls and each transmittal to foreign governments or foreign nationals may be made only with prior approval of the Air Force Armament Laboratory (ATRA), Eglin AFB, Florida 32542.

Reproduced by the
CLEARINGHOUSE
for Federal Scientific & Technical
Information Springfield, Va. 22151

AIR FORCE ARMAMENT LABORATORY

AIR FORCE SYSTEMS COMMAND • UNITED STATES AIR FORCE

EGLIN AIR FORCE BASE, FLORIDA



167

AN INVESTIGATION OF THE DYNAMIC BEHAVIOR OF A
SPLIT-SKIRT BOMB IN FREE FLIGHT

John D. Nelson, Jr.
Thomas A. Clare

This document is subject to special export controls and each transmittal to foreign governments or foreign nationals may be made only with prior approval of the Air Force Armament Laboratory (ATRA), Eglin AFB, Florida 32542.

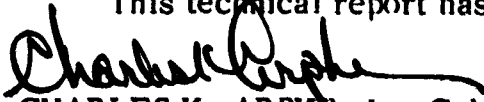
FOREWORD

This report documents work performed during the period June 1966 to June 1967 under the direction of Professor John D. Nicolaides, Principal Investigator, University of Notre Dame, Notre Dame, Indiana, under contract AF 08 (635)-5275 with the Air Force Armament Laboratory, Eglin Air Force Base, Florida.

The investigation was carried out by Mr. Thomas A. Clare, Aero-Space Engineer, U.S. Naval Weapons Laboratory, currently assigned as graduate student to the Aero-Space Engineering Department, University of Notre Dame. Mr. Carroll B. Butler (ATRA) monitored the program for the Armament Laboratory.

Information in this report is embargoed under the Department of State International Traffic in Arms Regulations. This report may be released to foreign governments by departments or agencies of the U.S. Government subject to approval of the Air Force Armament Laboratory (ATRA), Eglin AFB, Florida 32542, or higher authority with the Department of the Air Force. Private individuals or firms require a Department of State export license.

This technical report has been reviewed and is approved.



CHARLES K. ARPKE, Lt. Colonel, USAF
Acting Chief, Technology Division

ABSTRACT

An analysis is presented of the full scale, free flight dynamic behavior of a tri-partite bomb of split-skirt and variable drag configuration. The angular data was obtained from internal instrumentation from the drop at the Woomera Test Range in Salisbury, Australia by the Australian Weapons Research Establishment. This test was part of a joint research program on instrumented bombs undertaken by the United Kingdom, Australia, Canada, and the United States. The analysis was carried out by the Department of Aerospace Engineering, University of Notre Dame. The bomb was observed to experience Catastrophic Yaw in the early phase of the flight, while a Magnus instability was evident in the latter phase. An analysis of the last half of the flight data yielded an excellent determination of the aerodynamic stability coefficients: $C_{M\alpha}$, $C_{Mq} + C_{M\dot{\alpha}}$, $C_{M_{p\alpha}}$. An effort was also made to investigate the motion of the bomb as it passed through resonance. Roll lock-in was observed at this time coupled with a substantial increase in the magnitude of the complex angle of attack, thus indicating the possibility of induced side moment effects and Catastrophic Yaw. Fits of the Unified Linear Aeroballistic Theory to the data were successfully accomplished for this phase of the flight. An analysis of the motion yielded stability parameters which indicated the presence of an induced side moment at resonance. In this phase of this analysis, however, the numerical procedure used in fitting the data caused concern in that, at resonance, neither the Nutation Vector nor the Trim Vector are rotating (i.e. in body axes).

This document is subject to special export controls and each transmittal to foreign governments or foreign nationals may be made only with prior approval of the Air Force Armament Laboratory (ATBR), Eglin AFB, Florida 32542.

TABLE OF CONTENTS

Section		Page
I.	INTRODUCTION	1
II.	THEORY	2
III.	COMPUTATIONAL PROCEDURE	10
IV.	PRELIMINARY ANALYSIS	13
V.	ANALYSIS OF RESULTS	38
VI.	CONCLUSIONS	141
Appendixes		
I	Log Decrement Technique Applied to Precession Vector	143
II	NOI. Static Wind Tunnel Test Results	144
III	NOI. Dynamic Wind Tunnel Test Results	149
References		152

LIST OF FIGURES (continued)

Figure	Title	Page
1	Schematic of Split-Skirt Bomb	14
2	Angle of Attack Versus Time from Release	16
3	Angle of Sideslip Versus Time from Release	20
4	Magnitude of Complex Angle of Attack Versus Time from Release	24
5	Complex Angle of Attack	27
6	Trajectory Parameters Versus Time from Release	35
7	Probable Error of Fit Versus Time from Release	39
8	Magnitude of Nutation Vector Versus Time from Release for Split-Skirt Bomb (739)	45
9	Probable Error of Nutation Vector Versus Time from Release	48
10	Body Nutation Frequency Versus Time from Release	52
11	Probable Error of Body Nutation Frequency Versus Time from Release	55
12	Magnitude of Precession Vector Versus Time from Release	58
13	Probable Error of Precession Vector Versus Time from Release	59
14	Body Precession Frequency Versus Time from Release	61
15	Probable Error of Body Precession Frequency Versus Time from Release	62
16	Magnitude of Trim Vector Versus Time from Release	63
17	Probable Error of Trim Vector Versus Time from Release	66
18	Magnitude of Trim Vector Versus Frequency Ratio	69
19	Nutation Vector Dynamic Damping Factor Versus Time from Release	71
20	Probable Error of Nutation Vector Dynamic Damping Factor Versus Time from Release	74
21	Nutation Vector Dynamic Damping Factor Versus Time from Release	77
22	Nutation Vector Dynamic Damping Factor Versus Time from Release	80
23	Precession Vector Dynamic Damping Factor Versus Time from Release	83
24	Probable Error of Precession Vector Dynamic Damping Factor Versus Time from Release	84
25	Magnitude of Precession Vector Versus Time from Release	85

LIST OF FIGURES (continued)

Figure	Title	Page
26	Logarithm of Magnitude of Precession Vector Versus Time from Release	86
27	Precession Vector Dynamic Damping Factor Versus Time from Release	87
28	Normal Force Coefficient Derivative Versus Time From Release	89
29	Normal Force Coefficient Derivative Versus Mach Number	92
30	Pitching Moment Coefficient Derivative Versus Time from Release	93
31	Gyroscopic Stability Factor Versus Time from Release	96
32	Roll Orientation Angle Versus Time from Release	100
33	Magnitude of Complex Angle of Attack (Smoothed) Versus Time from Release	103
34	Pitch Damping Moment Coefficient Derivative Versus Time from Release	107
35	Pitch Damping Moment Coefficient Derivative Versus Time from Release	108
36	Precession Vector Dynamic Damping Factor Versus Time from Release	111
37	Magnus Moment Coefficient Derivative Versus Time from Release	114
38	Magnus Moment Coefficient Derivative Versus Time from Release	115
39	Dynamic Damping Factors Versus Time from Release	119
40	Dynamic Damping Factors Versus Time from Release	122
41	Dynamic Damping Factors Versus Time from Release	123
42	Induced Side Moment Term Versus Time from Release	124
43	Induced Side Moment Derivative Versus Time from Release	125
44	Induced Side Moment Coefficient Derivative Versus Time from Release	126
45	Induced Side Moment Coefficient Derivative Versus Time from Release	128
46	Roll Orientation Angle Versus Time from Release	129
47	Induced Side Moment Coefficient Derivative Versus Roll Orientation Angle	130

LIST OF FIGURES (concluded)

Figure	Title	Page
48	Induced Side Moment Derivative Versus Roll Orientation Angle	131
49	Pitching Moment Coefficient Derivative Versus Magnitude of Complex Angle of Attack and Mach Number	132
50	Pitching Moment Coefficient Versus Magnitude of Complex Angle of Attack and Mach Number	135
51	Pitching Moment Coefficient vs Angle of Attack (Comparison with wind tunnel and other free flight results)	136
52	Magnus Moment Coefficient Derivative Versus Magnitude of Complex Angle of Attack and Mach Number	138
53	Magnus Moment Coefficient Derivative Versus Magnitude of Complex Angle of Attack and Mach Number	139
Appendix II		
II-1	Normal Force Coefficient Derivative Versus Mach Number and Roll Orientation	145
II-2	Normal Force Coefficient Derivative (Averaged over Roll Orientation) Versus Mach Number	146
II-3	Pitching Moment Coefficient Derivative (Averaged over Roll Orientation) Versus Mach Number	147
II-4	Pitching Moment Coefficient Derivative (Averaged over Roll Orientation) Versus Mach Number	148
Appendix III		
III-1	Pitch Damping Moment Coefficient Derivative Versus Mach Number and Roll Orientation	150
III-2	Pitch Damping Moment Coefficient Derivative (Averaged over Roll Orientation) versus Mach Number	

LIST OF SYMBOLS

- A** Reference area, $\frac{\pi d^2}{4}$ (ft²)
- C_M** Pitching moment coefficient,
- C_{M_α}** Pitching moment coefficient derivative,
 $\frac{\partial C_M}{\partial \alpha}$ (rad⁻¹)
- C_{M_q}** Pitch damping moment coefficient derivative
 due to cross spin velocity, $\frac{\partial C_M}{\partial (\frac{q d}{2V})}$ (rad⁻¹)
- C_{M_{α̇}}** Pitch damping moment coefficient derivative
 due to change in angle of attack,
 $\frac{\partial C_M}{\partial (\frac{q d}{2V})}$ (rad⁻¹)
- C_{M_p}** Magnus moment coefficient derivative, $\frac{\partial C_M}{\partial (\frac{p d}{2V})}$ (rad⁻¹)
- C_{M_{pα}}** Magnus moment coefficient derivative,
 $\frac{\partial C_{M_p}}{\partial \alpha}$ (rad⁻²)
- C_{M_{α̇α}}** Induced side moment coefficient derivative
 $\frac{\partial C_{M(\dot{\alpha})}}{\partial \alpha}$ (rad⁻¹)
- C_Z** Normal force coefficient,
- C_{Z_α}** Normal force coefficient derivative, $\frac{\partial C_Z}{\partial \alpha}$ (rad⁻¹)
- d** Maximum body diameter (ft)
- I_x** Axial moment of inertia (slug-ft²)
- I** Transverse moment of inertia (slug-ft²)
- L** Missile length (ft)
- L** Rolling moment (ft-lb)
- L(_α)** Roll moment due to fin cant (ft-lb)

LIST OF SYMBOLS (concluded)

$L(p)$	Roll damping moment (ft-lb)
$L(\gamma, \alpha)$	Induced roll moment (ft-lb)
M	Pitching moment (ft-lb)
m	Mass (slugs)
N	Yawing moment (ft-lb)
p	Rolling velocity (rad/sec)
Q	Dynamic pressure, $\frac{1}{2} \rho V^2$ (lb/ft ²)
q	Magnitude of cross spin velocity, $\sqrt{q^2 + r^2}$ (rad/sec)
s	Gyroscopic stability factor
t	Time (sec)
τ	Ballistician's coefficient
u	Axial velocity (ft/sec)
V	Magnitude of total velocity (ft/sec)
Ξ	Normal force (lb)
α	Angle of attack (rad or deg)
β	Angle of sideslip (rad or deg)
$\tilde{\alpha}$	Complex angle of attack, $\beta + i\alpha$ (rad or deg)
ρ	Atmospheric density (slugs/ft ³)
λ_n	Nutation vector dynamic damping factor
λ_p	Precession vector dynamic damping factor
ω_n	Nutation vector frequency (rad/sec)
ω_p	Precession vector frequency (rad/sec)
$\tilde{\omega}$	Angular velocity of missile fixed axis system (rad/sec)

γ Roll orientation angle with angle measured between a reference fin and the plane of the complex angle of attack.

γ_4 denotes 4 fins.

SECTION I

INTRODUCTION

At the present time, it is well known that cruciform finned missiles and bombs demonstrate three basic types of instabilities: Magnus, Resonance, and Catastrophic Yaw. During the past few years at the Aero-Space Engineering Department of the University of Notre Dame, extensive research has been carried out on the dynamic behavior of cruciform finned missiles in order to develop a more fundamental understanding of these flight phenomena. This program has included both wind tunnel experimentation¹ and free flight data analysis.^{1,2}

Late in 1960, a joint research program on instrumented bombs was formulated. Engaged in this study are the British Royal Aircraft Establishment (RAE) and the Australian Weapons Research Establishment (WRE). At an early stage in the experimental program, contribution was made by the United States Navy, Air Force, and Army in the form of wind tunnel and computer facilities.³ In this joint program, effort was directed toward investigation of the dynamic characteristics of less conventional stabilizers. In particular, a split-skirt tail configuration was used for experimentation in the hope that it would eliminate one or more of the instabilities characteristic to cruciform finned missiles. However, free flight tests of this configuration, performed at the Woomera Test Range in Salisbury, Australia⁴, indicated the possibility of these instabilities.

It was felt that application of the techniques developed at the University of Notre Dame would be useful in examining the flight characteristics of this new bomb configuration. Thus, the purpose of this report is to analyze the dynamic behavior of one test round of a split-skirt bomb. Approximately 1000 points of telemetry records of the angular orientation data as a function of time were fitted to the Unified Linear Aeroballistic Theory by the Method of Differential Corrections as described in Reference 2. From the results of this fitting technique, the following aerodynamic stability coefficient derivatives were determined: pitching moment, $C_{m\alpha}$; pitch damping moment, $C_{m\dot{\alpha}} + C_{m\ddot{\alpha}}$; and Magnus moment, $C_{m\dot{\phi}}$. In addition, an extension of the Unified Linear Aeroballistic Theory was made in order to examine the effects of the induced side moment coefficient derivative, $C_{m\dot{\phi}} \sin 4\phi$, at resonance. The results of this portion of the analysis, however, are questionable due to a combination of the flight characteristics at resonance and the numerical procedures employed in fitting the data.

SECTION II

THEORY

For the sake of completeness, a development of the Six Degree of Freedom Equations of Motion, as well as the Unified Linear Aeroballistic Theory and its non-linear extension will be presented.

Six Degree of Freedom Equations of Motion

Consider two sets of orthogonal axes: a) space-fixed axes x, y, z ; and b) missile-fixed axes X, Y, Z . Beginning with Newton's Laws of Translational and Angular Motion, it is proposed to obtain a set of equations of motion for a missile with six degrees of freedom, whose solution will yield the criteria for dynamic stability with expressions for the pertinent aerodynamic forces and moments. It should be noted, however, that the aerodynamic parameters are with respect to the set of axes fixed to the missile and that Newton's Laws of motion are valid only for a set of axes which are stationary or translate with a constant velocity. According to Goldstein⁵, however, the following transformation from the missile-fixed axes to the space-fixed axes may be applied:

$$\left. \frac{d\vec{V}}{dt} \right|_{\text{space fixed}} = \left. \frac{d\vec{V}}{dt} \right|_{\text{wobbling axes}} + \vec{\Omega} \times \vec{V} \quad (1)$$

Where $\vec{\Omega}$ is the angular velocity of the coordinates of the wobbling axes.

Consider first, Newton's Law of Translational Motion applied to the space-fixed axes.

$$\vec{F} = \frac{d}{dt}(m\vec{V})_{xyz} \quad (2)$$

where

$$\vec{V} = \begin{bmatrix} u \\ v \\ w \end{bmatrix}$$

The components of \vec{V} are the linear velocity components with respect to the missile-fixed axes. Noting that mass is constant, application of Eq. (1) to Eq. (2) yields

$$\vec{F} = m \left(\frac{d\vec{V}}{dt} \right)_{xyz} = m \left[\left(\frac{d\vec{V}}{dt} \right)_{XYZ} + \vec{\Omega} \times \vec{V} \right]$$

where

$$\underline{\Omega} = \begin{bmatrix} \Omega_x \\ \Omega_y \\ \Omega_z \end{bmatrix}$$

, the angular velocity components of the coordinate system.

Thus,

$$\vec{F} = m \left\{ \frac{d}{dt} \begin{bmatrix} u \\ v \\ w \end{bmatrix} + \begin{bmatrix} \Omega_x \\ \Omega_y \\ \Omega_z \end{bmatrix} \times \begin{bmatrix} u \\ v \\ w \end{bmatrix} \right\} \quad (3)$$

In Aeroballistic axes*

$$\vec{\Omega} = \begin{bmatrix} \Omega_x \\ \Omega_y \\ \Omega_z \end{bmatrix} = \begin{bmatrix} 0 \\ q \\ r \end{bmatrix} \quad \text{where} \quad q = \sqrt{\dot{\phi}^2 + \dot{\psi}^2} \quad (4)$$

Thus, performing the indicated differentiation and vector operation in Eq. (3) and writing the force in terms of its components,

$F_X (= X)$, $F_Y (= Y)$, $F_Z (= Z)$ yields

$$\begin{aligned} X &= m\dot{u} + m(qv - rw) \\ Y &= m\dot{v} + mru \\ Z &= m\dot{w} - mqv \end{aligned} \quad (5)$$

Consider Newton's Law of Angular Motion applied to the space-fixed axes,

$$\vec{M} = \frac{d}{dt} (\vec{H})_{xyz} = \frac{d}{dt} (I \vec{\omega})_{xyz} \quad (6)$$

where

$$I = \begin{bmatrix} I_{xx} & I_{xy} & I_{xz} \\ I_{yx} & I_{yy} & I_{yz} \\ I_{zx} & I_{zy} & I_{zz} \end{bmatrix} \quad \text{the moment of inertia tensor,}$$

*Aeroballistic axes are orthogonal axes fixed to the missile but which do not roll with it. The origin is fixed at the center of gravity and the X axis is coincidental with the symmetric axis of the missile.

and,

$$\vec{\omega} = \begin{bmatrix} p \\ q \\ r \end{bmatrix}$$

the angular velocity components
in the missile-fixed axes.

Assuming the principal axis is coincident with the geometric axis, the moment of inertia tensor may be diagonalized, and assuming rotational mass symmetry, $I_y = I_z = I$. Thus,

$$I = \begin{bmatrix} I_x & 0 & 0 \\ 0 & I & 0 \\ 0 & 0 & I \end{bmatrix}$$

Application of Eq. (1) to Eq. (6) yields

$$\vec{M} = \frac{d}{dt}(I\vec{\omega})_{xyz} = \frac{d}{dt}(I\vec{\omega})_{xyz} + \vec{\omega} \times (I\vec{\omega})$$

or expanding into components for aeroballistic axes

$$\vec{M} = \begin{bmatrix} I_x & 0 & 0 \\ 0 & I & 0 \\ 0 & 0 & I \end{bmatrix} \begin{bmatrix} \dot{p} \\ \dot{q} \\ \dot{r} \end{bmatrix} + \begin{bmatrix} 0 \\ q \\ r \end{bmatrix} \times \begin{bmatrix} I_x & 0 & 0 \\ 0 & I & 0 \\ 0 & 0 & I \end{bmatrix} \begin{bmatrix} p \\ q \\ r \end{bmatrix} \quad (7)$$

Performing the indicated vector operations in Eq. (7) and writing the moment in terms of its components $M_x (= L)$, $M_y (= M)$, $M_z (= N)$ yields

$$\begin{aligned} L &= I_x \dot{p} \\ M &= I \dot{q} + p I_x r \\ N &= I \dot{r} - p I_x q \end{aligned} \quad (8)$$

Thus, Eqs. (5) and (8) represent the differential equations of motion in aeroballistic axes for a free flight missile having six degrees of freedom.

Unified Linear Aeroballistic Theory

The solution⁶ of these equations for the complex angle of attack, subject to the constraints of constant roll rate and velocity, is the following:

$$\vec{\alpha}_A = \vec{K}_{N_A} e^{(\lambda_{N_A} + i\omega_{N_A})t} + \vec{K}_{P_A} e^{(\lambda_{P_A} + i\omega_{P_A})t} + \vec{K}_{T_A} e^{i\dot{p}t} + \vec{K}_{R_A} \quad (9)$$

where

$\vec{\alpha}_A$ = complex angle of attack (aeroballistic)

\vec{K}_{N_A} = nutation vector (aeroballistic)

\vec{K}_{P_A} = precession vector (aeroballistic)

\vec{K}_{T_A} = trim vector (aeroballistic)

\vec{K}_{R_A} = yaw of repose vector (aeroballistic)

$$\lambda_{N_A, P_A} = \frac{QA}{2mV} \left[C_{Z\alpha} (1 \mp \tau) + \frac{md^2}{2I} (C_{M\dot{\alpha}} + C_{M\ddot{\alpha}}) (1 \pm \tau) \pm \frac{md^2}{I_x} C_{M\ddot{\alpha}} \tau \right] \quad (10)$$

$$\omega_{N_A, P_A} = \frac{pI_x}{2I} (1 \pm \frac{1}{\tau}) \quad (11)$$

$$\tau = \frac{1}{\sqrt{1 - \frac{1}{\tau}}} \quad (12)$$

$$s = \frac{(pI_x)^2}{4IA\dot{Q}C_{M\ddot{\alpha}}} \quad (13)$$

The solution for the complex angle of attack may be expressed in body axes* by application of the transformation

$$\vec{\alpha}_B = \vec{\alpha}_A e^{-i\dot{p}t} \quad (14)$$

* Body axes are aeroballistic axes which roll with the missile.

Thus, application of Eq. (14) to Eq. (9) yields the solution in terms of body axes:

$$\vec{\alpha}_B = \vec{K}_{NB} e^{(\lambda_{NB} + i\omega_{NB})t} + \vec{K}_{PB} e^{(\lambda_{PB} + i\omega_{PB})t} + \vec{K}_{TB} + \vec{K}_{RB} e^{-ipt} \quad (15)$$

where

$\vec{\alpha}_B$ = complex angle of attack (body)

\vec{K}_{NB} = nutation vector (body)

\vec{K}_{PB} = precession vector (body)

\vec{K}_{TB} = trim vector (body)

\vec{K}_{RB} = yaw of repose vector (body)

Recognizing the fact, however, that the only difference between the two axis systems is the rolling velocity, or $\vec{K}_{NB} = \vec{K}_{NB} - \vec{K}_{NB}$, $\lambda_{NB} = \lambda_{NB} = \lambda_{NB}$, etc.

$$\omega_{NB} = \omega_{NA} - p \quad (16)$$

and,

$$\omega_{PB} = \omega_{PA} - p \quad (17)$$

Thus, the solution for the complex angle of attack in body axes may be written as

$$\vec{\alpha}_B = \vec{K}_{NB} e^{(\lambda_{NB} + i\omega_{NB})t} + \vec{K}_{PB} e^{(\lambda_{PB} + i\omega_{PB})t} + \vec{K}_T + \vec{K}_R e^{-ipt} \quad (18)$$

where the vector dynamic damping factors and frequencies are defined by Eqs. (10) through (13), (16) and (17).

The necessary and sufficient conditions for the dynamic stability of a fin stabilized missile are as follows:

1. The gyroscopic stability factor must be negative, $s < 0$, and,
2. The nutation and precession dynamic damping factors must be negative, $\lambda_{NB} < 0$.

Catastrophic Yaw Theory⁶

A unique instability, not accounted for by the Unified Linear Aeroballistic Theory⁶, was occasionally observed in the trajectories of a certain fin-stabilized missile. This instability was characterized by two phenomena: 1) failure of the missile to attain its steady state rolling velocity, and 2) a rapid increase of the pitching and yawing motion to extremely large angles of attack. These phenomena are labeled "Roll Lock-In" and "Catastrophic Yaw," respectively.^{7,8,9}

Initially, the rolling velocity increases due to fin cant, but when it attains a value equal to the aeroballistic nutation frequency, it "locks in" at this particular value rather than continuing to seek its steady state rate, which is much larger. With respect to the pitching and yawing motion, however, initially the magnitude decreases; but when the rolling velocity locks in, the motion increases to extreme values which may even cause the missile to tumble.

When observed in special wind tunnel and full scale free flight tests, the phenomenon of roll lock-in appears to be traceable to the influence of the non-linear induced roll moment.^{10,11} Indeed, when this moment is introduced into the classical theory for pure rolling motion, a method for predicting the critical angle of attack and roll trim angle is available. Of major concern here, however, is the Catastrophic Yaw.

As established by Nicolaides⁸ and supplemented by flight performance data, the catastrophic growth of the pitching and yawing motion occurs when the missile is in "lunar motion," that is, when the angle between a reference fin and the plane of complex angle of attack is constant. The Unified Linear Aeroballistic Theory predicts, for a statically stable missile, that this type of motion may exist for any of three cases: 1) pure nutational motion in which the roll rate is equal to the aeroballistic nutation frequency, 2) pure trim in which lunar motion exists for all values of the rolling velocity, and 3) a combination of both in which the rolling velocity is equal to the aeroballistic nutation frequency. The Linear Theory, applied to pure nutational motion, fails to account for the catastrophic growth observed. Also, maximum amplification of the trim occurs when the rolling velocity equals the aeroballistic nutation frequency, which is known as "Resonance Instability." Initially, one would suspect this phenomenon to be the cause of the observed motion; this amplification, however, may be extracted from the linear theory, which also yields approximate values when non-linearities exist in the force and moment system. In neither case does the linear theory account for the observed catastrophic growth of complex angle of attack. Thus, it is evident that a further understanding and evaluation of the fluid forces and moments acting on the missile is necessary.

While the dependence on roll orientation* is automatically detected from the linear theory, its essential role in the explanation of roll lock-in suggests that there may be a force and moment associated with it. Indeed, wind tunnel tests do reveal two additional effects of roll orientation: 1) the normal force and its moment are modified, and more important, 2) a side force and moment are found to exist. The side moment was observed to vary sinusoidally with the roll orientation.

Thus, in addition to the forces and moments involved in the linear theory, the following are now introduced (for a cruciform finned missile):

$$\vec{Z}(\gamma, \alpha) = Z_{\gamma\alpha} \vec{\alpha} \sin 4\gamma = C_{Z_{\gamma\alpha}} \vec{\alpha} Q A \sin 4\gamma \quad (19a)$$

and

$$\vec{M}(\gamma, \alpha) = M_{\gamma\alpha} \vec{\alpha} \sin 4\gamma = C_{M_{\gamma\alpha}} \vec{\alpha} Q A d \sin 4\gamma \quad (19b)$$

In order to determine the contribution of these forces and moments to the dynamic stability of a missile, they must be added to the classical aerodynamic system. A general solution for the complex motion involving these new terms is not possible; however, according to Nicolaides⁶, if the characteristic motion is assumed to be "lunar" an approximate solution is possible. Employment of the perturbation approach to this type of motion, as presented in Reference 6, yields a variation, due to the additional forces and moments, in the equation for the dynamic damping factors. Thus, neglecting changes in the normal force due to roll orientation, this equation assumes the following form:

$$\lambda_{N,P}^* = \frac{Q A}{2 m V} \left[C_{Z_\alpha} (1 \pm \tau) + \frac{m d^2}{2 I_x} (C_{M_\eta} + C_{M_{\dot{\alpha}}}) (1 \pm \tau) \pm \frac{m d^2}{I_x} C_{M_{P\alpha}} \tau \right] \pm \frac{Q A d}{I_x P} C_{M_{\gamma\alpha}} (\sin 4\gamma) \tau \quad (20)$$

Comparison with the resulting dynamic damping factors from linear theory, Eq. (10), and denoting them as $\lambda_{N,P}^*$, yield the following relation:

$$\lambda_{N,P}^* = \lambda_{N,P} \pm \frac{Q A d}{I_x P} C_{M_{\gamma\alpha}} (\sin 4\gamma) \tau \quad (21)$$

*Roll orientation angle, γ , is defined as the angle between a reference fin and the plane formed by the complex angle of attack.

It should be noted that while in stability derivative notation, a subscript implies partial differentiation with respect to the variables, $C_{m_{\dot{\gamma}}}$ is not a derivative with respect to $\dot{\gamma}$ but a function of it. Thus, it is completely consistent with the notation, $C_{m_{\dot{\gamma}}} \rightarrow C_{m_{\dot{\gamma}}}(\dot{\gamma})$. Hence, in Catastrophic Yaw Theory the necessary and sufficient conditions for the dynamic stability of a fin-stabilized missile are as follows:

1. The gyroscopic stability factor must be negative, $s < 0$, and,
2. The nutation and precession vector dynamic damping factors must be negative, $\lambda_{N,P} < 0$.

SECTION III

COMPUTATIONAL PROCEDURE

The computer program of Reference 12 was used to fit the complex angular data⁴ to the quadricyclic equation, Eq. (18), by the Method of Differential Corrections^{13,14}. The stability parameters, $\lambda_N, \rho, \omega_N, \rho_N, K_N, P, T, R$, were determined as a function of time from release by fitting the Unified Linear Aeroballistic Theory to small segments of the data and overlapping these segments.

Two assumptions are made in using this technique to obtain the stability parameters.

1. The segment of fit is chosen small enough to insure that the total velocity and roll rate are essentially constant in the time interval defining the segment.
2. Enough points of the complex angular data are fitted in each of these segments to well define the stability parameters for the time interval defining that segment.

The fact that these segments are overlapped enables one to obtain the stability parameters as continuous functions of time from release.

If the complex angular motion is such that both the Nutation and Precession Vectors, their damping factors and frequencies may be obtained from the fitting procedure; the aerodynamic stability derivatives, $C_{M_{\dot{\alpha}}}$, $C_{M_{\dot{\omega}}}$, and $C_{M_{\dot{\omega}}}$ may be computed as found in Reference 2. This general procedure is applied in the following manner:

1. Substituting Eqs. (16), (17), (18), (13), (12) into Eq. (11) and solving for $C_{M_{\dot{\alpha}}}$ yields,

$$C_{M_{\dot{\alpha}}} = \frac{B I}{\pi \rho d^3 V^2} [(\omega_N + p)(\omega_N + \dot{p})] \quad (22)$$

2. Using predetermined values for $C_{E_{\dot{\alpha}}}$, $C_{M_{\dot{\alpha}}} + C_{M_{\dot{\omega}}}$ may be computed by adding the expressions for λ_N and λ_P , and solving for $C_{M_{\dot{\alpha}}} + C_{M_{\dot{\omega}}}$ yields,

$$C_{M_{\dot{\alpha}}} + C_{M_{\dot{\omega}}} = \frac{2 I}{m d^3} \left[-C_{E_{\dot{\alpha}}} + \frac{m V}{Q A} (\lambda_N + \lambda_P) \right] \quad (23)$$

3. Having solved for $C_{M_q} + C_{M_{\dot{\alpha}}}$, solving either the λ_N or λ_P expression for $C_{M_{P\alpha}}$ yields,

$$C_{M_{P\alpha}} = \pm \frac{I_x}{m d^2 \tau} \left[\frac{2mV}{QA} (\lambda_N, \lambda_P) - C_{Z\alpha} (1 \mp \tau) - \frac{m d^2}{2I} (C_{M_q} + C_{M_{\dot{\alpha}}}) (1 \pm \tau) \right] \quad (24)$$

If, however, the complex angular motion is such that the Precession Vector is zero or is small that the fitting routine is not able to determine it within a reasonable degree of accuracy,

1. Substituting Eqs. (16), (13), and (12) into the expression for ω_{NB} Eq. (11), and solving for $C_{M_{\alpha}}$ yields,

$$C_{M_{\alpha}} = \frac{-(\omega_{NB} + p)I}{AdQ} \left[\omega_{NB} + p \left(1 - \frac{I_x}{I} \right) \right] \quad (25)$$

Since in this case, λ_P is not known, an analytical solution for $C_{M_q} + C_{M_{\dot{\alpha}}}$ is not possible. Thus, in order to calculate $C_{M_{P\alpha}}$, $C_{M_q} + C_{M_{\dot{\alpha}}}$ must be known. If this is the case, $C_{M_{P\alpha}}$ may still be calculated as follows:

2. Solve the λ_N expression for $C_{M_{P\alpha}}$ yielding

$$C_{M_{P\alpha}} = \frac{I_x}{m d^2 \tau} \left[\frac{2mV}{QA} \lambda_N - C_{Z\alpha} (1 - \tau) - \frac{m d^2}{2I} (C_{M_q} + C_{M_{\dot{\alpha}}}) (1 + \tau) \right] \quad (26)$$

In the Catastrophic Yaw Theory, consider Eq. (21),

$$\lambda_{NP}^* = \lambda_{NP}' \pm \frac{QAd}{I_x p} C_{M_{\alpha}} (\sin 4\gamma) \tau \quad (21)$$

solving for the induced side moment term,

$$\frac{QAd}{I_x p} C_{M_{\alpha}} (\sin 4\gamma) \tau = \lambda_N^* - \lambda_N' \quad (27a)$$

$$\frac{QAd}{I_x p} C_{M_{\alpha}} (\sin 4\gamma) \tau = \lambda_P' - \lambda_P^* \quad (27b)$$

and making use of Eq. (19b),

$$\frac{M_{Y_{4\alpha}}(\sin 4\gamma)}{I_x p} \tau = (\lambda_N^* - \lambda_N') \quad (28a)$$

or,

$$\frac{M_{Y_{4\alpha}}(\sin 4\gamma)}{I_x p} \tau = (\lambda_P' - \lambda_P^*) \quad (28b)$$

Thus, the induced side moment coefficient derivative may be obtained

$$C_{M_{Y_{4\alpha}} \sin 4\gamma} = \frac{I_x p}{\tau Q_{Ad}} (\lambda_N^* - \lambda_N') \quad (29a)$$

or

$$C_{M_{Y_{4\alpha}} \sin 4\gamma} = \frac{I_x p}{\tau Q_{Ad}} (\lambda_P' - \lambda_P^*) \quad (29b)$$

SECTION IV

PRELIMINARY ANALYSIS

Configurational Description and Free Flight Conditions

The configuration analyzed is a free flight, variable drag bomb with a split-skirt tail, which has a skirt opening of 10 degrees. A schematic is presented in Fig. 1. The mass parameters for this test, Round 739, are presented in Table 1.

This bomb was dropped from an altitude of 45000 feet; the time of fall was recorded as 67.47 seconds. Angular orientation data was determined from .002 second to 63.39 seconds from release at intervals of .047 second.

The angular orientation data⁴ for this analysis consists of the two components of the complex angle of attack ($\beta + i\alpha$) in body axes. These components are presented in Figs. 2 and 3 as a function of time from release, and the magnitude of the complex angle of attack, $|\alpha|$, is shown in Fig. 4, while the complex motion is presented in Fig. 5. This report consists of a dynamic stability analysis from 12.05 to 62.13 seconds from release.

The following trajectory parameters for Round 739 are presented in Fig. 6 as a function of time from release: roll rate, velocity, Mach number, dynamic pressure, and Reynolds number per foot. Upon preliminary examination of this data, it was noted that the roll rate, while increasing initially, levels off at approximately 12 seconds until 20 seconds at which time it speeds up towards its steady state value at the end of the flight. This phenomenon, combined with the observed magnitude of complex angle of attack at approximately the same time, indicated the possibility of Roll Lock-In and Catastrophic Yaw effects in the early phase of the flight. It was further noted that, although Mach number variations were not extremely large, the flight was characterized by transonic velocities from approximately 35 seconds to 42 seconds from release.

From the magnitude of the complex motion, two dominant characteristics of the motion were observed: a) the rapid increase and decrease of the magnitude of complex angle of attack at approximately 14 seconds from release, and b) the characteristically undamped motion from 25 seconds from release to the end of the flight. Referring these observations to the complex motion, Fig. 5, it was noted that, at approximately 14 seconds from release, one of the vector frequencies changed sign, i.e., one of the "loops," characteristic to the motion, reversed direction. Since the motion is in body axes, a change in sign of the body nutation frequency would indicate that the bomb had passed through resonance at this time. Also, from Fig. 5 it was noted that from 25 seconds from release to the end of the flight, the motion

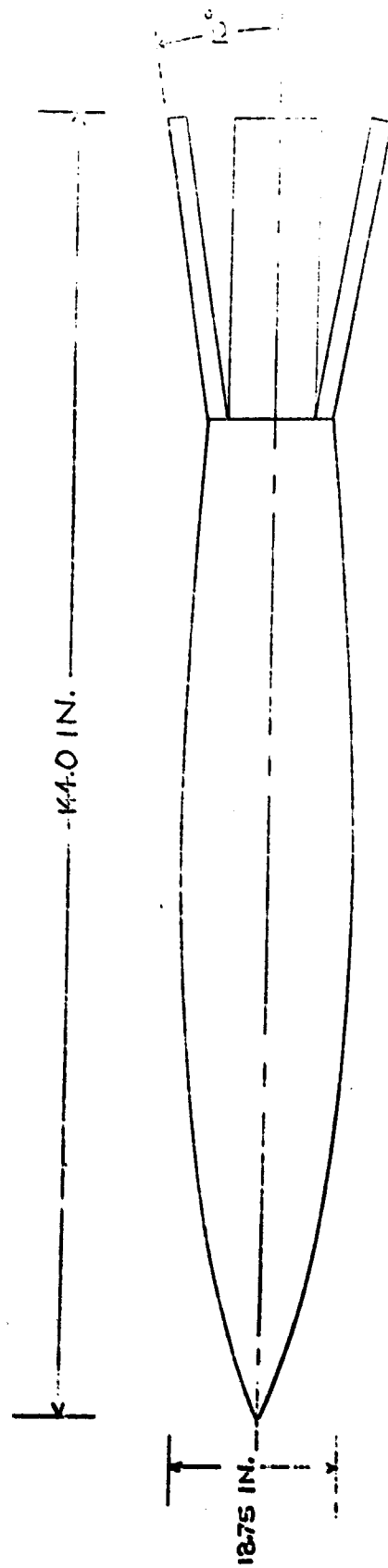


FIG. 1 SCHEMATIC OF SPLIT-SKIRT BOMB

TABLE I. MASS PARAMETERS OF SPLIT-SKIRT BOMB

Release Weight (lb)	939.0
Length (in.)	144.0
Maximum Body Diameter (in.)	18.75
Axial Moment of Inertia (slug-ft ²)	8.8
Transverse Moment of Inertia (slug-ft ²)	171.3
C. G. Position from Nose (% body length)	30.7

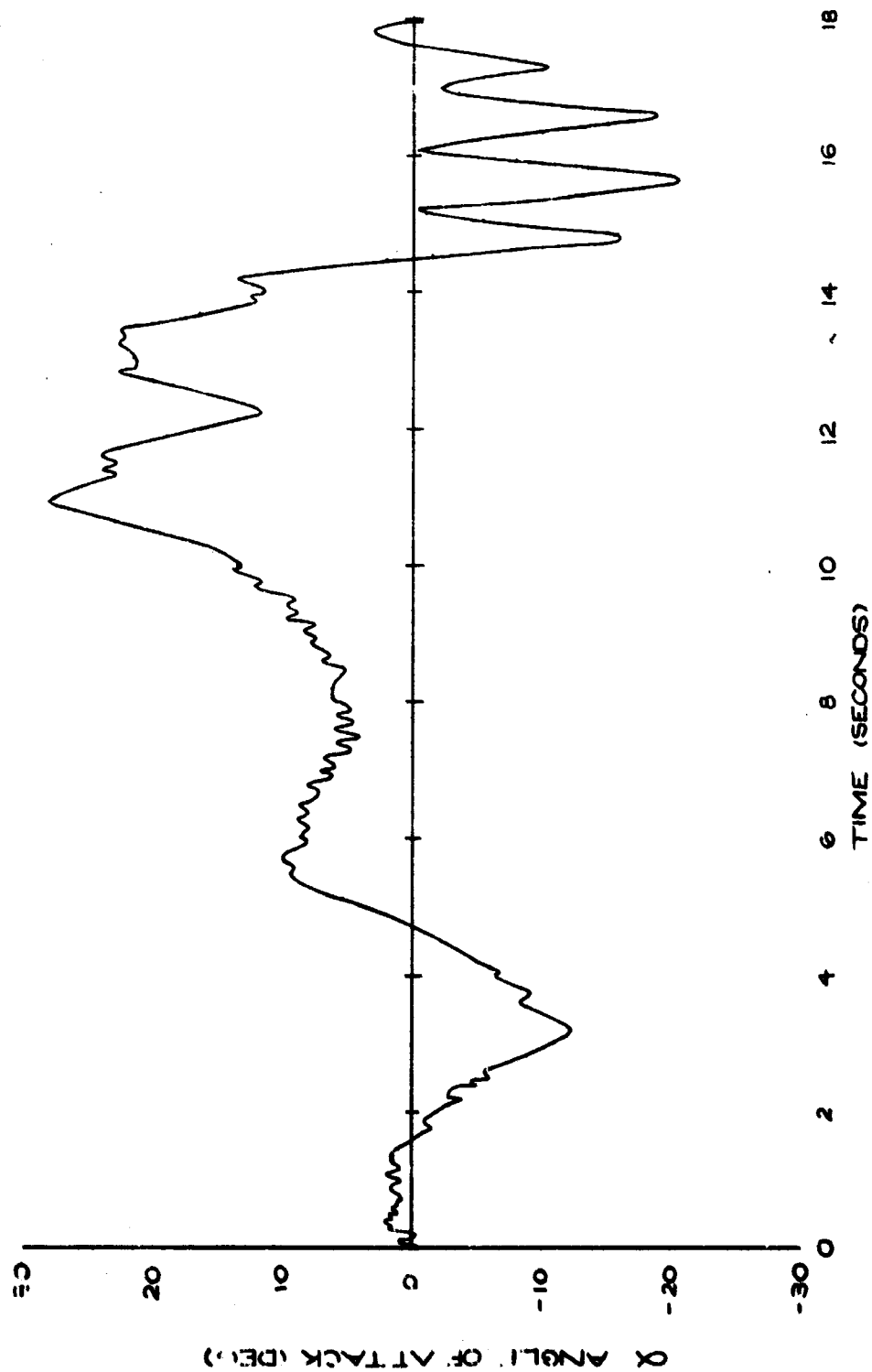


FIG. 2a. ANGLE OF ATTACK VERSUS
TIME FROM RELEASE FOR
SPLIT-SKIRT BOMB (739)

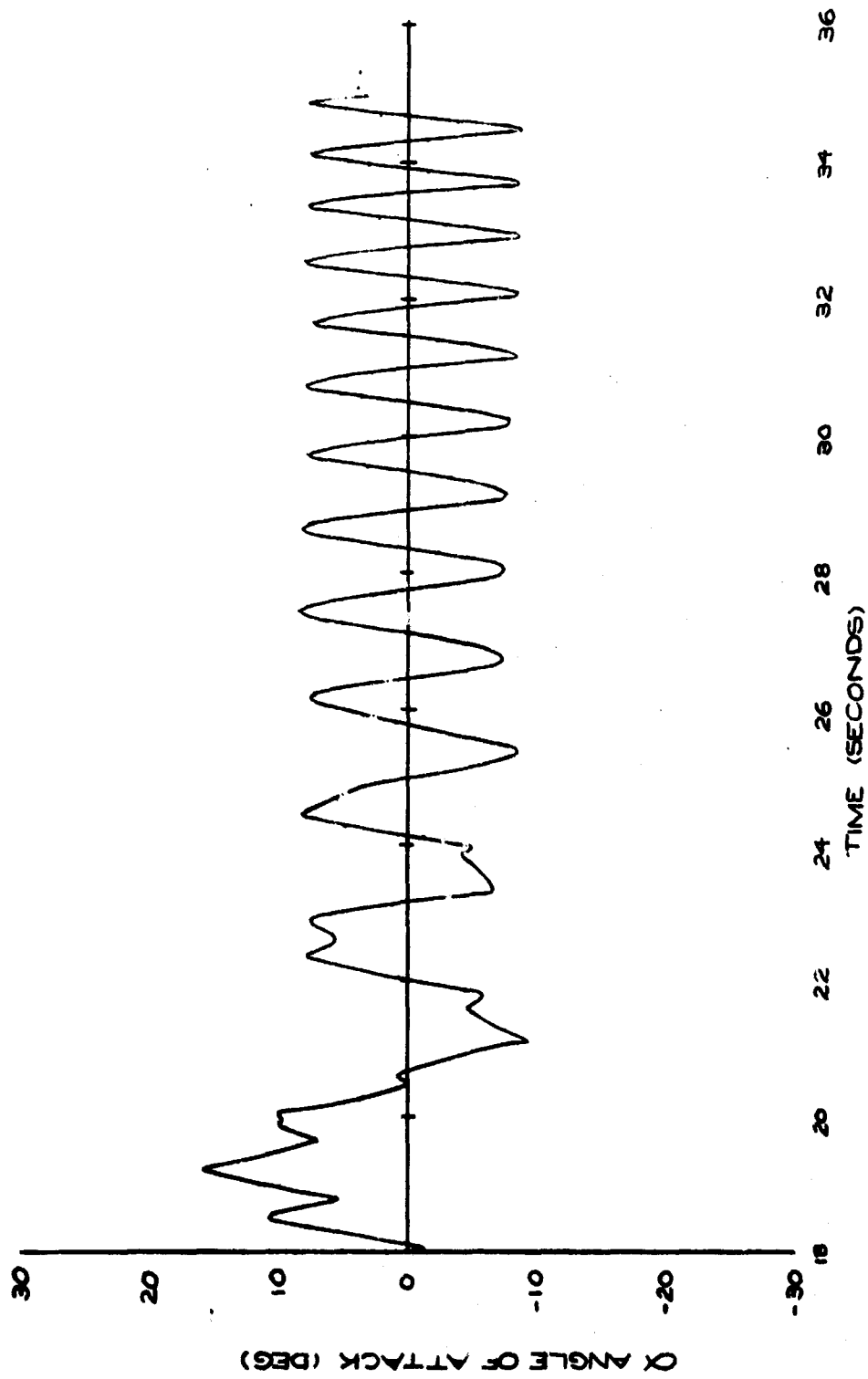


FIG. 2b ANGLE OF ATTACK VERSUS
TIME FROM RELEASE FOR
SPLIT-SKIRT BOMB (739)

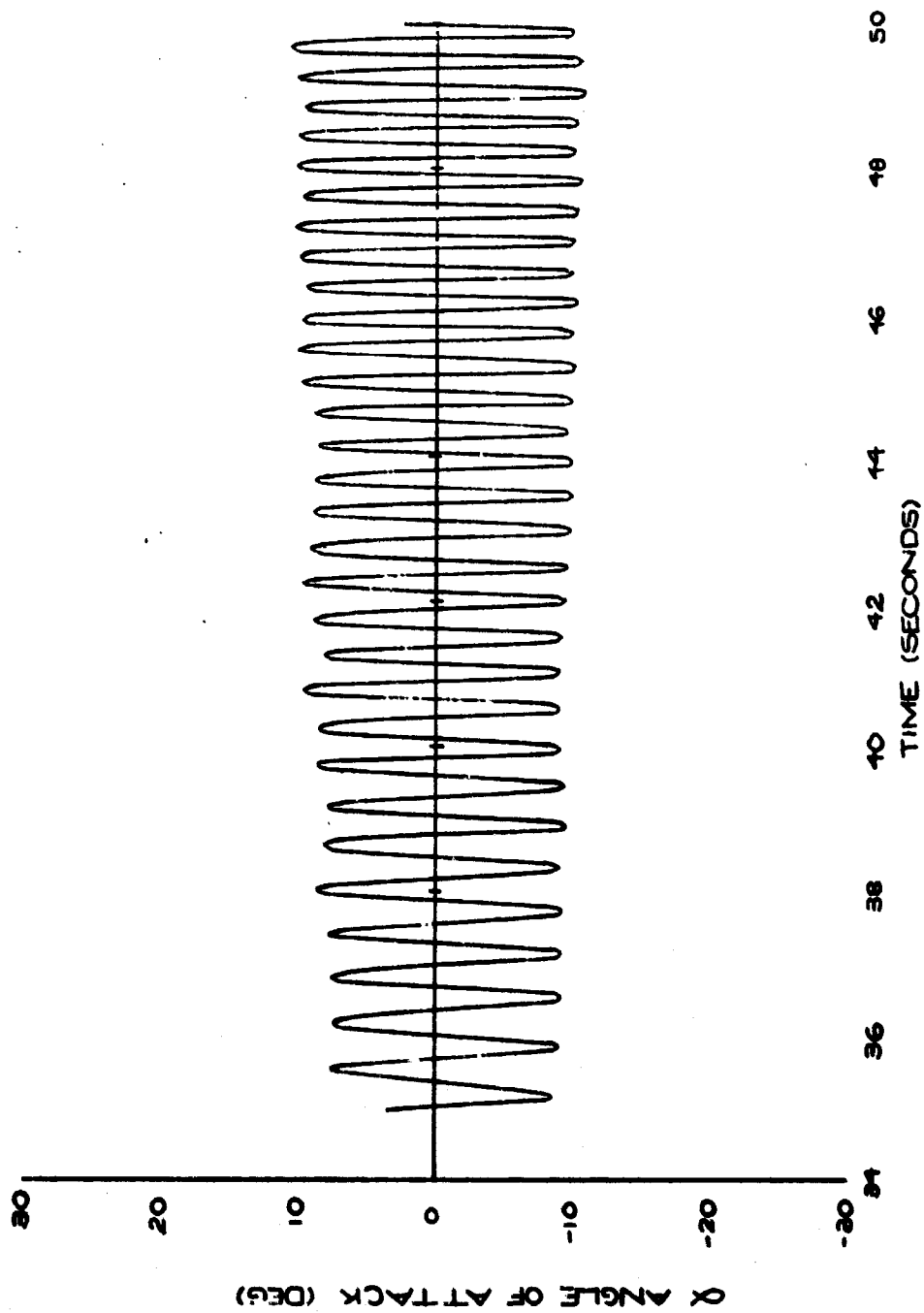


FIG. 2C ANGLE OF ATTACK VERSUS
TIME FROM RELEASE FOR
SPLIT-SKIRT BOMB (739)

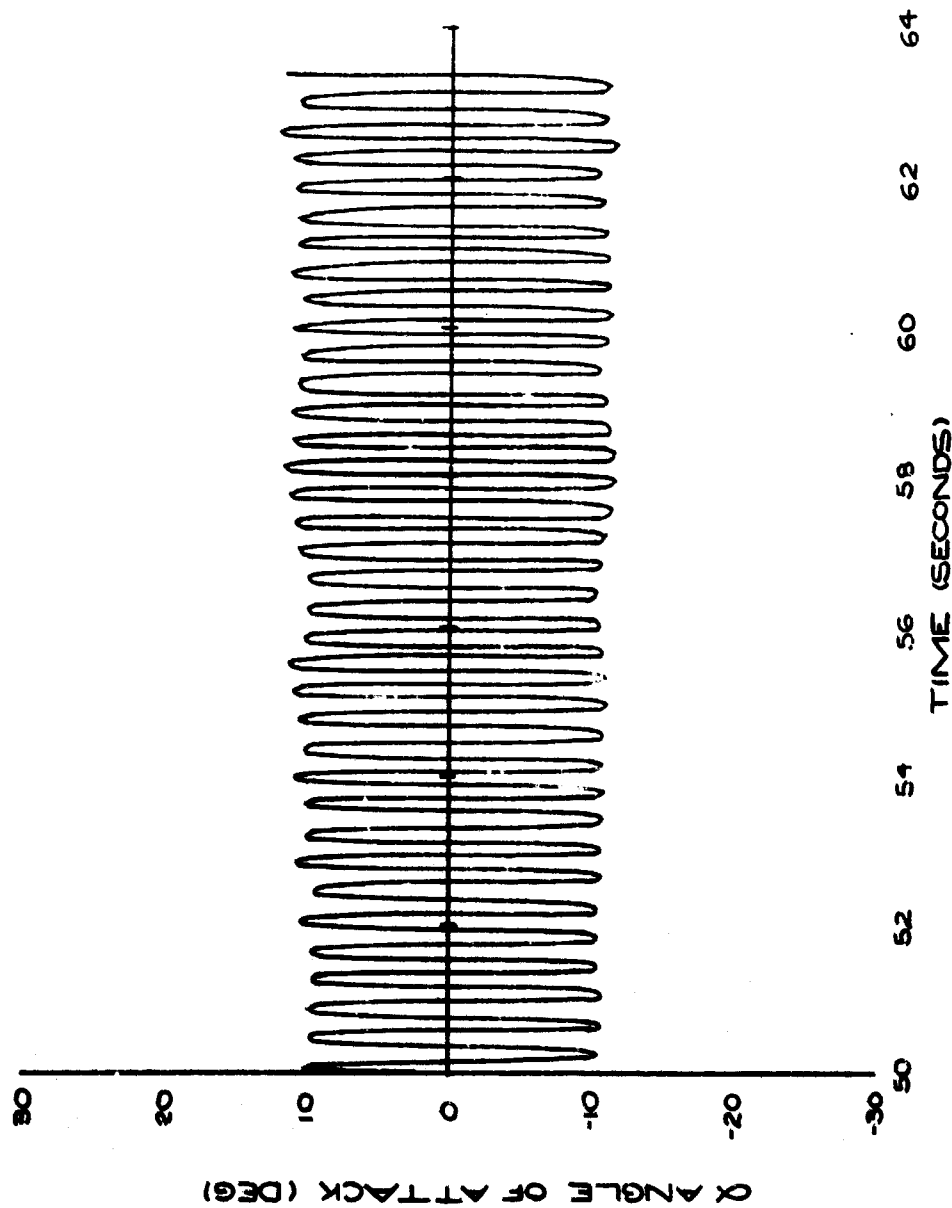


FIG. 2d ANGLE OF ATTACK VERSUS
TIME FROM RELEASE FOR
SPLIT-SKIRT BOMB (739)

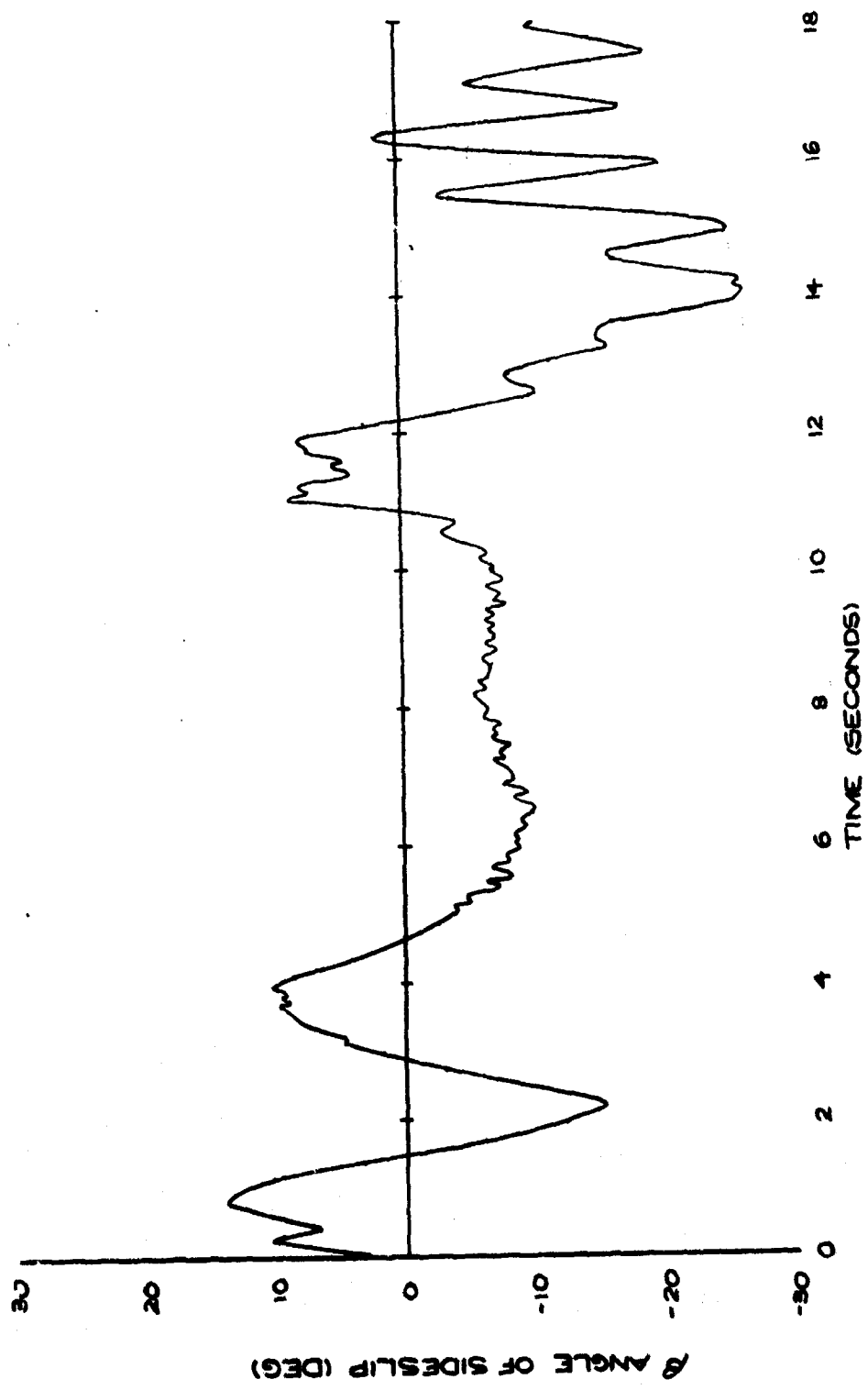


FIG. 3a. ANGLE OF SIDESLIP VERSUS
TIME FROM RELEASE FOR
SPLIT-SKIRT BOMB (739)

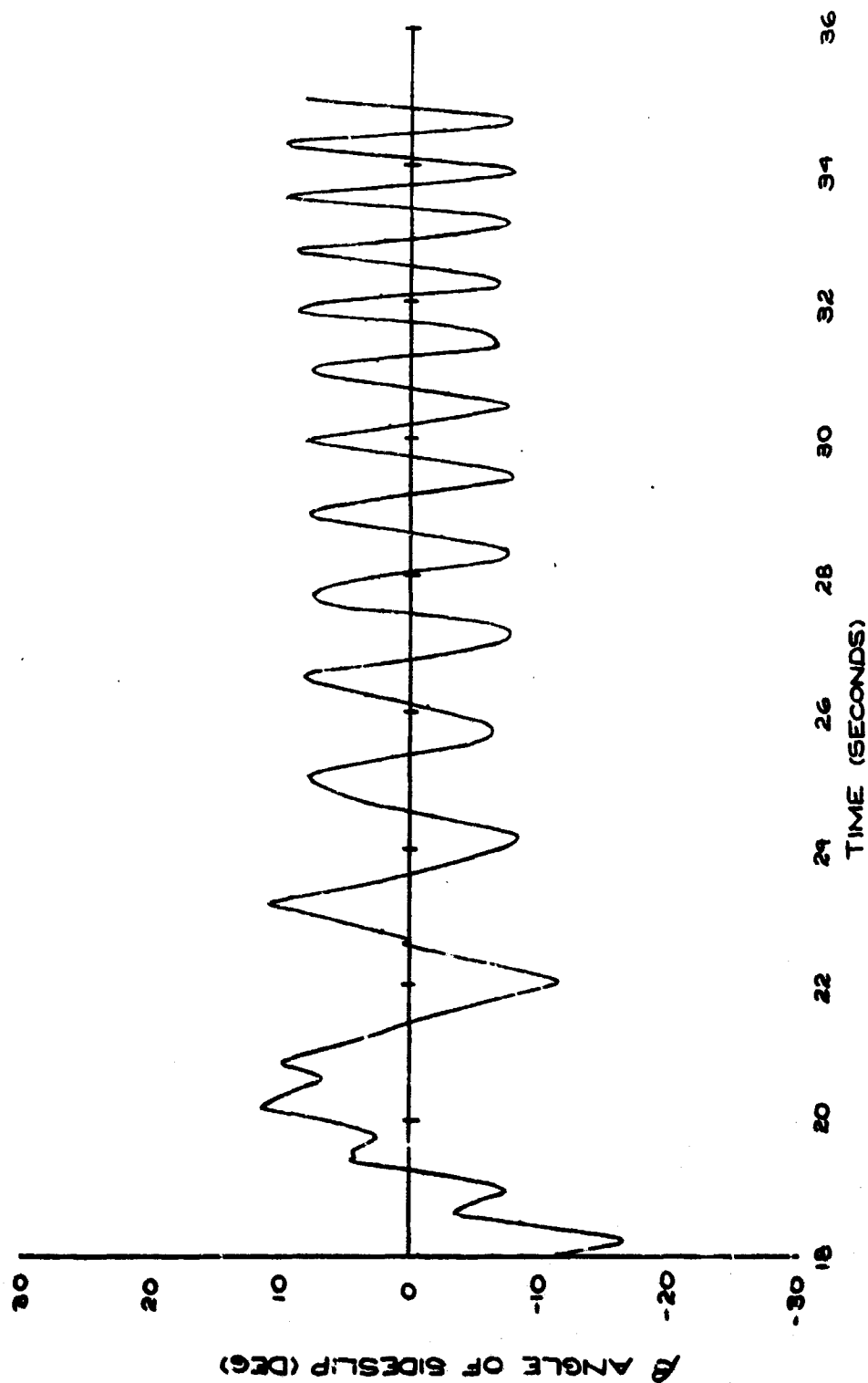


FIG. 36 ANGLE OF SIDESLIP VERSUS
TIME FROM RELEASE FOR
SPLIT-SKIRT BOMB (739)

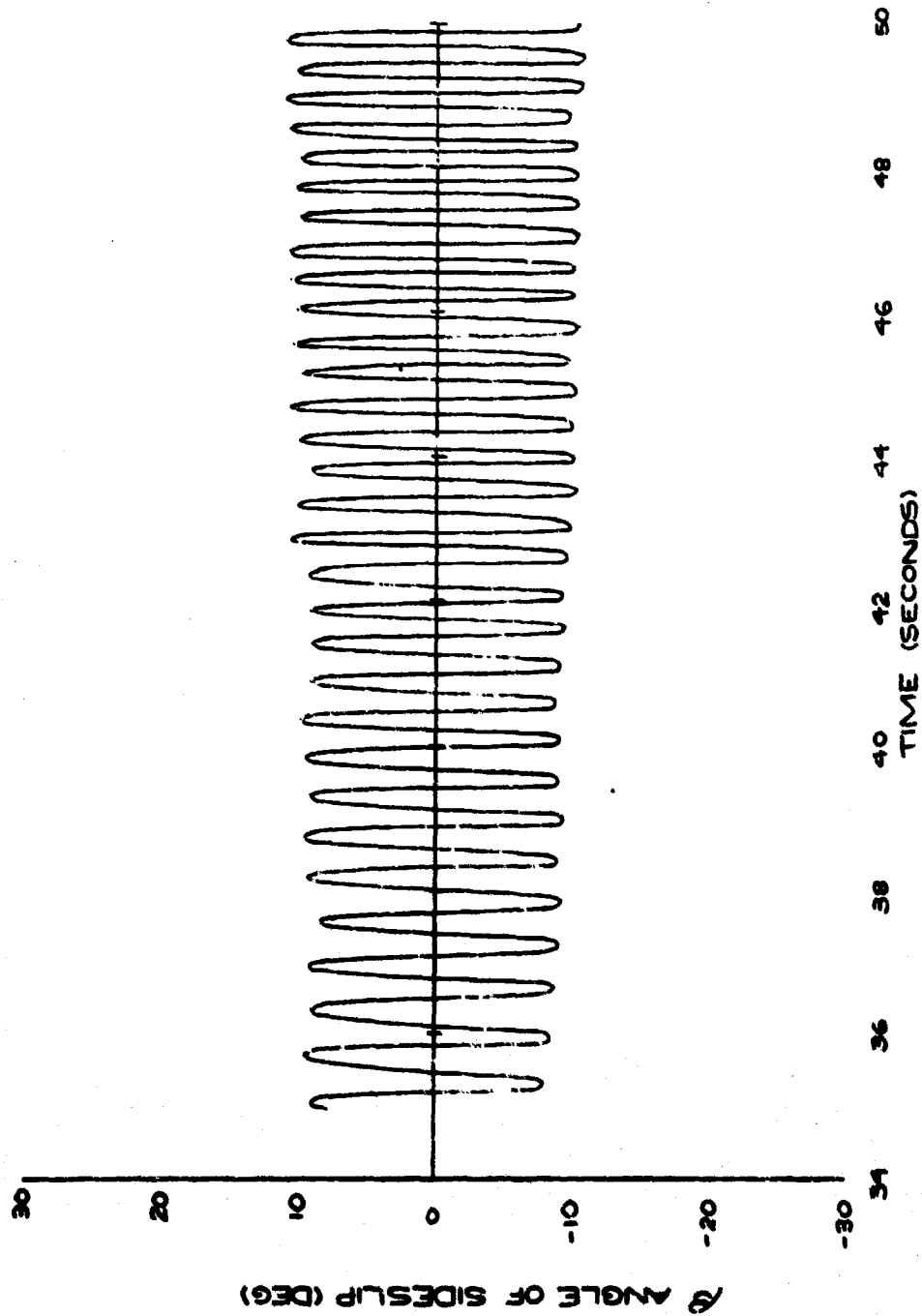


FIG. 3C ANGLE OF SIDESLIP VERSUS
TIME FROM RELEASE FOR
SPLIT-SKIRT BOMB (739)

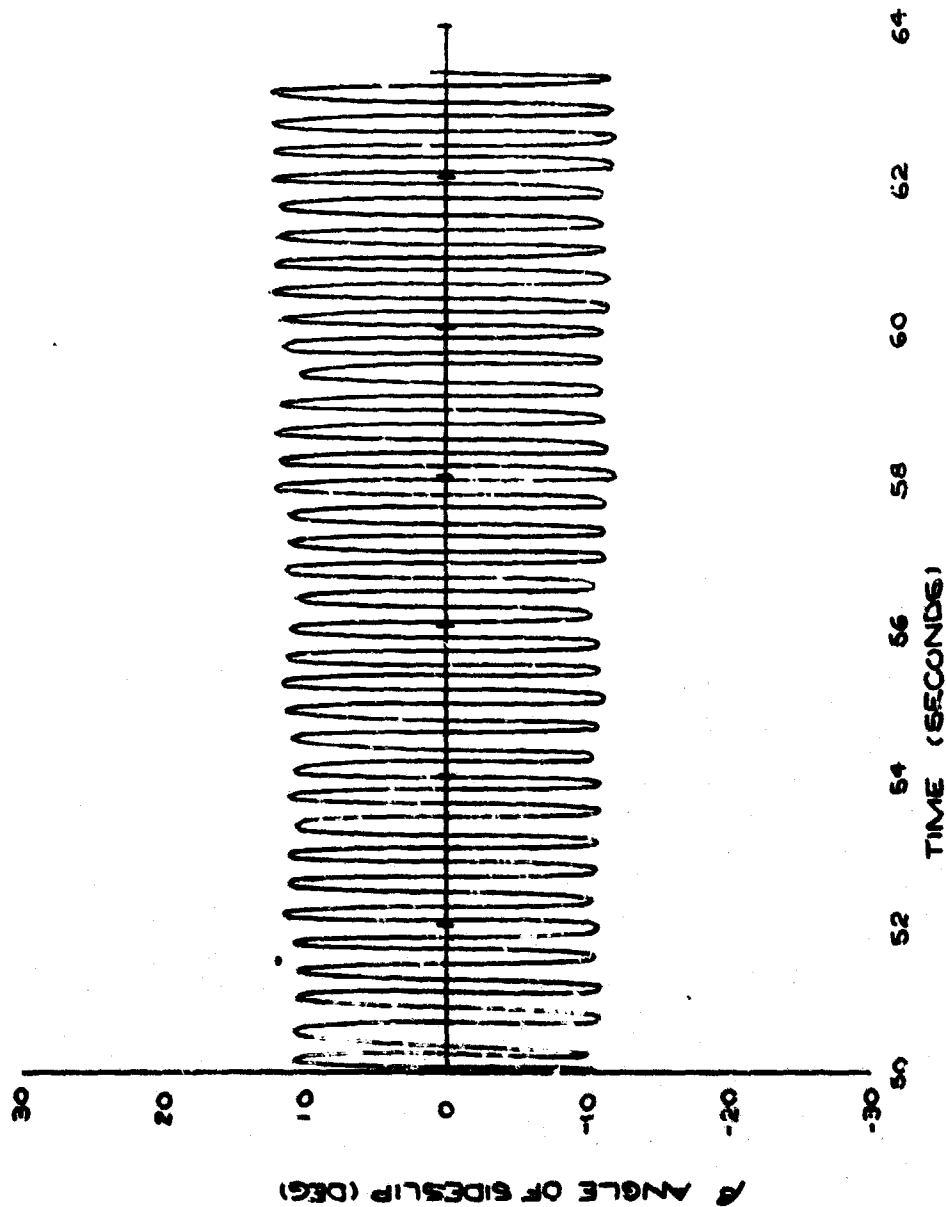


FIG. 3d ANGLE OF SIDESLIP VERSUS
TIME FROM RELEASE FOR
SPLIT-SKIRT BOMB (739)

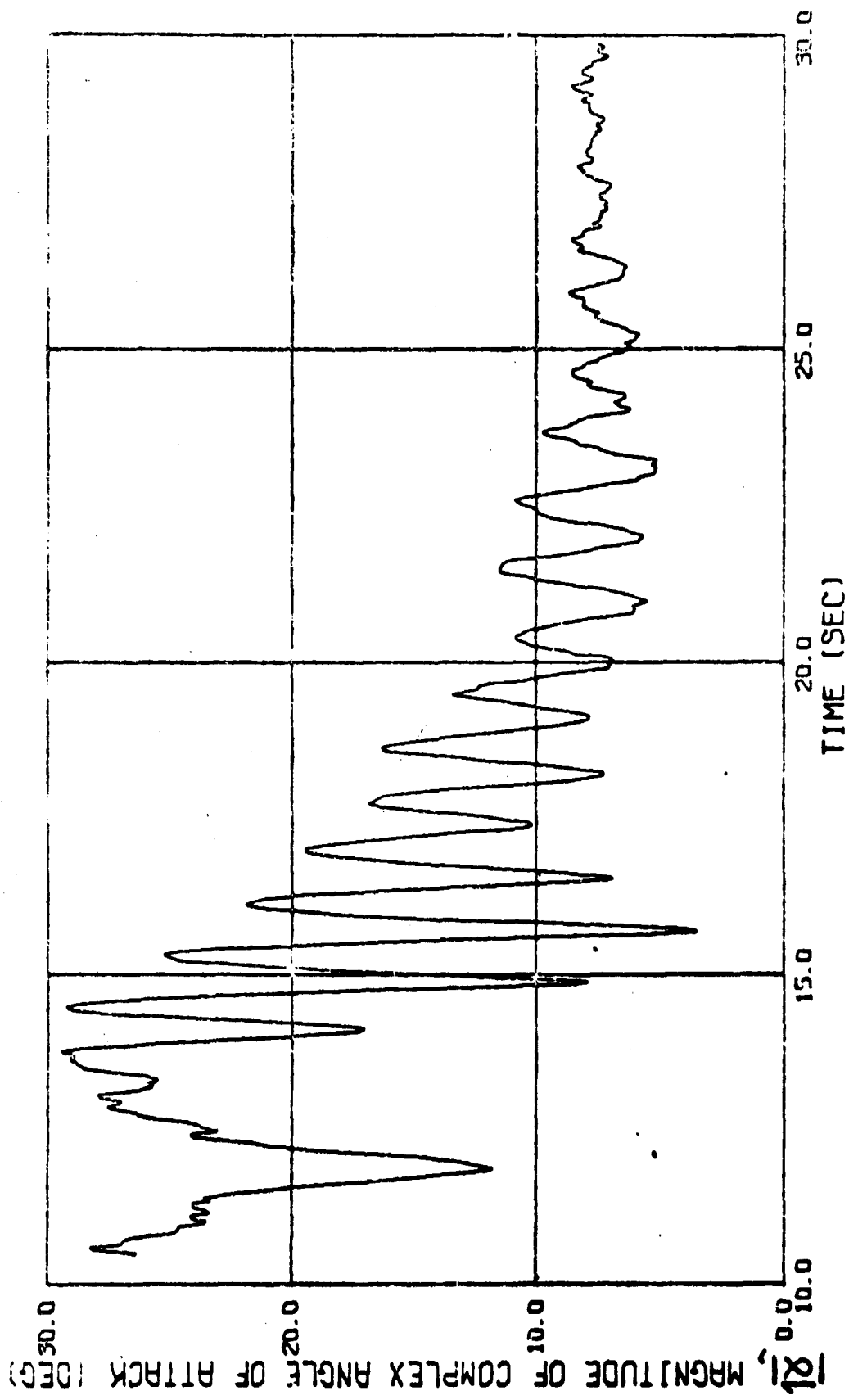


Fig. 4a MAGNITUDE OF COMPLEX ANGLE OF ATTACK VERSUS TIME FROM RELEASE
FOR SPLIT-SKIRT BOMB (739)

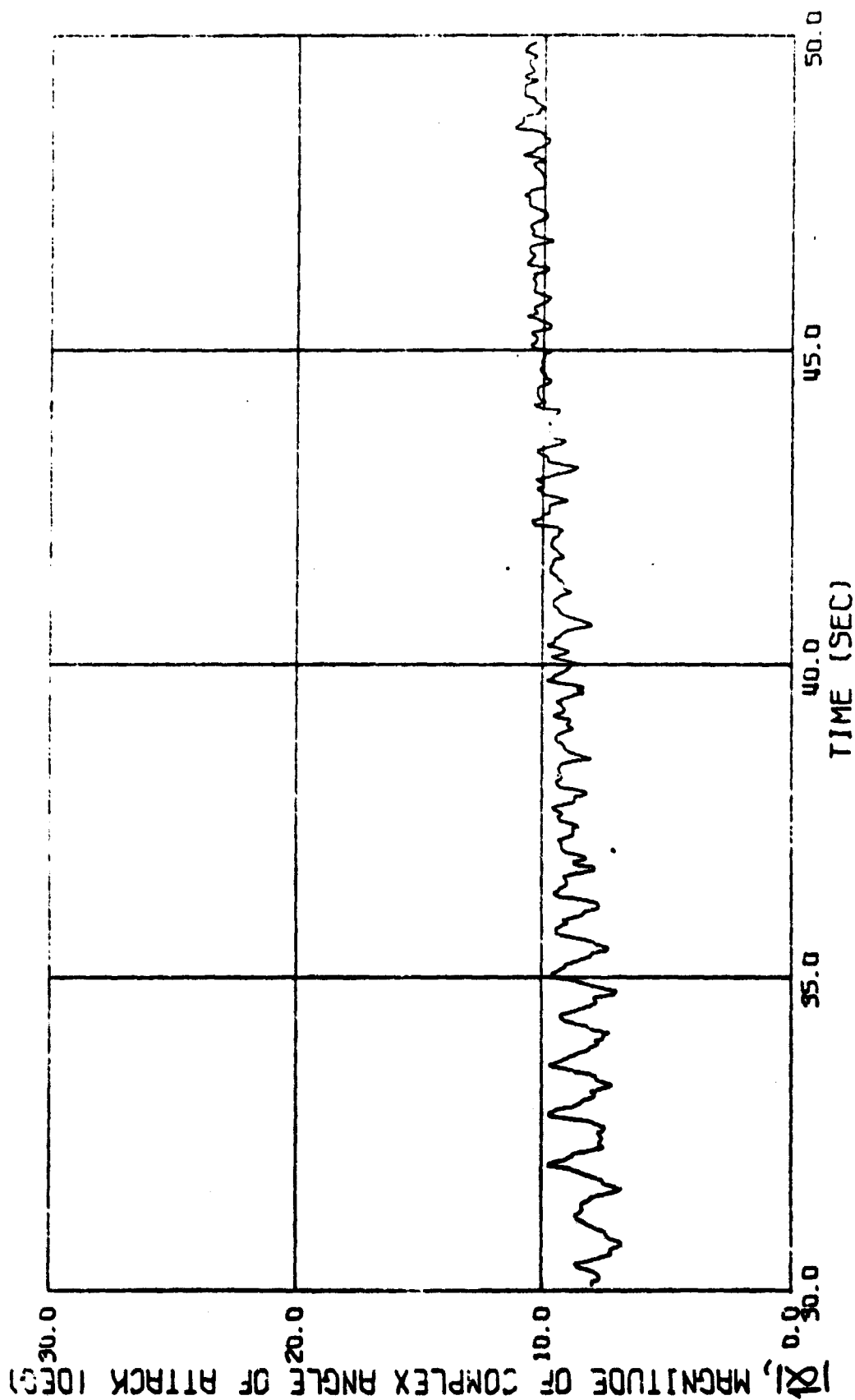


Fig. 4b MAGNITUDE OF COMPLEX ANGLE OF ATTACK VERSUS TIME FROM RELEASE
FOR SPLIT-SKIRT BOMB (739)

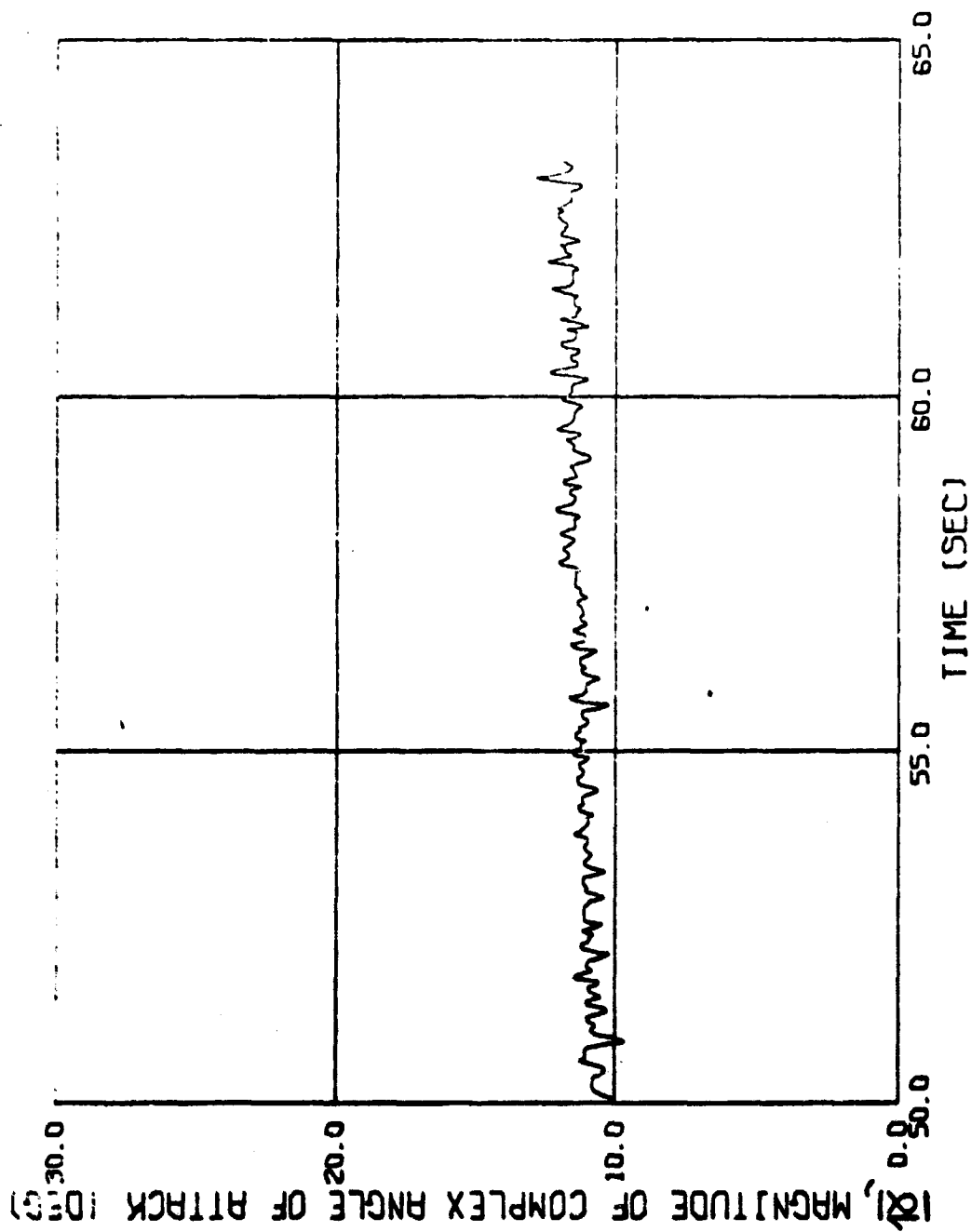


Fig. 4c MAGNITUDE OF COMPLEX ANGLE OF ATTACK VERSUS TIME FROM RELEASE FOR SPLIT-SKIRT BOMB (739)

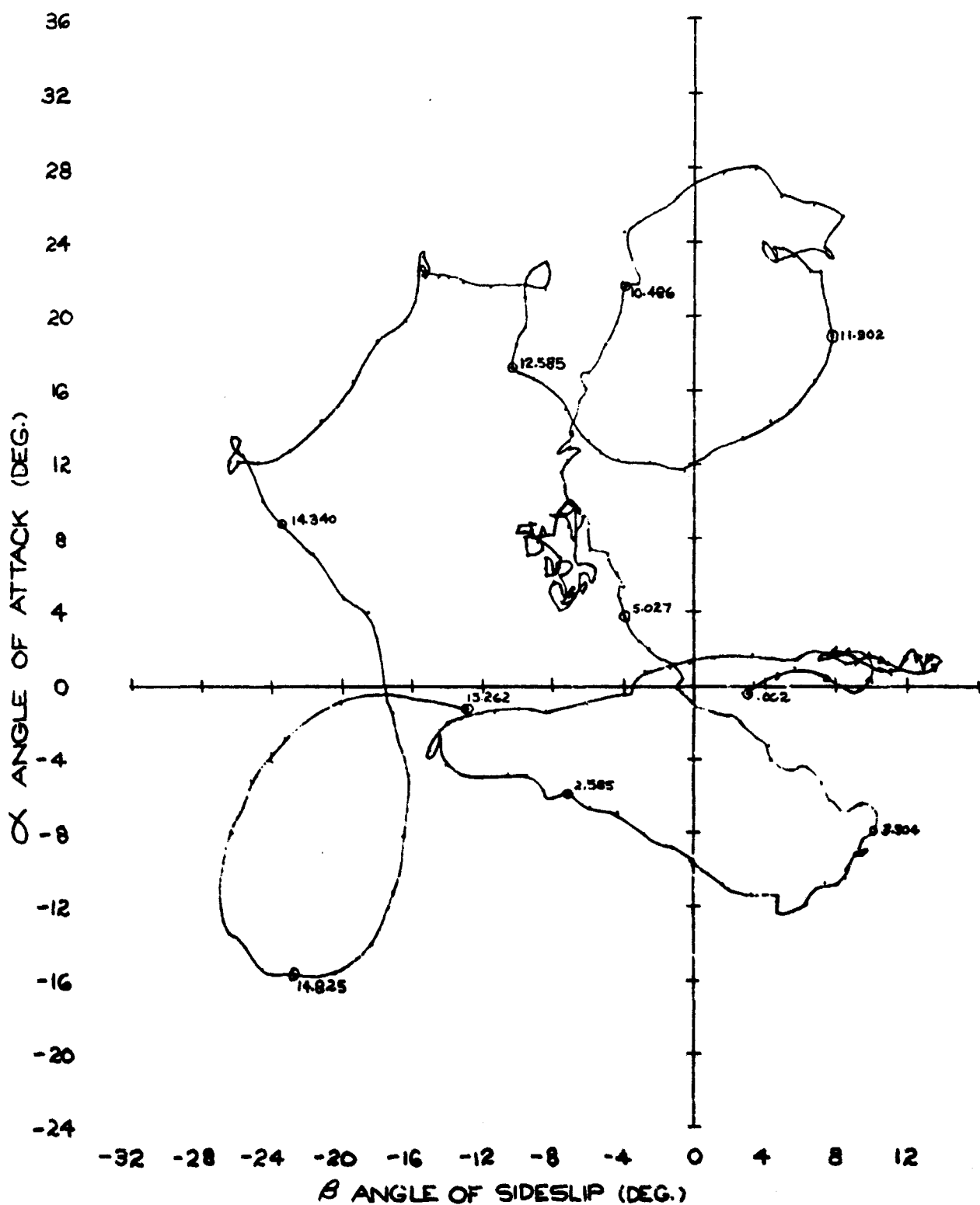


FIG. 52 COMPLEX ANGLE OF
ATTACK FOR SPLIT-
SKIRT BOMB (739)

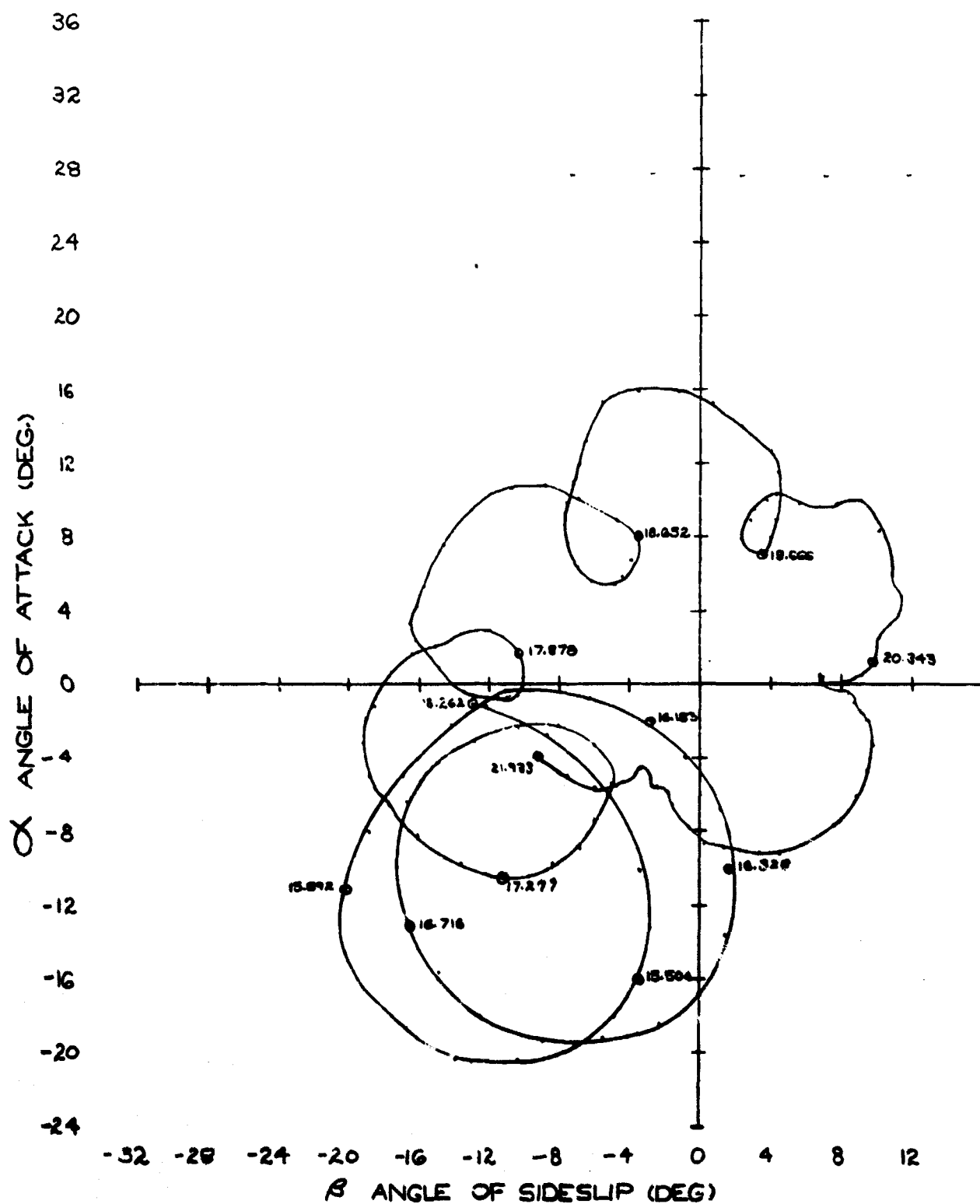


FIG. 5b COMPLEX ANGLE OF
ATTACK FOR SPLIT-
SKIRT BOMB (739)

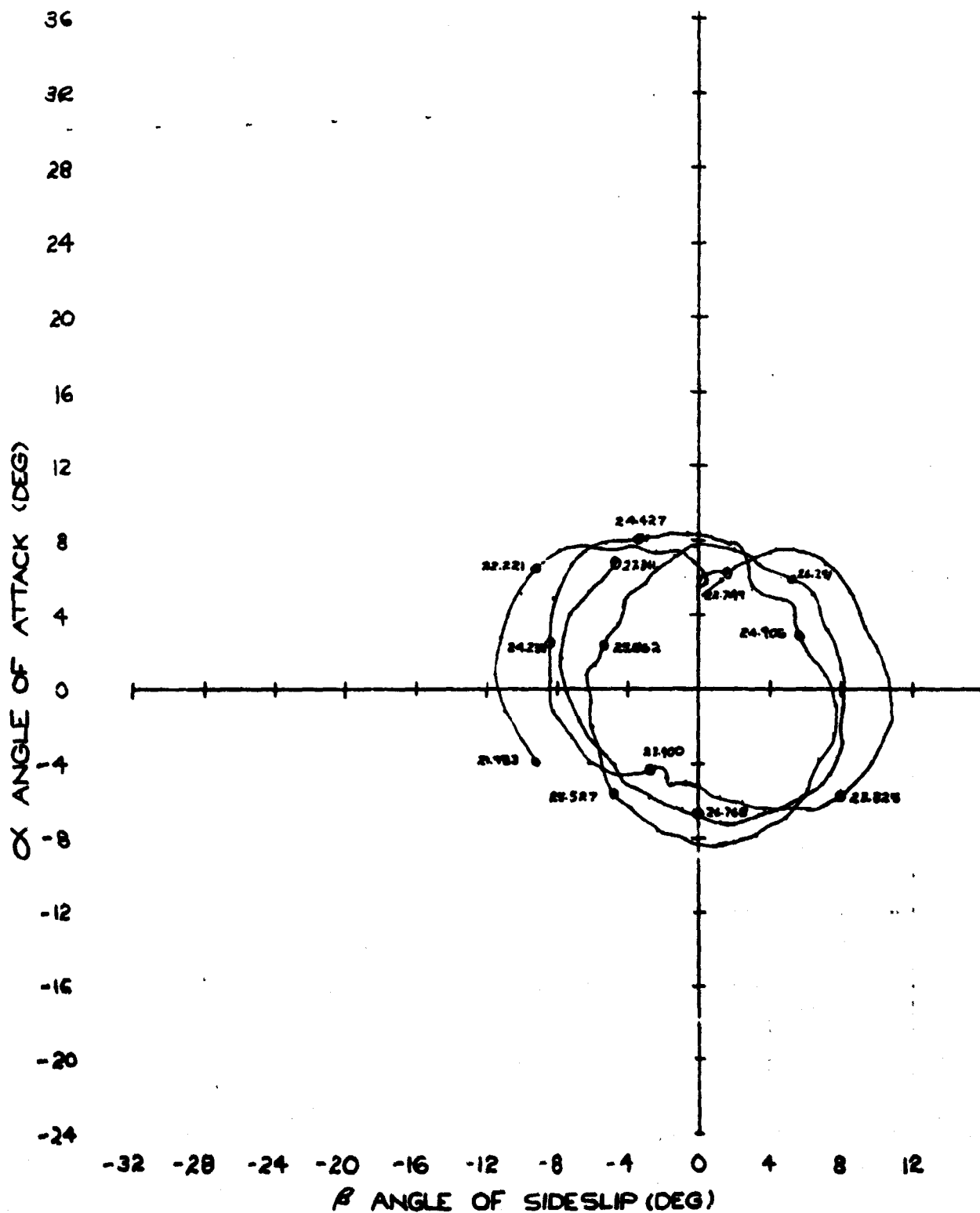


FIG 5C COMPLEX ANGLE OF
ATTACK FOR SPLIT-
SKIRT BOMB (739)

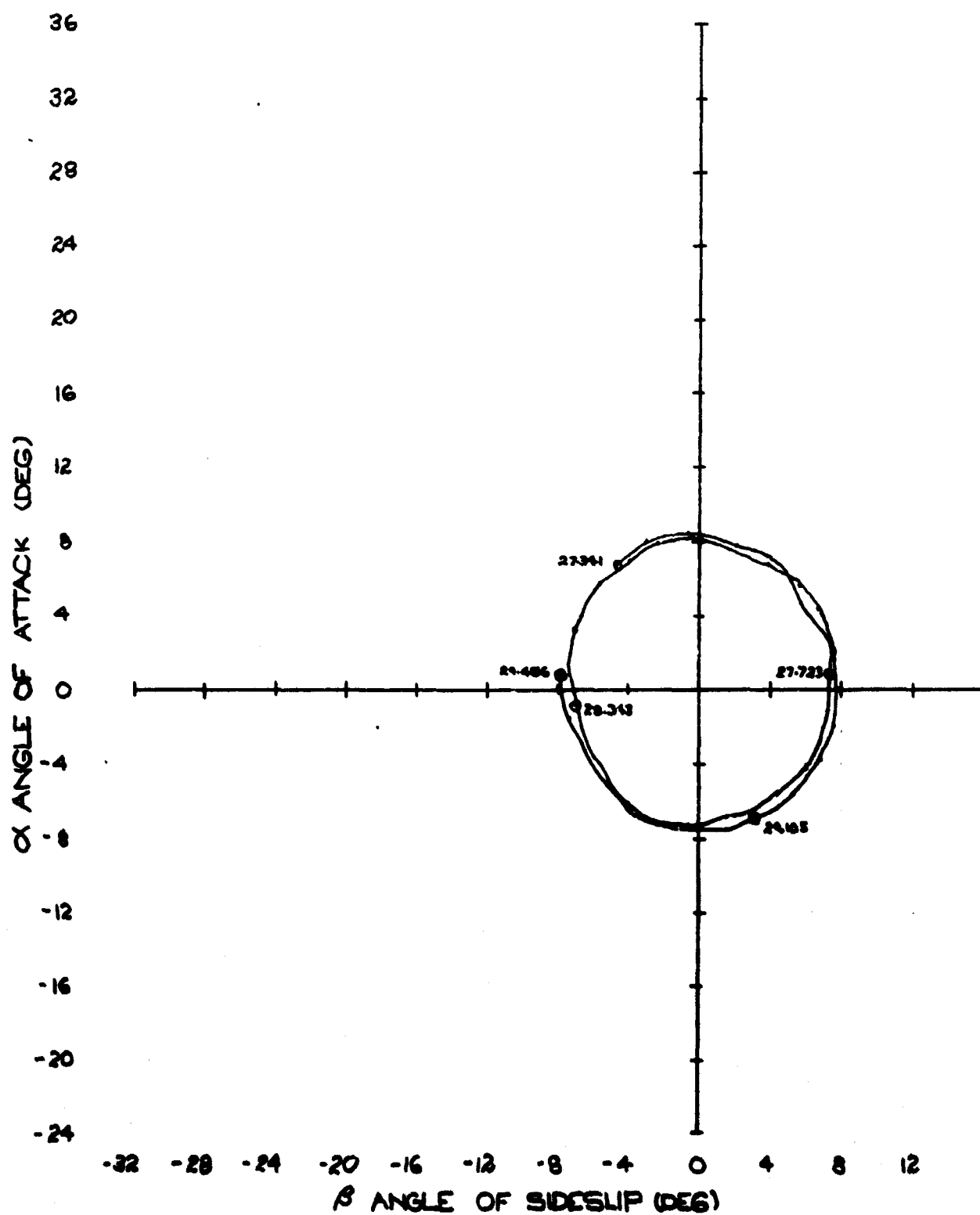


FIG 5d COMPLEX ANGLE OF
ATTACK FOR SPLIT-
SKIRT BOMB (739)

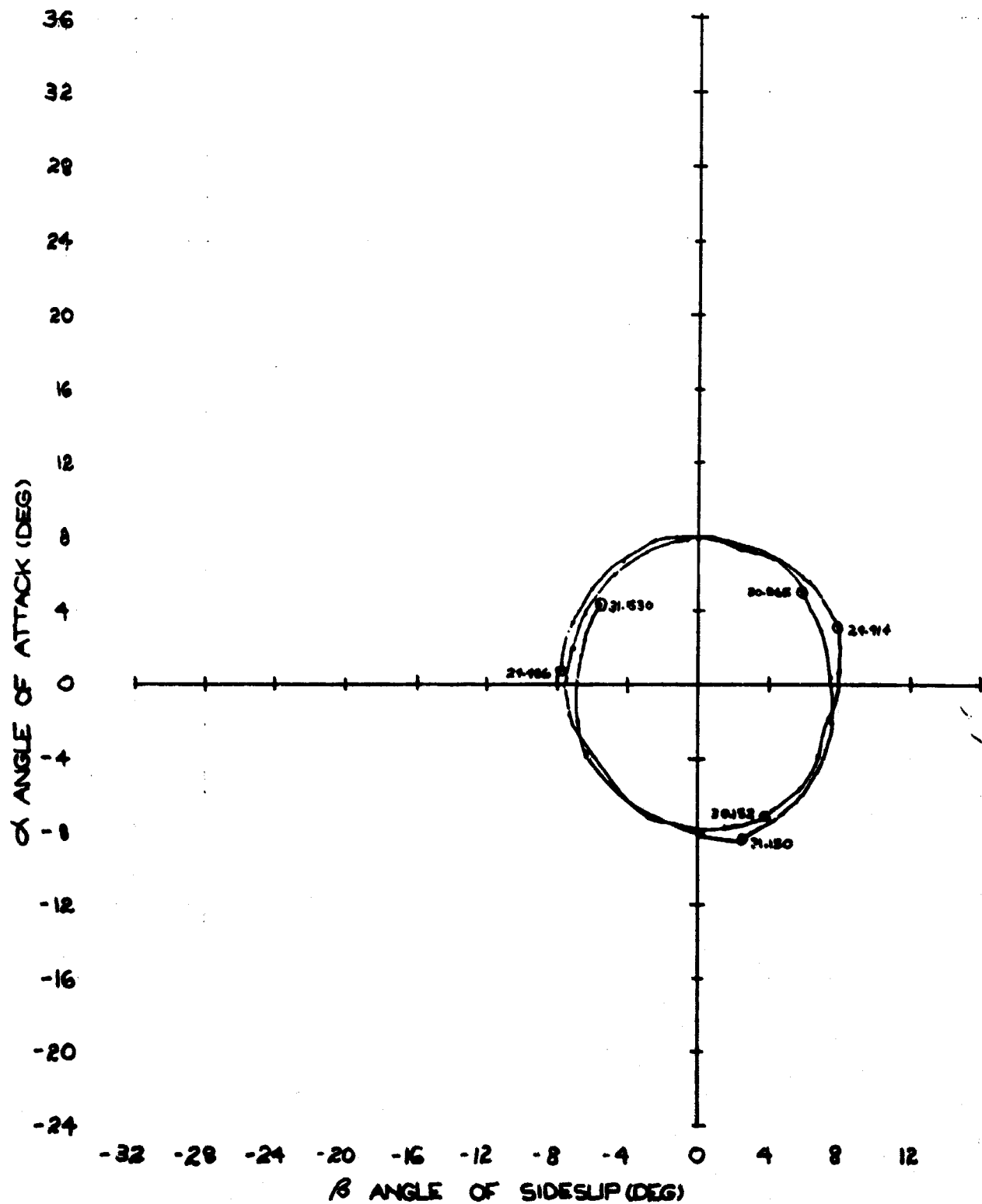


FIG. 5c COMPLEX ANGLE OF
ATTACK FOR SPLIT-
SKIRT BOMB (739)

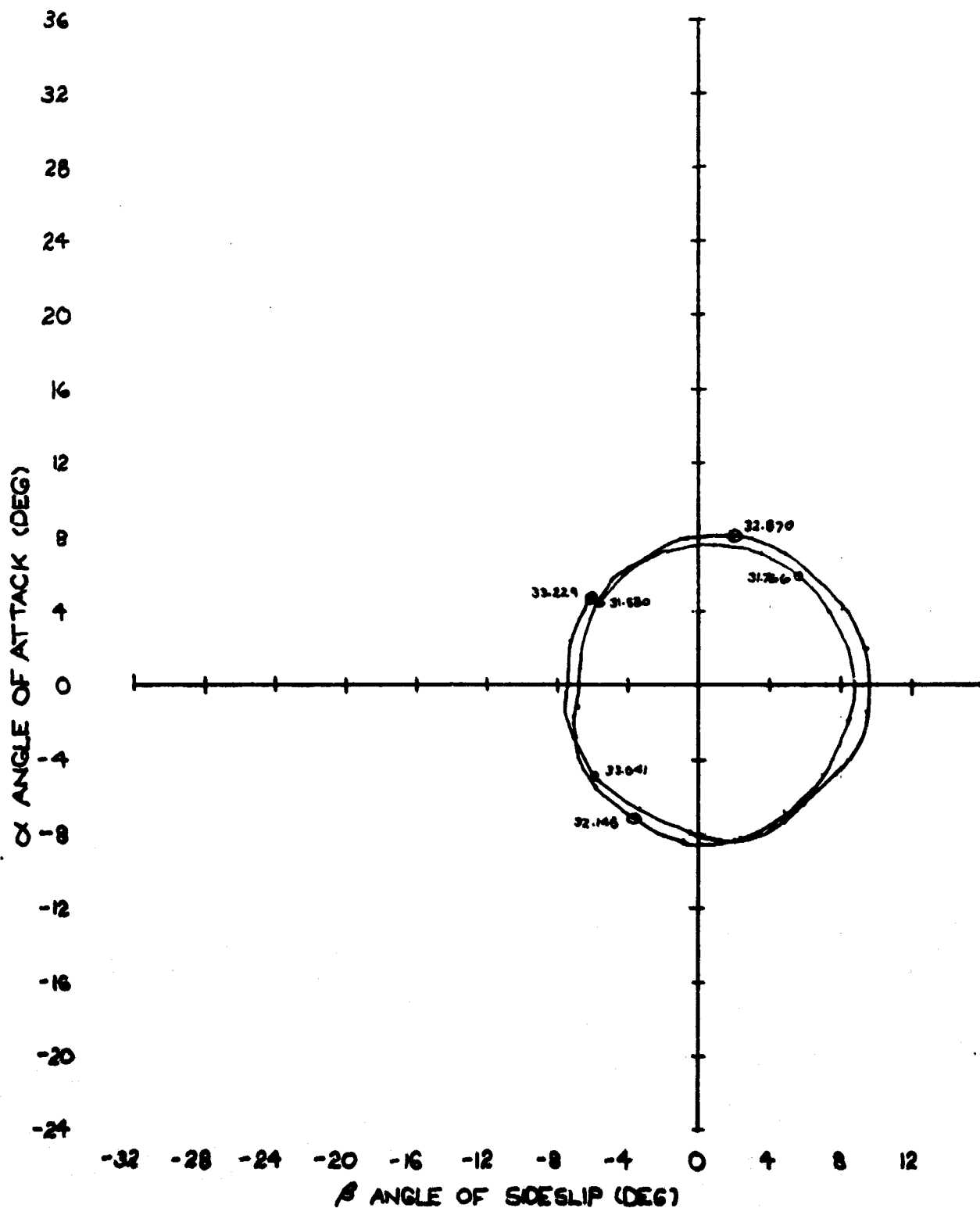


FIG. 5f COMPLEX ANGLE OF
ATTACK FOR SPLIT-
SKIRT BOMB (739)

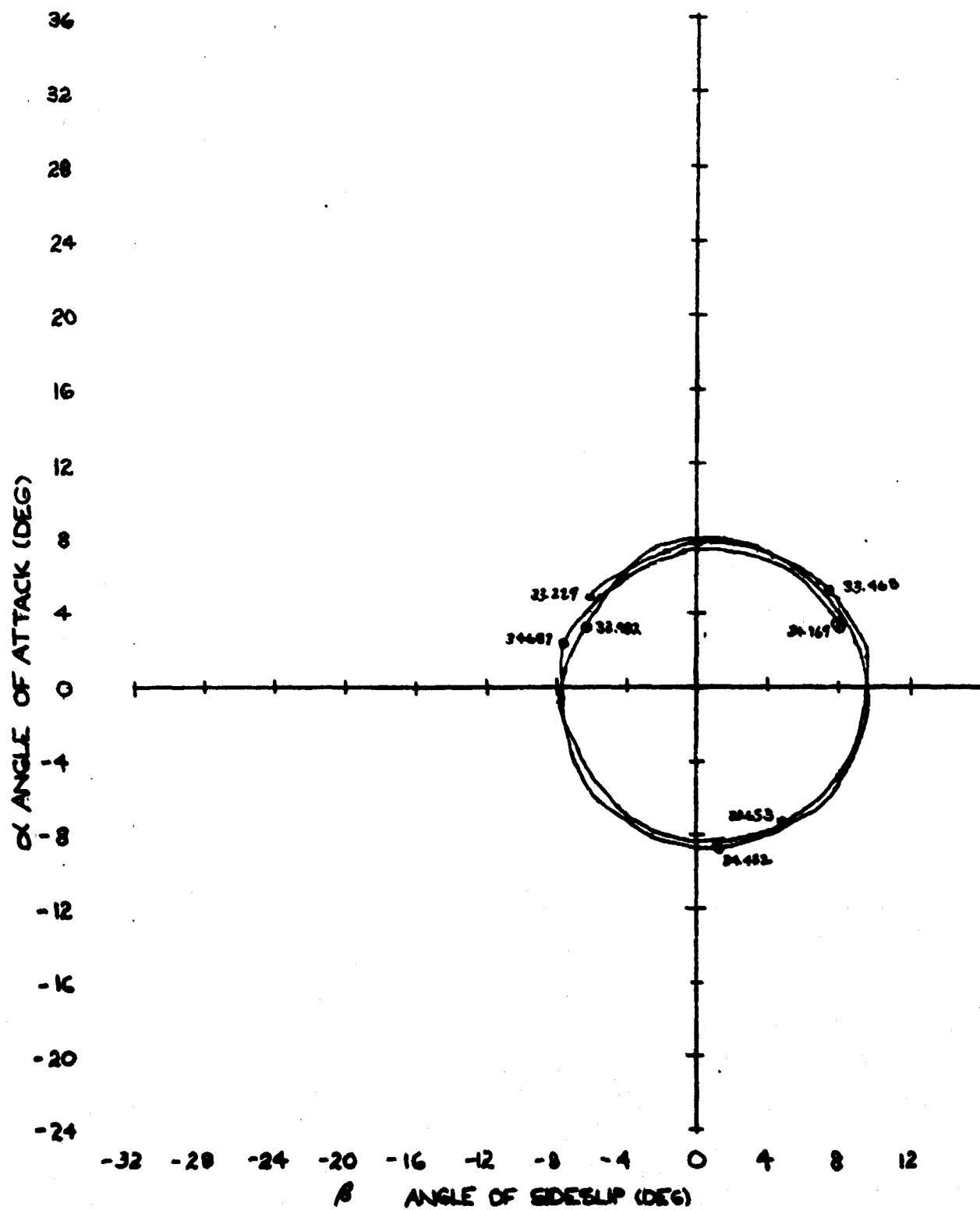


FIG 58 COMPLEX ANGLE OF
ATTACK FOR SPLIT-
SKIRT BOMB (739)

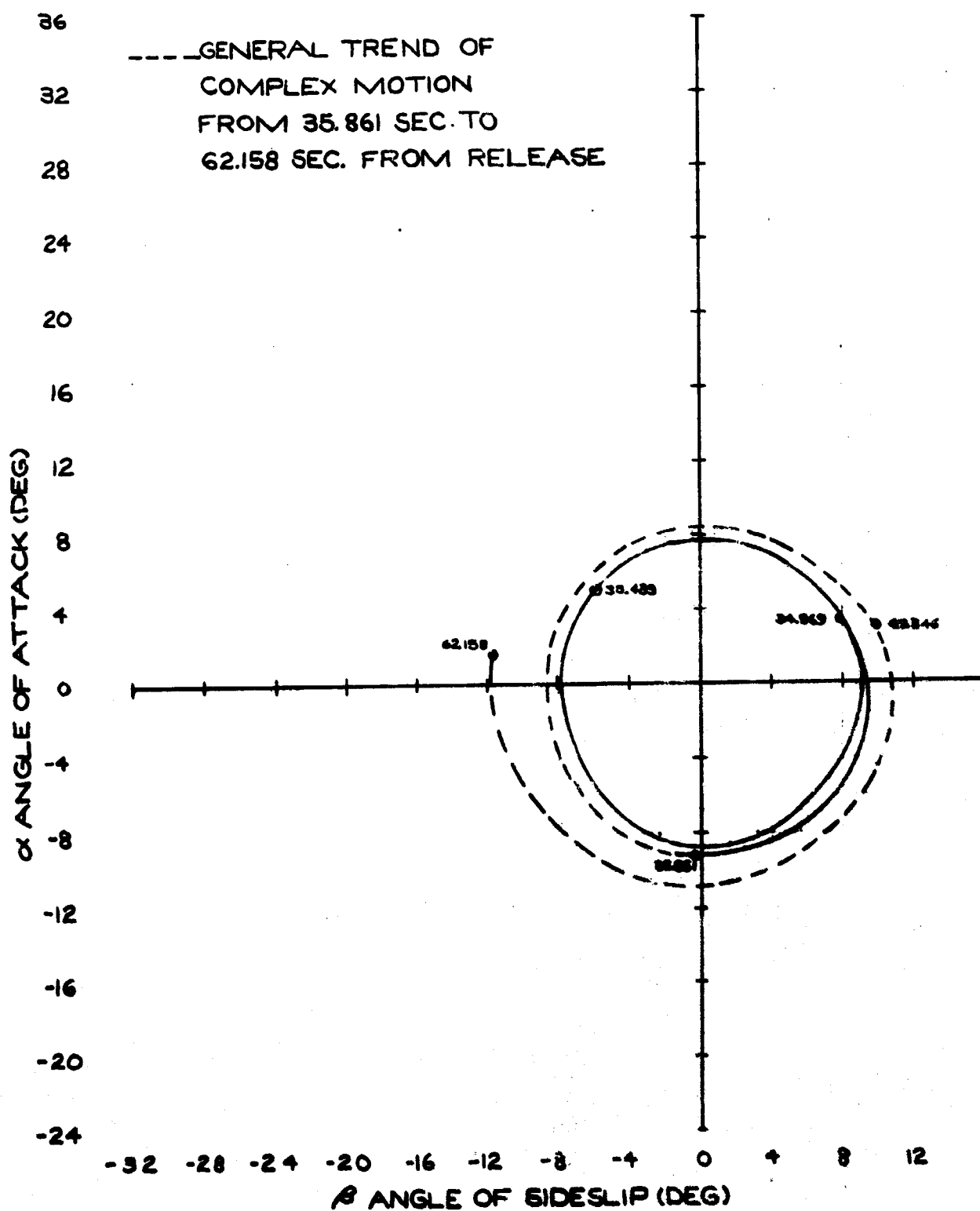


FIG. 5h COMPLEX ANGLE OF
 ATTACK FOR SPLIT-
 SKIRT BOMB (739)

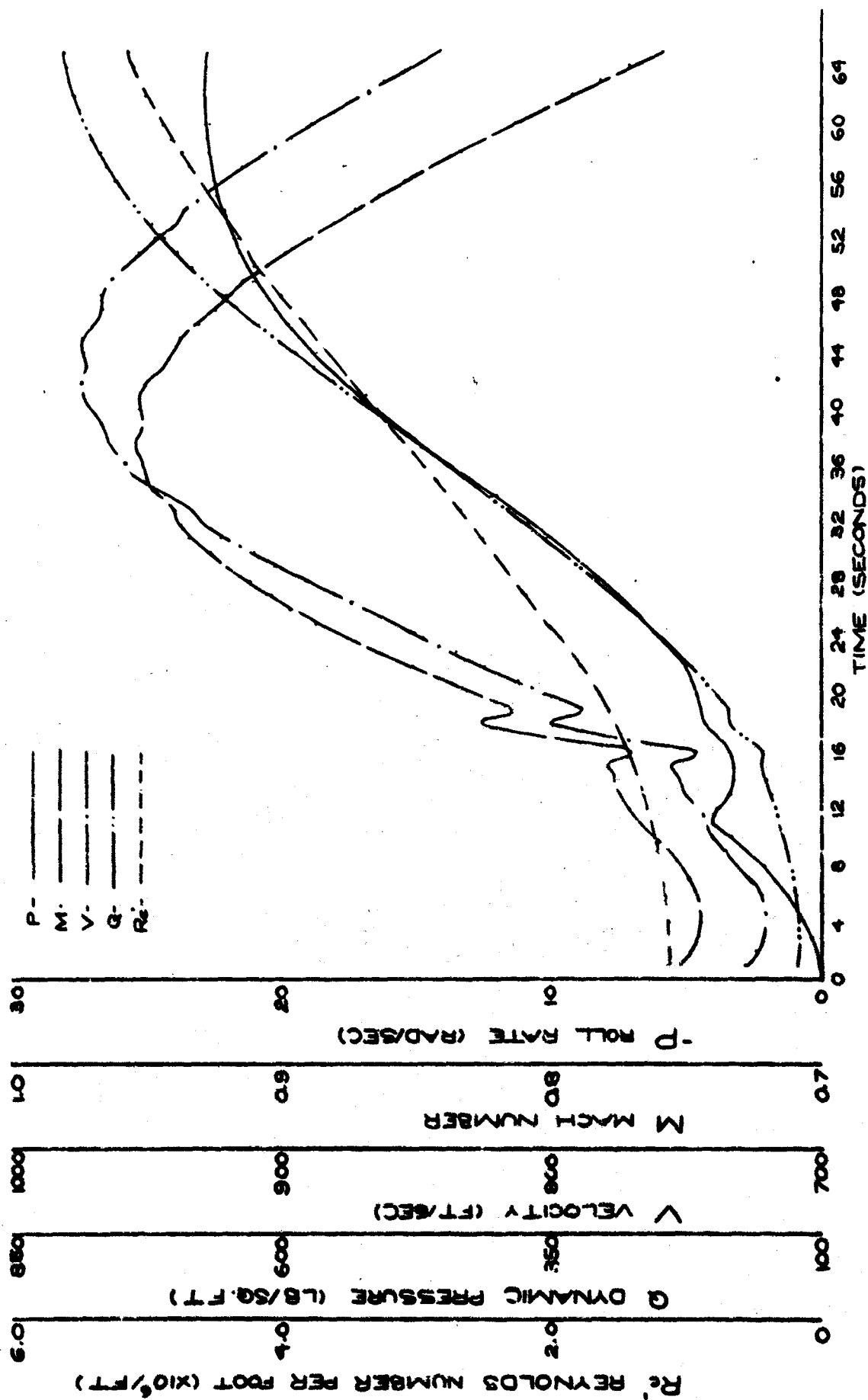


FIG. 6 TRAJECTORY PARAMETERS VERSUS TIME

FROM RELEASE FOR SPLIT-SKIRT BOMB (739)

is characterized by undamping concentric circular motion indicative of a Magnus instability. Thus, preliminary investigation of the angular orientation data indicated that two of the three basic types of instabilities characteristic to cruciform finned missiles might be present: Resonance and Magnus Instability.

Fitting Procedure

The fitting technique of Reference 12 is organized in such a manner as to allow considerable flexibility in its application to various sets of data. In the case of six degree of freedom data, the motion's characteristics, such as rate of change of the magnitude of the angle of attack and changes in the shape of the complex motion (circular, elliptical, etc.) generally dictate the procedures to be followed to obtain the best possible fit. Another important factor which must be considered is the possibility of error in the data and how this error may affect the results. Both factors were investigated in great detail prior to application of the fitting routine.

In order to detect possible error in the data, investigation was directed towards the magnitude of the complex motion, Fig. 4, in which considerable oscillations were observed. Up to approximately 25 seconds from release, at which time the complex motion assumes a circular pattern, it was assumed that these oscillations, which decreased in amplitude with time, were due to the superposition of a damping vector with the vector dominant in the motion. After 25 seconds from release, however, the motion is circular about a center at nearly zero complex angle of attack, indicating that the motion is probably monocyclic with a small trim. Thus, it was thought that the observed oscillations might be due to inherent error in the data. Rhodes and Shannon³ indicate that the differential pressure incidence meter used to measure the angular orientation data has phase lags associated with the tube lengths leading from the surface tapping points to the pressure transducers. These phase lags are estimated in Reference 15. From previous experience with the fitting routine², it was thought that these oscillations might influence the determination of the dynamic damping factors.

The procedure to be followed in fitting the angular orientation data was heavily dependent on the general characteristics of the complex motion. From 12.05 seconds from release to approximately 16.6 seconds, the complex motion consists of large "loops." At this time, the "loops" become much smaller and begin to damp out while the overall motion is elliptical. At 24.5 seconds the motion is of a circular nature and continues in this manner until the end of the flight. The angular orientation data, tabulated at every 0.047 second, was fitted to the quadricyclic equation, Eq. (18), over various numbers of cycles of the complex motion, depending on what section of the data was being fitted. Beginning at 16.62 seconds, the fit was receded in time in increments of 0.047 second, each sectional fit encom-

passing 0.5 cycle, until the effects of the release disturbance were felt at 12.05 seconds and the fit was terminated. The fit was then advanced from 16.62 seconds at increments of 0.13 second, each sectional fit encompassing 0.75 cycle, until 24.5 seconds at which time the Precession Vector had damped to such an extent that the fitting routine could not determine it, its dynamic damping factor, and frequency to within a reasonable degree of accuracy. In the previous two sections of data fitted, the character of the motion was changing rapidly, thus dictating that each fit encompass only a fraction of a cycle. In this case the number of points per cycle was sufficiently large to insure a good fit.

At 24.5 seconds, initial conditions with sufficient accuracy to commence the fit were not able to be extracted from the data. At 34.97 seconds, however, initial conditions were obtained, and the fit was receded in time to 24.5 seconds at increments of 0.141 second, each sectional fit encompassing 2 cycles. The ability to obtain an accurate fit with a larger number of cycles is due to the fact that the character of the motion was not changing too severely from 24.5 seconds to 34.97 seconds. From 34.97 seconds to the end of the flight, the motion is essentially circular. Thus, more cycles may be included per sectional fit without loss of accuracy. This increase in the number of cycles is also necessary since the number of points per cycle was decreasing. Therefore, from 34.97 seconds from release to the end of the flight, the fit was advanced 0.23 second, each sectional fit encompassing 3 cycles, until the fit was terminated at 62.13 seconds from release. A summary of the parameters and techniques used in the fitting procedure is presented in Table II.

Thus, by overlapping these sectional fits the stability parameters of Eq. (18) were determined as a function of time from release. Using position coordinate data and the magnitude of the complex angle of attack, the functional dependence of the stability derivatives with Mach number, Reynolds number, and angle of attack was analyzed.

TABLE II. FITTING ROUTINE AND PARAMETERS

<u>Initial</u> <u>Time (sec)</u>	<u>Final</u> <u>Time (sec)</u>	<u>Time</u> <u>Increment (sec)</u>	<u>Number of Cycles</u> <u>per Sectional Fit</u>
16.62	12.05	-.047	.5
16.62	24.5	.13	.75
34.97	24.5	-.141	2.0
34.97	62.13	.23	3.0

SECTION V

ANALYSIS OF RESULTS

The fit of the complex angular motion to the quadricyclic equation, Eq. (18), yielded a total probable error which ranges from 0.12 degree to 2.3 degrees. Fig. 7 shows the probable error of fit (Figs. 7a to 7c) and the percent error of fit (Figs. 7d to 7f) as a function of time from release. The percent error is with respect to the magnitude of the vectors fitted. It is seen that the maximum percent error obtained is approximately 7% of the total motion, which indicates a good fit of the theory to the data. At 24.5 seconds from release, there is a sharp increase in the probable error from 0.2 degree to 0.6 degree. There are two reasons for this discontinuity: 1) At the end of the previous fit (24.5 seconds) the magnitude of the Precession Vector had damped to such an extent that the fitting routine was no longer able to determine it, its dynamic damping factor and frequency. Hence, at the beginning of the next fit, these small values of the Precession Vector appeared in the residuals as error until the vector damped to a negligible amplitude at approximately 26.5 seconds from release. 2) A higher probable error at the beginning of a fit has been found to be characteristic to the fitting procedure due to the fact that it takes several iterations for the initial approximations to attain sufficient accuracy. Thus, a combination of these observations, one characteristic to the data, the other to the fitting procedure, led to the discontinuity observed in the probable error. The amplitude of the probable error, indicating an extremely good fit to the complex angular data, implied generally accurate fits to the linear stability parameters of the quadricyclic equation.

Linear Stability Parameters and Probable Errors

In fitting the complex angular motion, Fig. 5, to the quadricyclic equation, Eq. (18), it was found that the Nutation Vector and Trim Vector were present throughout the entire flight. The Precession Vector, however, was not fitted after 24.5 seconds from release, while the Yaw of Repose Vector was found to be negligibly small throughout the entire flight.

Nutation Vector and Frequency

Figs. 8 and 9 show the magnitude of Nutation Vector and its probable error as a function of time from release. The fit yielded an accuracy which ranged from 0.04 degree to 1.1 degrees. It should be noted that the largest probable error, 1.1 degrees, occurred when the magnitude was approximately 33 degrees. Comparison of the magnitude of R_n and the magnitude of the complex motion from 25 seconds until the end of the flight indicates that practically the entire motion was pure nutation. The slight oscillations appearing in the magnitude are felt to be due to the inherent error in the

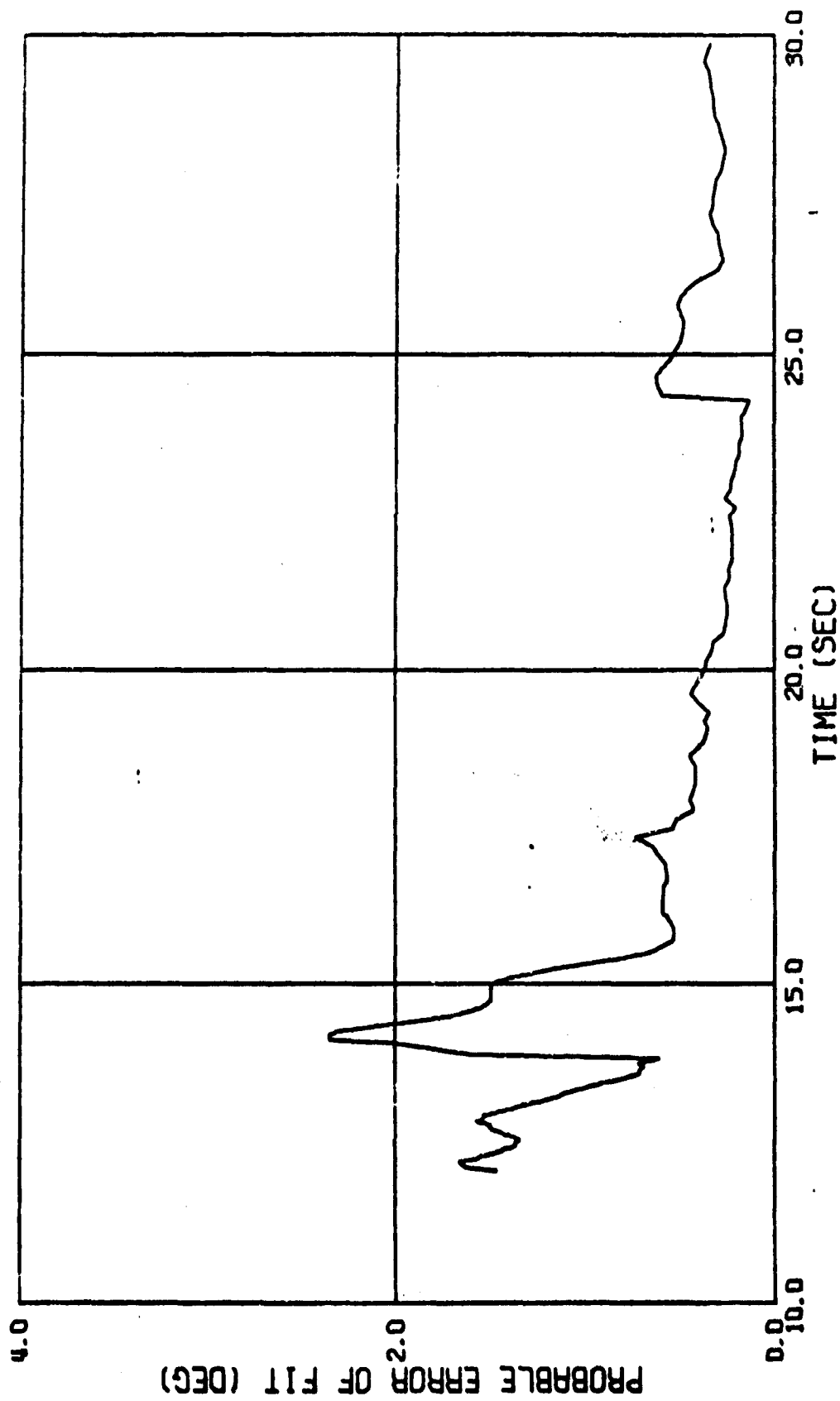


Fig. 7a PROBABLE ERROR OF FIT VERSUS TIME FROM RELEASE FOR SPLIT-SKIRT BOMB (739)

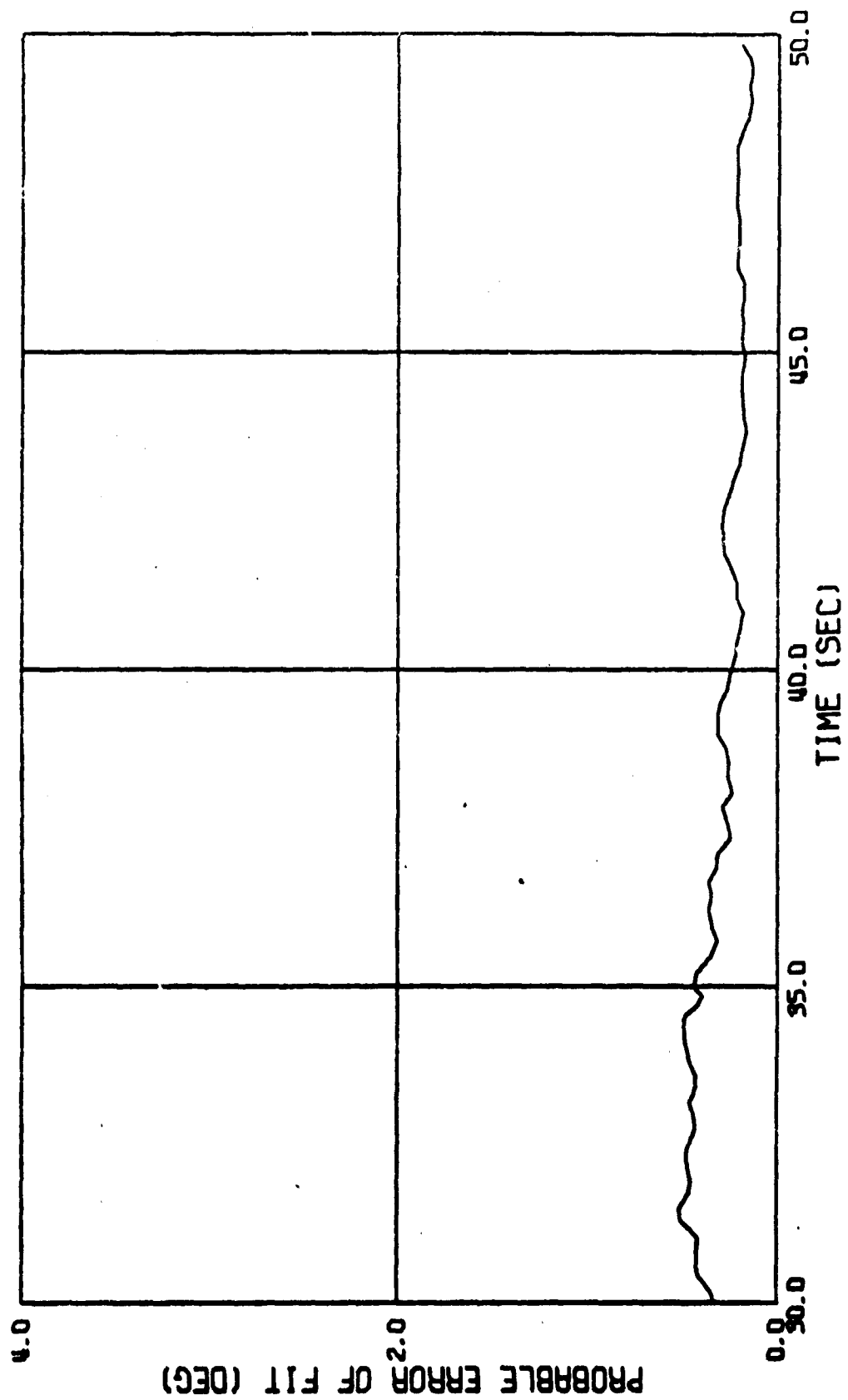


Fig. 7b PROBABLE ERROR OF FIT VERSUS TIME FROM RELEASE FOR SPLIT-SKIRT BOMB (739)

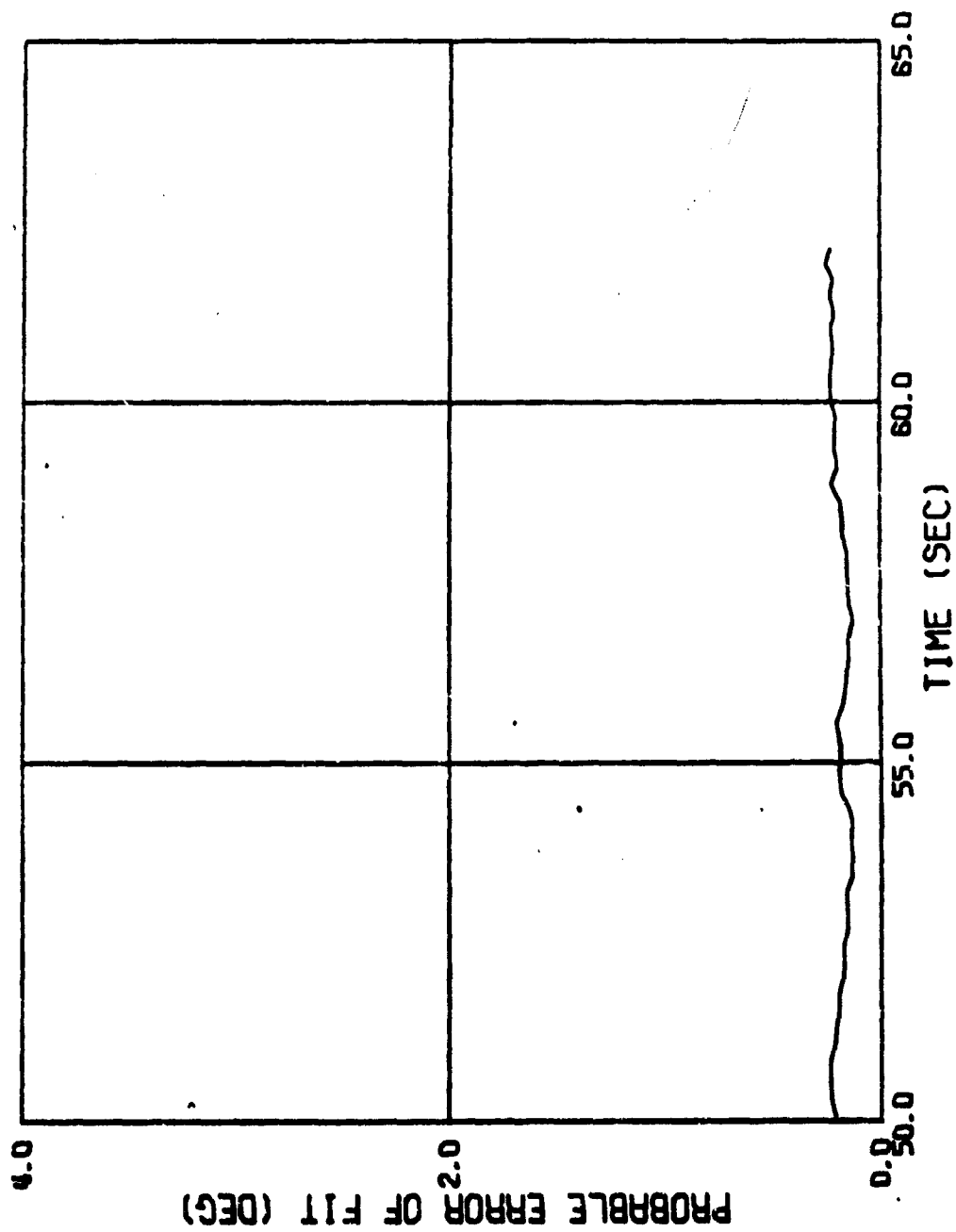


Fig. 7c PROBABLE ERROR OF FIT VERSUS TIME FROM RELEASE
FOR SPLIT-SKIRT BOMB (739)

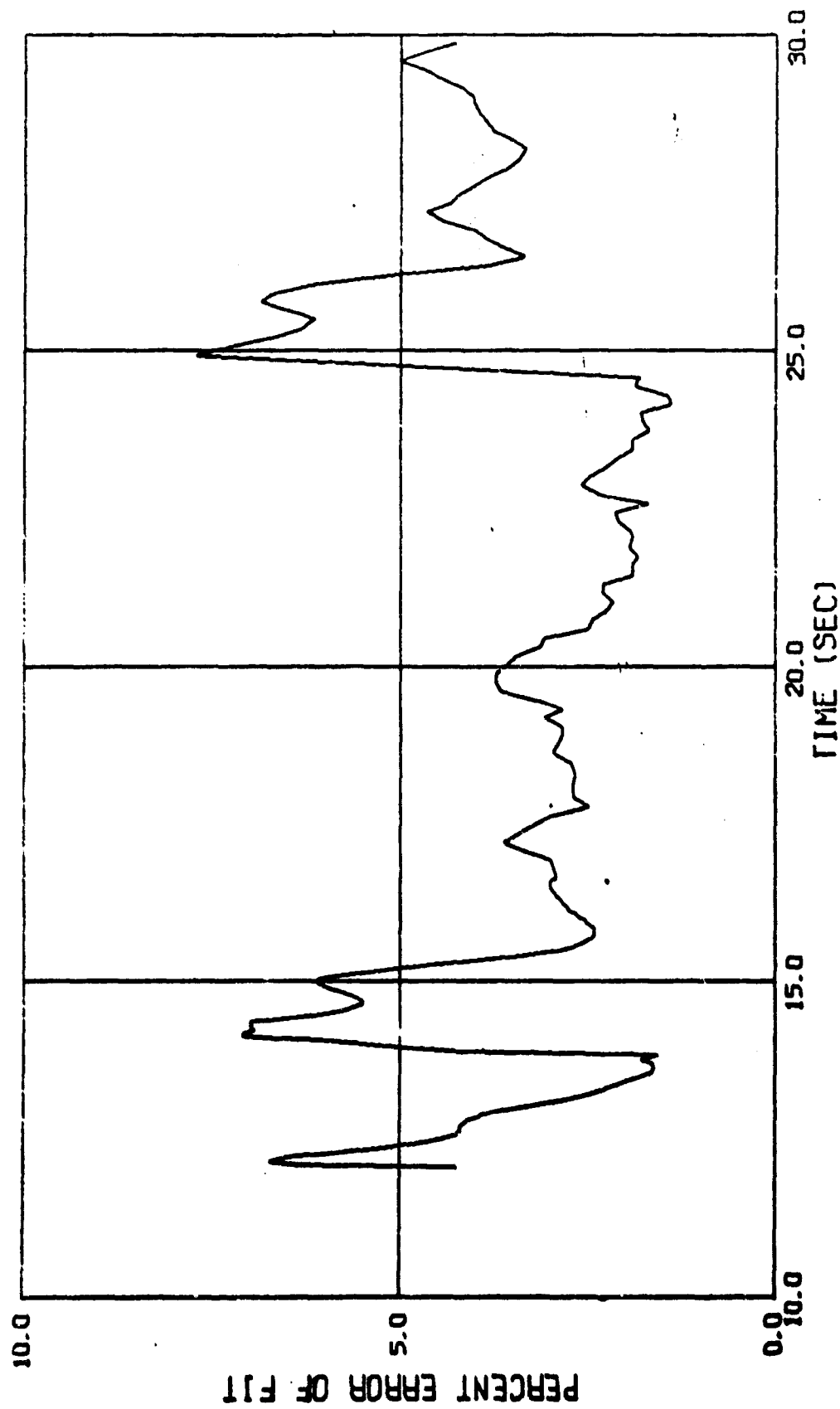


Fig. 7d PERCENT ERROR OF FIT VERSUS TIME FROM RELEASE FOR SPLIT-SKIRT BONIB (739)

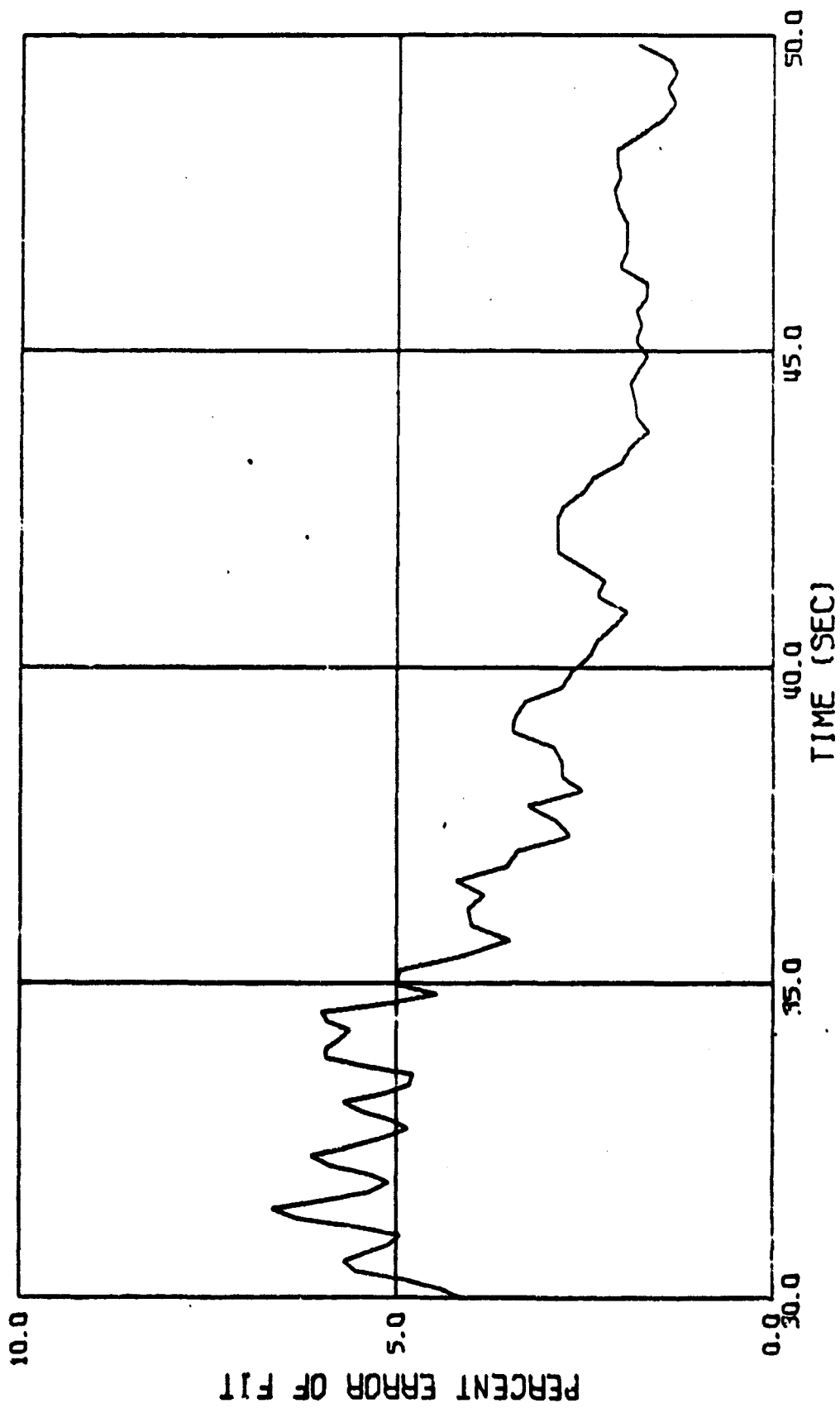


Fig. 7e PERCENT ERROR OF FIT VERSUS TIME FROM RELEASE FOR SPLIT-SKIRT BOMB (739)

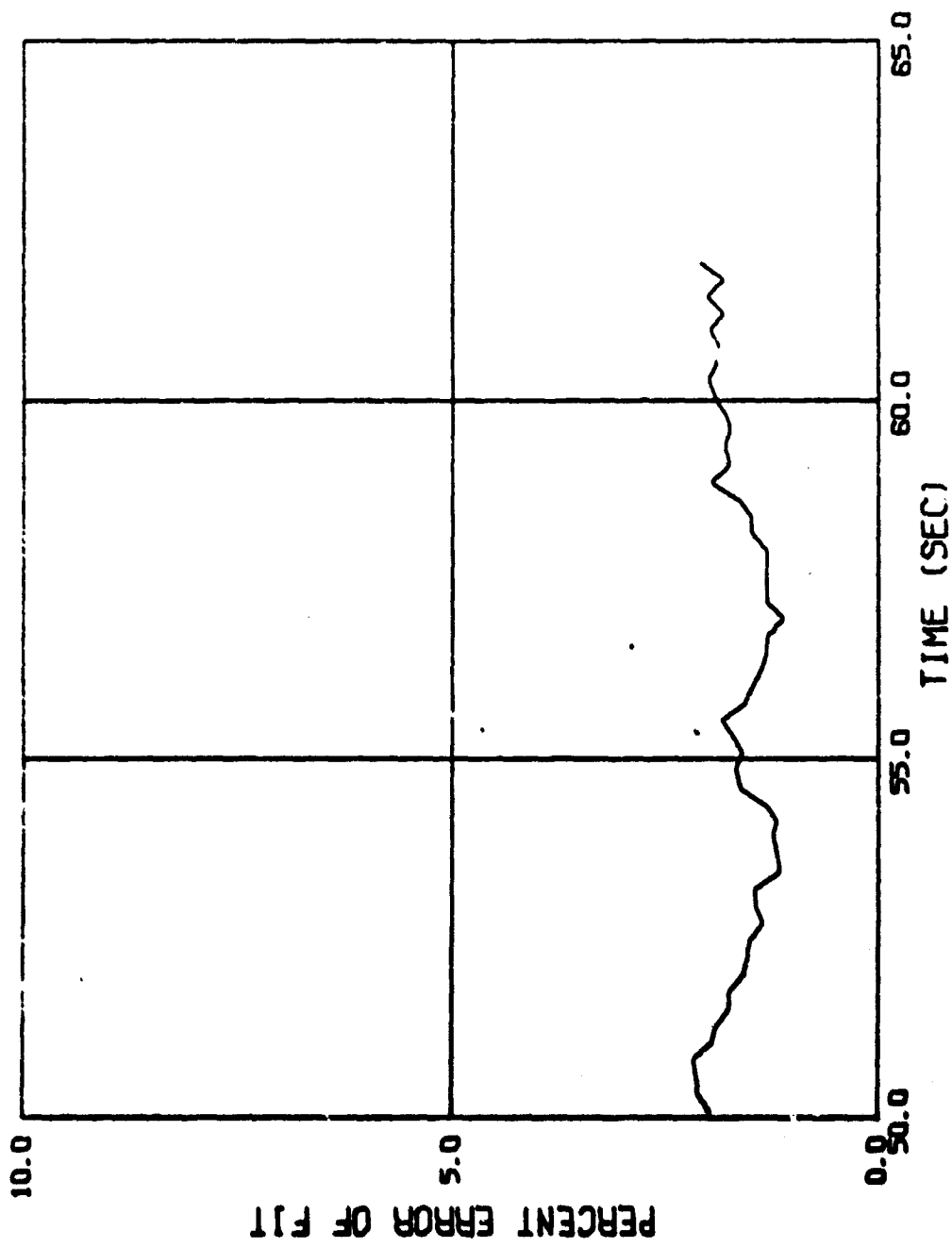


Fig. 71 PERCENT ERROR OF FIT VERSUS TIME FROM RELEASE
FOR SPLIT-SKIRT BOMB (739)

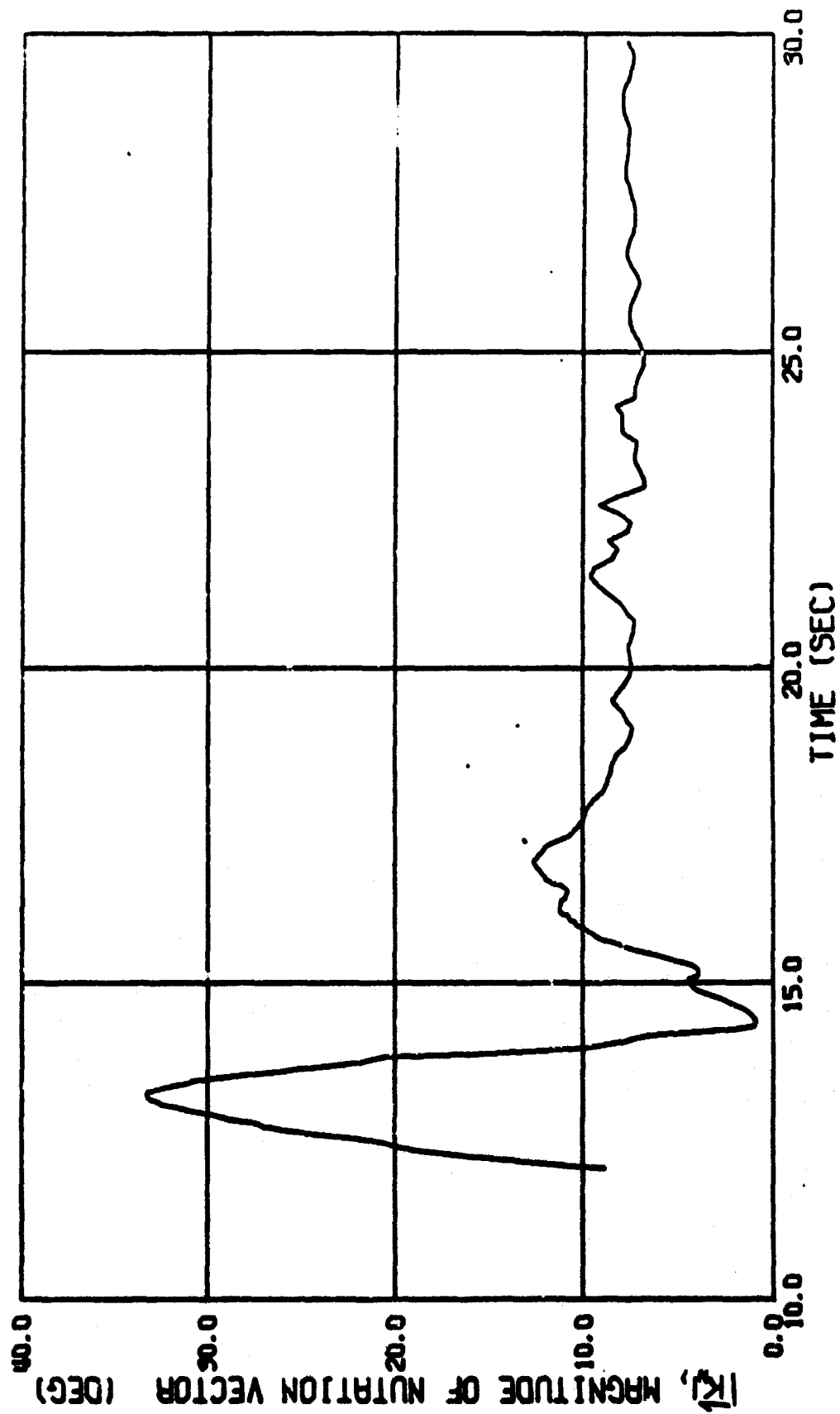


Fig. 8a MAGNITUDE OF NUTATION VECTOR VERSUS TIME FROM RELEASE FOR SPLIT-SKIRT BOMB (739)

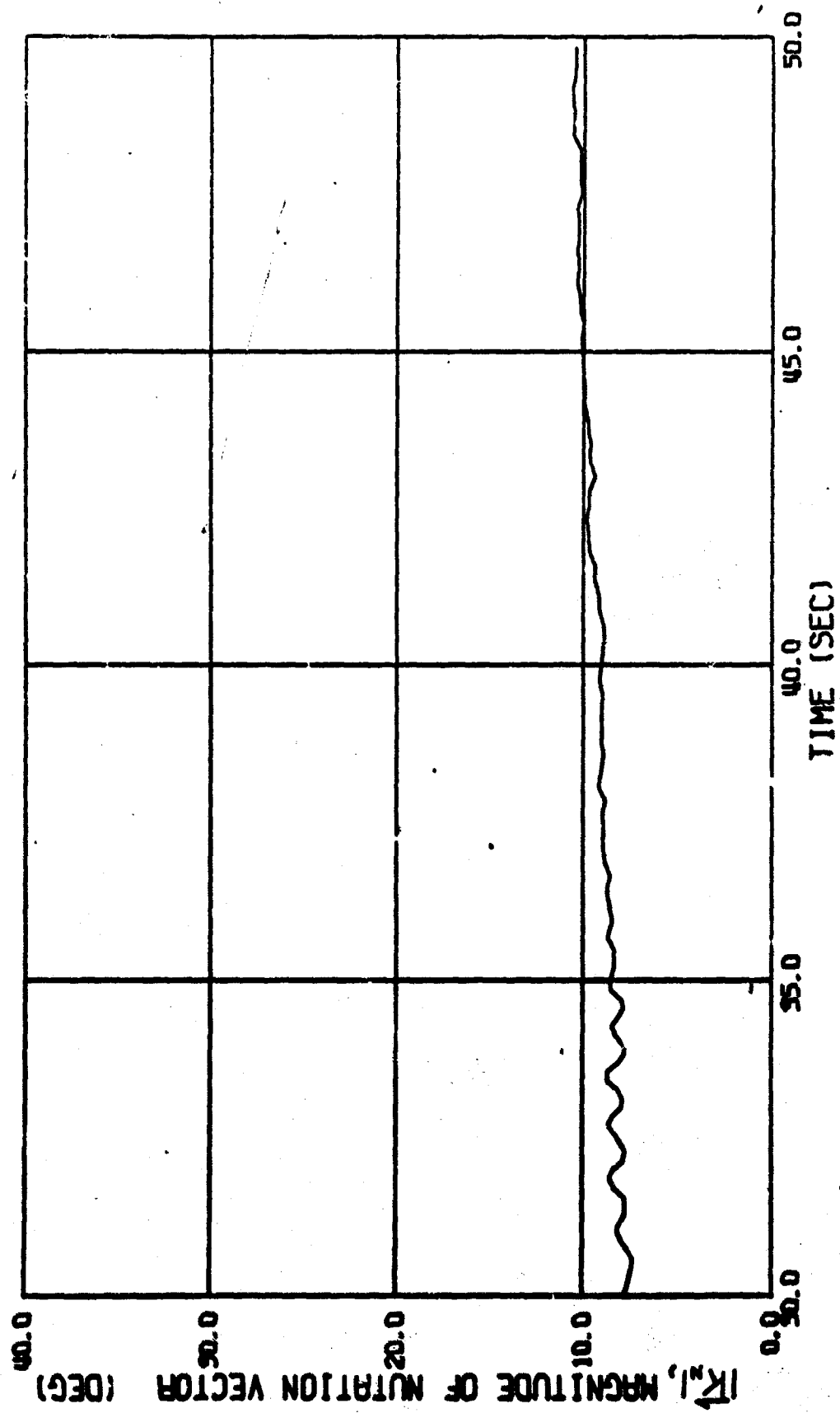


Fig. 8b MAGNITUDE OF NUTATION VECTOR VERSUS TIME FROM RELEASE FOR SPLIT-SKIRT BOMB (739)

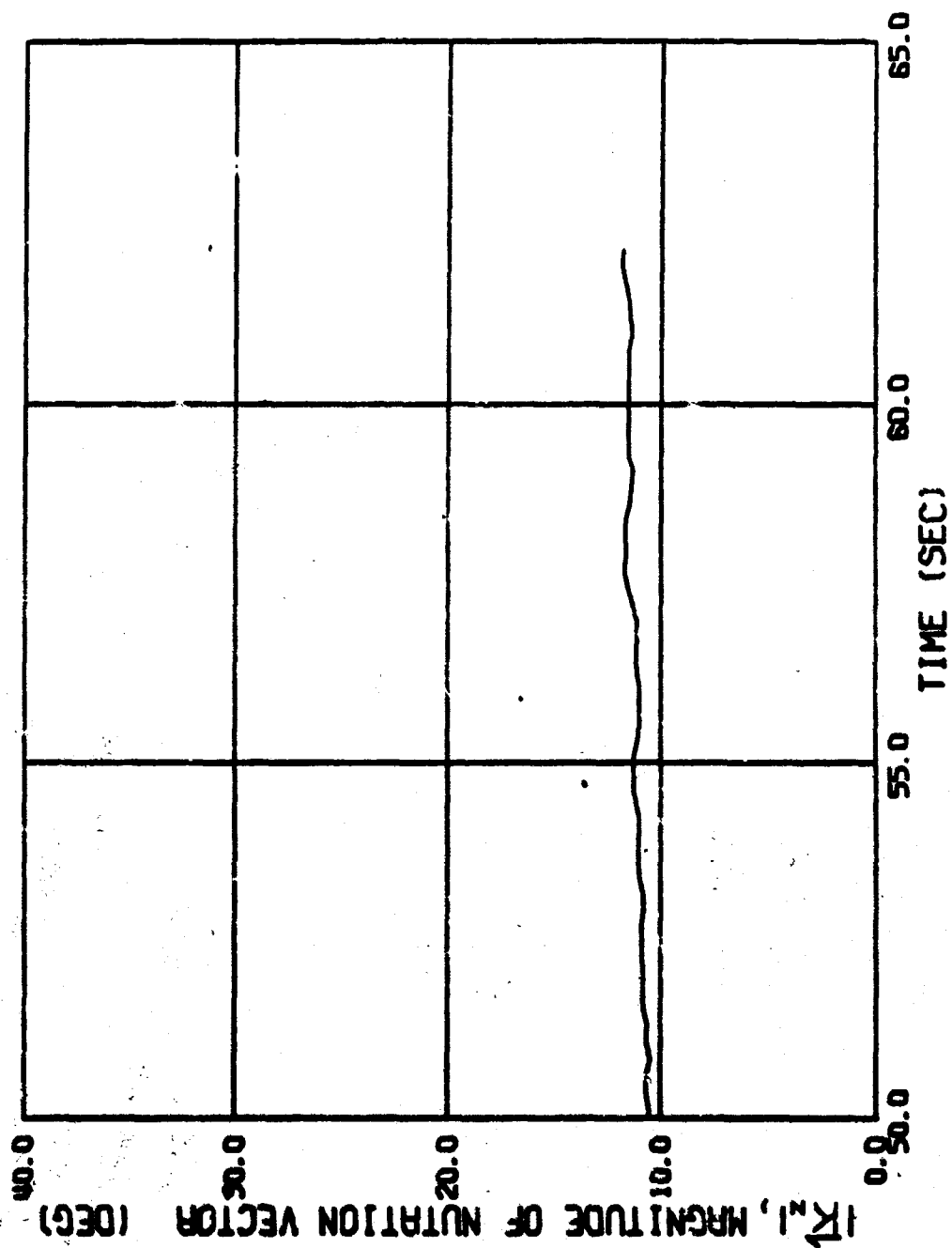


Fig. 8c MAGNITUDE OF NUTATION VECTOR VERSUS TIME FROM
RELEASE FOR SPLIT-SKIRT BOMB (739)

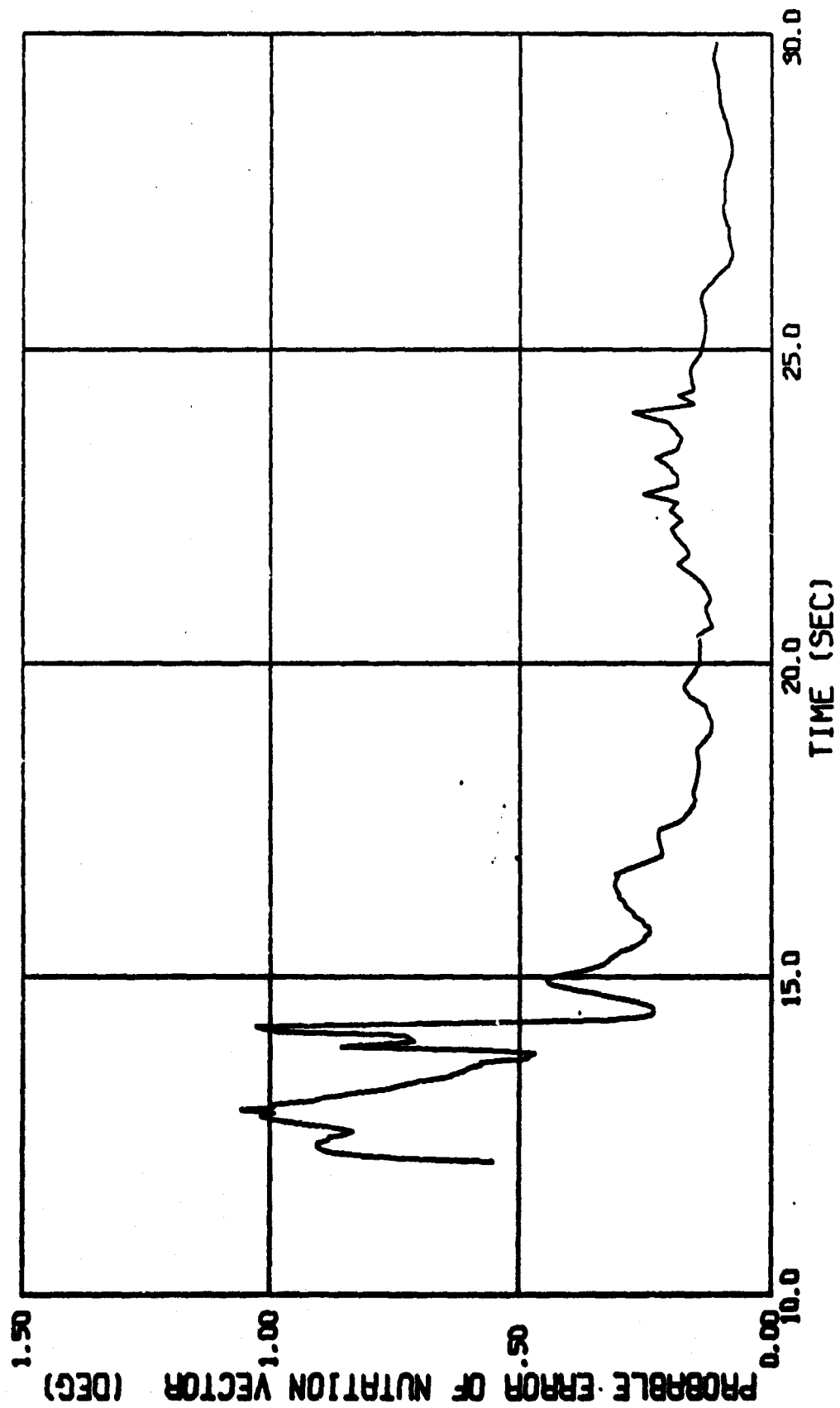


Fig. 9a PROBABLE ERROR OF NUTATION VECTOR VERSUS TIME FROM RELEASE FOR SPLIT-SKIRT BOMB (739)

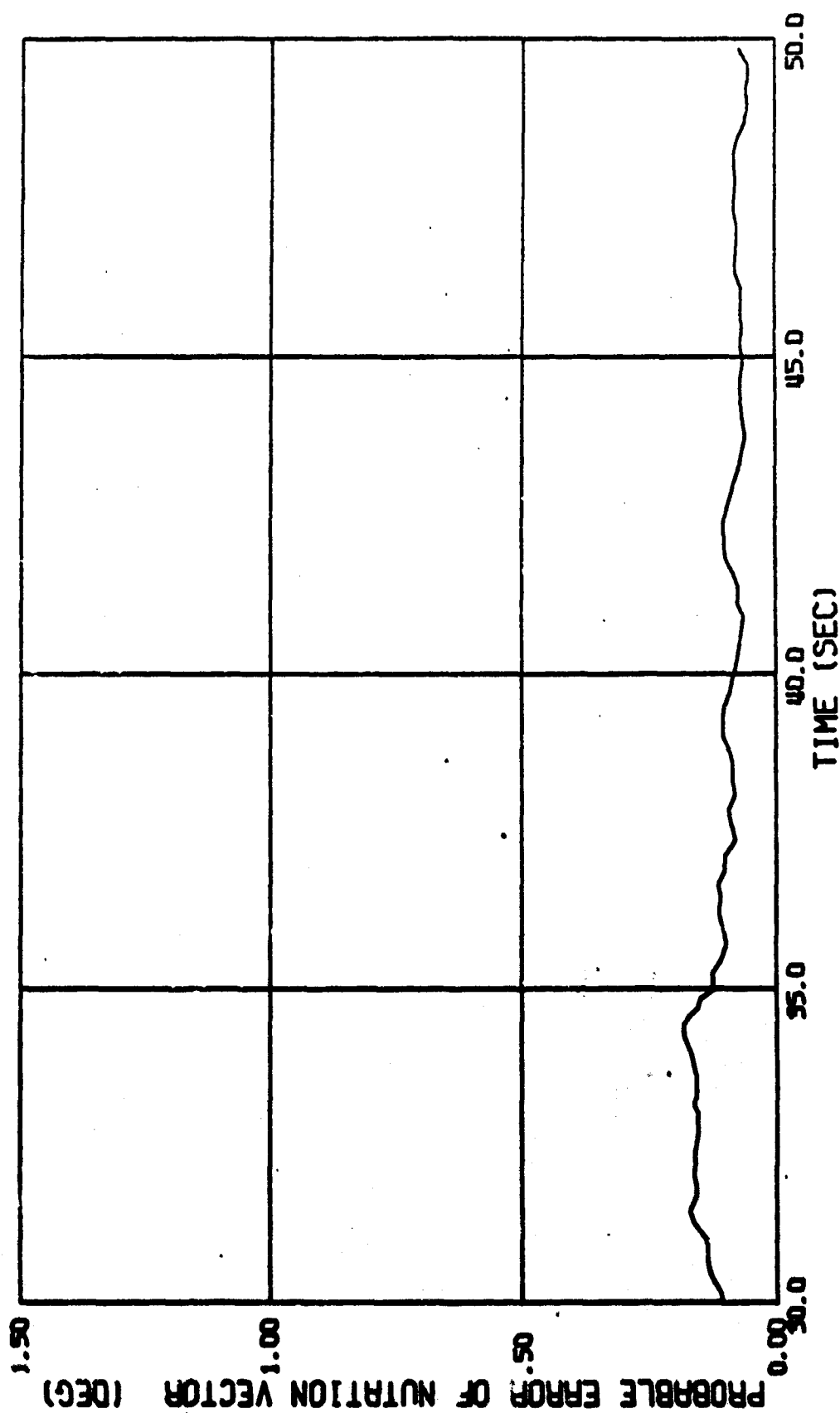


Fig. 9b PROBABLE ERROR OF NUTATION VECTOR VERSUS TIME FROM RELEASE FOR SPLIT-SKIRT BOMB (739)

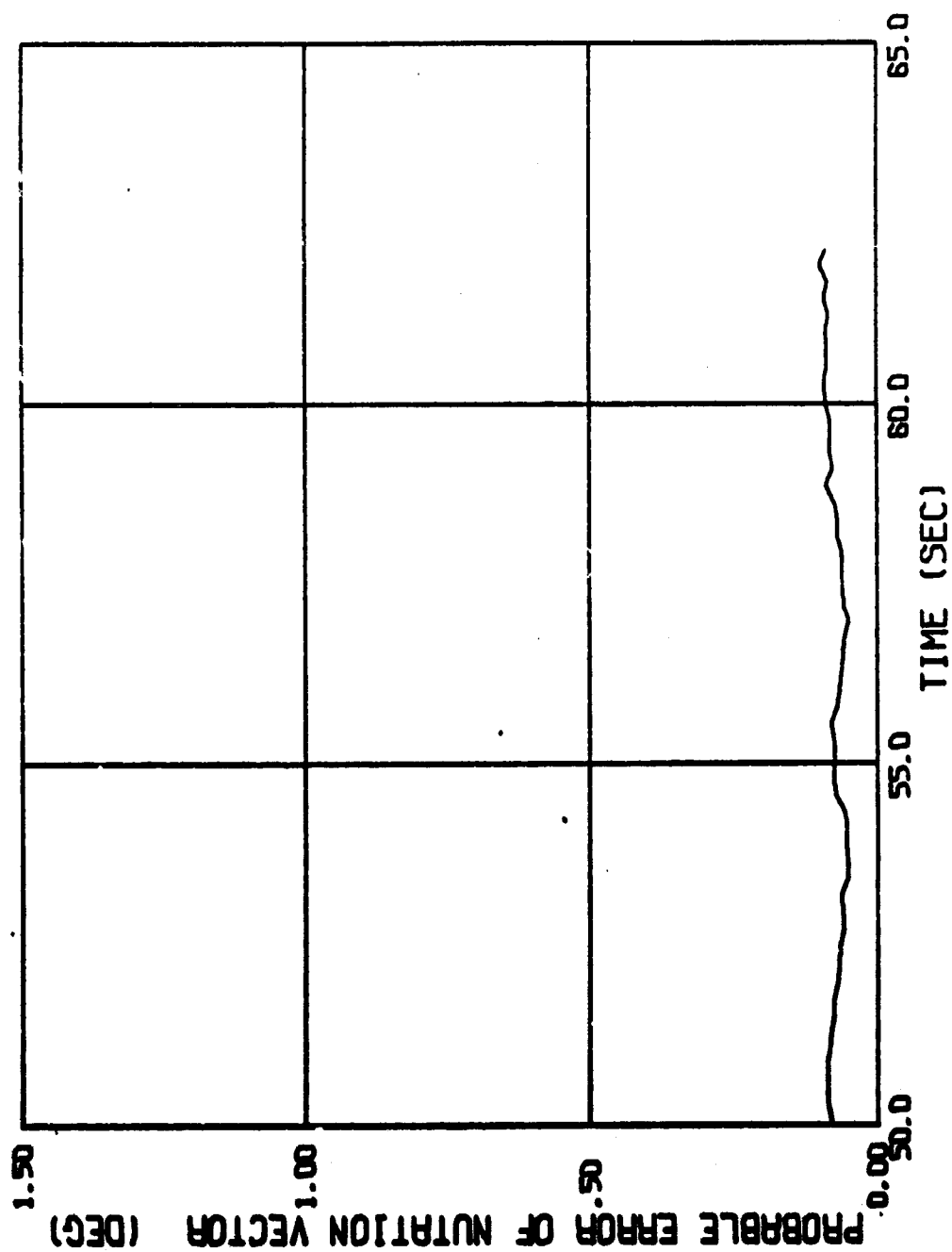


Fig. 9c PROBABLE ERROR OF NUTATION VECTOR VERSUS TIME
FROM RELEASE FOR SPLIT-SKIRT BOMB (739)

data, as discussed in the Preliminary Analysis.

The nutation frequency, in body axes, and its probable error are presented as a function of time from release in Figs. 10 and 11. Fig. 10 shows an approximately linear increase in ω_{nb} from 0.6 rad/sec at 14.7 seconds to 16.3 rad/sec at 57 seconds, at which time it remains constant until 61 seconds when a slight decrease is observed. The results of Fig. 11 indicate an extremely accurate fit. This was expected, however, from previous experience with the fitting procedure which indicated that, in general, the vector frequencies were the most accurately determined parameters. Fig. 11 shows a range of probable errors from .007 rad/sec to 0.075 rad/sec. In this case, however, the maximum probable error did not occur when the frequency was the largest. On the contrary, the frequency was changing sign at this time. From Eq. (16) it is obvious that at this time the aeroballistic nutation frequency is equal to the rolling velocity, i.e., the bomb is at resonance. This is in complete agreement with the observations made in the Preliminary Analysis.

The largest probable error occurring at the time of zero body nutation frequency is felt to be of considerable importance. In the fitting procedure, the number of points to be fitted per section is determined from a calculation involving division by the nutation frequency. Hence, if the angular data is in body axes, the number of points to be fitted at resonance will go to infinity. In order to avoid this, a slight alteration was made in the fitting routine: the number of points to be fitted was held constant when the magnitude of the nutation frequency was near 0 rad/sec. This alteration induced a large rate of change of ω_{nb} through resonance as shown in Fig. 10a. Therefore, in this small time range, the linear theory was violated. This explains the sharp increase in probable error of fit obtained at this time, as shown in Fig. 7. Similar effects were noted in the probable errors of the stability parameters at this time.

Precession Vector and Frequency

The magnitude of the Precession Vector and its probable error are presented in Figs. 12 and 13. The magnitude ranges from 14 degrees at approximately 14 seconds to 1 degree at 24.5 seconds. At 24.5 seconds the vector decreased to such a small magnitude that it was no longer able to be extracted from the data as the Precession Vector. The larger probable error of fit at this time indicated that $|K_p|$ appeared in the residuals as error until its magnitude was negligible. The greatest error in $|K_p|$.0 .62 degree, occurred at approximately 14 seconds from release, when the magnitude of the vector was the largest. The sharp peak in the probable error at this time is felt to result directly from the violation of the linear theory as discussed previously. The error is seen to become slightly more random as the vector begins to damp out of the motion.

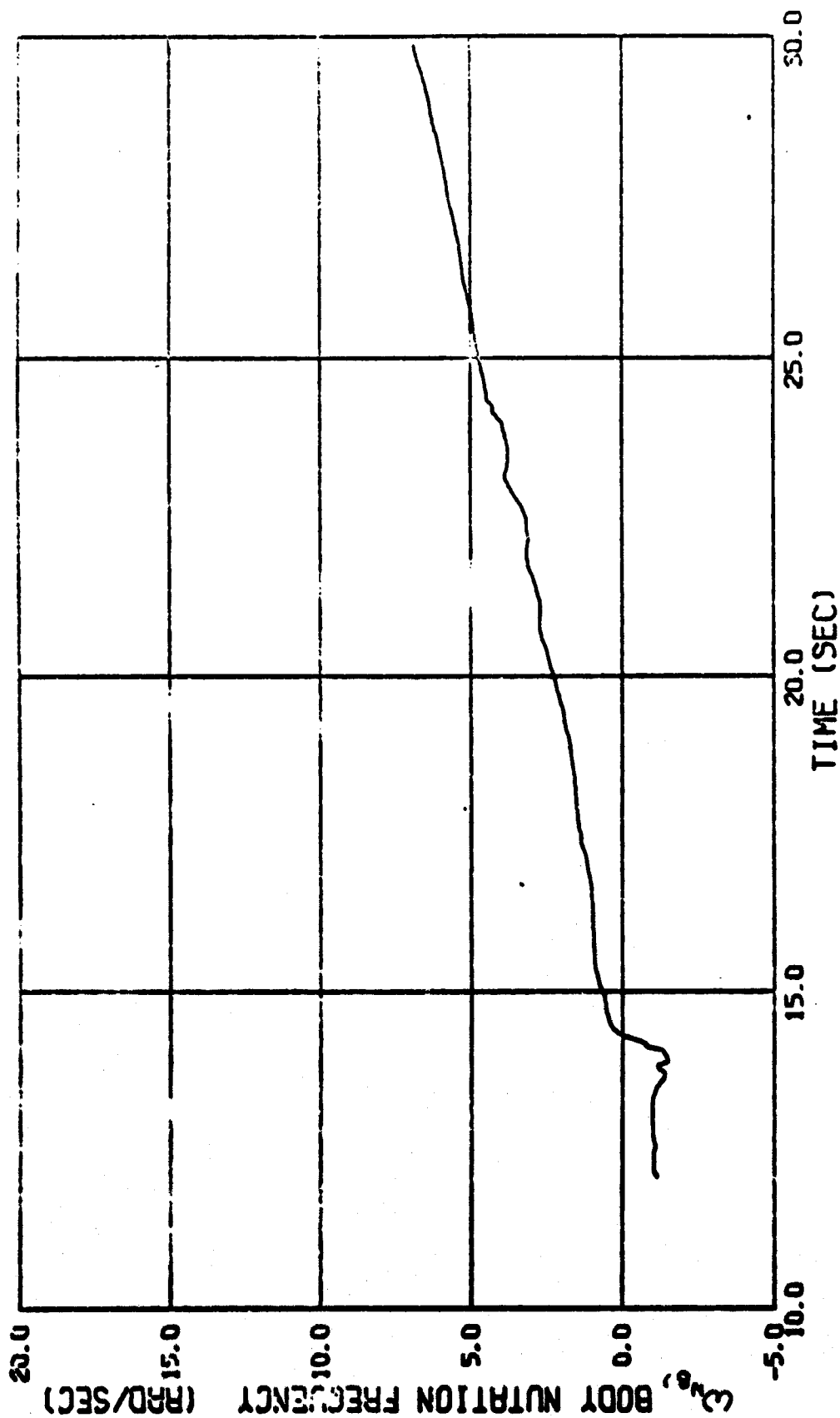


Fig. 10a BODY NUTTATION FREQUENCY VERSUS TIME FROM RELEASE FOR SPLIT-SKIRT BOMB (739)

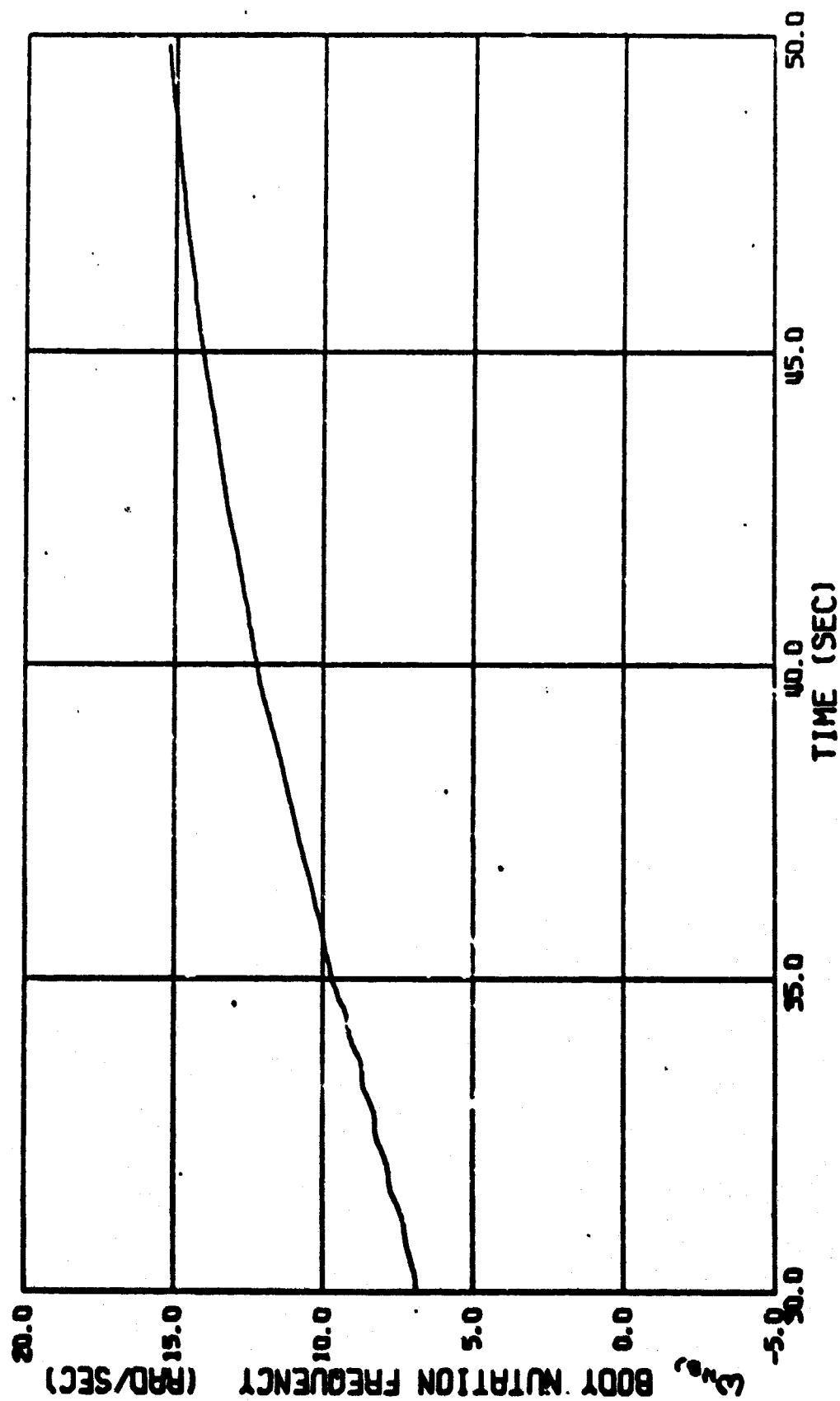


Fig. 10b BODY NUTATION FREQUENCY VERSUS TIME FROM RELEASE FOR SPLIT-SKIRT BOMB (739)

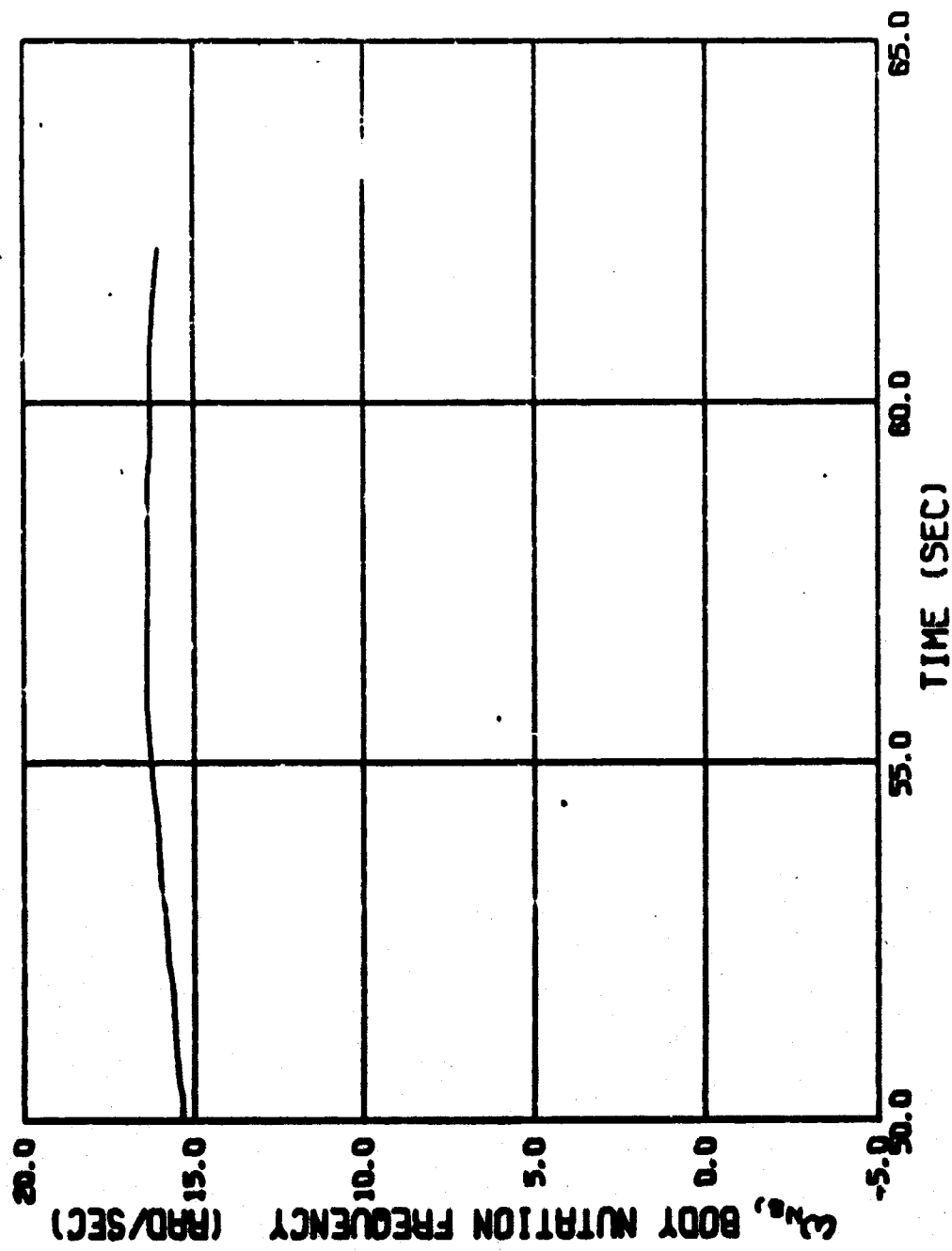


Fig. 10c BODY NUTATION FREQUENCY VERSUS TIME FROM RELEASE
FOR SPLIT-SKIRT BOMB (739)

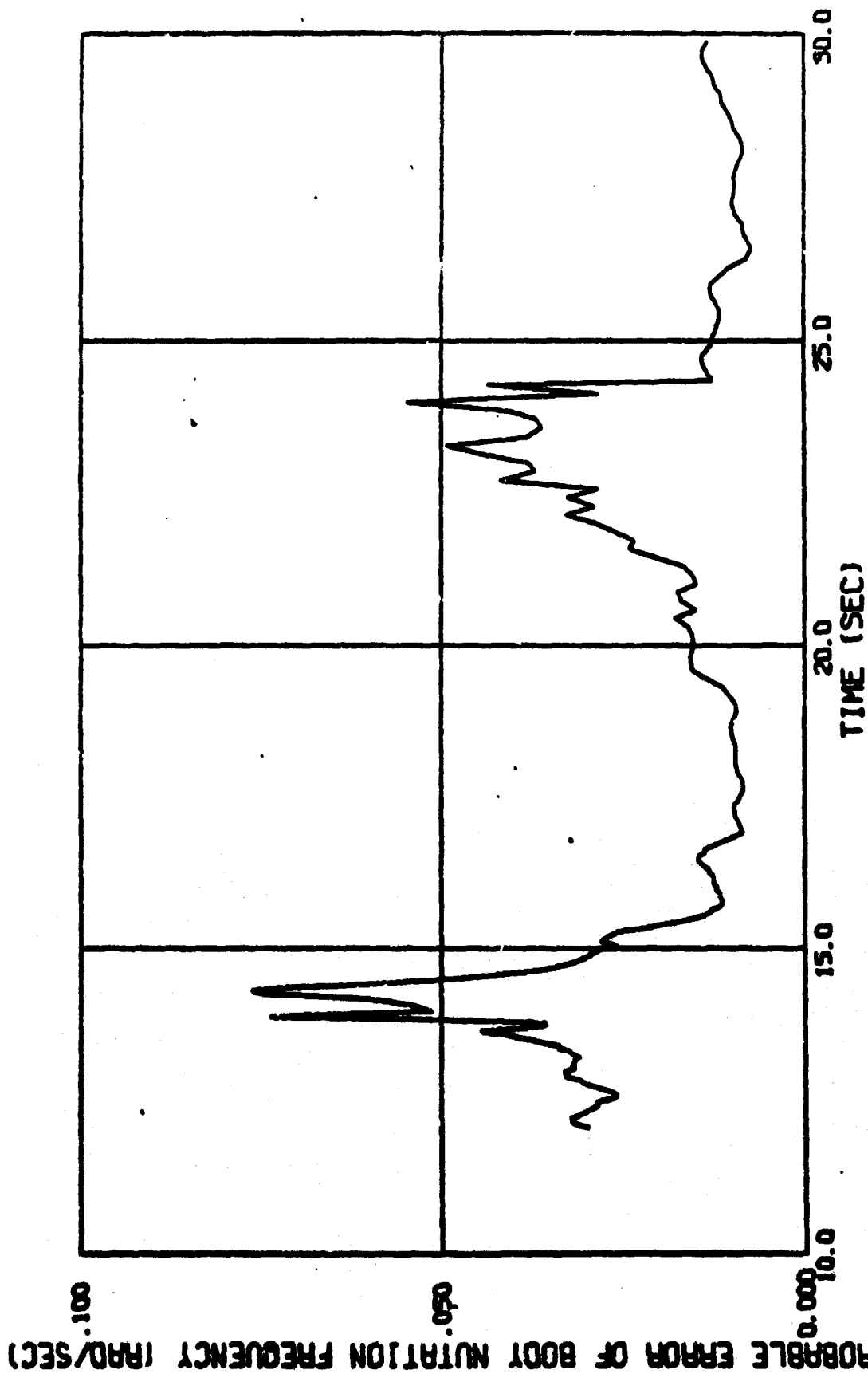


Fig. 11a PROBABLE ERROR OF BODY NUTATION FREQUENCY VERSUS TIME FROM RELEASE FOR SPLIT-SKIRT BOMB (739)

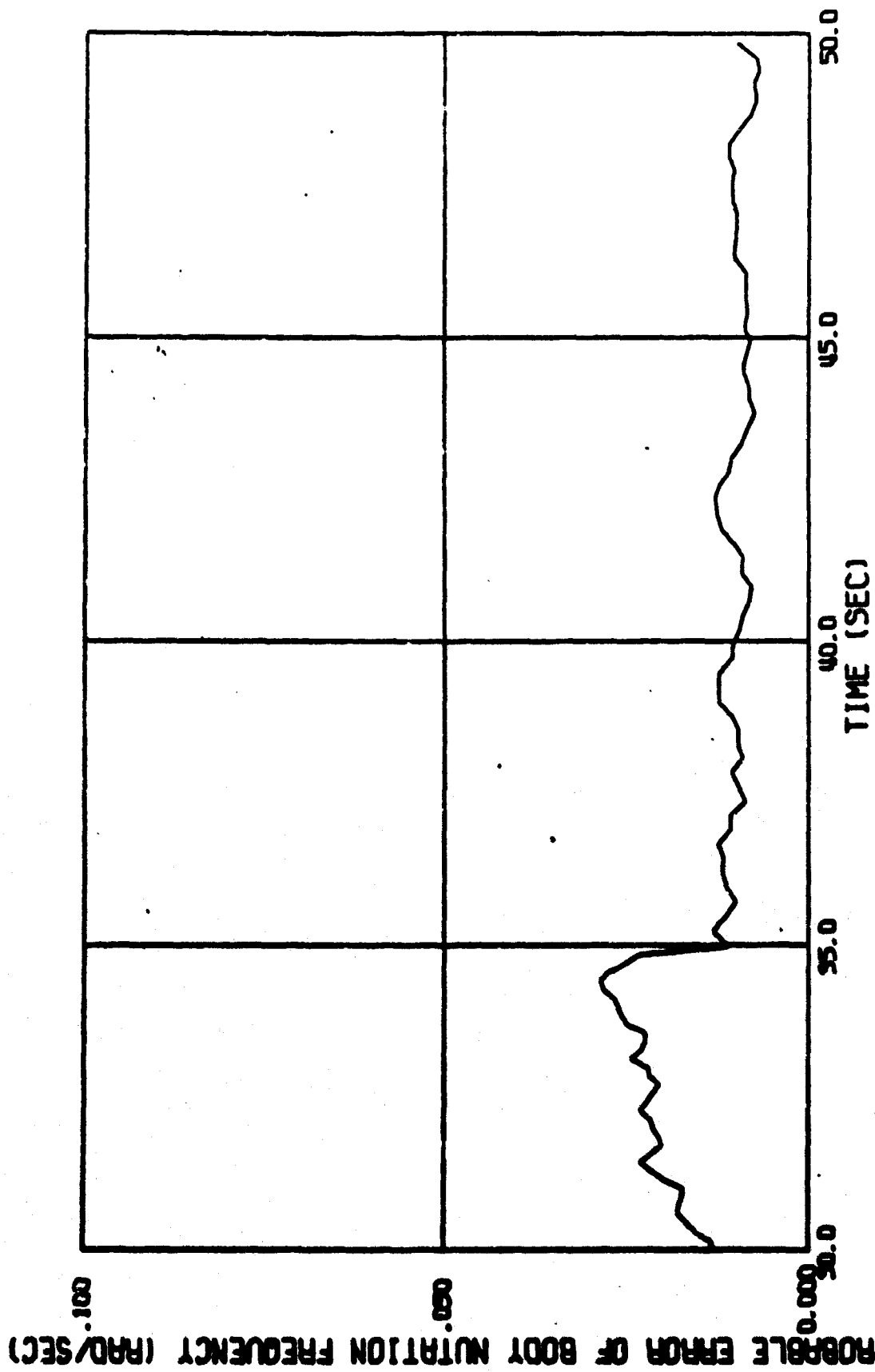


Fig. 11b PROBABLE ERROR OF BODY NUTATION FREQUENCY VERSUS TIME FROM
RELEASE FOR SPLIT-SKIRT BOMB (739)

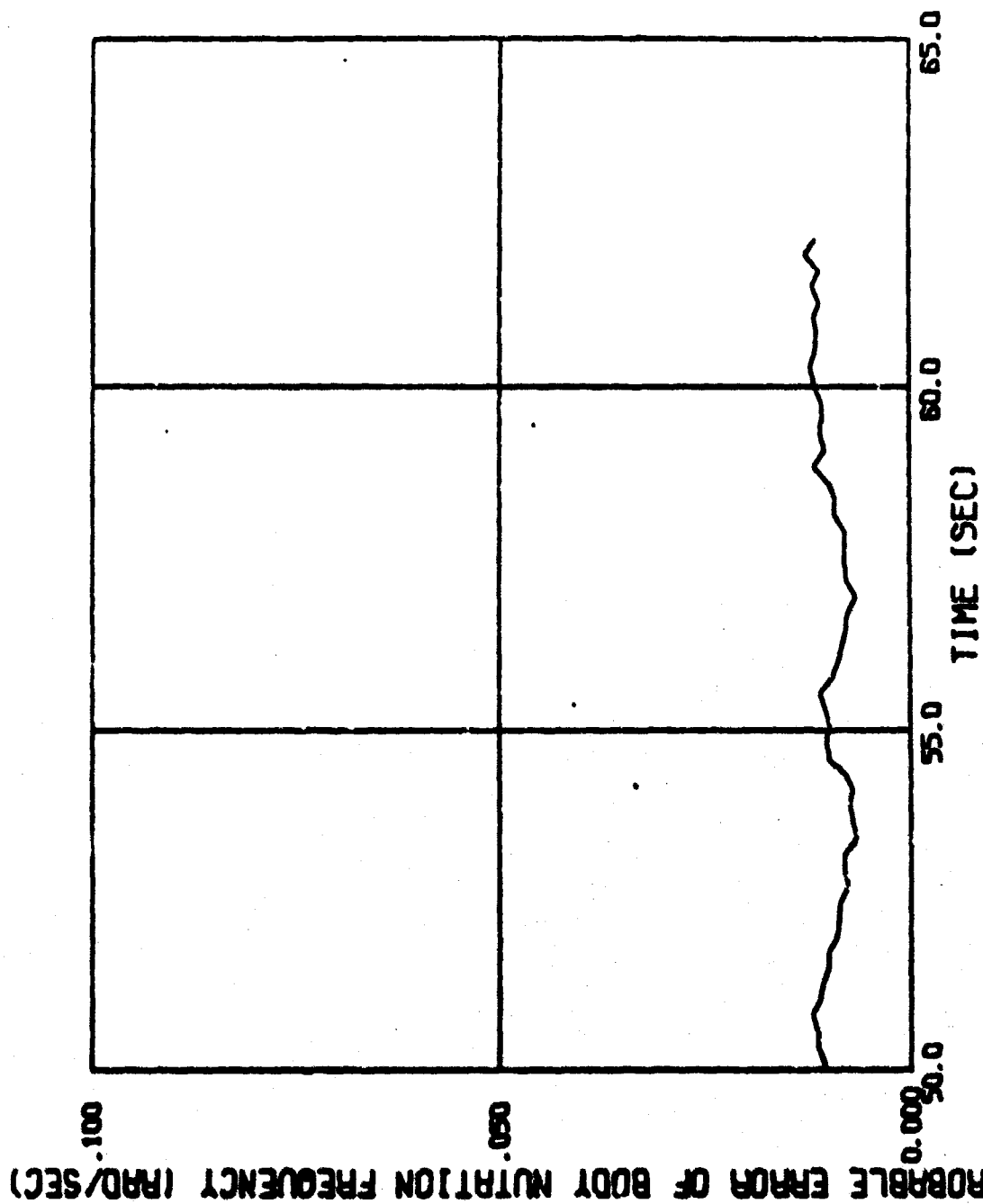


Fig. 11c PROBABLE ERROR OF BODY NUTATION FREQUENCY VERSUS
TIME FROM RELEASE FOR SPLIT-SKIRT BOMB (739)

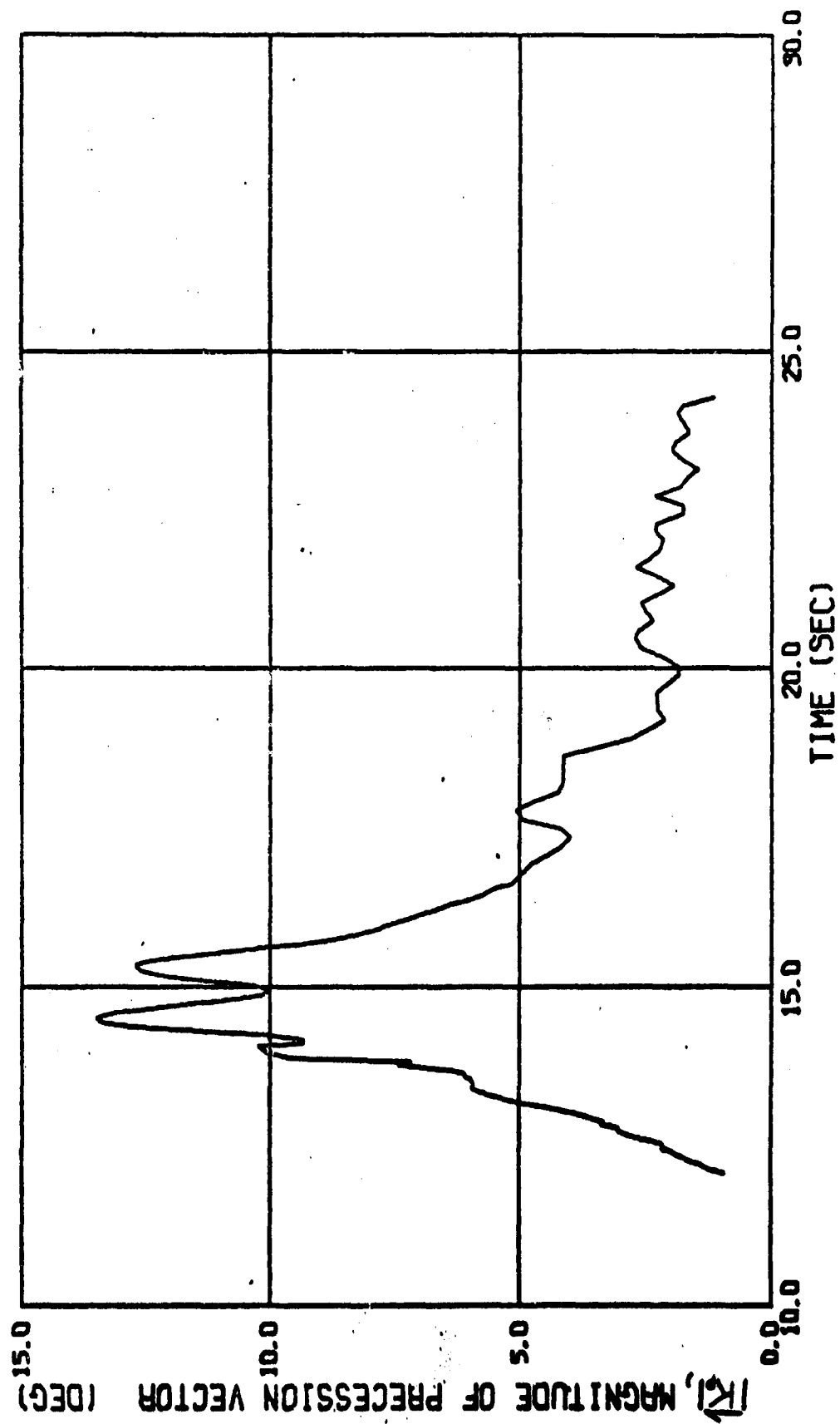


Fig. 12 MAGNITUDE OF PRECESSION VECTOR VERSUS TIME FROM RELEASE FOR SPLIT-SKIRT BOMB (739)

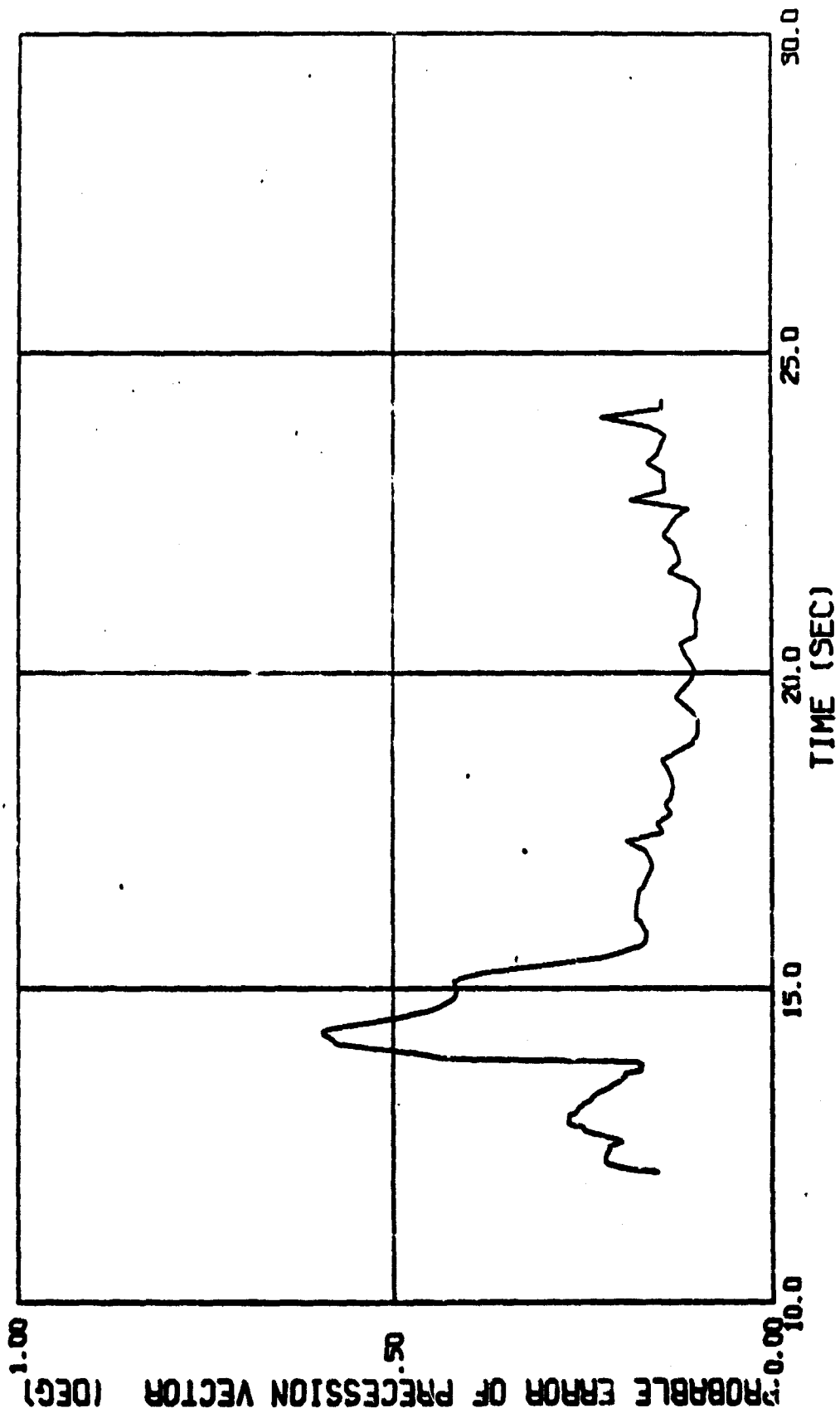


Fig. 13 PROBABLE ERROR OF PRECESSION VECTOR VERSUS TIME FROM RELEASE FOR
SPLIT-SKIRT ECMB (739)

As presented in Fig. 14, the body precession frequency varies slightly throughout the section fitted, ranging from 6 rad/sec at 12.05 seconds to 11 rad/sec at 24.5 seconds. The probable error, shown in Fig. 15, increases from 0.03 rad/sec at 13 seconds to 0.25 rad/sec at 24.5 seconds. The slight increase observed as the fit approaches its termination at 12.05 seconds is felt to be due to the effect of release disturbance. The increase in probable error beginning at approximately 22 seconds results from the fact that the Precession Vector is in the process of damping out at this time. The effects are seen in the slight variations of ω_{p8} in Fig. 14.

Trim Vector

The Trim Vector, shown in Fig. 16, is seen to reach its maximum value, 21 degrees, at approximately 14.2 seconds, the resonant condition, as expected from the analysis of the body nutation frequency, Fig. 10. The probable error, presented in Fig. 17, indicates an extremely good fit even though the magnitude of the Trim Vector is very nearly zero degrees during the last 37 seconds out of the flight. Again, the maximum probable error occurs when the magnitude of the vector is also a maximum. As in the case of the Precession Vector, the sharp increase in the probable error occurs when the linear theory was violated.

At approximately 24 seconds from release, when the complex motion begins to assume a circular nature, the Trim Vector is almost negligible. This, combined with the magnitude of the Nutation Vector and the loss of the Precession Vector, completely explains the concentric circular motion about an almost zero degree trim observed in the complex plane. A comparison of the magnitude of the Nutation, Precession, and Trim Vectors at resonance indicate that the major cause of the large angle of attack observed is the amplification of the Trim Vector. Fig. 18 shows $|R_T|$ as a function of the ratio of the roll rate to the aeroballistic nutation frequency. The Trim Vector is seen to reach maximum amplitude at the point where the ratio is 1.

Nutation and Precession Dynamic Damping Factors

As anticipated in the Preliminary Analysis, the oscillations in the angular orientation data had an undesirable effect on the determination of the dynamic damping factors. This effect was predominant when the magnitude of the complex angle of attack was not larger than approximately 1° degrees. This occurred from 16.6 seconds to the end of the flight. At these times the complex motion was characterized by quasi-circular and circular motion. That is, from 16.6 seconds to 24.5 seconds, the Precession Vector was in the process of damping out, and from this time until the end of the flight the motion was characteristically nutational. Up to 16.6 seconds, however, the magnitude of the angle of attack was either extremely large,

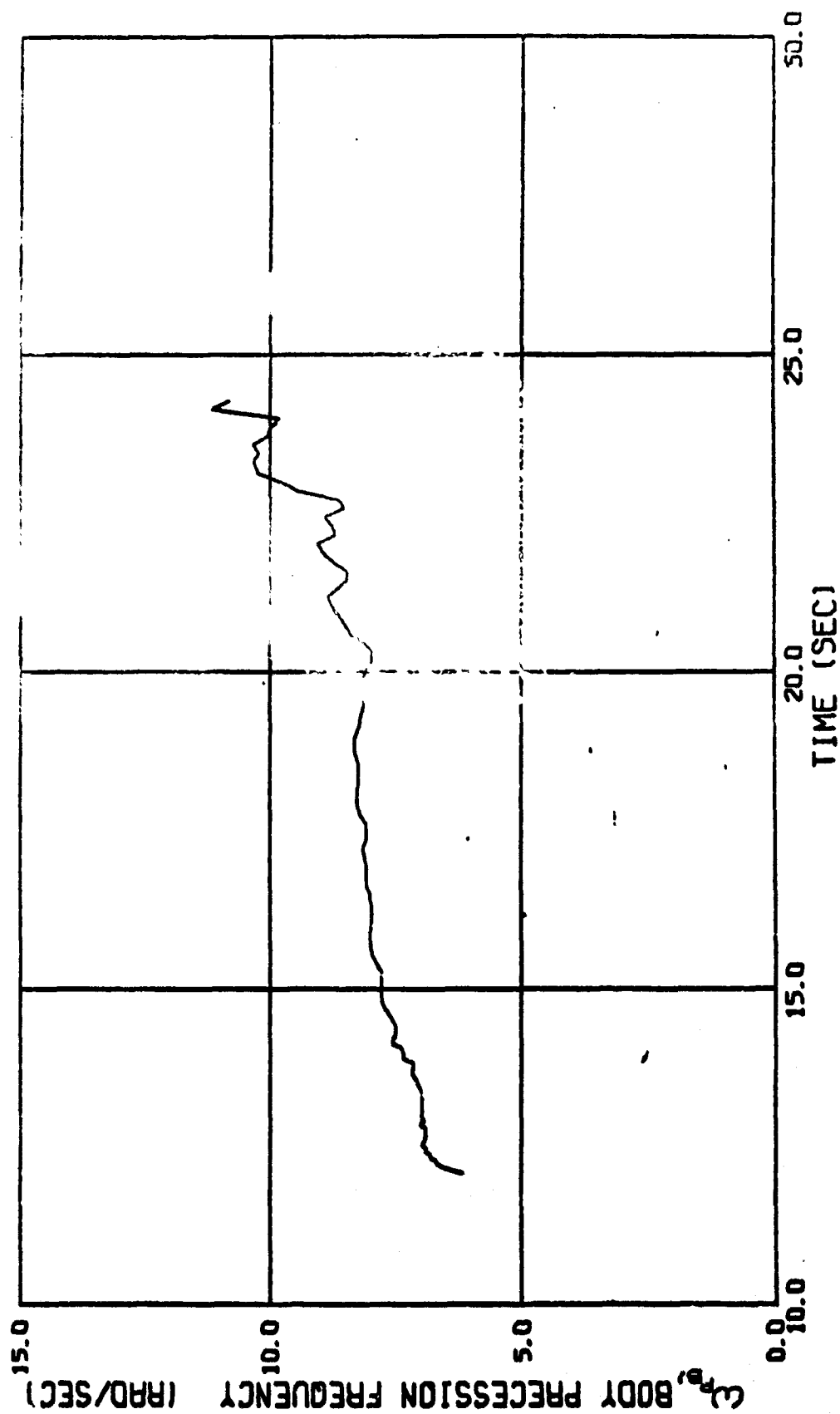


Fig. 14 BODY PRECESSION FREQUENCY VERSUS TIME FROM RELEASE FOR SPLIT-SKIRT BOMB (739)

PROBABLE ERROR OF BODY PRECESSION FREQUENCY (RAD/SEC)

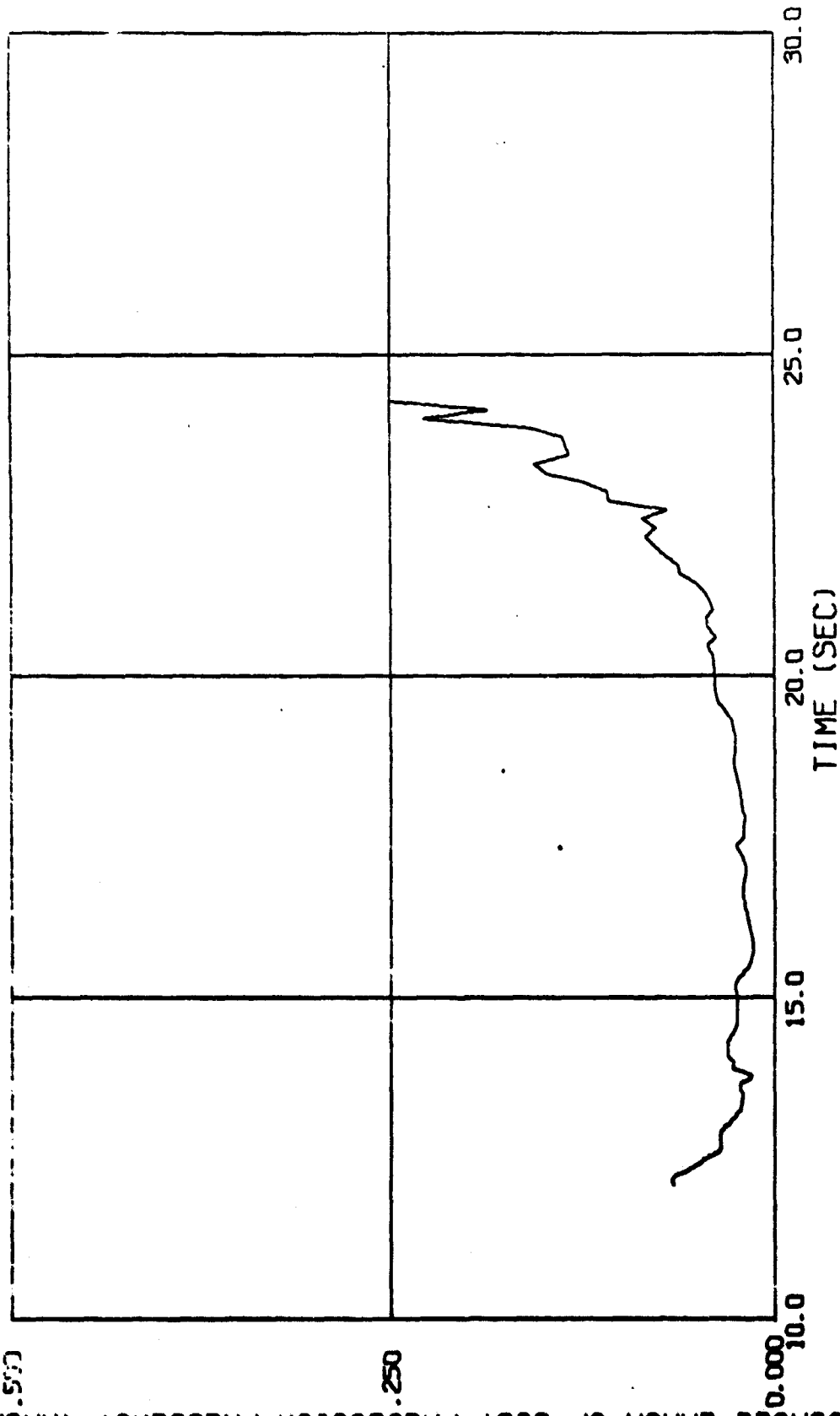


Fig. 15 PROBABLE ERROR OF BODY PRECESSION FREQUENCY VERSUS TIME FROM RELEASE FOR SPLIT-SKIRT BOMB (739)

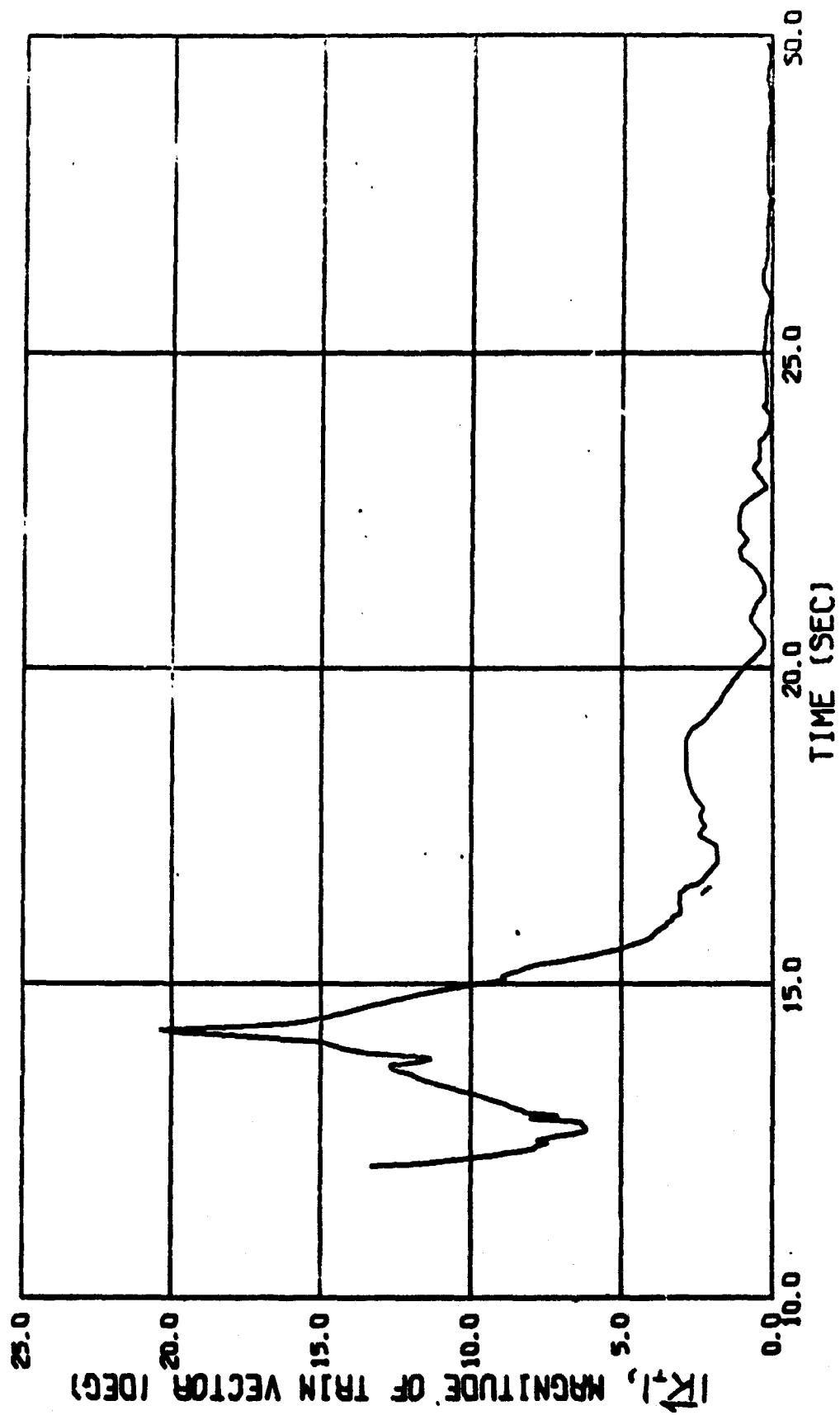


Fig. 16a MAGNITUDE OF TRIM VECTOR VERSUS TIME FROM RELEASE FOR SPLIT-SKIRT BOMB (739)

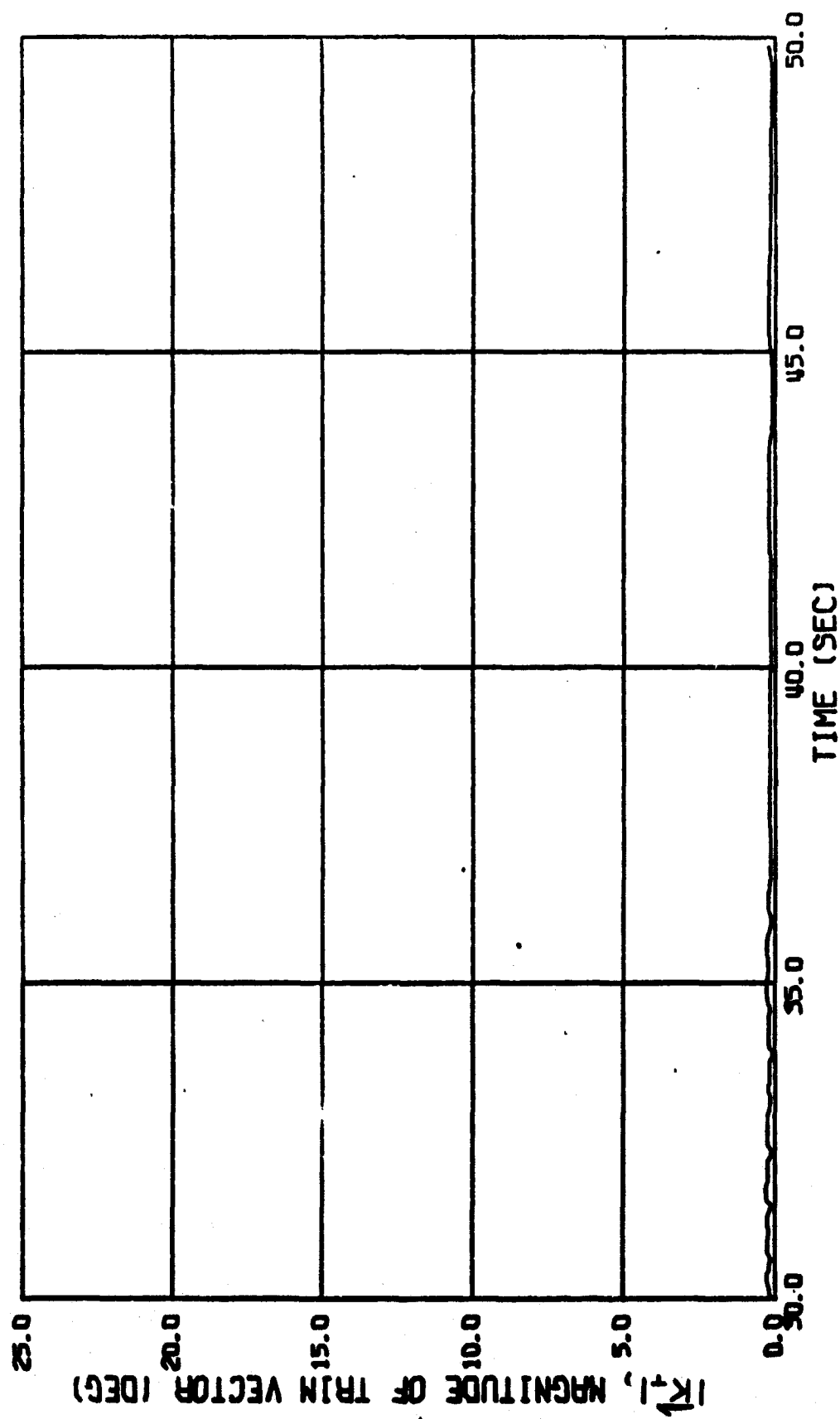


Fig. 16b MAGNITUDE OF TRIM VECTOR VERSUS TIME FROM RELEASE FOR SPLIT-SKIRT BOMB (739)

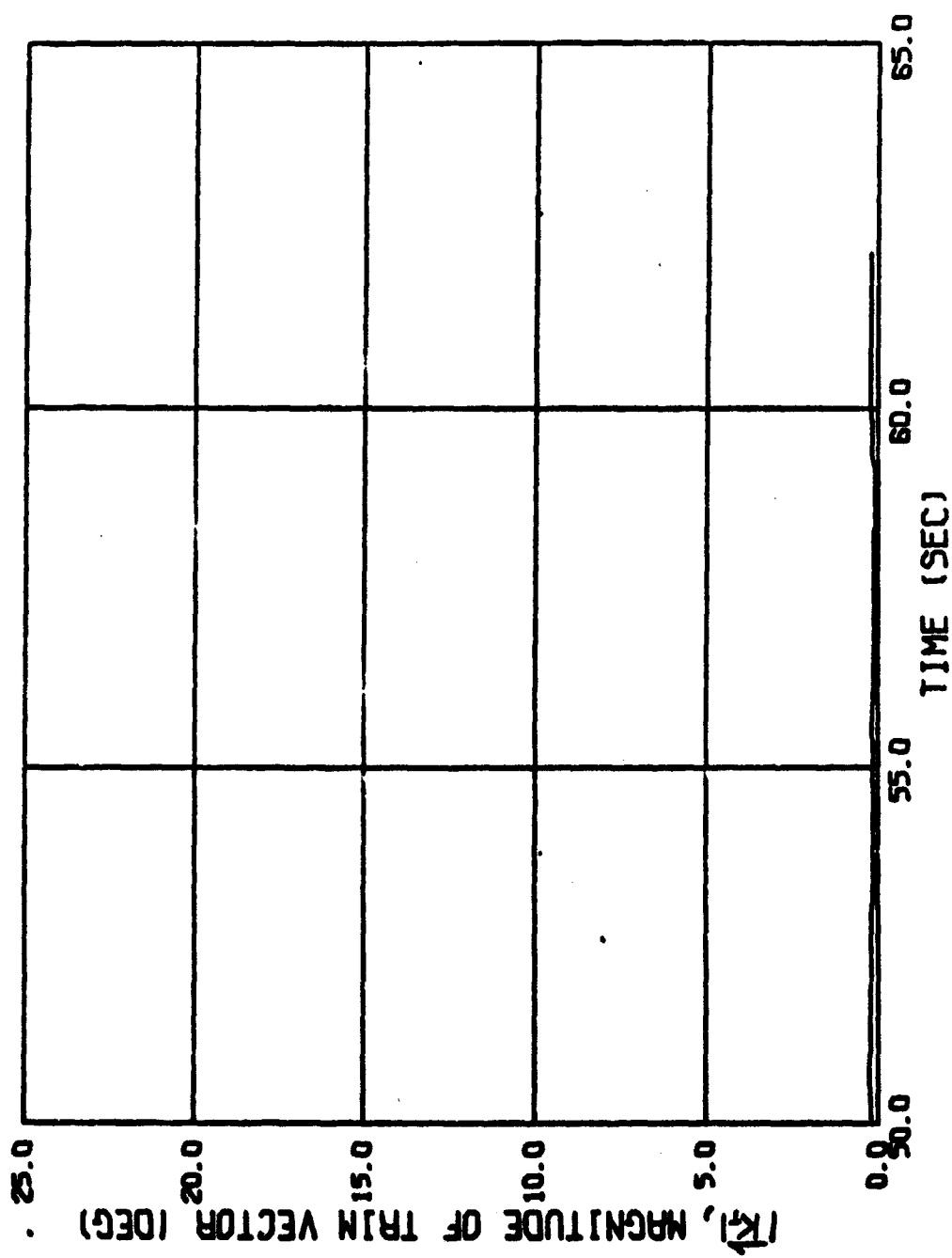


Fig. 16c MAGNITUDE OF TRIM VECTOR VERSUS TIME FROM
RELEASE FOR SPLIT-SKIRT BOMB (739)

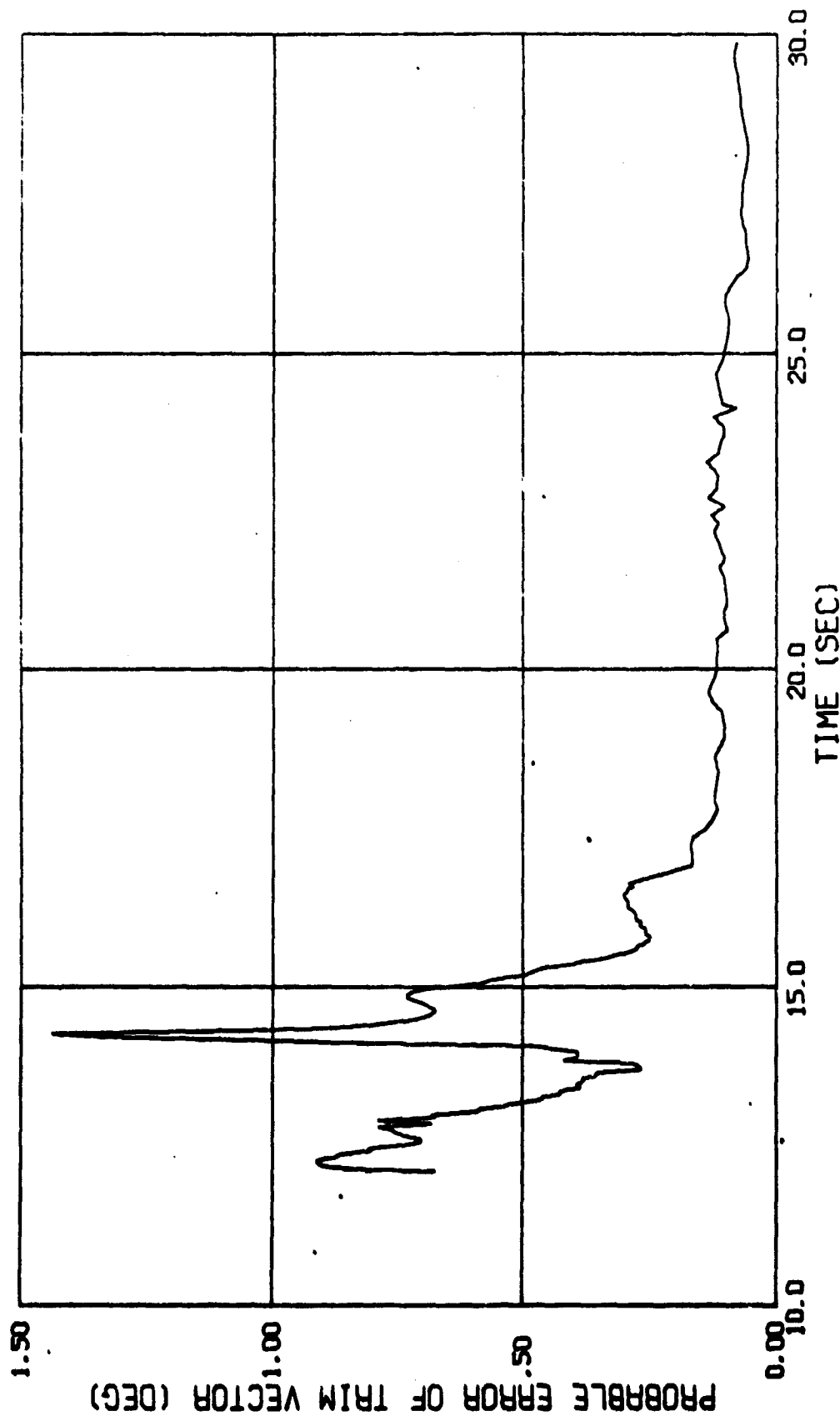


Fig. 17a PROBABLE ERROR OF TRIM VECTOR VERSUS TIME FROM RELEASE FOR SPLIT-SKIRT BOMB (739)

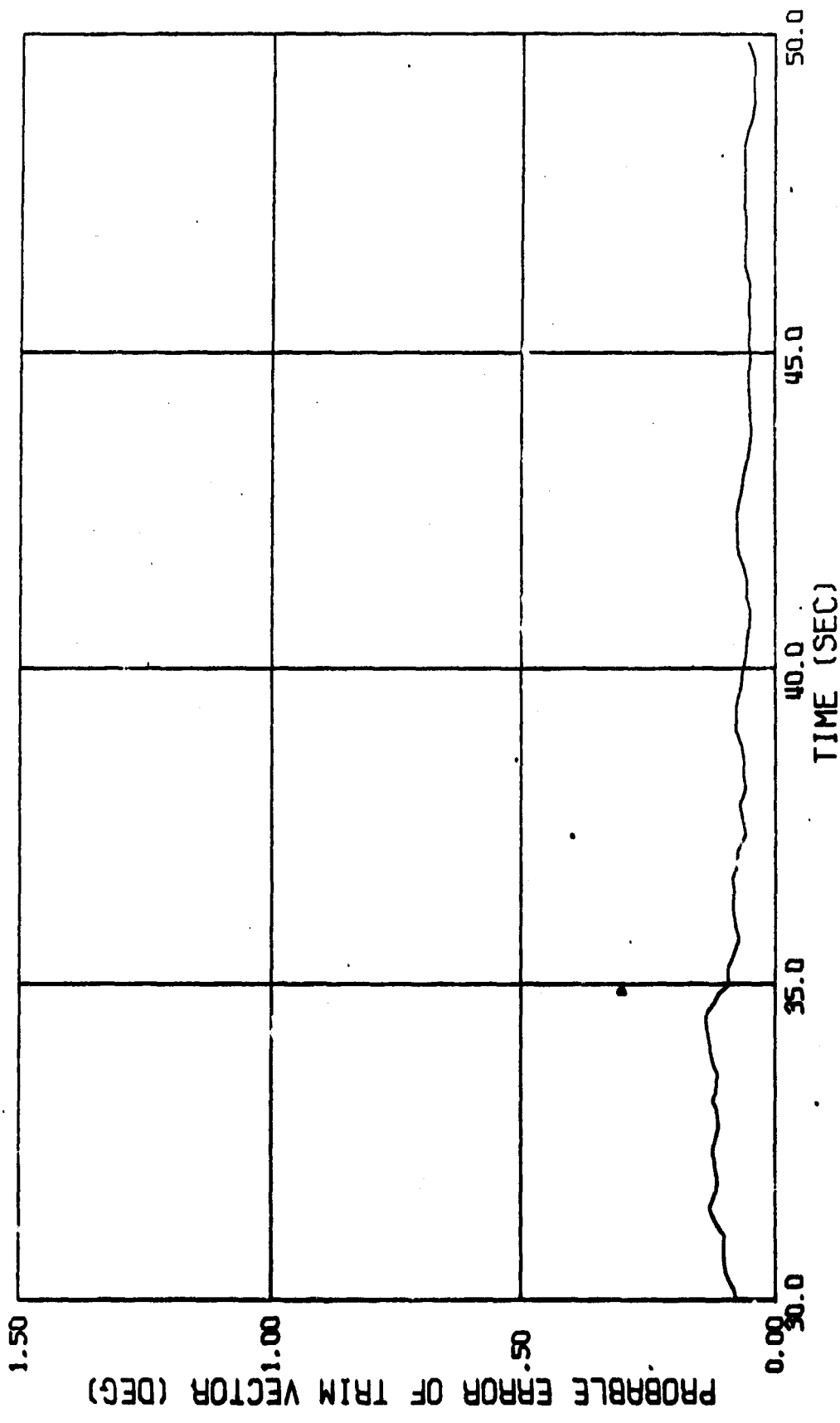


Fig. 17b PROBABLE ERROR OF TRIM VECTOR VERSUS TIME FROM RELEASE FOR SPLIT-SKIRT BOMB (739)

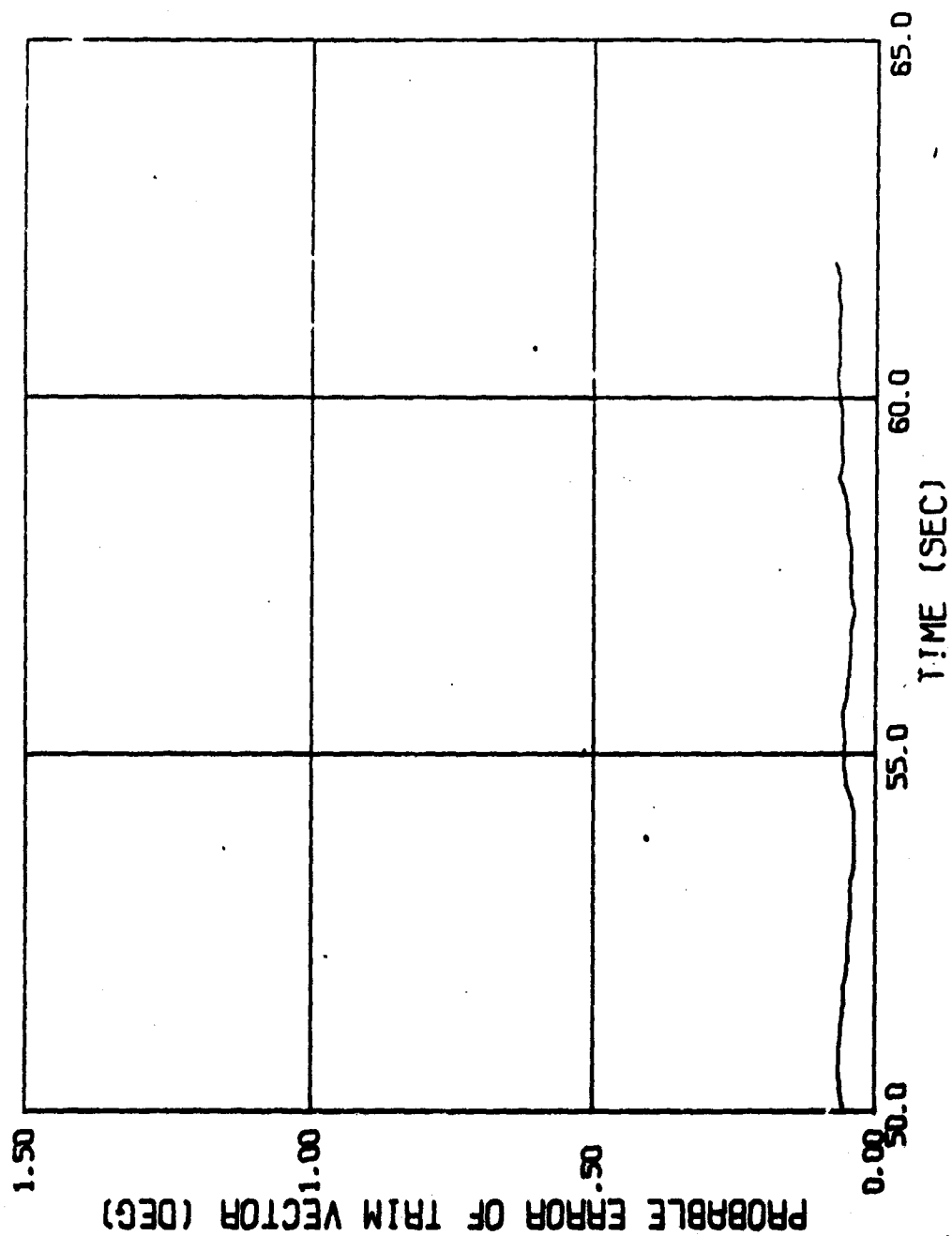


Fig. 17c PROBABLE ERROR OF TRIM VECTOR VERSUS TIME FROM
RELEASE FOR SPLIT-SKIP BOMB (739)

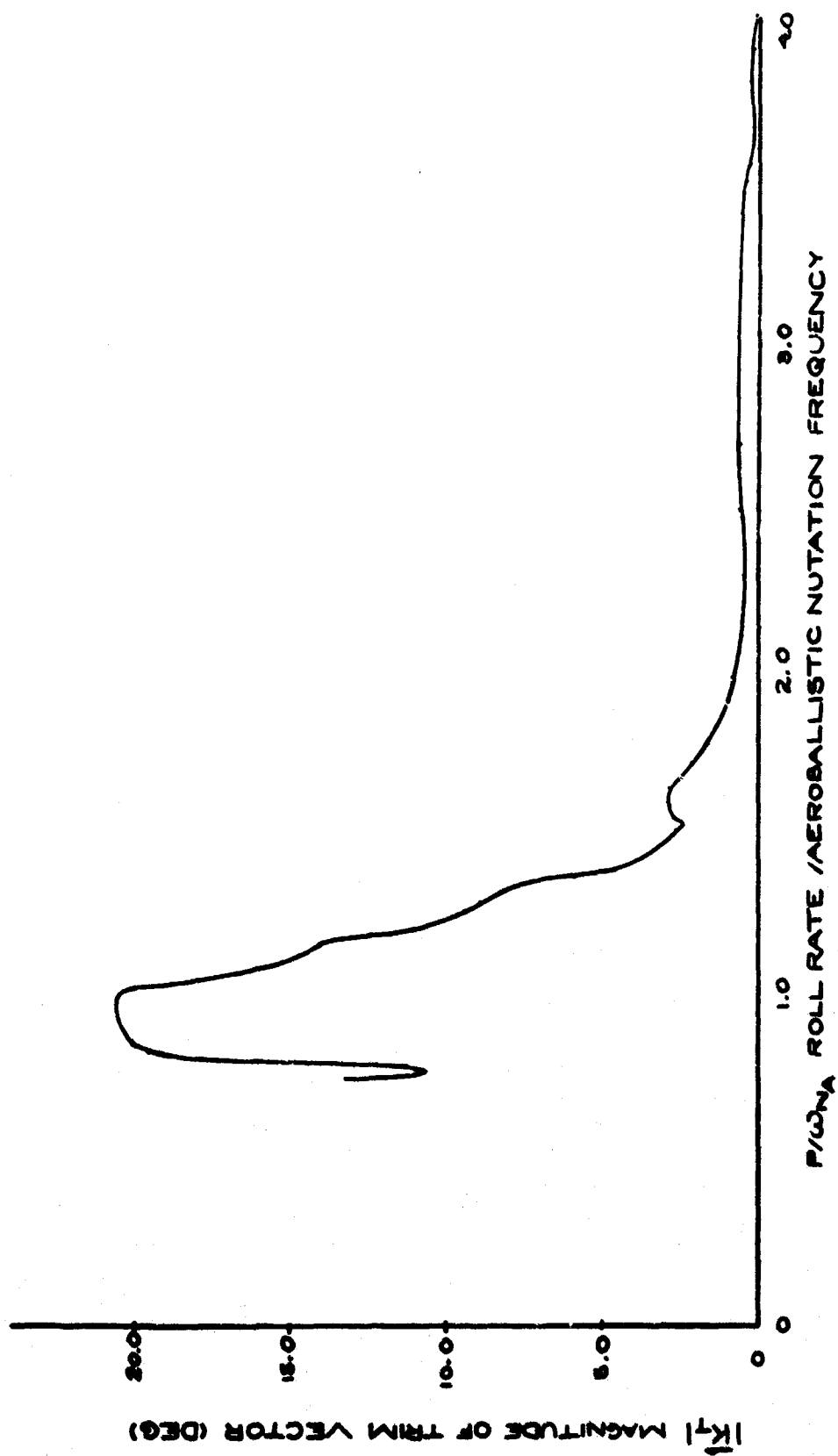


FIG. 18 MAGNITUDE OF TRIM VECTOR
VERSUS FREQUENCY RATIO
FOR SPLIT-SKIRT BOMB (739)

or was changing so rapidly that the oscillations were concealed. Furthermore, the times at which the oscillations played an important role in the determination of the dynamic damping factors were characterized by either a very small value in the nutational mode or the termination of the vector in the precessional mode. Thus, since the dynamic damping factors play an important role in the determination of the aerodynamic coefficients, considerable care was employed in evaluating the results.

Fig. 19 shows the Nutation Vector dynamic damping factor as a function of time from release. As is evident from this figure, the oscillations appear at 16.6 seconds and remain until the end of the flight. Up to 16.6 seconds, however, the values of λ_n are well determined. In order to obtain meaningful results from any calculations involving λ_n from 16.6 seconds to the end of the flight, the oscillations had to be removed. Since the scatter shown in Fig. 19 is small, it was felt that the general trend of λ_n was truly represented. Hence a curve was smoothed through the fitted values as shown in Fig. 21. The results of the fitted and smoothed values of λ_n , which were used in the determination of the aerodynamic stability derivative coefficients, are presented in Fig. 22.

As in the case of the nutational mode, the Precession Vector dynamic damping factors were well determined up to 16.6 seconds as shown in Figs. 23 and 24. After this time, however, the precessional mode began to become extremely small and eventually become indeterminate at 24.5 seconds from release. As $|R_p|$ decreased, λ_p was more difficult to determine accurately. The larger scatter of λ_p shown in Fig. 23 and the increasing probable error shown in Fig. 24 indicate that the results were not representative of the general trend of the precessional mode. Thus, to smooth the results did not appear reliable. Therefore, in order to obtain a characteristic dynamic damping factor for the precessional mode from 16.6 seconds to 24.5 seconds from release, the magnitude of the Precession Vector as a function of time from release was analyzed. $|R_p|$, too, was characterized by oscillations. Thus, in order to obtain bona fide dynamic damping factors, $|R_p|$ as a function of time from release was smoothed as shown in Fig. 25. From this smoothed curve, the natural logarithm of $|R_p|$ as a function of time from release was obtained as presented in Fig. 26. By taking the local slopes of this curve, the Precession Vector dynamic damping factor was obtained as a function of time from release from 16.6 seconds to 24.5 seconds. An explanation of this procedure is given in Appendix I. The combined results of λ_p as a function of time from release are presented in Fig. 27.

It should be noted that the interpretation of the results of the fitting procedure in the resonance region are felt to be questionable. At resonance, both the Nutation and Trim arms are fixed (in body axes), and the ability of the fitting technique to distinguish between the two is uncertain. For the purpose of this analysis, however, the resulting stability parameters were

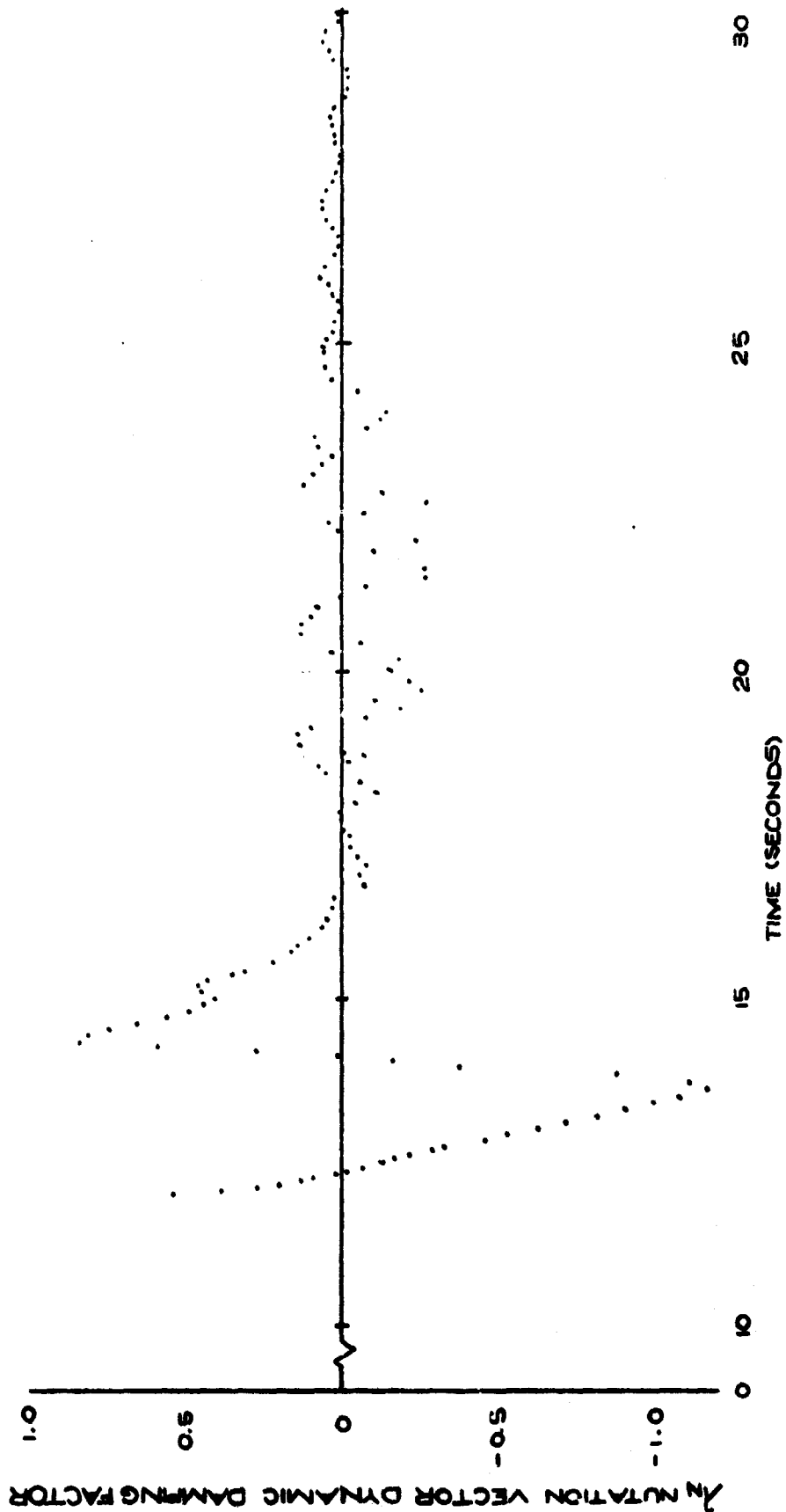


FIG. 19a NUTATION VECTOR DYNAMIC DAMPING
FACTOR VERSUS TIME FROM RELEASE
FOR SPLIT-SKIRT BOMB (739)

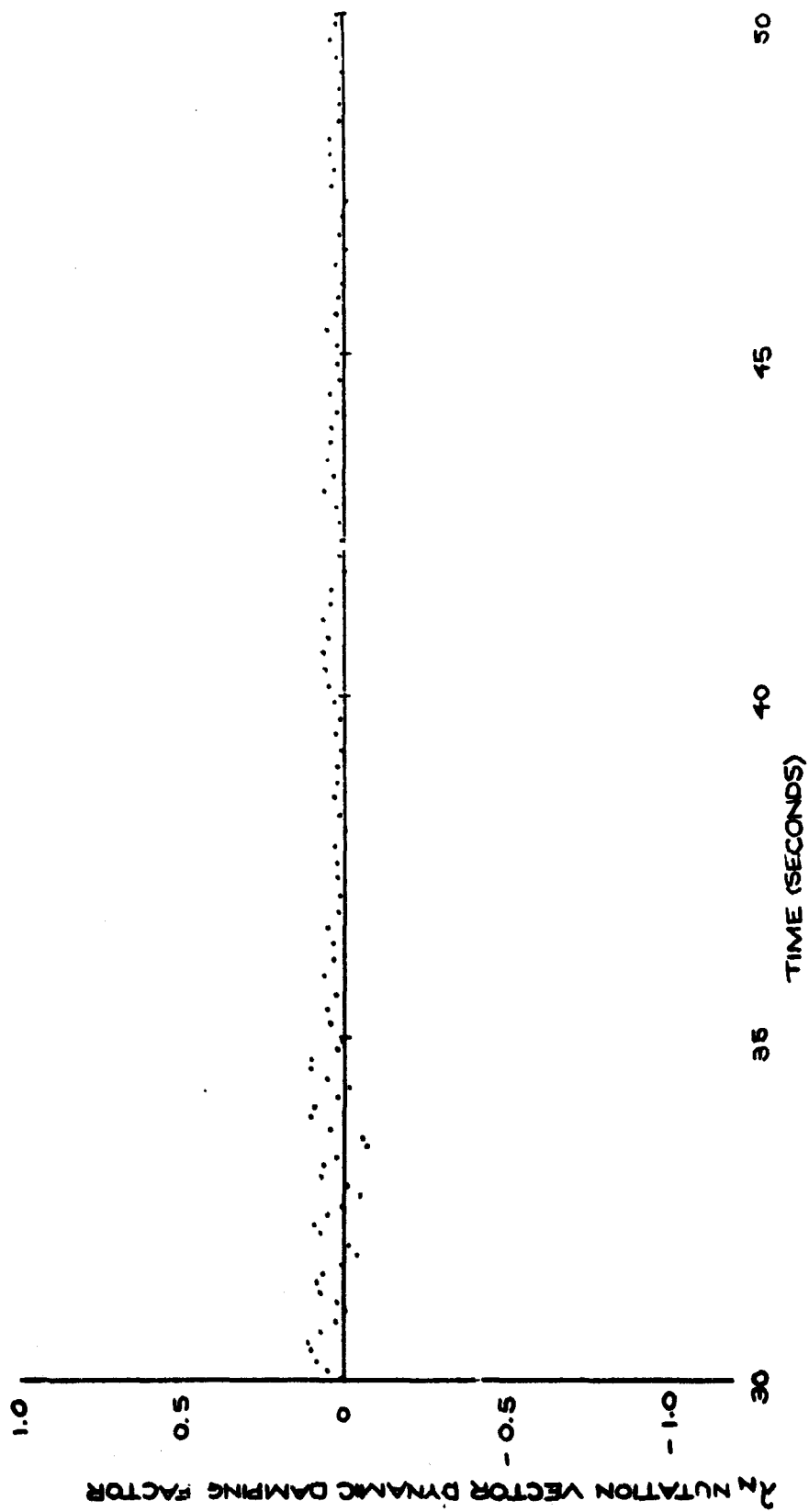


FIG.19b NUTATION VECTOR DYNAMIC DAMPING
FACTOR VERSUS TIME FROM RELEASE
FOR SPLIT-SKIRT BOMB (739)

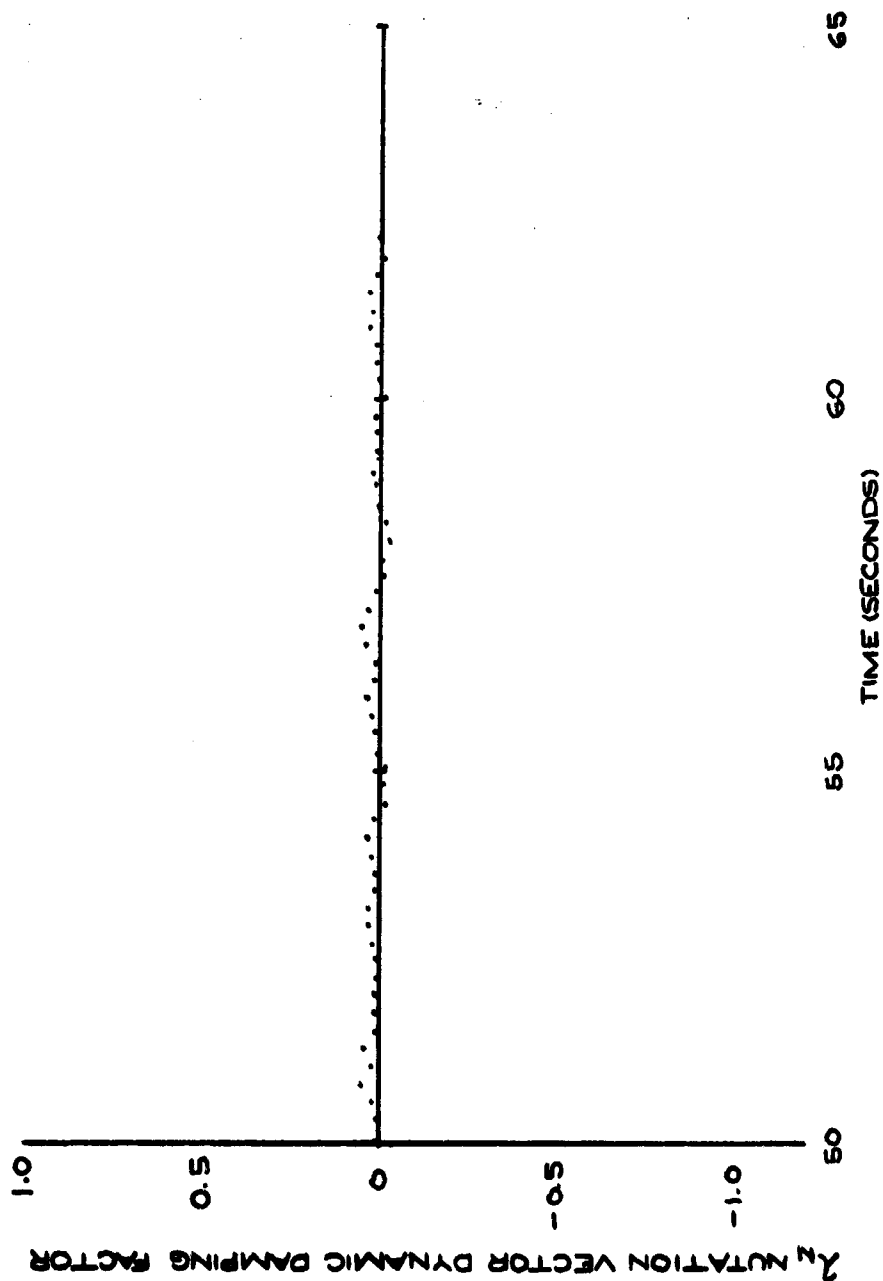


FIG.19C NUTATION VECTOR DYNAMIC DAMPING
FACTOR VERSUS TIME FROM RELEASE
FOR SPLIT-SKIRT BOMB (739)

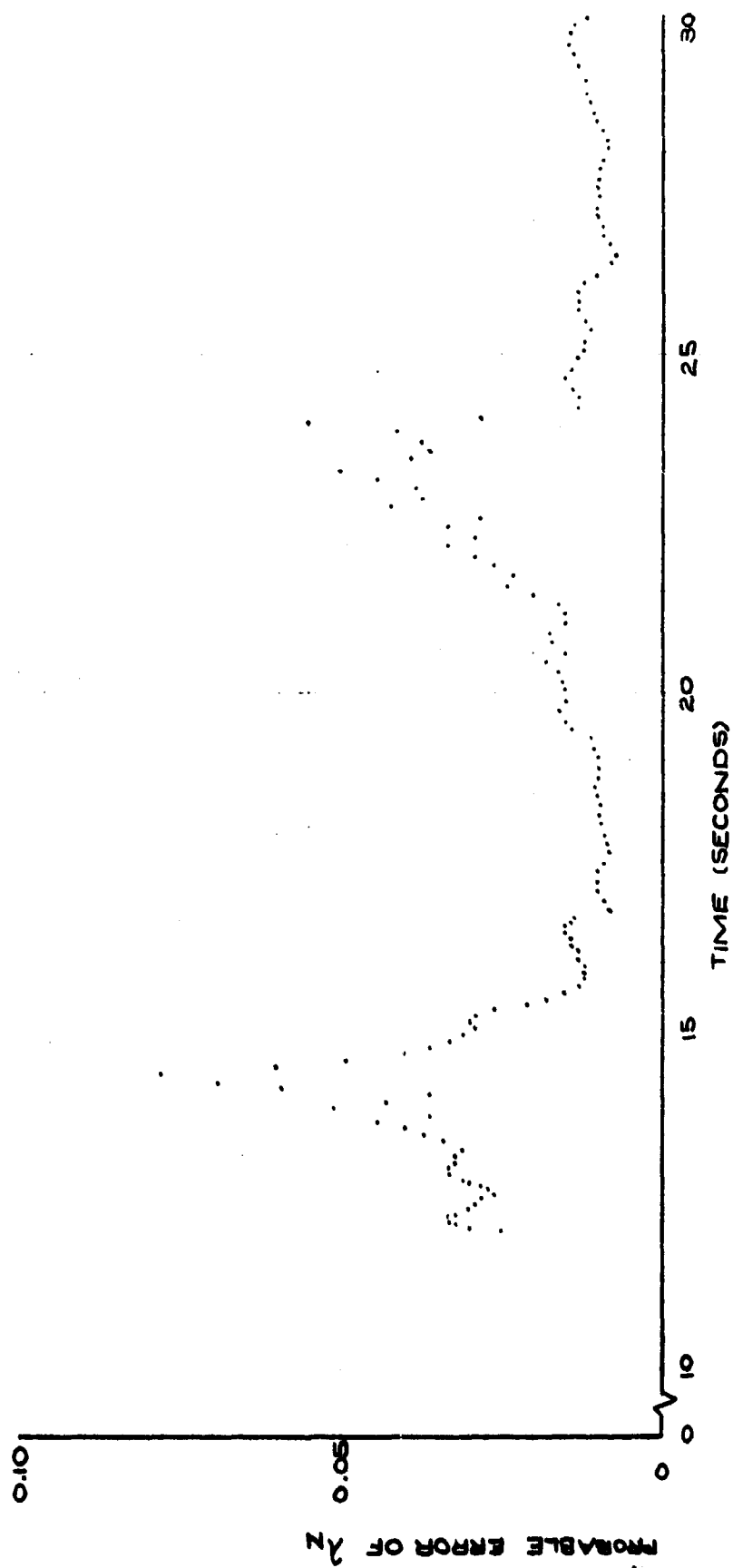


FIG. 20a PROBABLE ERROR OF NUTATION VECTOR
DYNAMIC DAMPING FACTOR VERSUS TIME
FROM RELEASE FOR SPLIT-SKIRT BOMB (739)

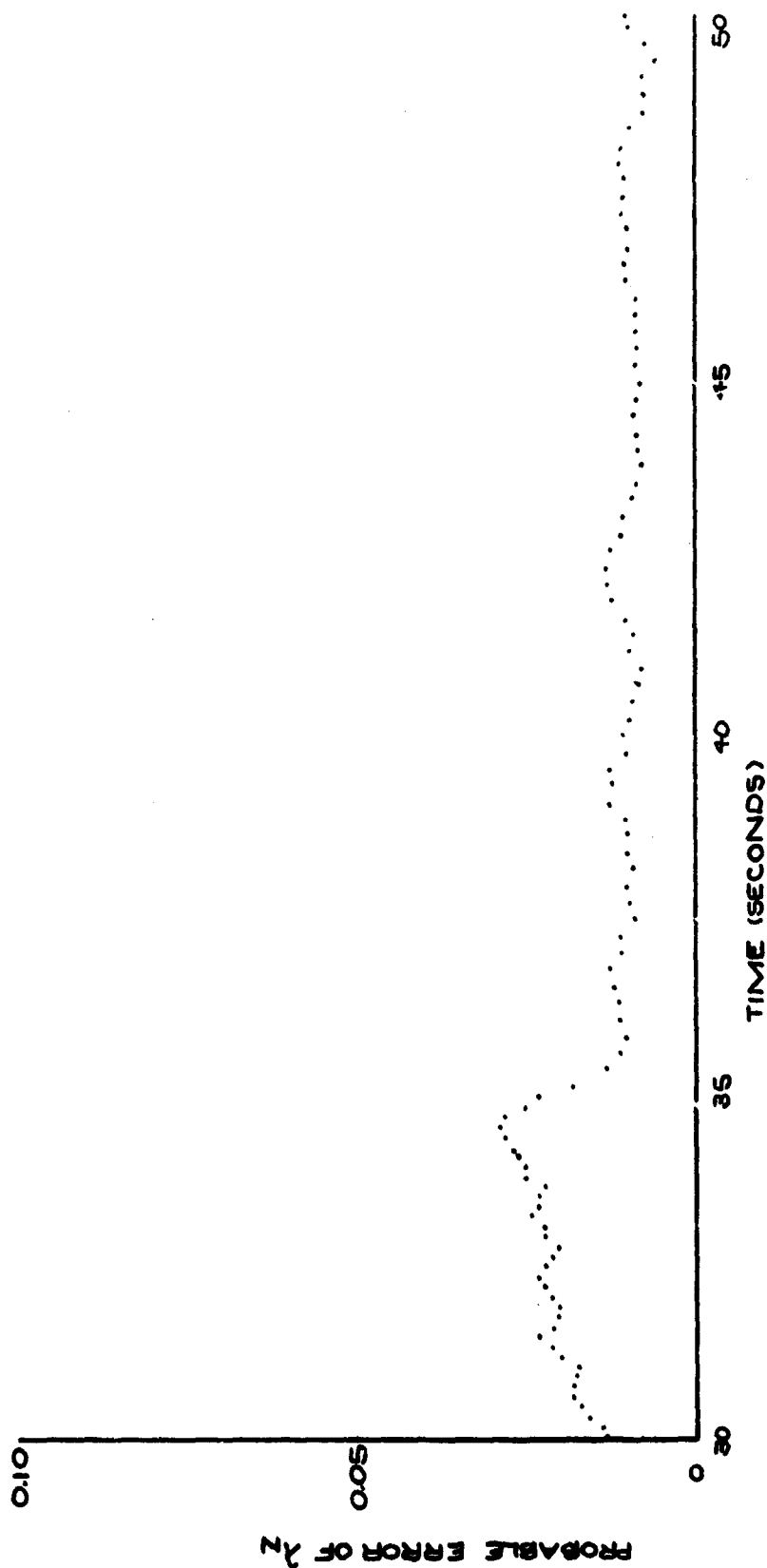


FIG. 20b PROBABLE ERROR OF NUTATION VECTOR
 DYNAMIC DAMPING FACTOR VERSUS TIME
 FROM RELEASE FOR SPLIT-SKIRT BOMB (739)

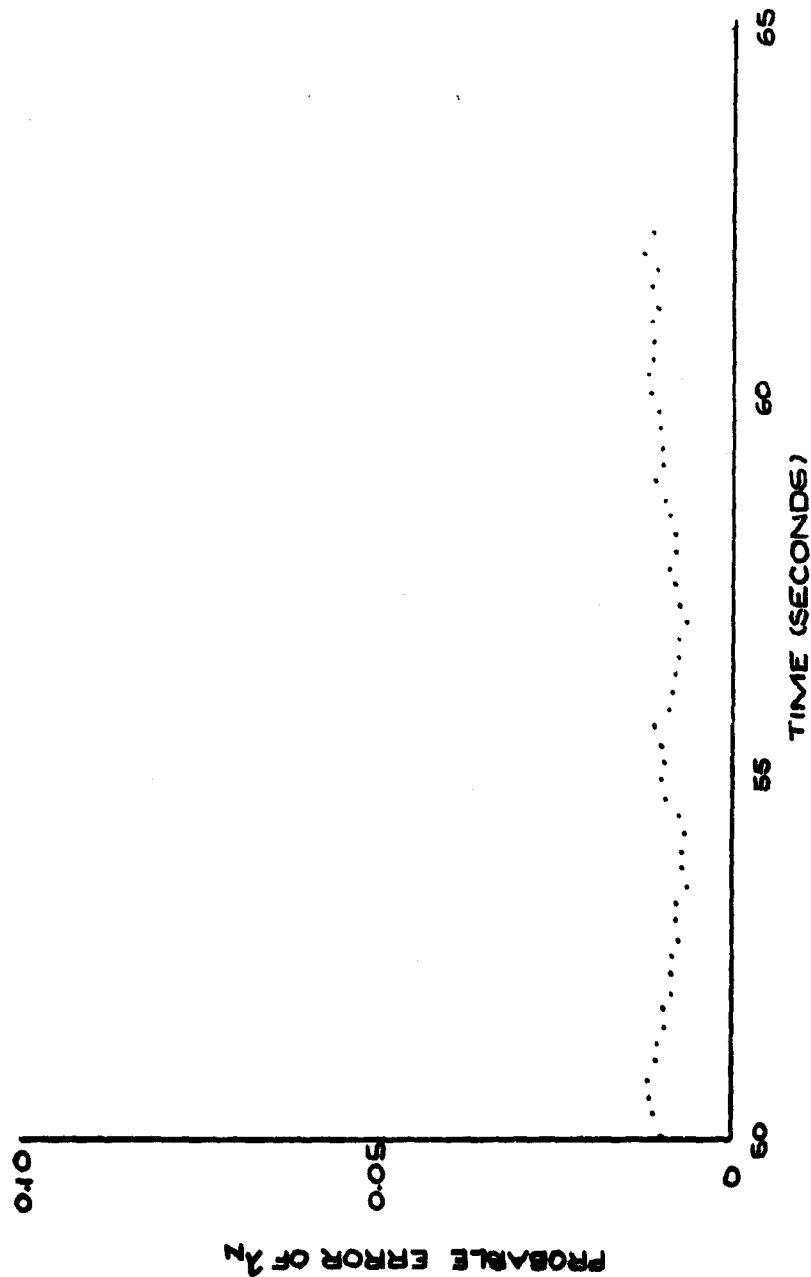


FIG. 20C PROBABLE ERROR OF NUTATION VECTOR

DYNAMIC DAMPING FACTOR VERSUS TIME

FROM RELEASE FOR SPLIT-SKIRT BOMB (739)

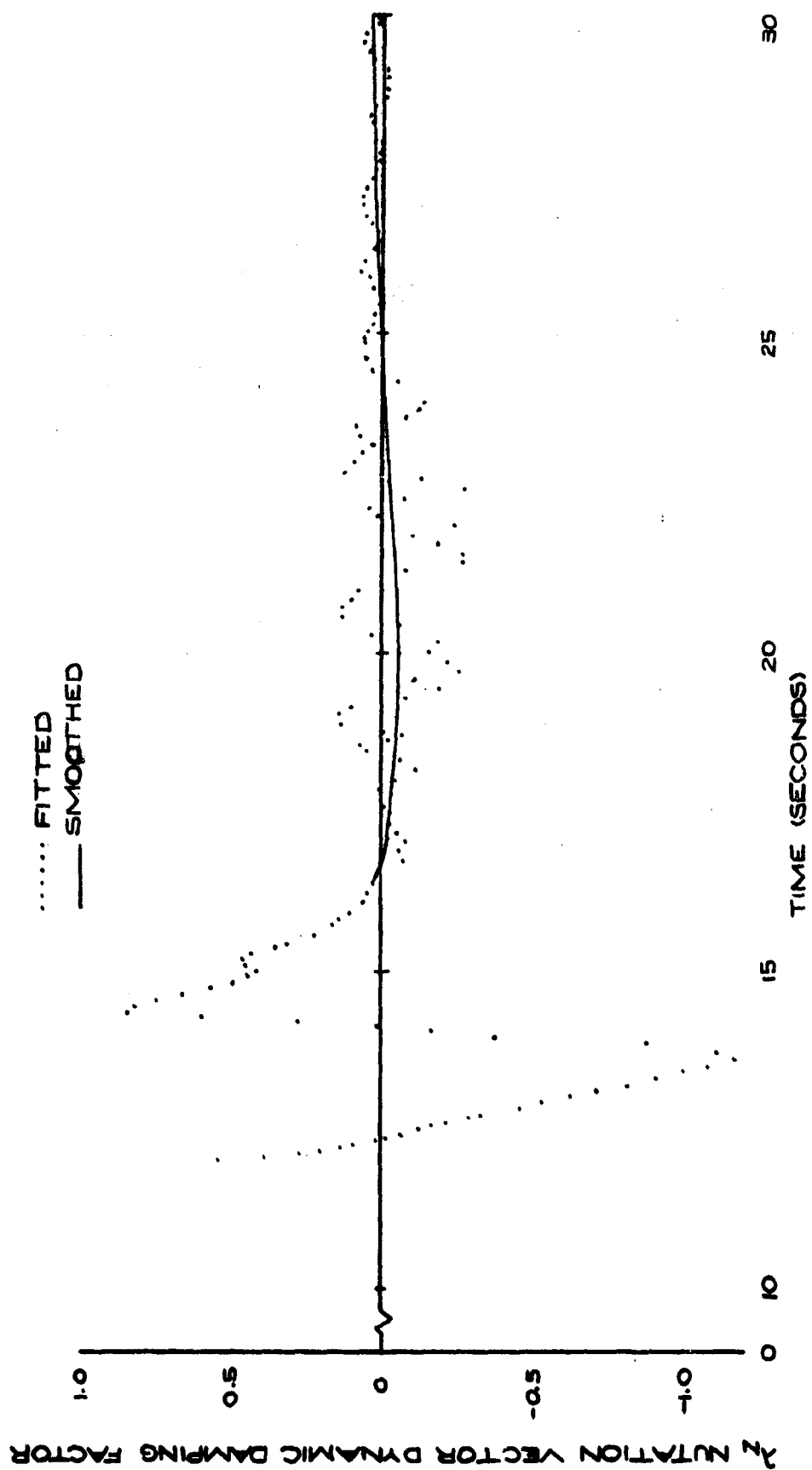


FIG. 21a NUTATION VECTOR DYNAMIC DAMPING
 FACTOR VERSUS TIME FROM RELEASE
 FOR SPLIT-SKIRT BOMB (739)

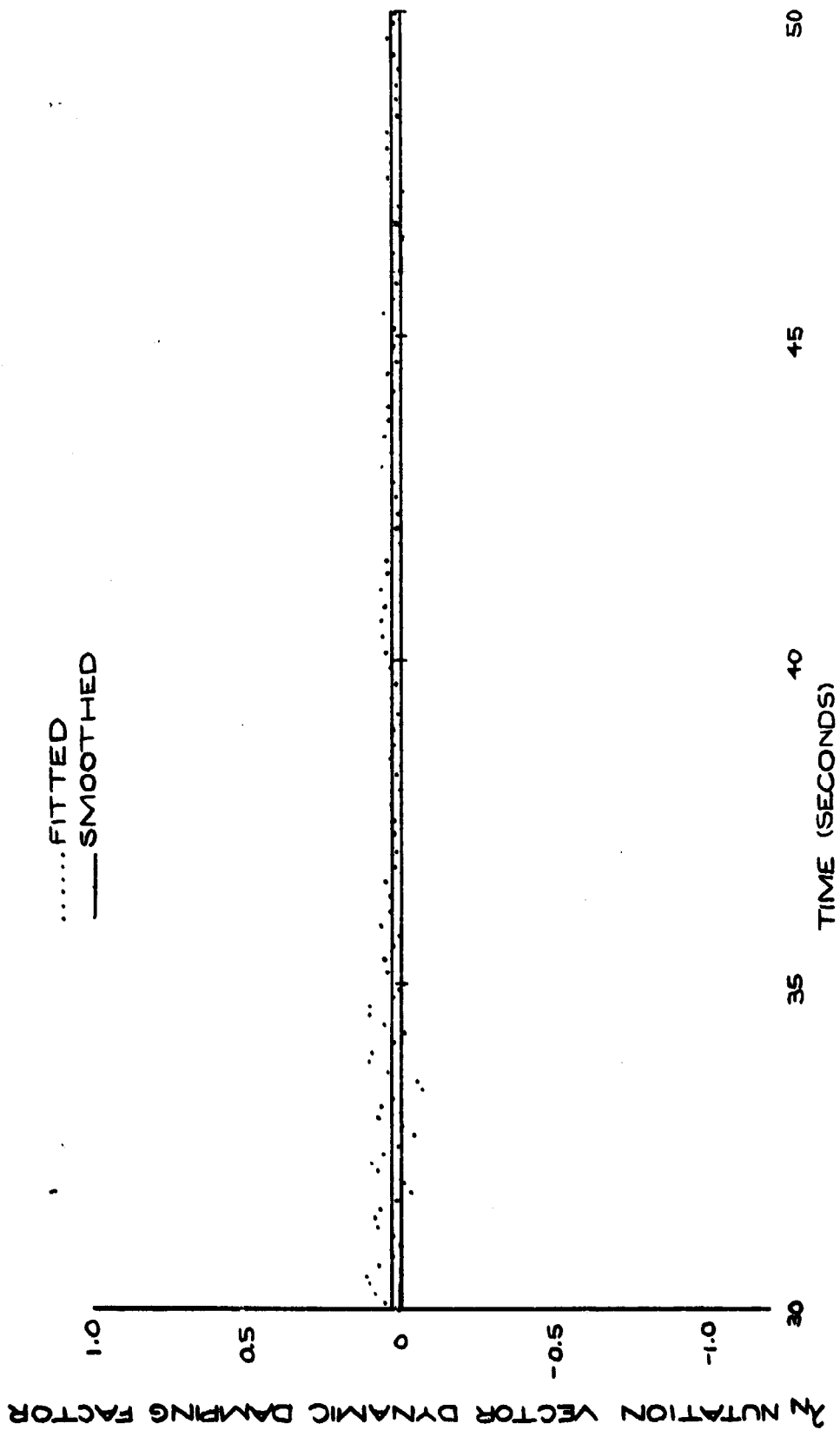


FIG. 21b NUTATION VECTOR DYNAMIC DAMPING
 FACTOR VERSUS TIME FROM RELEASE
 FOR SPLIT-SKIRT BOMB (739)

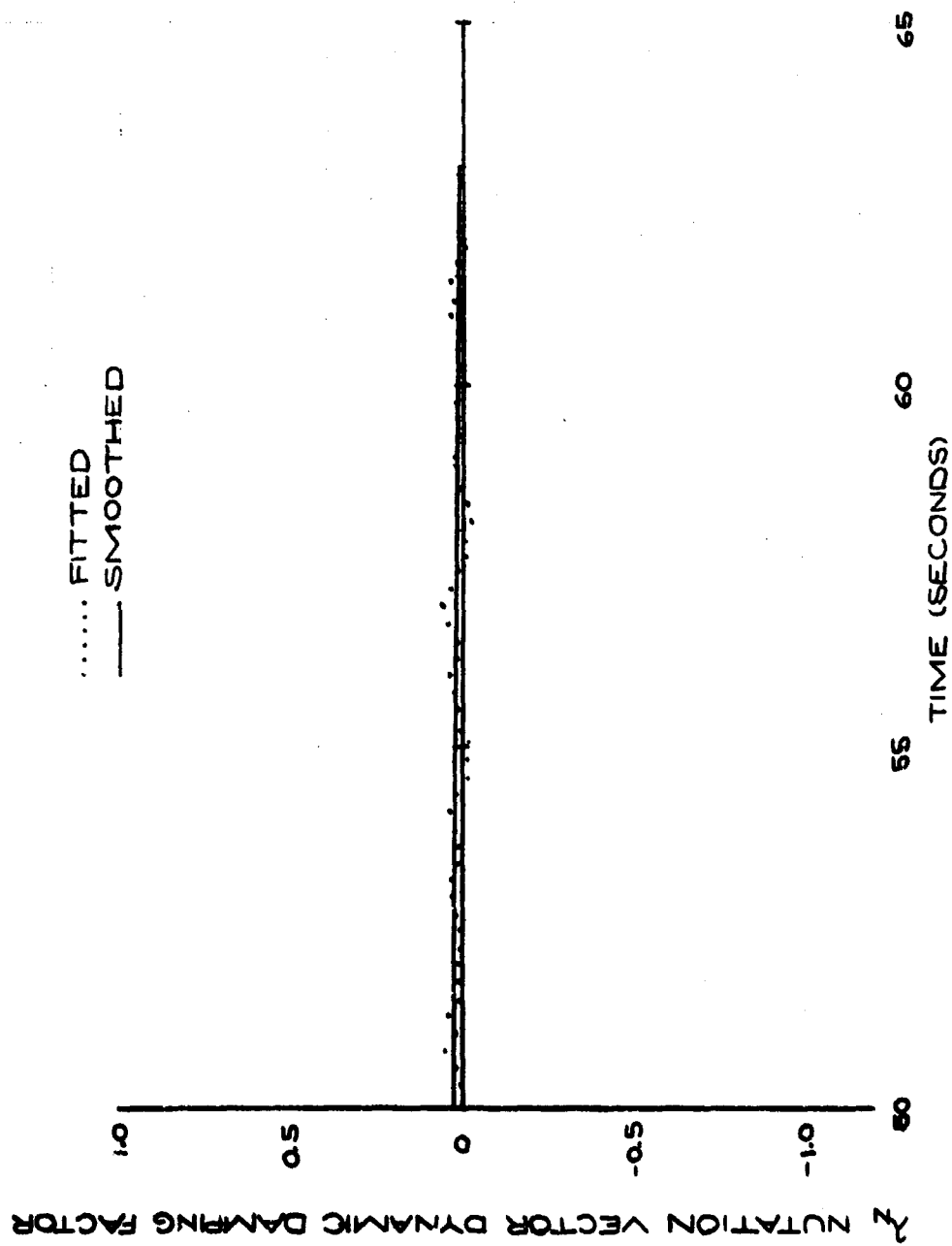


FIG.21C NUTATION VECTOR DYNAMIC DAMPING
 FACTOR VERSUS TIME FROM RELEASE
 FOR SPLIT-SKIRT BOMB (739)

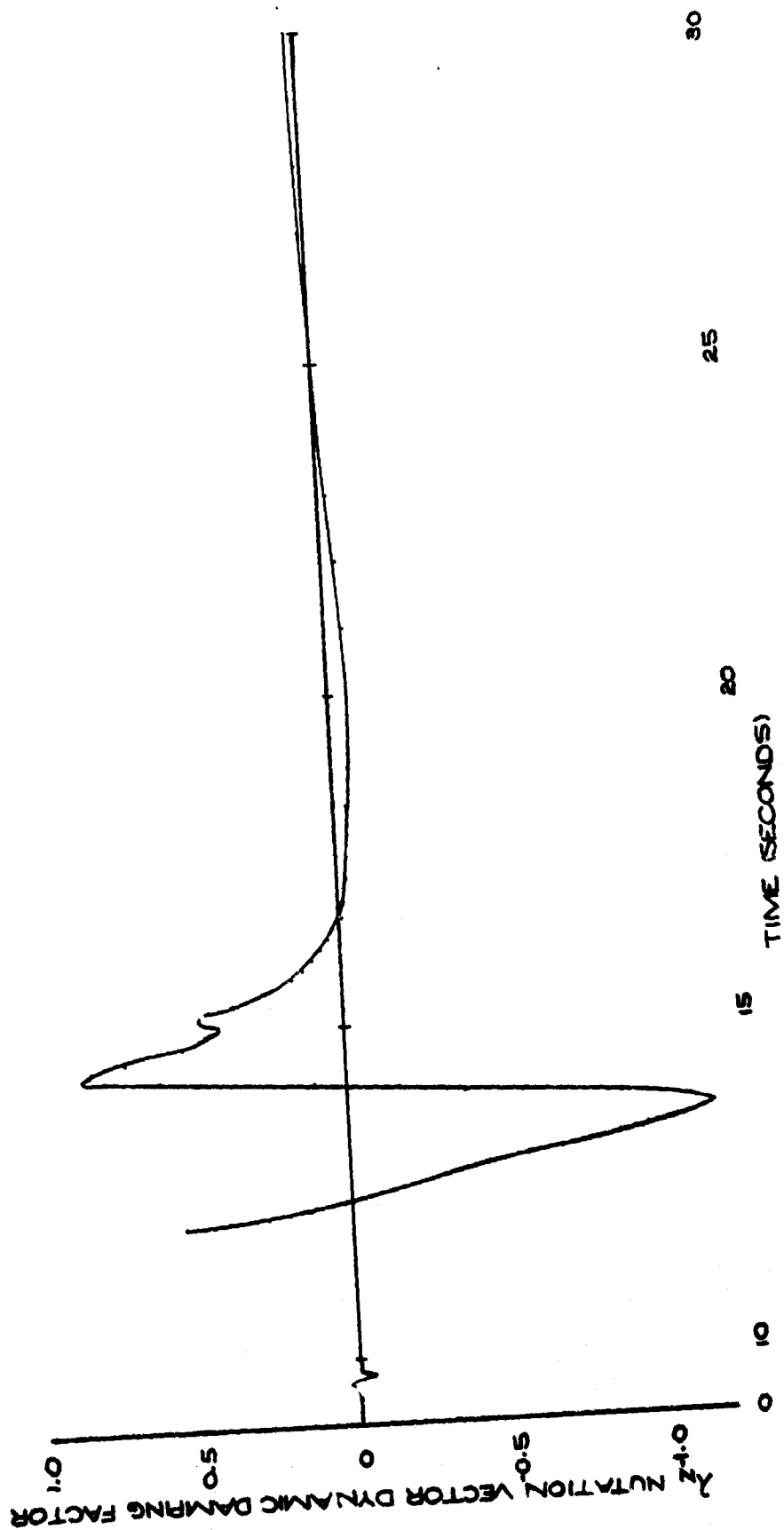


FIG. 22a NUTATION VECTOR DYNAMIC DAMPING
FACTOR VERSUS TIME FROM RELEASE
FOR SPLIT-SKIRT BOMB (739)

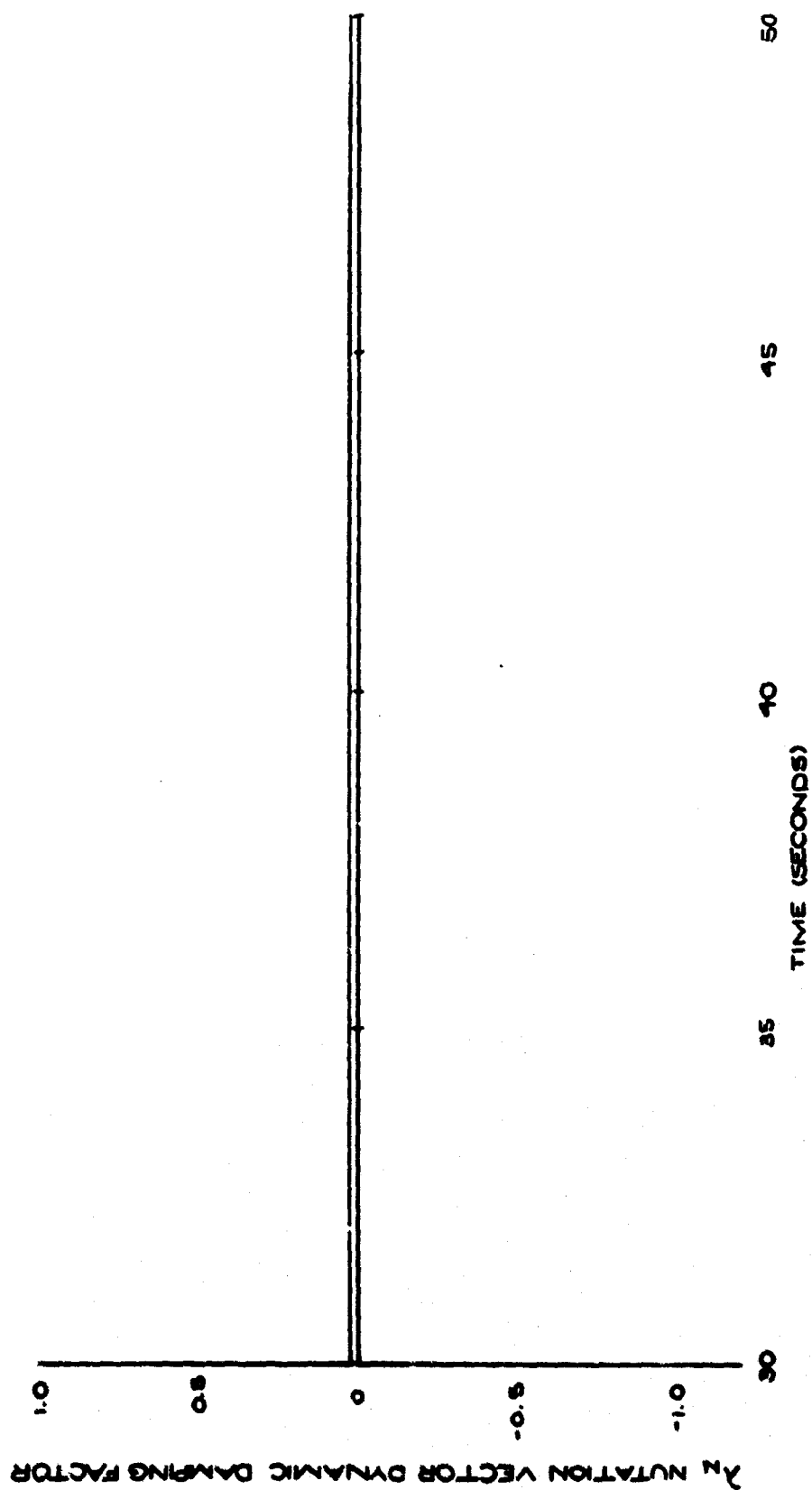


FIG. 22b NUTATION VECTOR DYNAMIC DAMPING
FACTOR VERSUS TIME FROM RELEASE
FOR SPLIT-SKIRT BOMB (739)

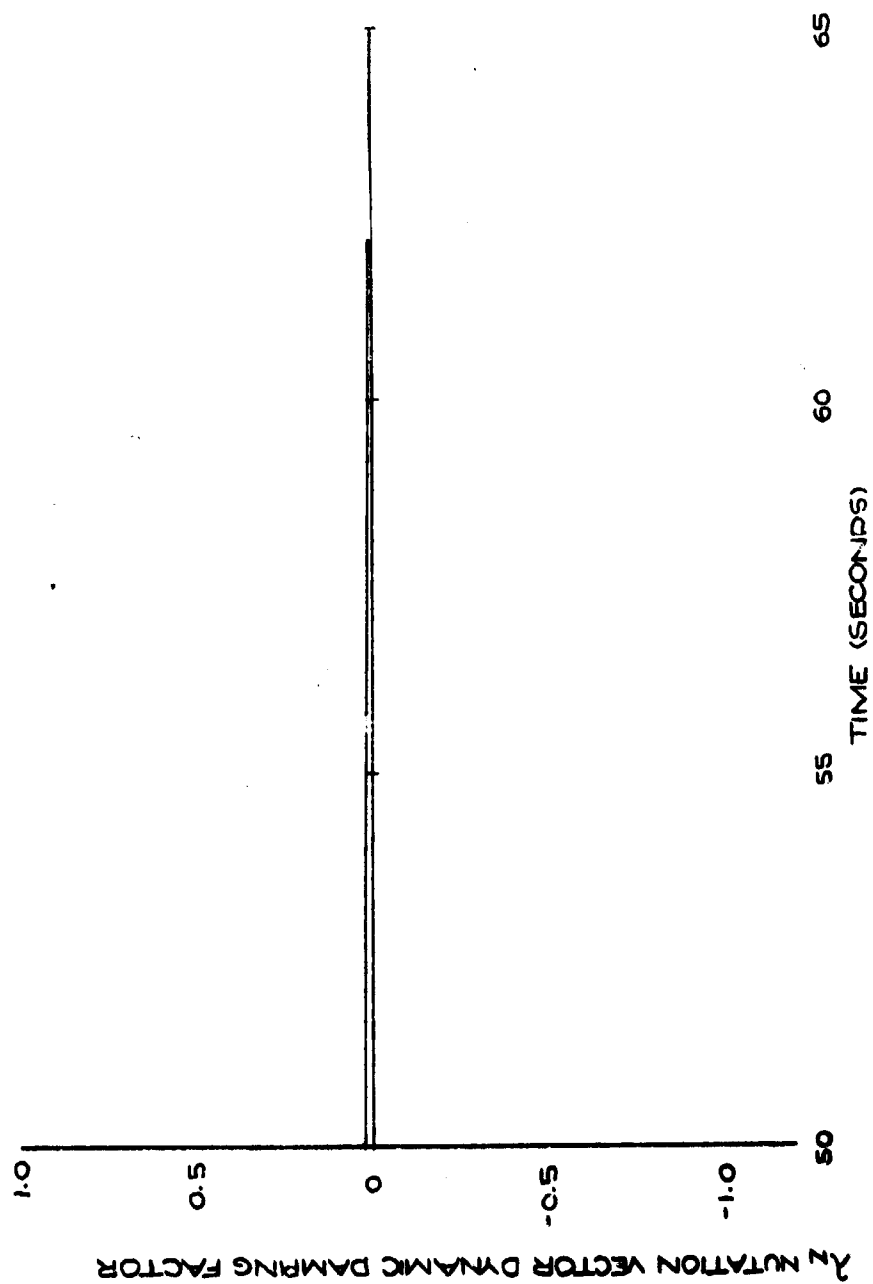


FIG. 22c NUTATION VECTOR DYNAMIC DAMPING
FACTOR VERSUS TIME FROM RELEASE
FOR SPLIT-SKIRT BOMB (739)

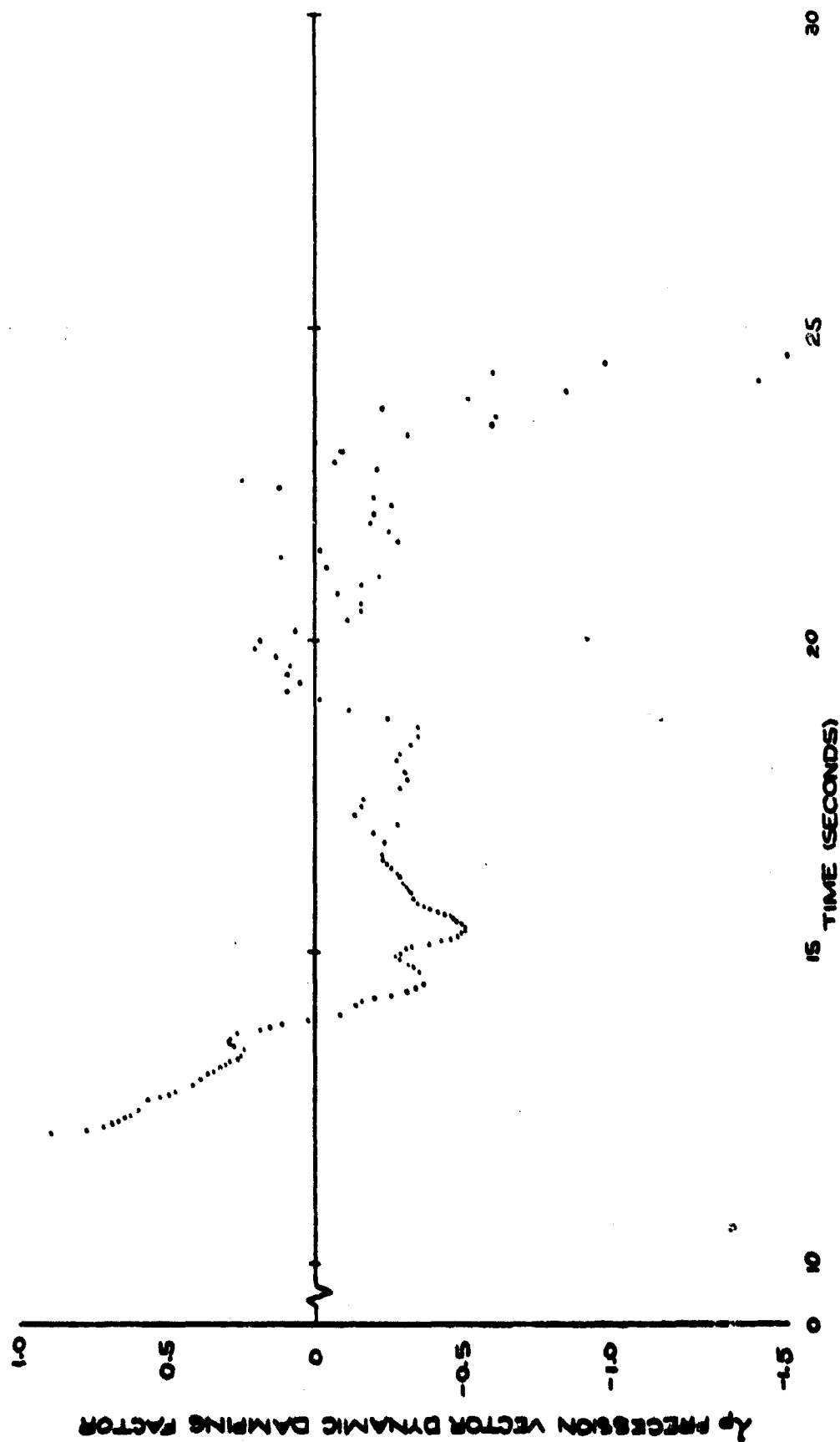


FIG 23 PRECESSION VECTOR DYNAMIC DAMPING FACTOR
VERSUS TIME FROM RELEASE FOR SPLIT-SKIRT BOMB (739)

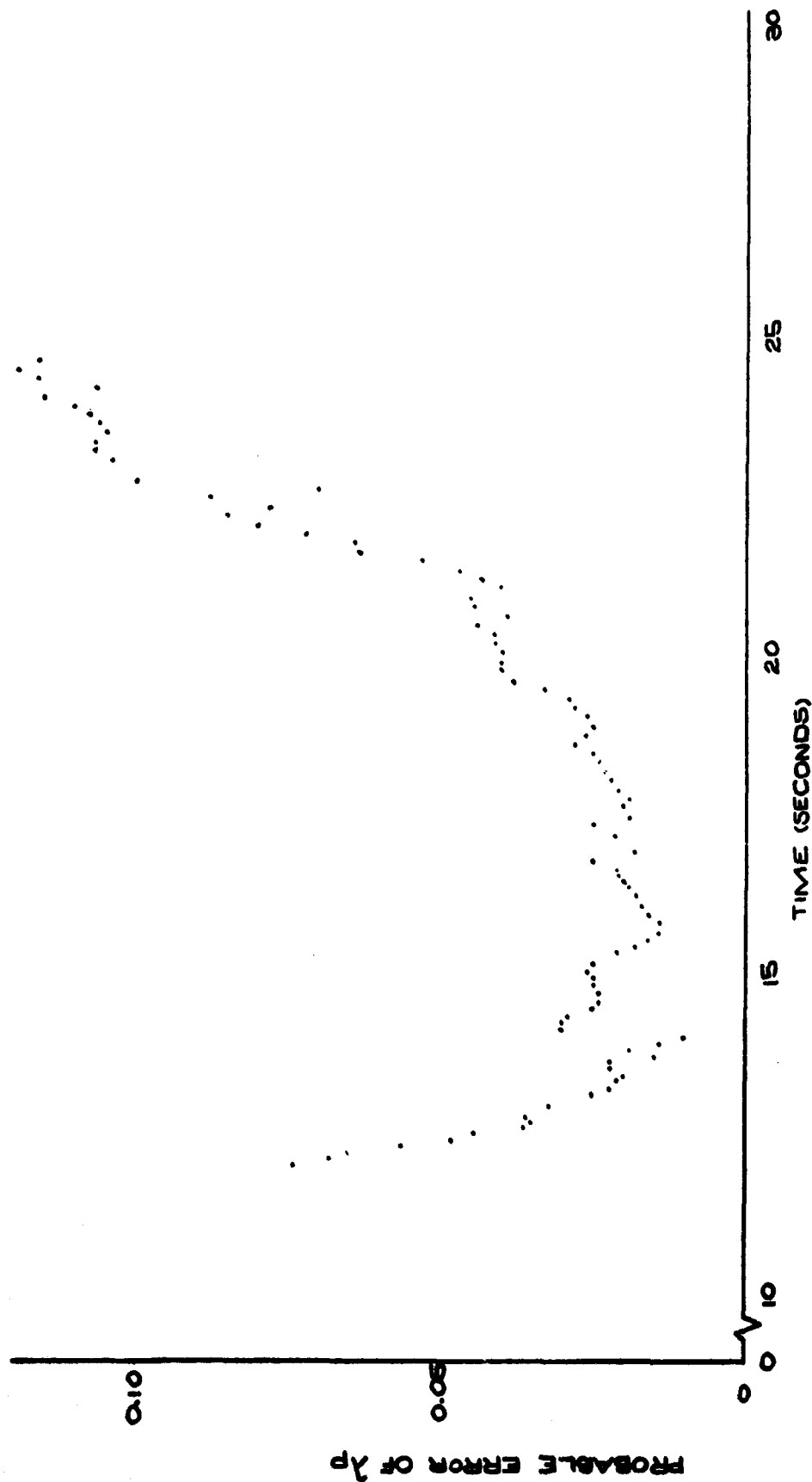


FIG.24 PROBABLE ERROR OF PRECESSION VECTOR
DYNAMIC DAMPING FACTOR VERSUS TIME
FROM RELEASE FOR SPLIT-SKIRT BOMB (739)

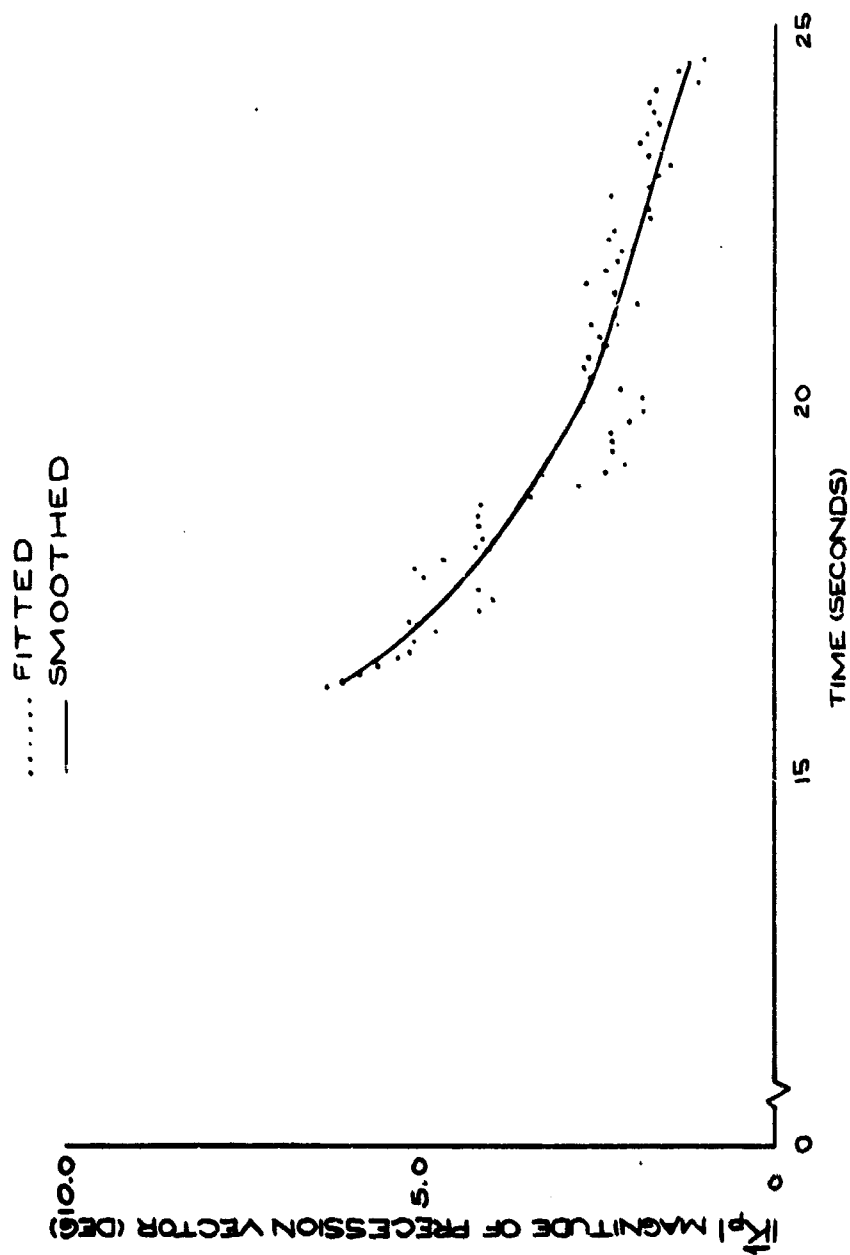


FIG. 25 MAGNITUDE OF PRECESSION
VECTOR VERSUS TIME FROM
RELEASE FOR SPLIT-SKIRT BOMB (739)

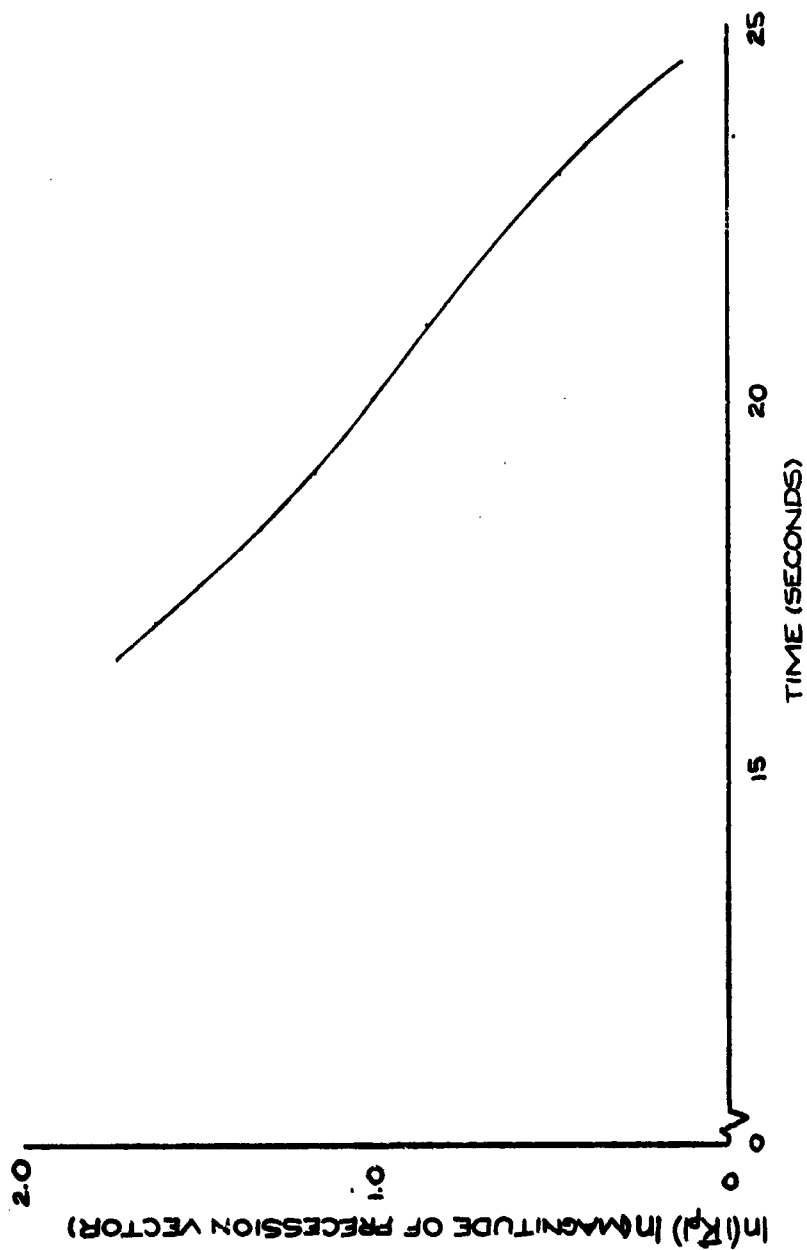


FIG.26 LOGARITHM OF MAGNITUDE
OF PRECESSION VECTOR
VERSUS TIME FROM RELEASE
FOR SPLIT-SKIRT BOMB(739)

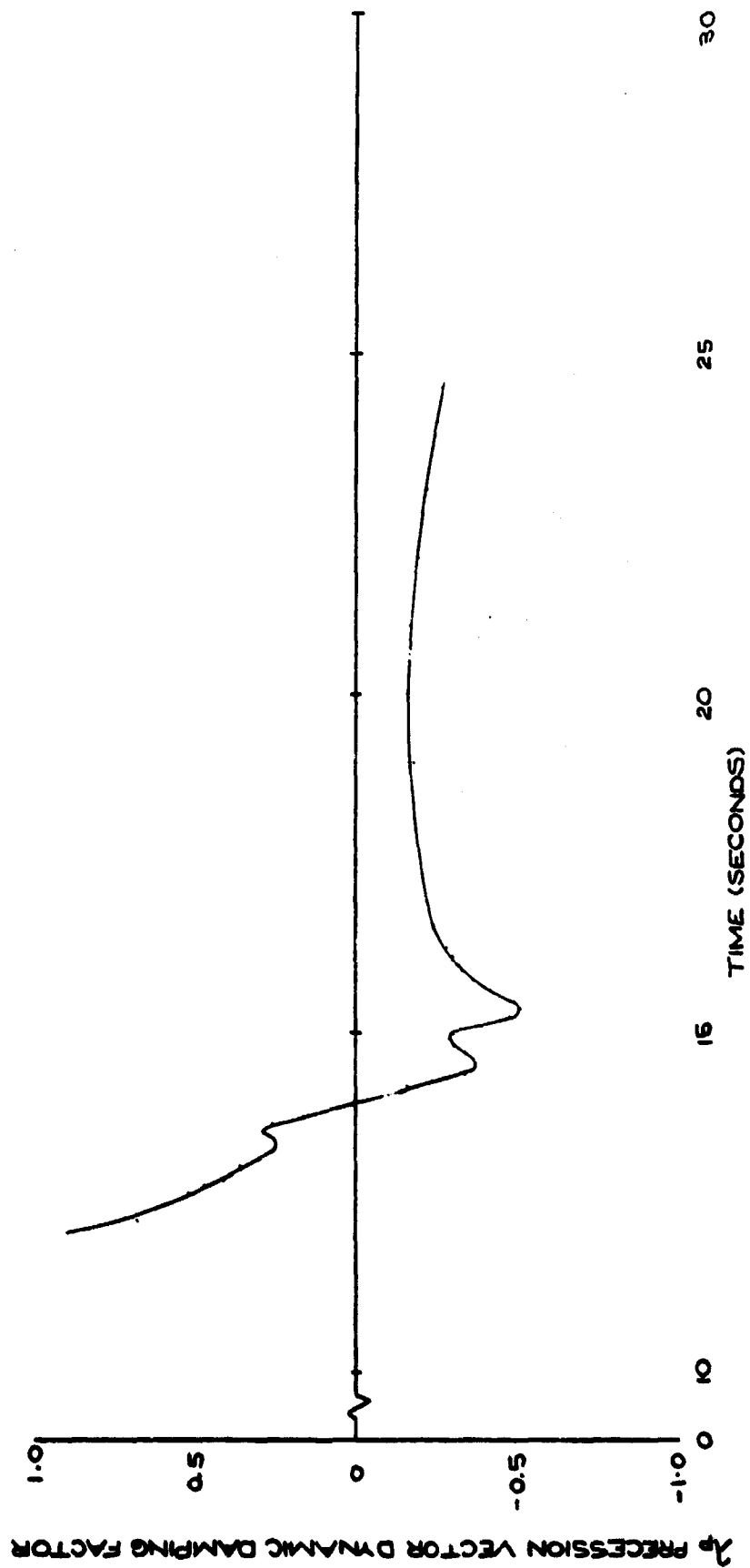


FIG.27 PRECESSION VECTOR DYNAMIC DAMPING
FACTOR VERSUS TIME FROM RELEASE
FOR SPLIT-SKIRT BOMB (739)

interpreted as indicated by "Wobble".¹²

Aerodynamic Stability Derivatives

As indicated in the Computational Procedure, known values for the normal force coefficient derivative, $C_{Z\alpha}$, are necessary for calculations yielding values for the pitch damping moment coefficient derivative, $C_{M\dot{\alpha}} + C_{M\ddot{\alpha}}$, and the Magnus moment coefficient derivative, $C_{M\dot{\alpha}}$. Figs. 28 and 29 present $C_{Z\alpha}$ as a function of time from release and Mach number, respectively. The wind tunnel test results¹⁶ from which $C_{Z\alpha}$ was obtained, are presented in Appendix I.

In order to determine $C_{M\alpha}$ as a function of time from release, Eq. (22) or Eq. (25) may be used, depending on whether or not the precessional mode is present. One method is to use Eq. (22) from 12.05 seconds to 24.5 seconds, at which time the precessional mode is no longer able to be determined by the fit, and to use Eq. (25) from 24.5 seconds to the end of the flight. This procedure has one inherent disadvantage, however, in that for a few seconds beyond 24.5 seconds the precessional mode is still present but is too small to be extracted from the data; thus, a slight discontinuity will appear in $C_{M\alpha}$ as a function of time from release at 24.5 seconds. Therefore, in order to avoid this, Eq. (25) was used to determine $C_{M\alpha}$ throughout the entire flight.

Using values of ω_{ND} as a function of time from release, determined from the fitting procedure, and the roll rate, as taken from Reference 4, $C_{M\alpha}$ was determined as a function of time from release by Eq. (25). These results are presented in Fig. 30.

From these values of $C_{M\alpha}$, the gyroscopic stability factor, s , was determined as a function of time from release by Eq. (13). These results, presented in Fig. 31, indicate gyroscopic stability throughout the entire flight. Near resonance, however, s becomes very small. This is a direct result of the large values of $C_{M\alpha}$ and the small values of rolling velocity at this time.

An examination of the dynamic damping factors, Figs. 22 and 27, and the gyroscopic stability factor, Fig. 31, leads to the result that, according to the linear theory, the bomb is dynamically stable from 16.6 seconds to 25 seconds from release. That is, it is only during this time interval that both necessary and sufficient conditions for the dynamic stability occur: $\lambda_{NP} < 0$, and $s < 0$.

In order to calculate the pitch damping moment coefficient derivative, $C_{M\dot{\alpha}} + C_{M\ddot{\alpha}}$, both dynamic damping factors must be known. As noted previously, the precessional mode was not able to be extracted from the data

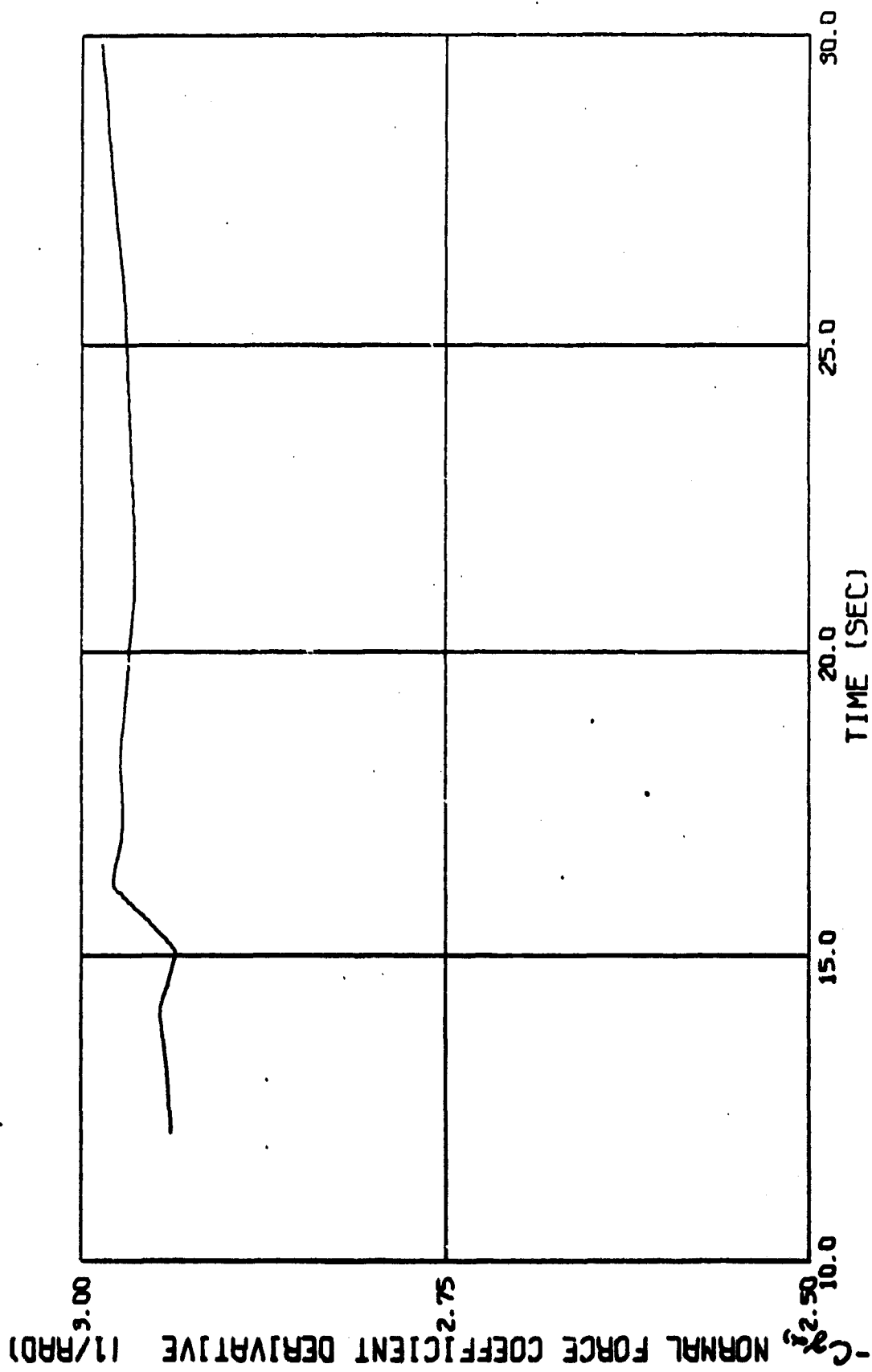


Fig. 28a NORMAL FORCE COEFFICIENT DERIVATIVE VERSUS TIME FROM RELEASE
FOR SPLIT-SKIRT BOMB (739)

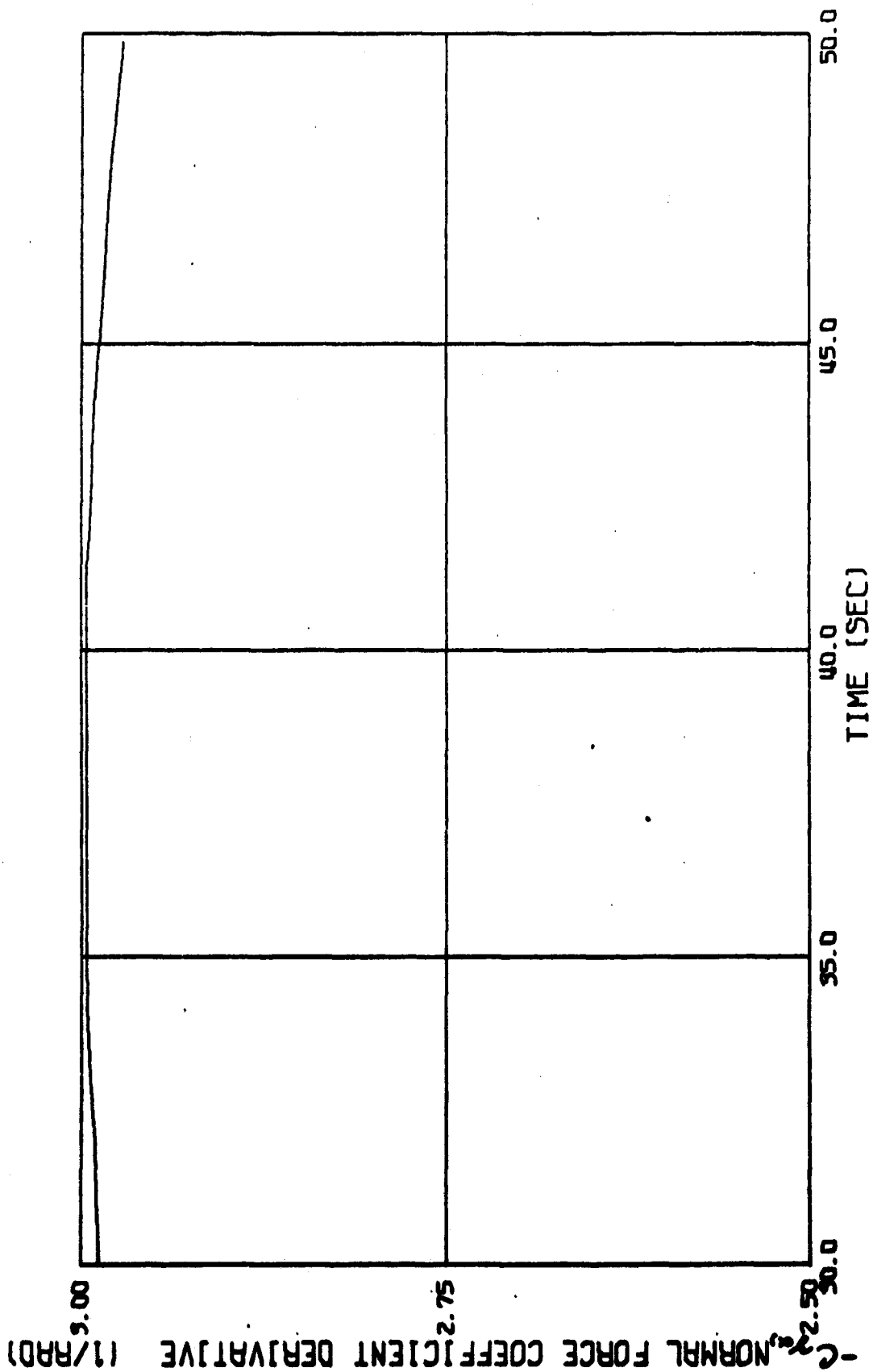


Fig. 28b NORMAL FORCE COEFFICIENT DERIVATIVE VERSUS TIME FROM RELEASE
FOR SPLIT-SKIRT BOMB (739)

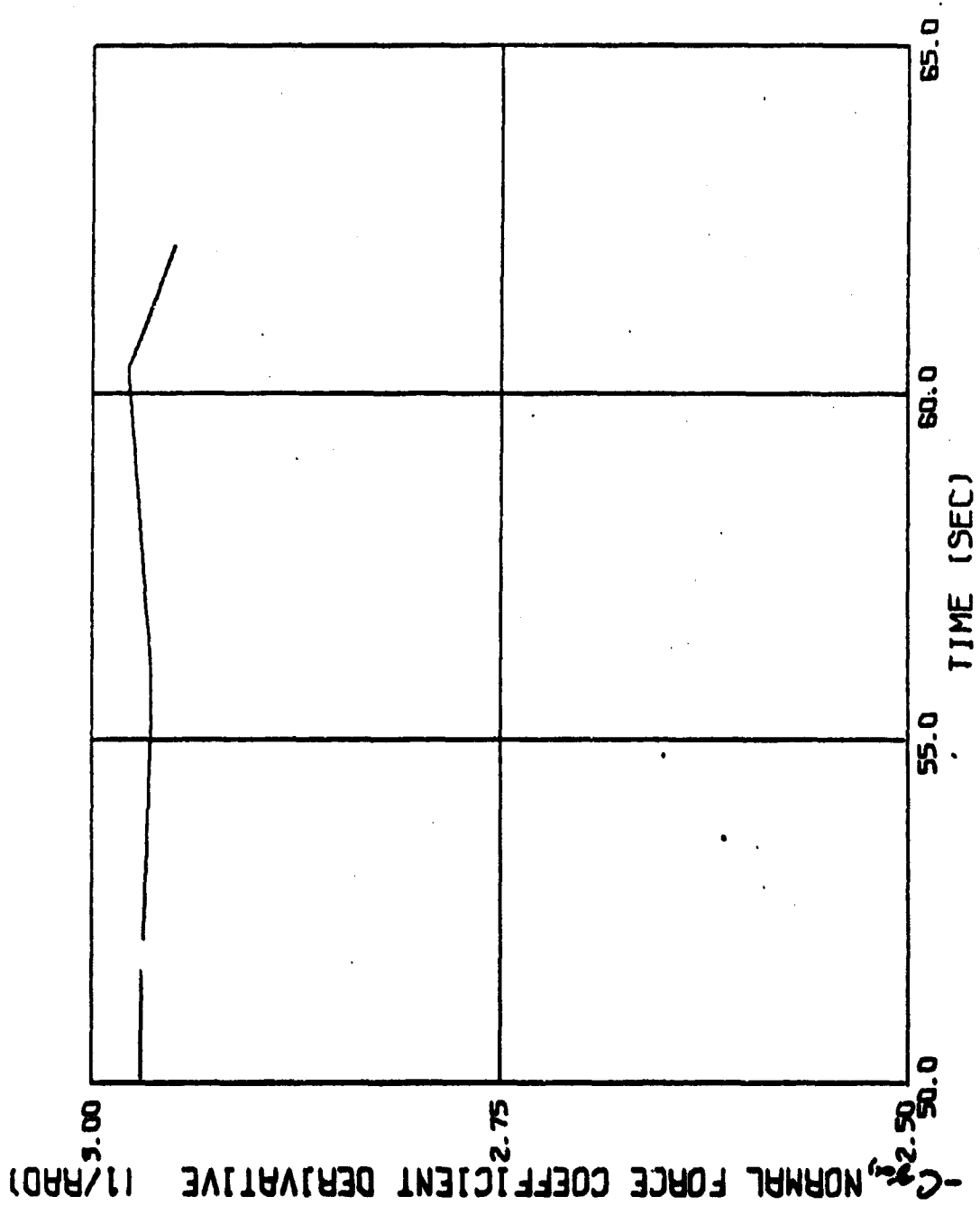


Fig. 28c NORMAL FORCE COEFFICIENT DERIVATIVE VERSUS
TIME FROM RELEASE FOR SPLIT-SKIRT BOMB (739)

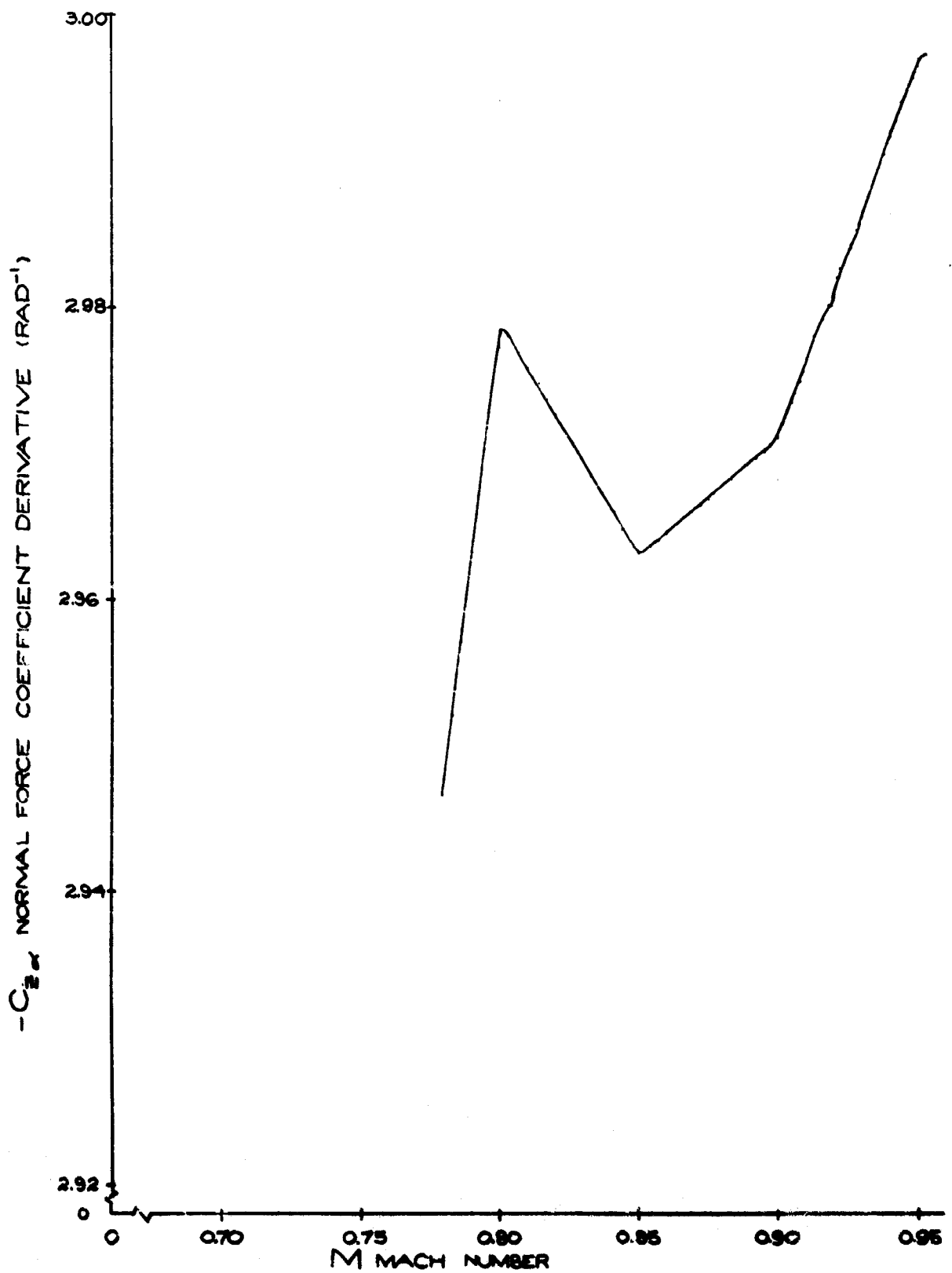


FIG 29 NORMAL FORCE COEFFICIENT
DERIVATIVE VERSUS MACH
NUMBER FOR SPLIT-SKIRT BOMB(739)

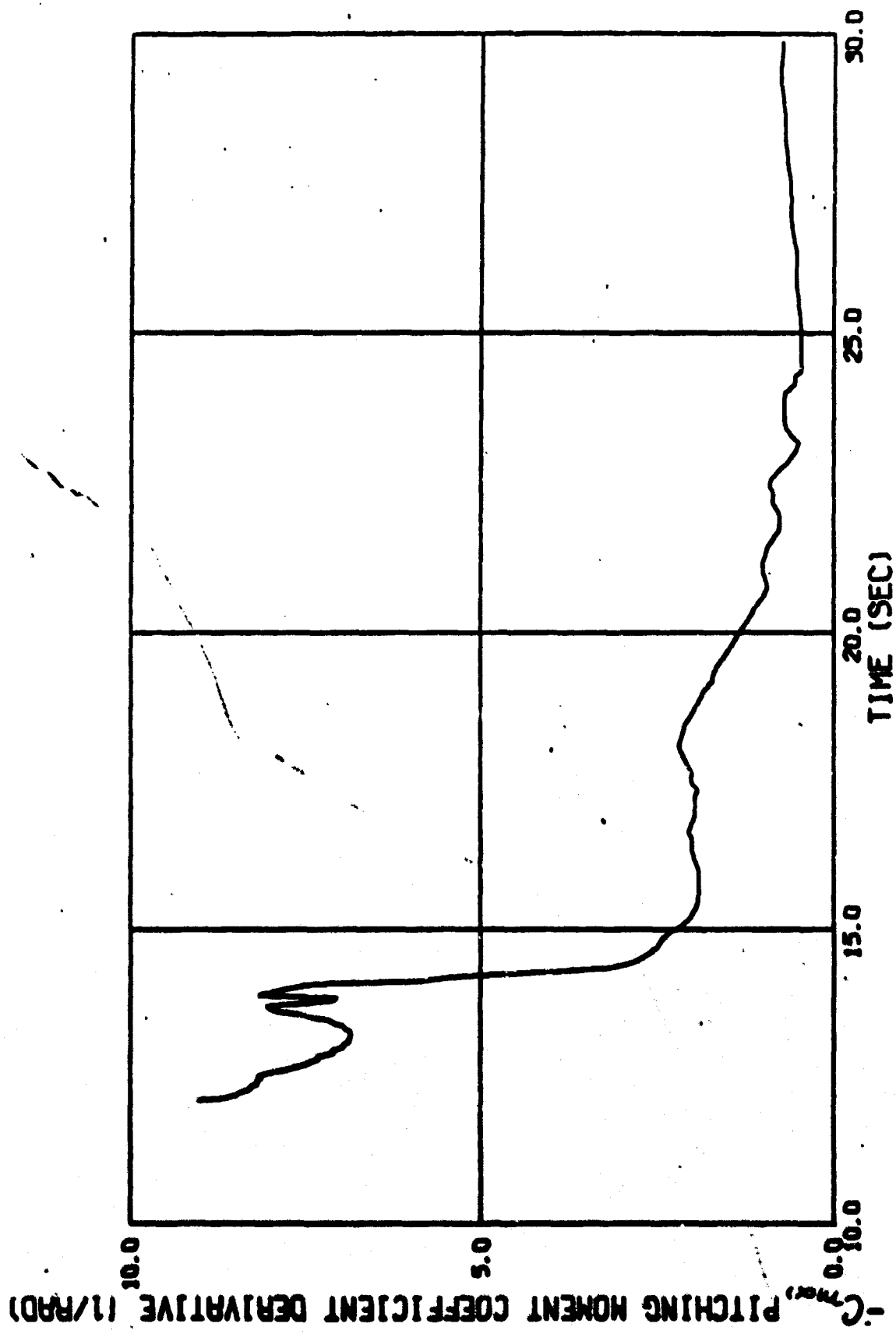


Fig. 30a PITCHING MOMENT COEFFICIENT DERIVATIVE VERSUS TIME FROM RELEASE
FOR SPLIT-SKIRT BOMB (739)

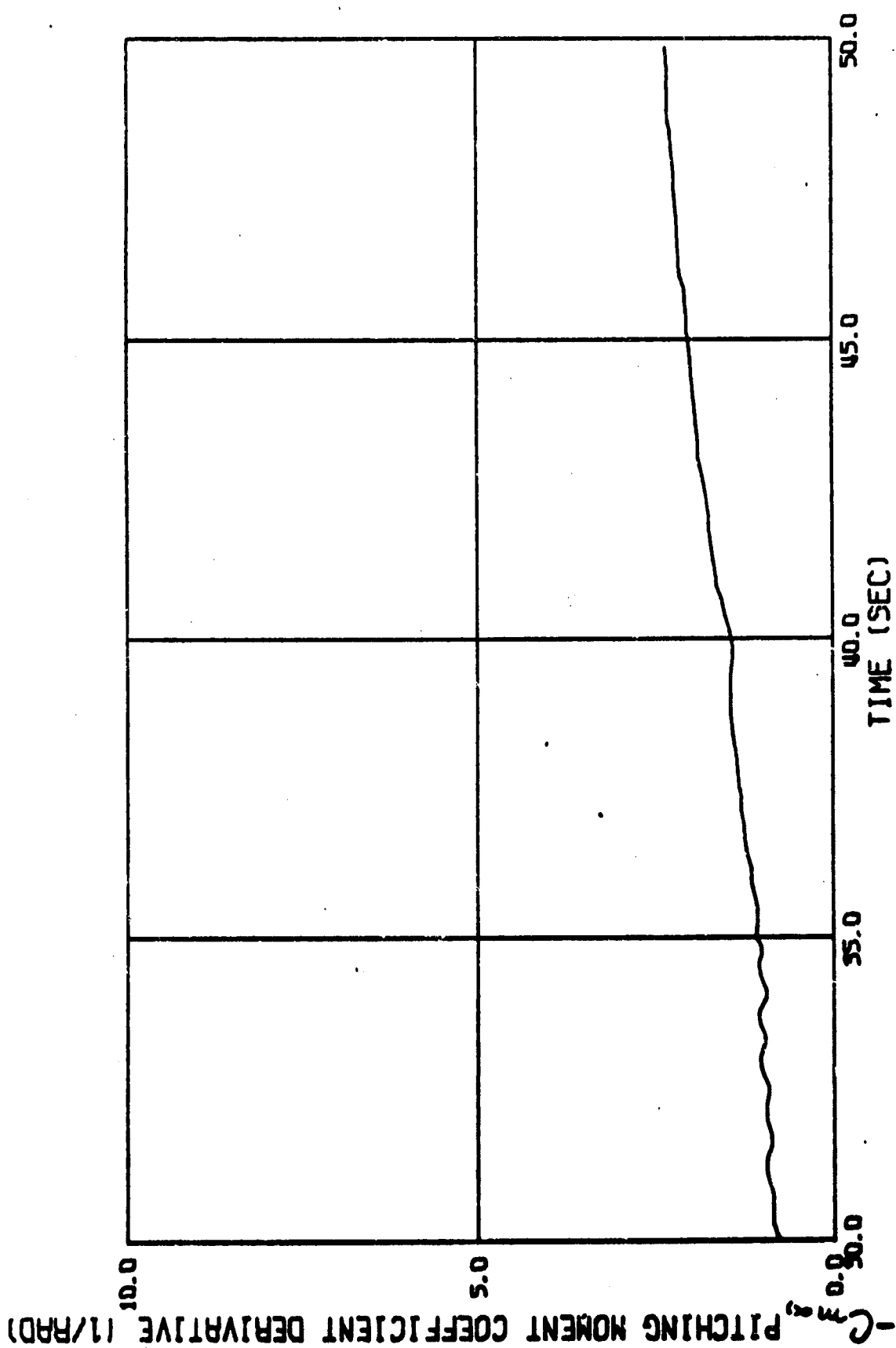


Fig. 30b PITCHING MOMENT COEFFICIENT DERIVATIVE VERSUS TIME FROM RELEASE FOR
SPLIT-SKIRT BOMB (739)

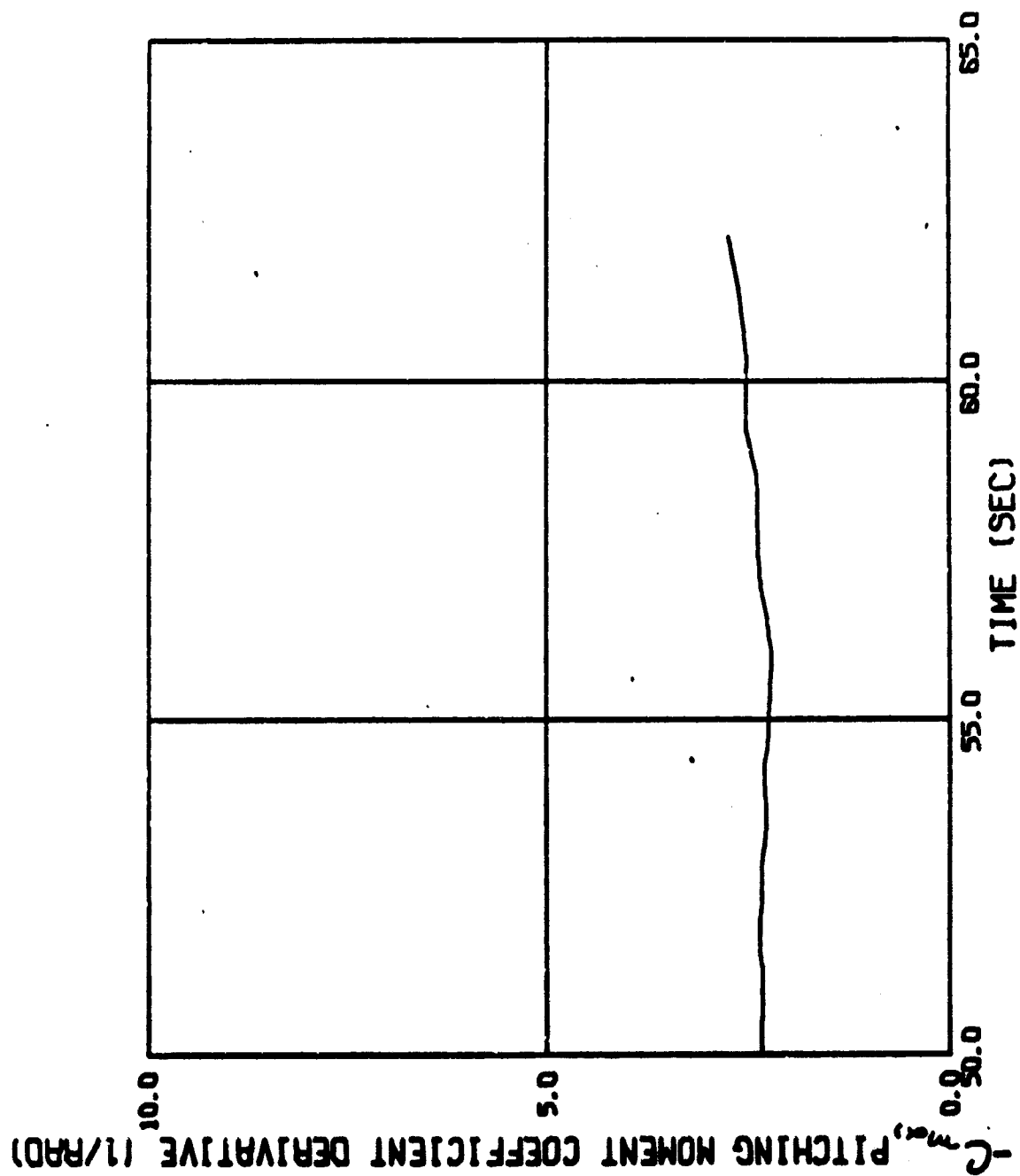


Fig. 30c PITCHING MOMENT COEFFICIENT DERIVATIVE VERSUS
TIME FROM RELEASE FOR SPLIT-SKIRT BOMB (739)

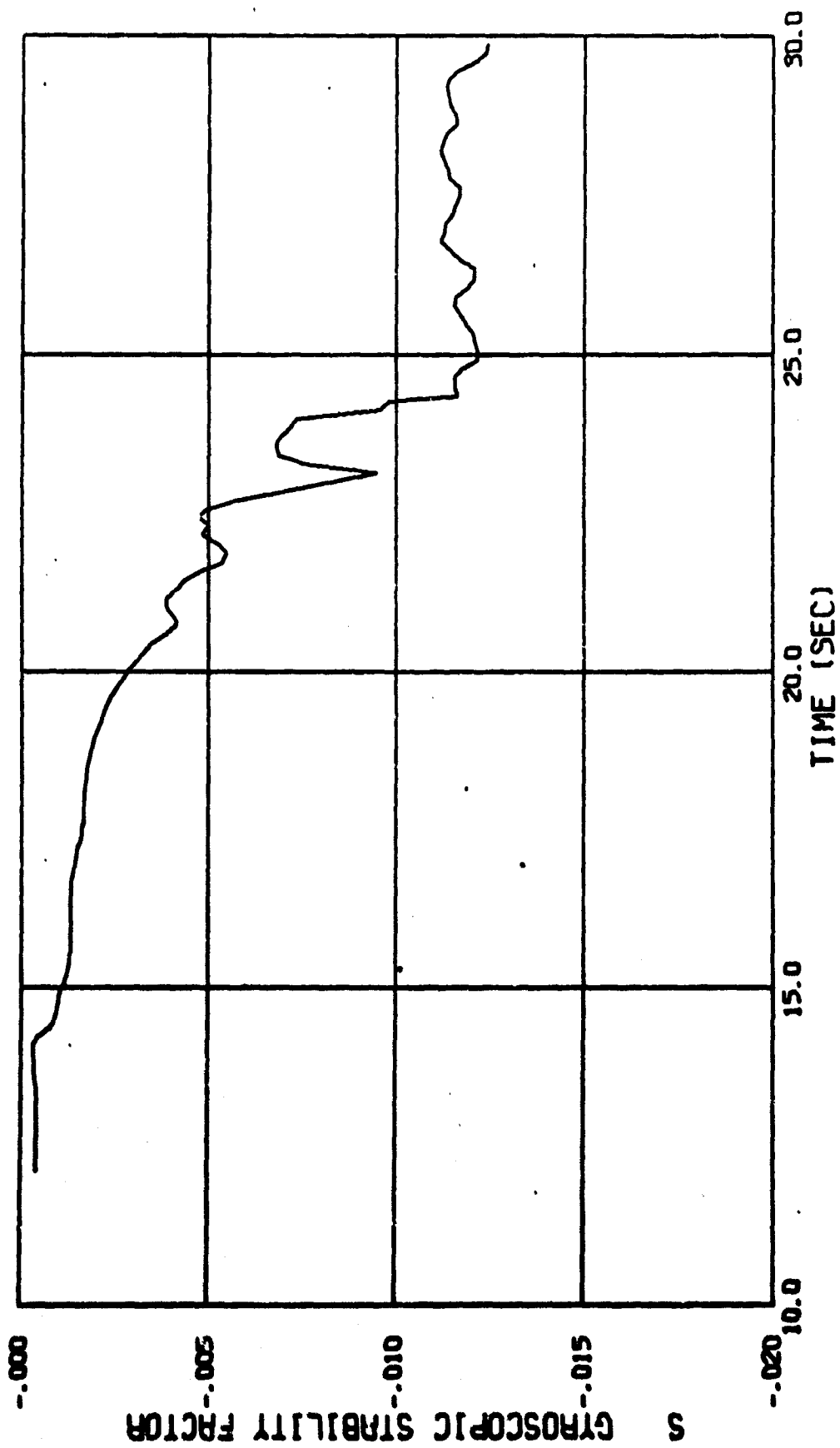


Fig. 31a GYROSCOPIC STABILITY FACTOR VERSUS TIME FROM RELEASE FOR SPLIT-SKIRT BOMB (739)

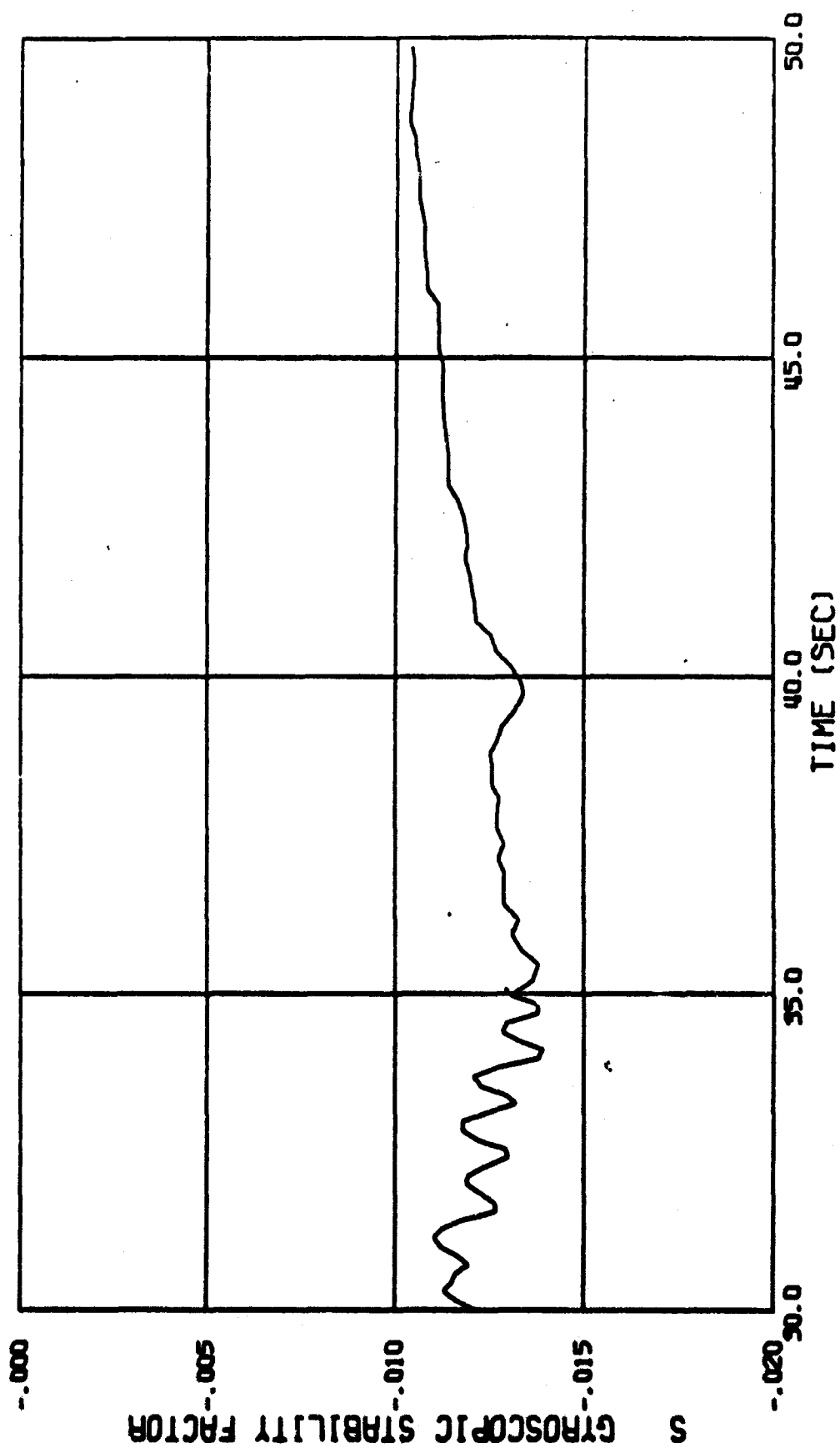


Fig. 31b GYROSCOPIC STABILITY FACTOR VERSUS TIME FROM RELEASE FOR SPLIT - SKIRT BOMB (739)

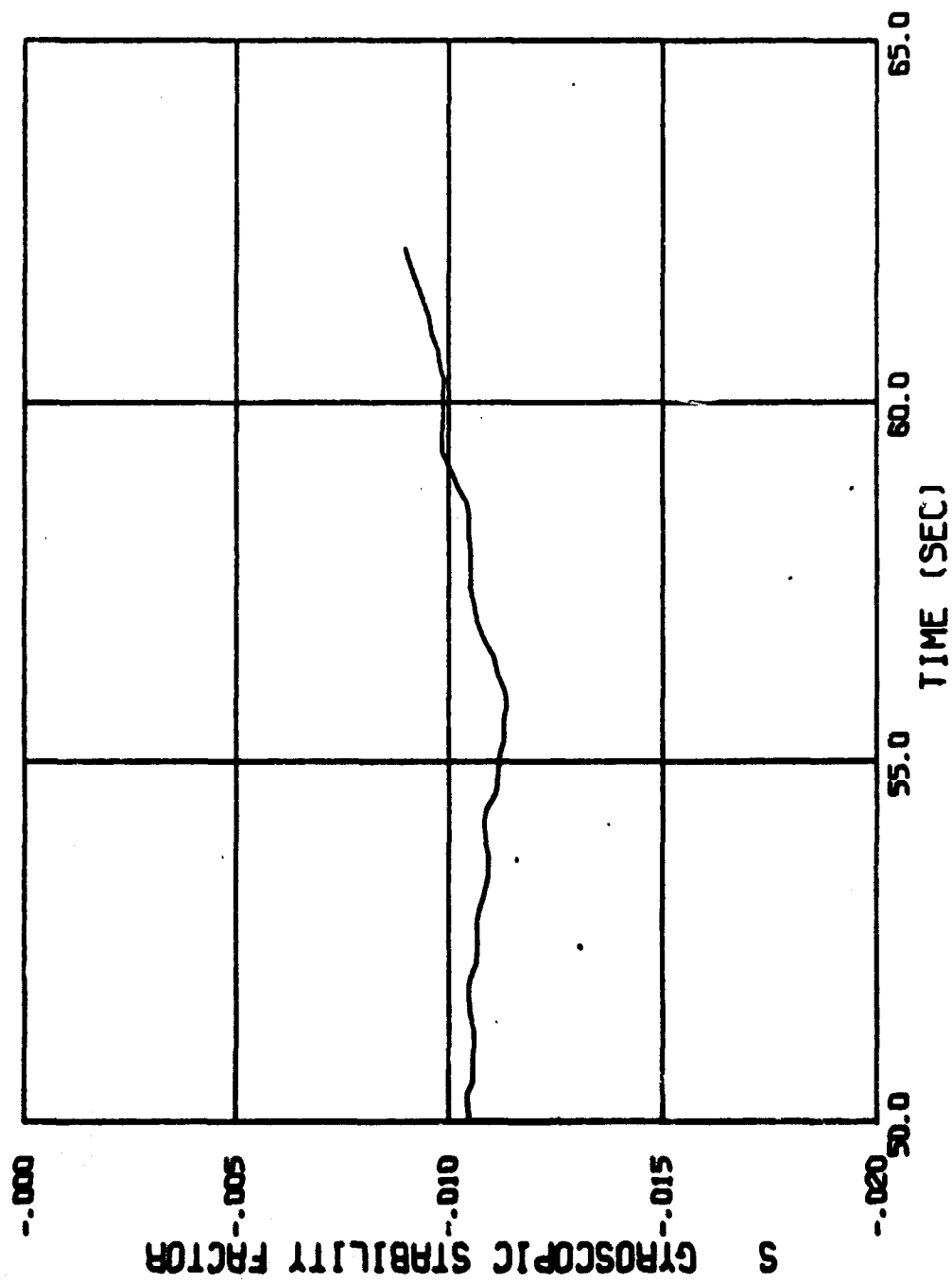


Fig. 31c GYROSCOPIC STABILITY FACTOR VERSUS TIME FROM
RELEASE FOR SPLIT-SKIRT BOMB (739)

after 24.5 seconds, thus, $C_{m\dot{\alpha}} + C_{m\dot{\beta}}$ may be calculated from Eq. (23) only up to 24.5 seconds from release. In making these calculations it was found that the pitch damping moment coefficient derivative assumed an essentially constant value of -49.3 rad^{-1} from 20.75 seconds to 24.5 seconds from release. During the time previous to this, however, $C_{m\dot{\alpha}} + C_{m\dot{\beta}}$ ranged from -339.3 rad^{-1} to 488.3 rad^{-1} , changing sign at approximately 14.2 seconds from release. Results of this nature are unorthodox to the linear theory. An examination of the dynamic damping factors, from which $C_{m\dot{\alpha}} + C_{m\dot{\beta}}$ is calculated, in this time period indicates that these results would indeed occur since both λ_n and λ_p change sign in the neighborhood of 14 seconds from release. Furthermore, calculations of the Magnus moment coefficient derivative from 12.05 seconds to 24.5 seconds from release from Eq. (24) yielded results of a similar nature. That is, previous to 20.75 seconds from release, $C_{m\dot{\alpha}}$ assumes values ranging from -642.2 rad^{-1} to 415.9 rad^{-1} , changing sign at approximately 14.2 seconds from release. Both of these results led to an investigation of the presence of some other phenomenon at this time aside from resonance. Again, it should be noted that these results may have occurred due to a confusion of the Nutation and Trim arms at resonance.

In the Preliminary Analysis, it was noted that, from 12 seconds to 20 seconds from release, the rolling velocity assumed a fairly constant value, which led to the thought that Roll Lock-In and Catastrophic Yaw effects might also be present. In order to investigate these phenomena, however, a knowledge of the roll orientation as a function of time from release was necessary.

The required information was found in Reference 4. Fig. 32 shows the roll orientation angle, γ , as a function of time from release. It was immediately noted that, from 12 seconds to approximately 21 seconds from release, the bomb experienced the effects of roll orientation. From 21 seconds to the end of the flight, however, the effect was cancelled out. For purposes of comparison, the magnitude of the complex angle of attack as a function of time from release was smoothed and is presented in Fig. 33. Comparison of Figs. 32a and 33a shows the undesirable effect of γ on $|R|$ up to approximately 21 seconds from release. Correlation of the roll orientation angle as a function of time, Fig. 32a, with the rolling velocity as a function of time, Fig. 6, shows that the missile was on the threshold of "lock-in" in the vicinity of 14 seconds from release. Had the roll moment due to cant been smaller, or the induced roll moment been slightly larger in magnitude, it is felt that the bomb would have experienced Roll Lock-In and Catastrophic Yaw. A small change in the flexible tail configuration could well induce these effects.

Thus, although the bomb did not experience Roll Lock-In and Catastrophic Yaw per se, the effects of the induced side moment associated with these phenomena were felt up to approximately 21 seconds from release. Therefore, the unorthodox results obtained by applying the damping equation of the linear theory, Eq. (10), to the data from 12.05 seconds to 20.75

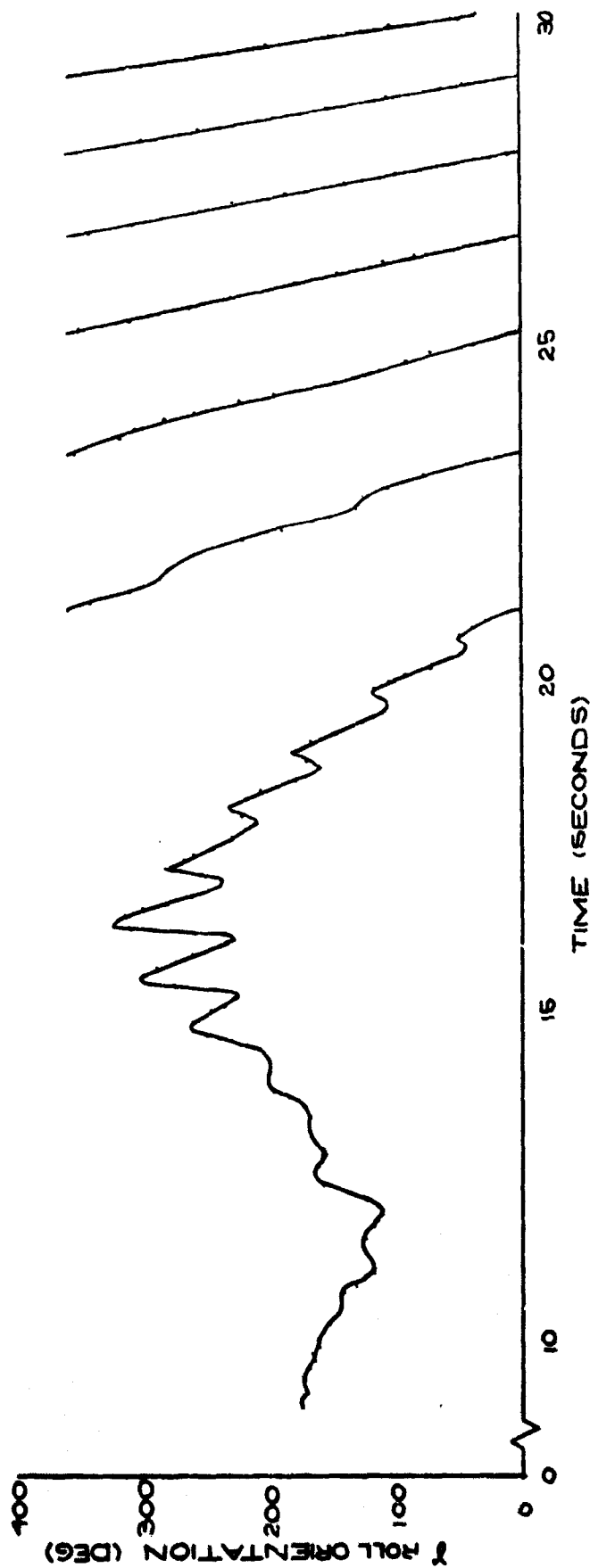


FIG. 32a ROLL ORIENTATION ANGLE VERSUS
TIME FROM RELEASE FOR
SPLIT-SKIRT BOMB (739)

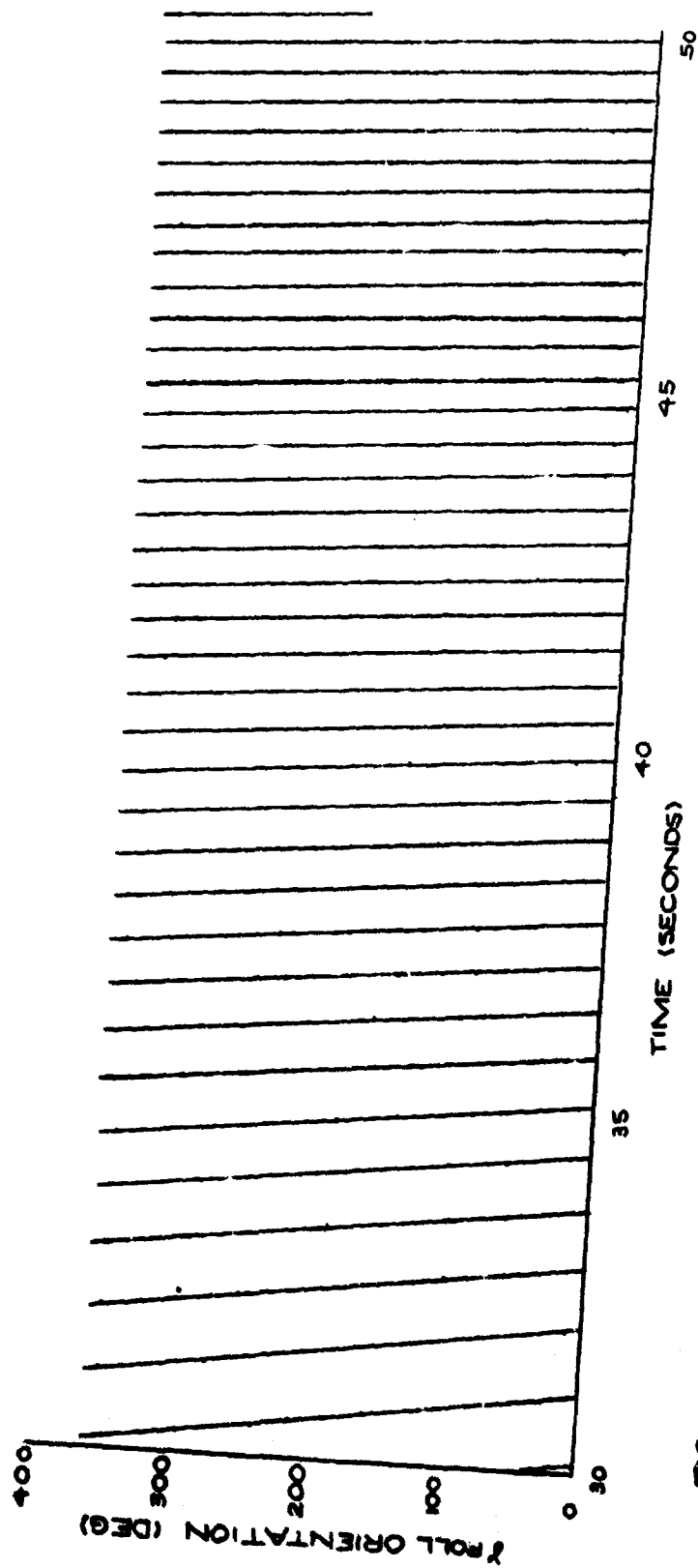


FIG. 32 b ROLL ORIENTATION ANGLE VERSUS
TIME FROM RELEASE FOR
SPLIT-SKIRT BOMB (739)

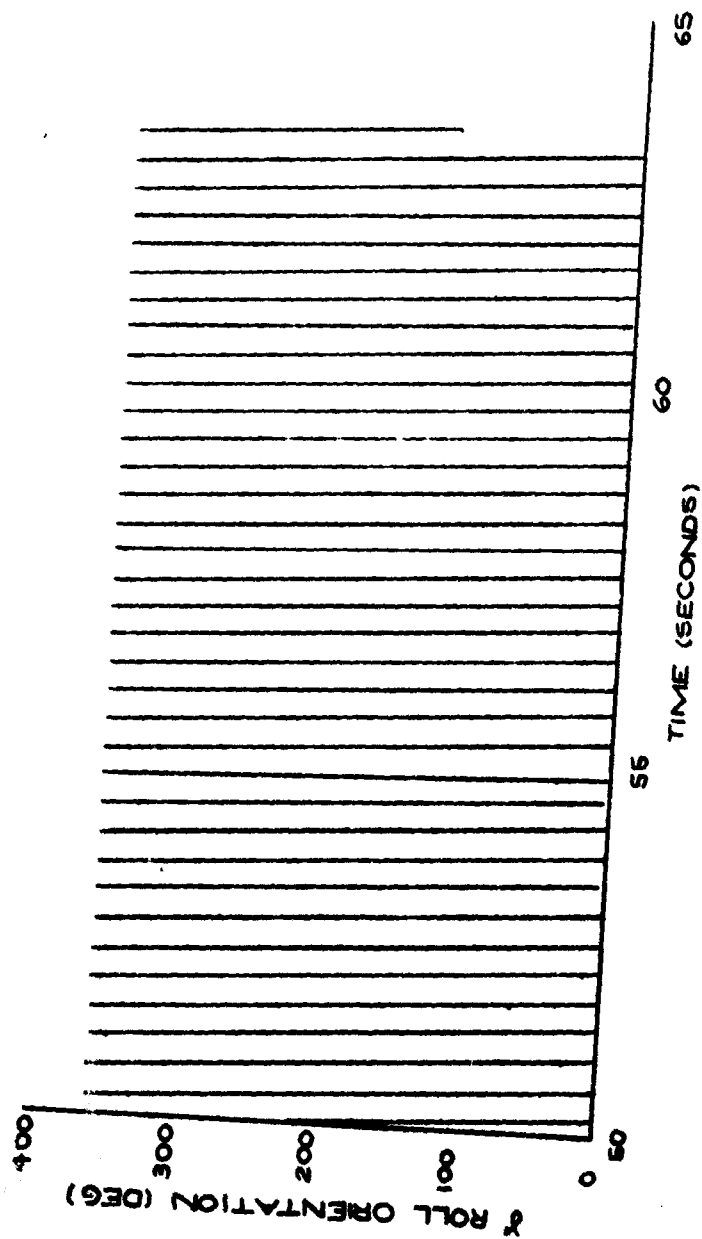


FIG-32C ROLL ORIENTATION ANGLE VERSUS
TIME FROM RELEASE FOR
SPLIT-SKIRT BOMB (739)

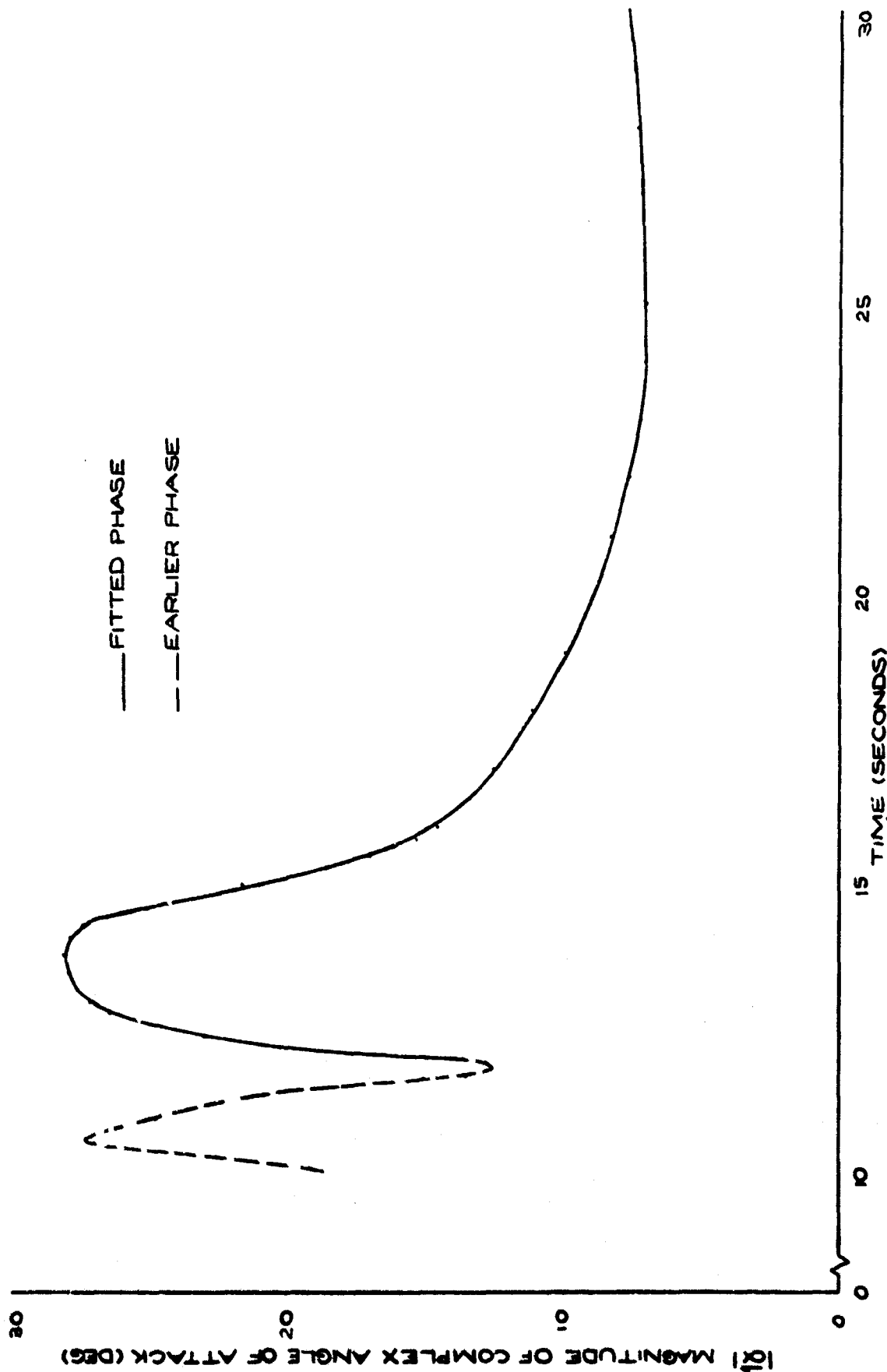


FIG. 33a MAGNITUDE OF COMPLEX ANGLE OF ATTACK (SMOOTHED)

VERSUS TIME FROM RELEASE FOR SPLIT-SKIRT BOMB (739)

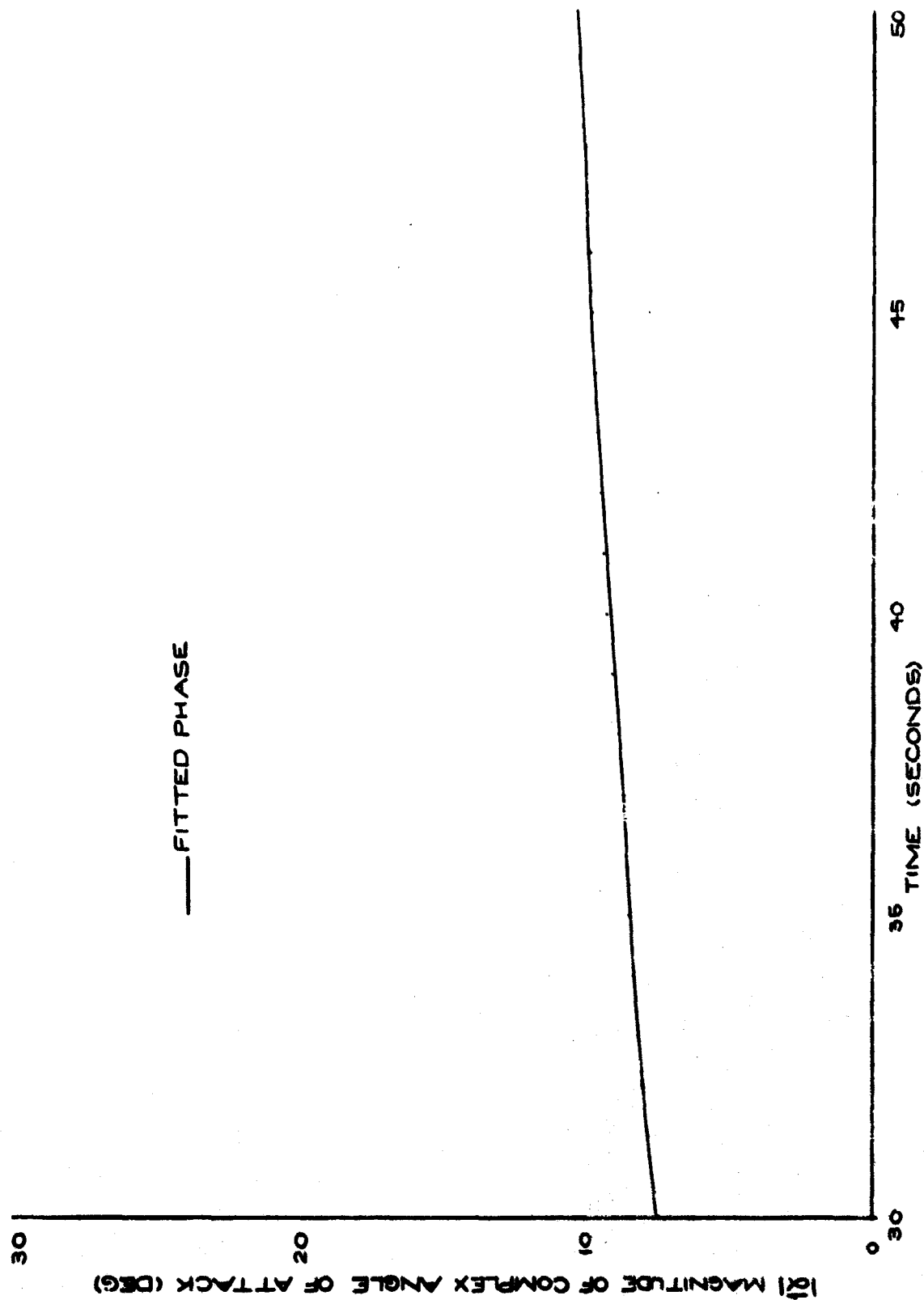


FIG. 38 b MAGNITUDE OF COMPLEX ANGLE OF ATTACK (SMOOTHED)
VERSUS TIME FROM RELEASE FC SPLIT-SKIRT BOMB (739)

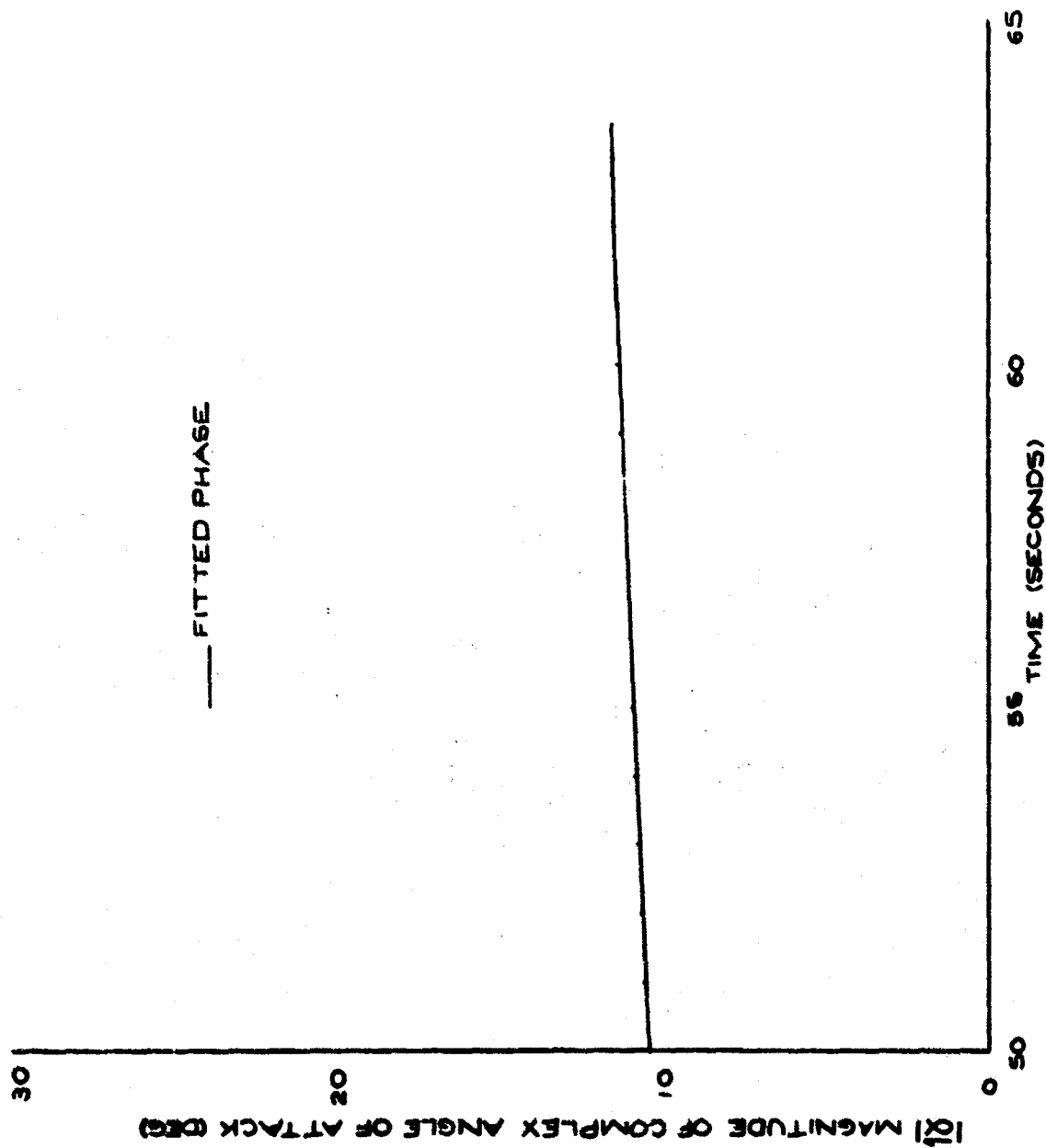


FIG. 33c MAGNITUDE OF COMPLEX ANGLE OF ATTACK (SMOOTHED)

VERSUS TIME FROM RELEASE FOR SPLIT-SKIRT BOMB (739)

seconds from release were attributed to the presence of the induced side moment during this time. Hence, the dynamic damping factors obtained from the fitting procedure from 12.05 seconds to 20.75 seconds from release are actually $\lambda_{N,p}^*$ of the Catastrophic Yaw Theory.

In order to apply the resulting equation of the Catastrophic Yaw Theory, Eq. (20), certain assumptions had to be made. Fig. 34 shows $C_{M\dot{\alpha}} + C_{M\dot{\beta}}$ as a function of time from release calculated from the linear theory from 16.7 seconds to 24.5 seconds and the extrapolated values. As seen from this figure, $C_{M\dot{\alpha}} + C_{M\dot{\beta}}$ was assumed constant from 20.75 seconds back to 12.05 seconds. Also, since λ_p was not extracted from the fitting procedure beyond 24.5 seconds from release, $C_{M\dot{\alpha}} + C_{M\dot{\beta}}$ was assumed constant from this point to the end of the flight. The linear theory, Eq. (23), yielded an essentially constant value of $C_{M\dot{\alpha}} + C_{M\dot{\beta}}$ from 20.75 seconds to 24.5 seconds from release. Thus, in extrapolating $C_{M\dot{\alpha}} + C_{M\dot{\beta}}$ on both sides of this time interval, the assumed value was found to be the same on each side, -49.3^{-1} . It is felt that this assumption of constant $C_{M\dot{\alpha}} + C_{M\dot{\beta}}$ was justified for two reasons: 1) the constant value obtained from the fitting procedure from 20.75 seconds to 24.5 seconds, and 2) the wind tunnel results¹⁷ show that, although the moment reference position is different than the free flight case, $C_{M\dot{\alpha}} + C_{M\dot{\beta}}$ varies very slightly in the Mach number range experienced in free flight. See Appendix III. Therefore, the pitch damping moment coefficient derivative was obtained as a function of time from release for the entire time of flight and is presented in Fig. 35. From the extrapolated values of $C_{M\dot{\alpha}} + C_{M\dot{\beta}}$ from 24.5 seconds to the end of the flight, the Precession Vector dynamic damping factor during this time period was calculated from Eq. (10), and is shown in Fig. 36 as a function of time from release. It is felt that the fact that these calculations yielded a curve which is continuous with the fitted values of λ_p at 24.5 seconds, and which follows the trend of the fitted values, enhances the justifications made in extrapolating the values of $C_{M\dot{\alpha}} + C_{M\dot{\beta}}$.

Another assumption was necessary concerning the Magnus moment coefficient derivative, $C_{M\dot{p}}$ in order to investigate the resonant phase of the flight. Fig. 37 shows the values of $C_{M\dot{p}}$ obtained from the linear theory, Eq. (24), for the portion of the flight from which λ_N and λ_p were extracted. These values are seen to increase sharply at 20.75 seconds from release. Thus, in order to facilitate investigation of induced side moment effects, $C_{M\dot{p}}$ was assumed constant, having a value of 13.5 rad^{-1} , from 12.05 seconds to 20.75 seconds from release. This extrapolation is shown in Fig. 37. From 24.5 seconds from release to the end of the flight, $C_{M\dot{p}}$ was calculated from Eq. (26) using the extrapolated values of $C_{M\dot{\alpha}} + C_{M\dot{\beta}}$. These results are shown in Fig. 38. Upon examination of Eq. (10) it was noted that a positive $C_{M\dot{p}}$ has a stabilizing effect on the precessional mode. Hence, after resonance, the already small magnitude of R_p was coupled with the increasing dynamic pressure and the stabilizing $C_{M\dot{p}}$ to cause the precessional mode to damp out halfway through the flight. On the other hand, the nutational mode, which is predominant after

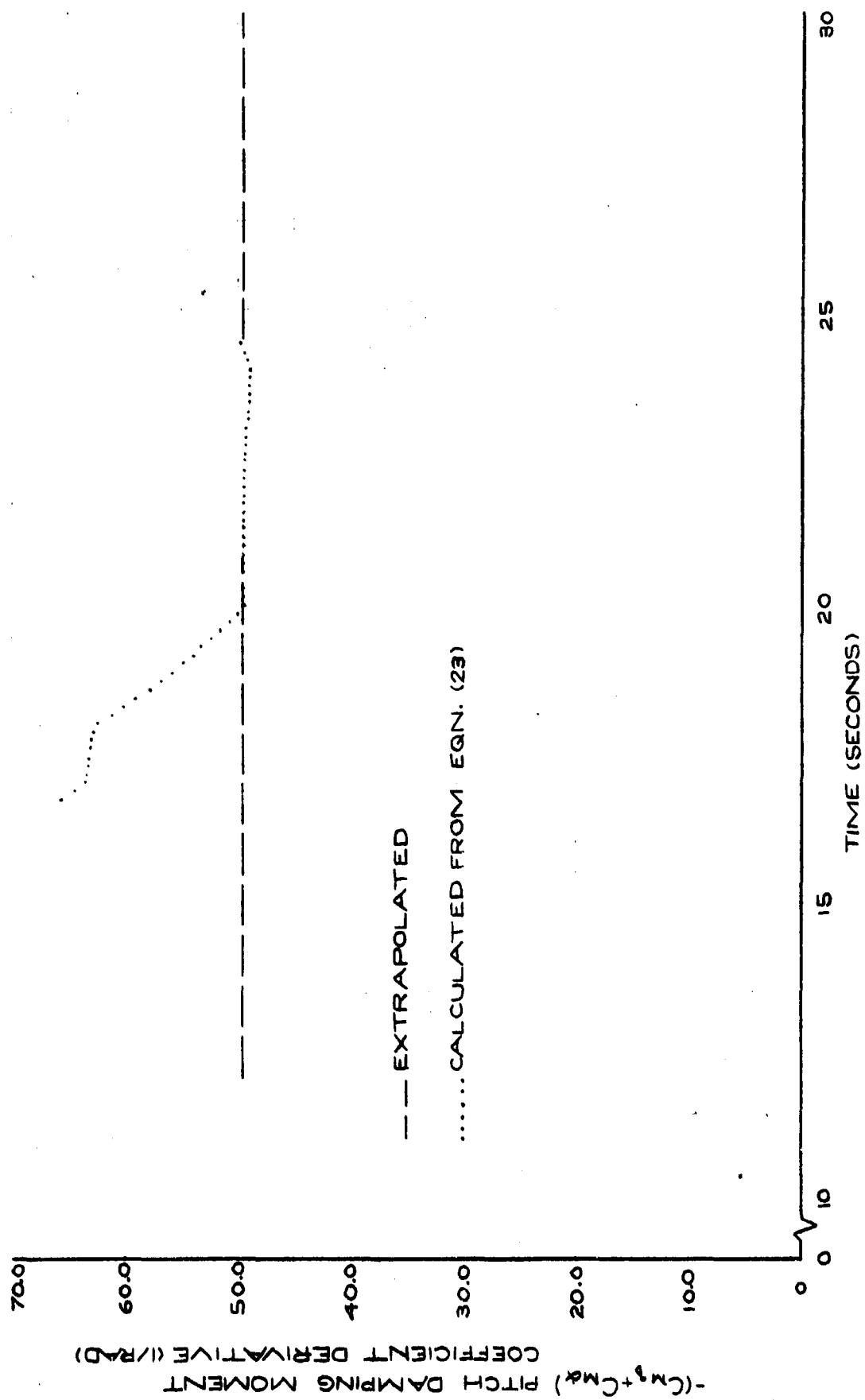


FIG. 34 PITCH DAMPING MOMENT COEFFICIENT
DERIVATIVE VERSUS TIME FROM
RELEASE FOR SPLIT-SKIRT BOMB (739)

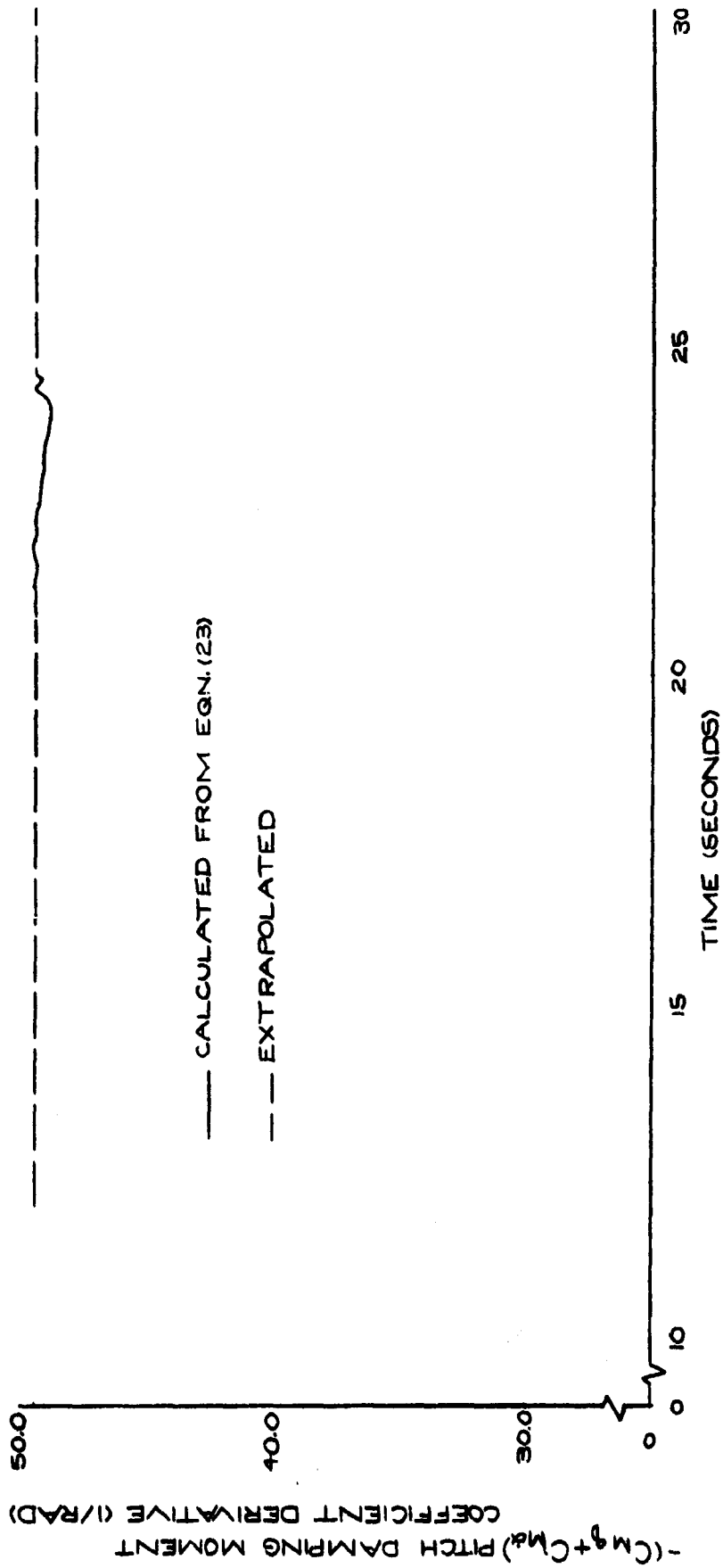


FIG. 35a PITCH DAMPING MOMENT COEFFICIENT
DERIVATIVE VERSUS TIME FROM
RELEASE FOR SPLIT-SKIRT BOMB (739)

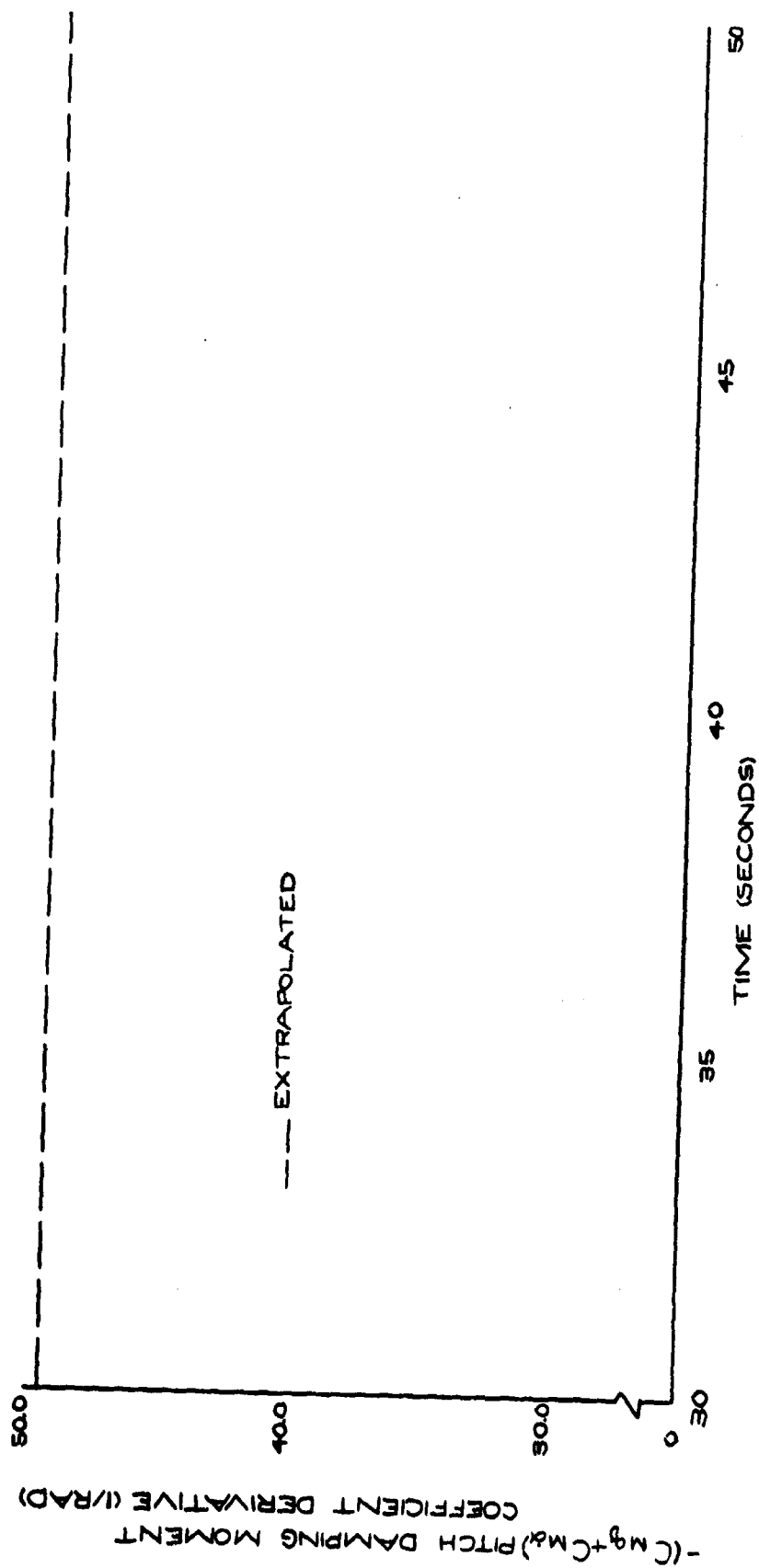


FIG. 35 b PITCH DAMPING MOMENT COEFFICIENT
DERIVATIVE VERSUS TIME FROM
RELEASE FOR SPLIT-SKIRT BOMB (739)

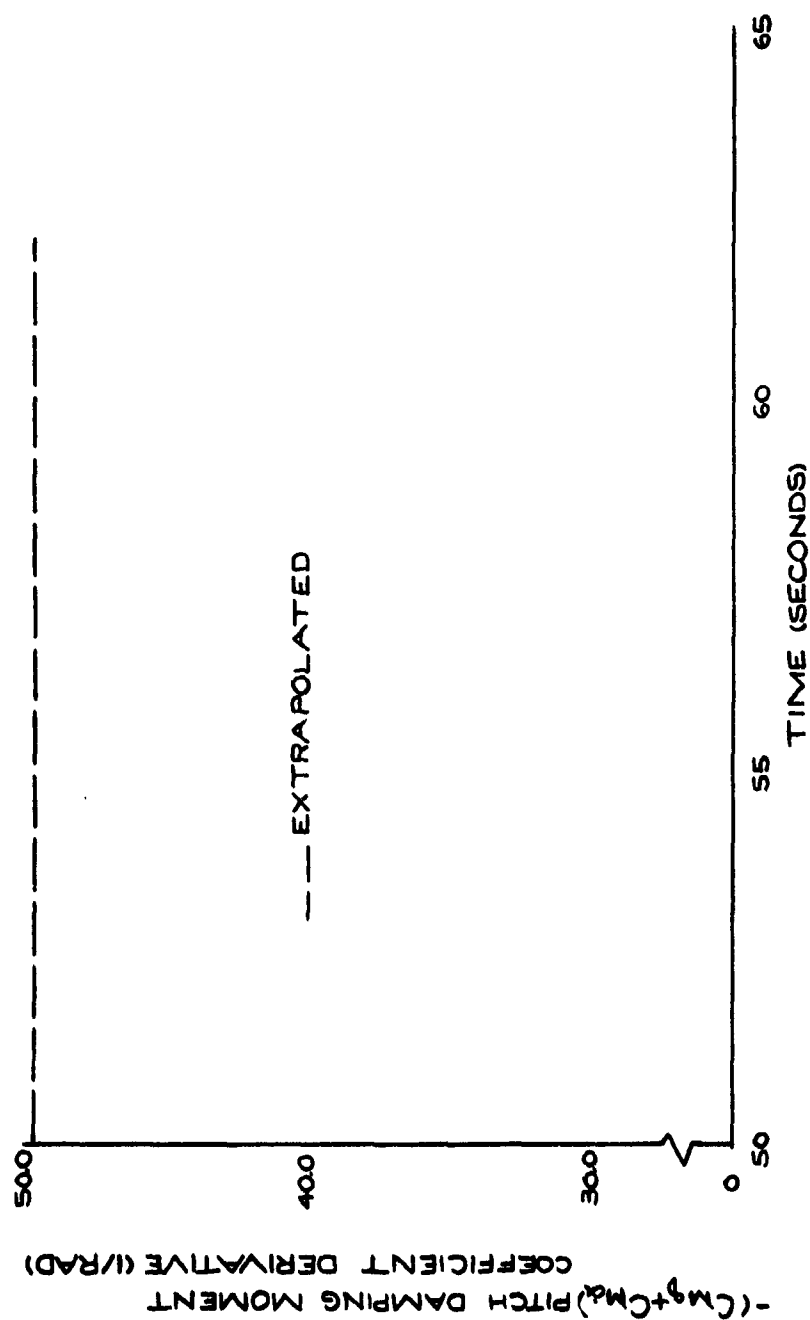


FIG 35c PITCH DAMPING MOMENT COEFFICIENT
DERIVATIVE VERSUS TIME FROM
RELEASE FOR SPLIT-SKIRT BOMB (739)

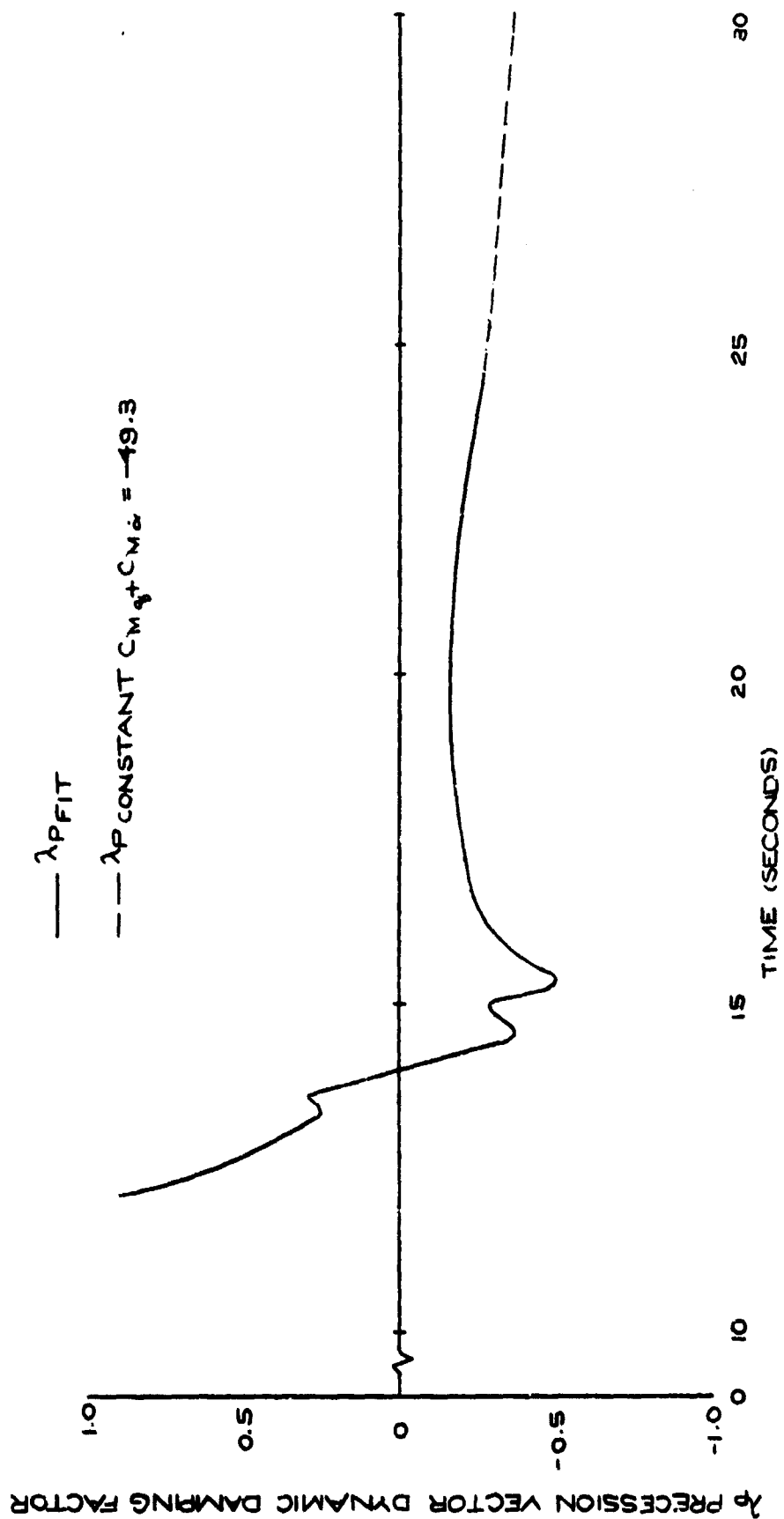


FIG. 36a PRECESSION VECTOR DYNAMIC DAMPING
FACTOR VERSUS TIME FROM RELEASE
FOR SPLIT-SKIRT BOMB (739)

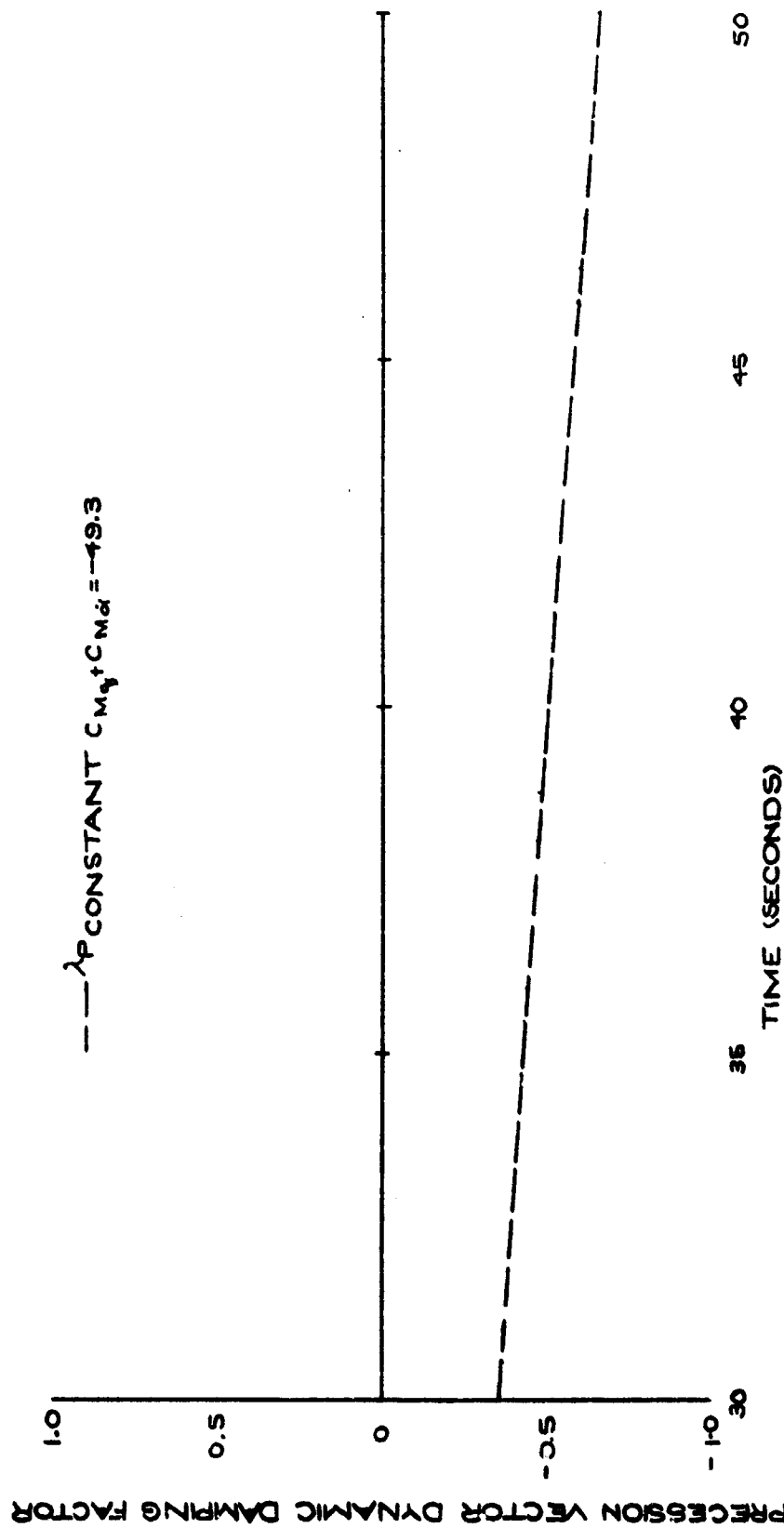


FIG. 36 b PRECESSION VECTOR DYNAMIC DAMPING
 FACTOR VERSUS TIME FROM RELEASE
 FOR SPLIT-SKIRT BOMB (739)

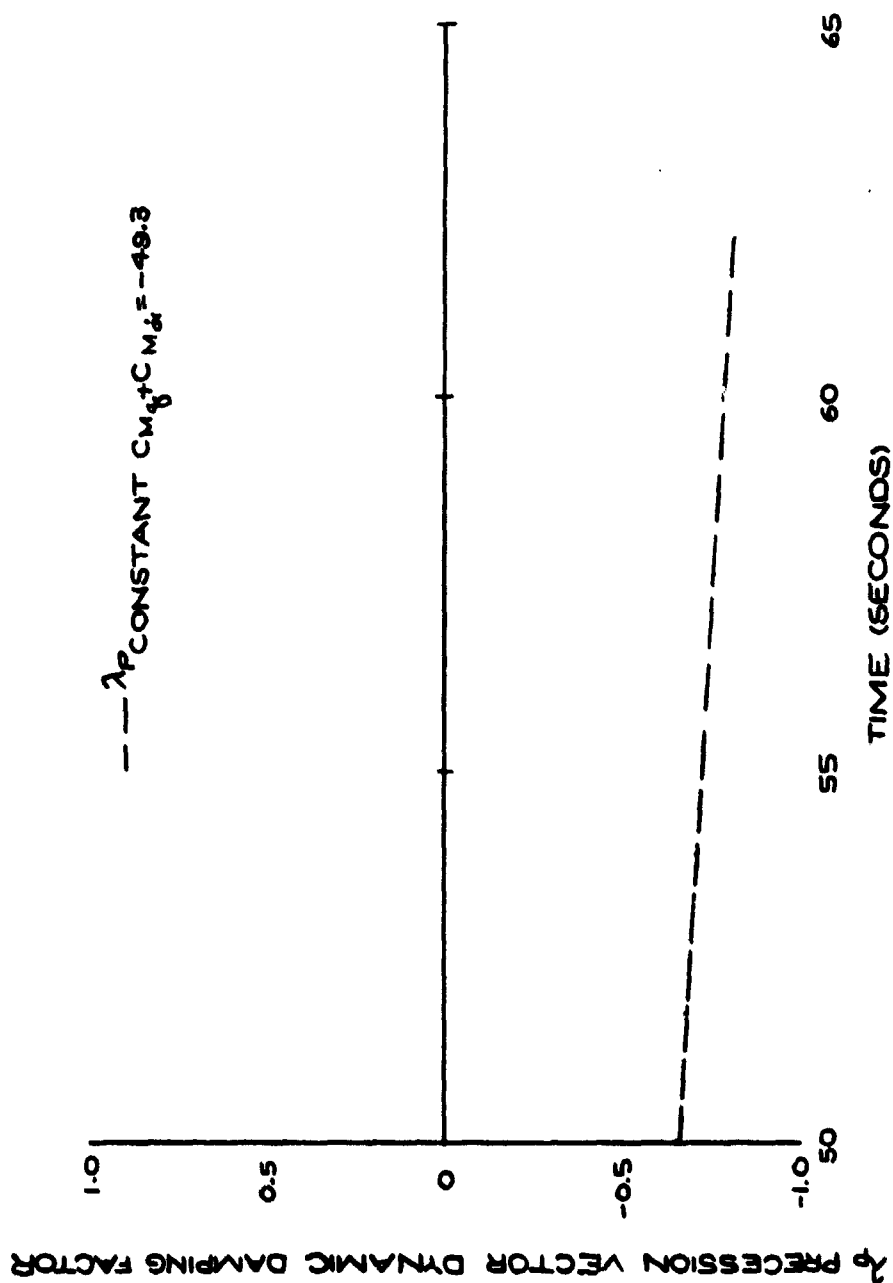


FIG. 36C PRECESSION VECTOR DYNAMIC DAMPING
FACTOR VERSUS TIME FROM RELEASE
FOR SPLIT-SKIRT BOMB (739)

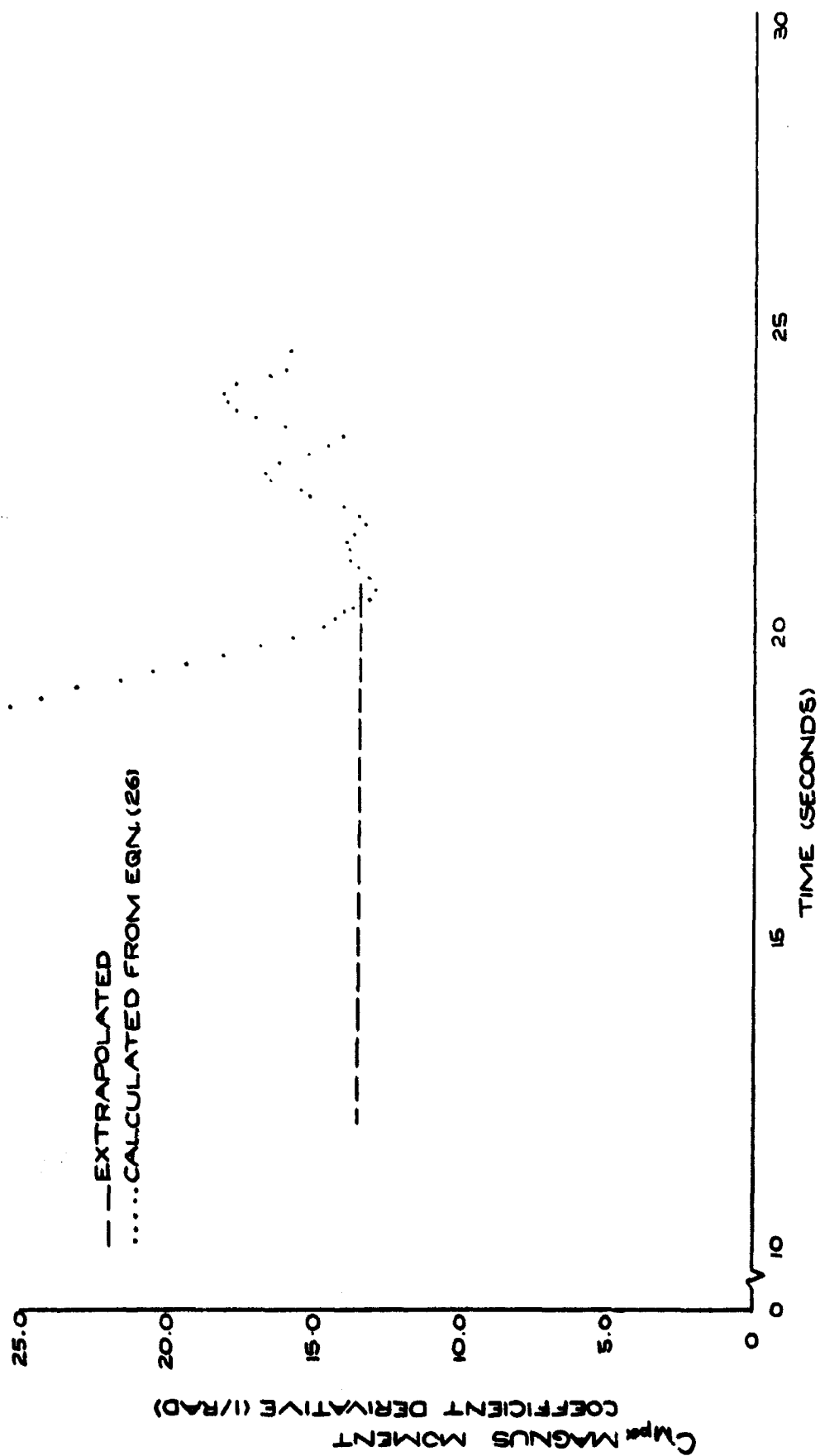


FIG. 37 MAGNUS MOMENT COEFFICIENT
DERIVATIVE VERSUS TIME FROM
RELEASE FOR SPLIT-SKIRT BOMB (739)

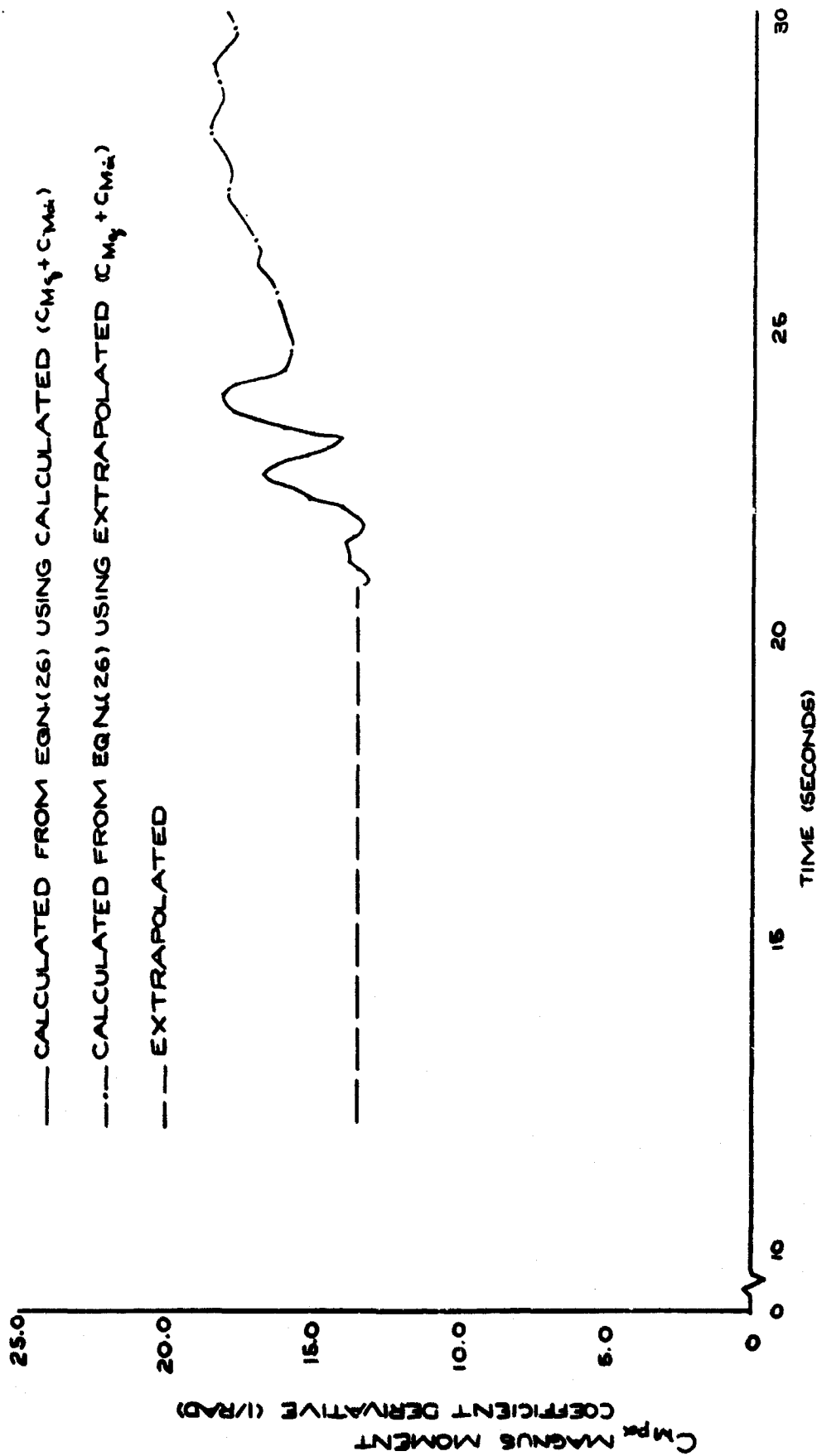


FIG. 38a MAGNUS MOMENT COEFFICIENT
DERIVATIVE VERSUS TIME FROM
RELEASE FOR SPLIT-SKIRT BOMB (739)

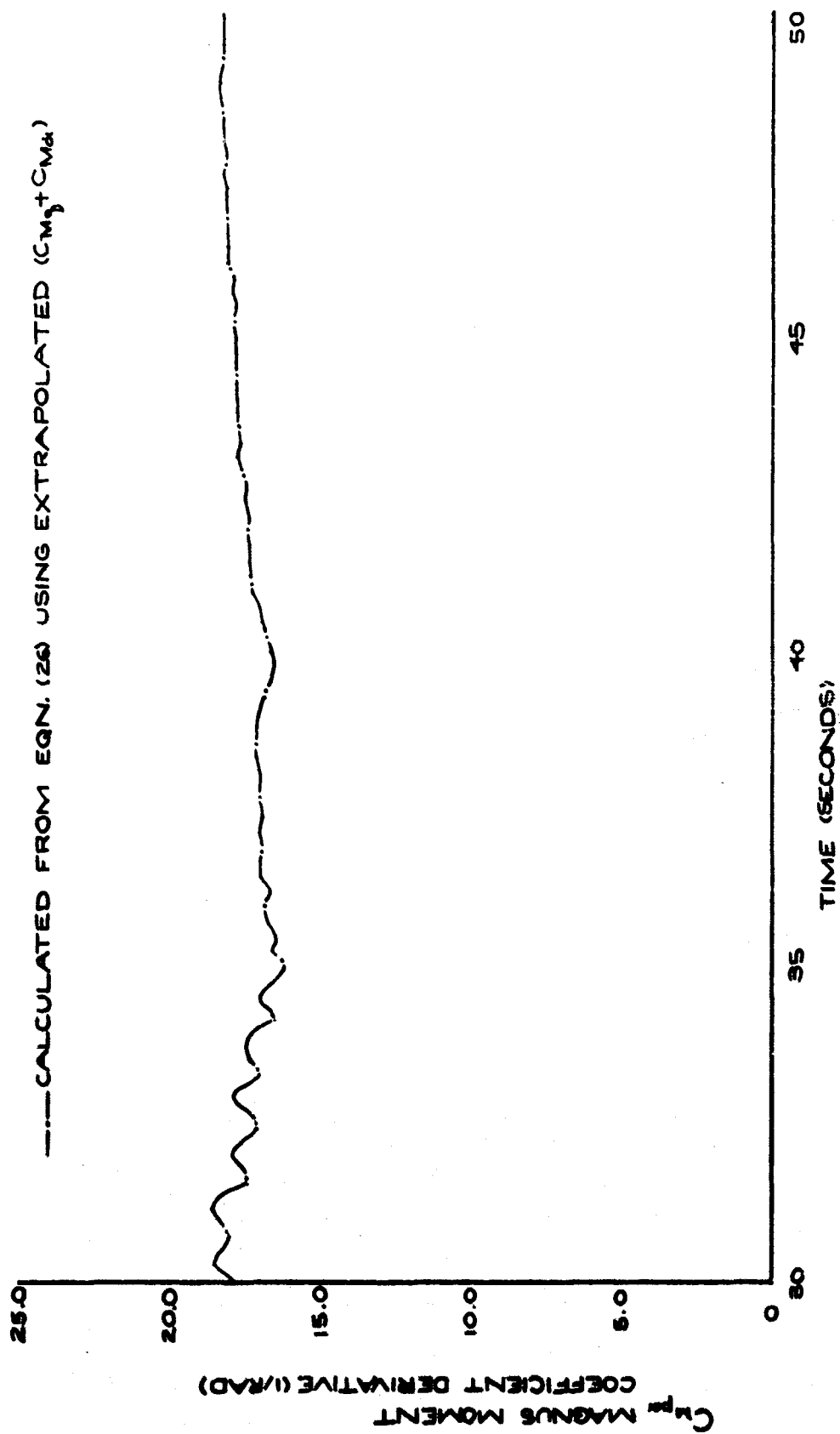


FIG. 38 b MAGNUS MOMENT COEFFICIENT
DERIVATIVE VERSUS TIME FROM
RELEASE FOR SPLIT-SKIRT BOMB (739)

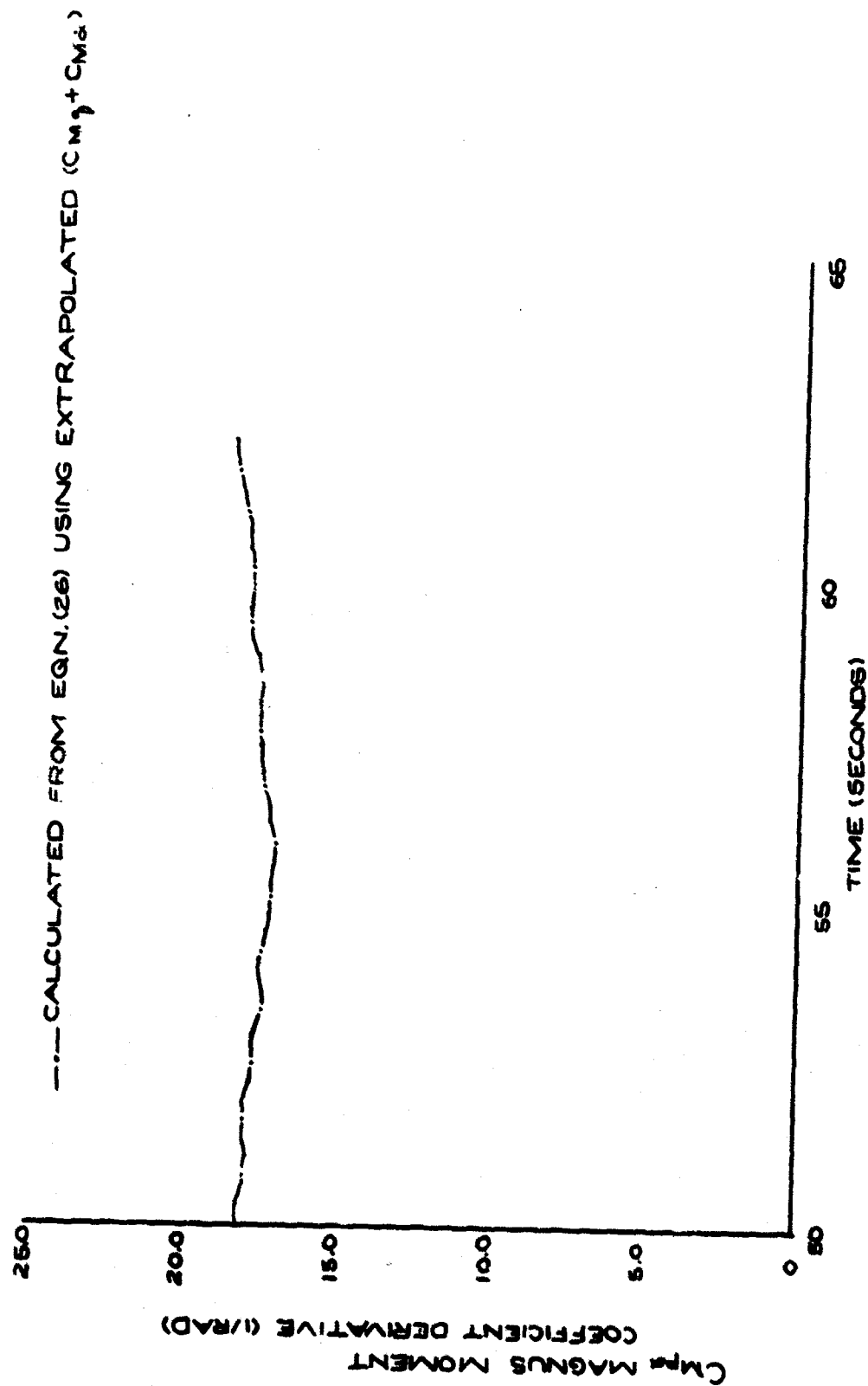


FIG. 38c MAGNUS MOMENT COEFFICIENT
DERIVATIVE VERSUS TIME FROM
RELEASE FOR SPLIT-SKIRT BOMB (739)

24.5 seconds, is destabilized by the positive Magnus term. It should be noted, however, that a positive $C_{M_{\dot{\alpha}}}$ does not necessarily imply an undamping of the Nutation Vector. The combination of parameters in the Magnus term of Eq. (10) must be larger in magnitude than the combination of parameters in the pitch damping term. In this case, this was indeed the situation. Hence, the cause of the undamped motion observed in the latter half of the flight may be attributed directly to a Magnus instability.

As soon as the values of $C_{M_{\dot{\alpha}}} + C_{M_{\dot{\beta}}}$ and $C_{M_{\dot{\gamma}}}$ were determined in the period from 12.05 seconds to 20.75 seconds from release, further investigation of the Catastrophic Yaw effects was made. Of primary interest are the dynamic damping factors during this time period, which are presented in Fig. 39. It should be noted that, since $C_{M_{\dot{\alpha}}} + C_{M_{\dot{\beta}}}$ is directly proportional to the mean of λ_N and λ_P , and inversely proportional to the dynamic pressure, the constant value of $C_{M_{\dot{\alpha}}} + C_{M_{\dot{\beta}}}$ was maintained as a result of the increasing value of Q . The fact that the observed Magnus instability was slight may also be attributed to the increasing value of Q . The values of the dynamic damping factors previous to 20.75 seconds are, adopting Nicolaides' notation, $\lambda_{N,P}^i$. Using the values of $C_{M_{\dot{\alpha}}} + C_{M_{\dot{\beta}}}$ and $C_{M_{\dot{\gamma}}}$ between 12.05 seconds and 20.75 seconds from release, the linear dynamic damping factors may be calculated from Eq. (10). These results are shown as a function of time in Fig. 40. Fig. 41 presents a complete picture of the effect of the induced side moment of the Catastrophic Yaw Theory on the dynamic damping factors.

Employing the results of Fig. 41 and Eqs. (28a) and (28b), where $\lambda_{N,P}^i$ corresponds to the linear dynamic damping factors, yielded the induced side moment term of Eq. (20) as a function of time from release as shown in Fig. 42. From Eq. (19b) and the pertinent trajectory parameters, the induced side moment derivative was calculated and is presented in Fig. 43. Eqs. (29a) and (29b) yielded $C_{M_{\dot{\gamma}}} \sin 4\gamma$, which is shown in Fig. 44 as a function of time from release.

It is immediately obvious from the results of Figs. 42, 43, and 44 that the calculations from the nutational and precessional modes do not yield the same results. This is a direct result of the asymmetry of the dynamic damping factors as seen in Fig. 41. Of the two results obtained, it is felt that the calculations involving the nutational mode are more indicative of the actual phenomena for two reasons: 1) the accuracy to which the Nutation Vector dynamic damping factor was determined was significantly greater than that of the precessional mode, and 2) the cause of the termination of the fitting routine at 12.05 seconds was due to the inability of the iteration procedure to converge to a value of $|K_P|$ and λ_P . As can be seen from Fig. 41, the Precession Vector dynamic damping factor starts to decrease at 13.6 seconds but reverses direction at 13.35 seconds and becomes indeterminate at 12.05 seconds. An average value of $C_{M_{\dot{\gamma}}} \sin 4\gamma$ was calculated from values obtained from the nutational and precessional modes. For the

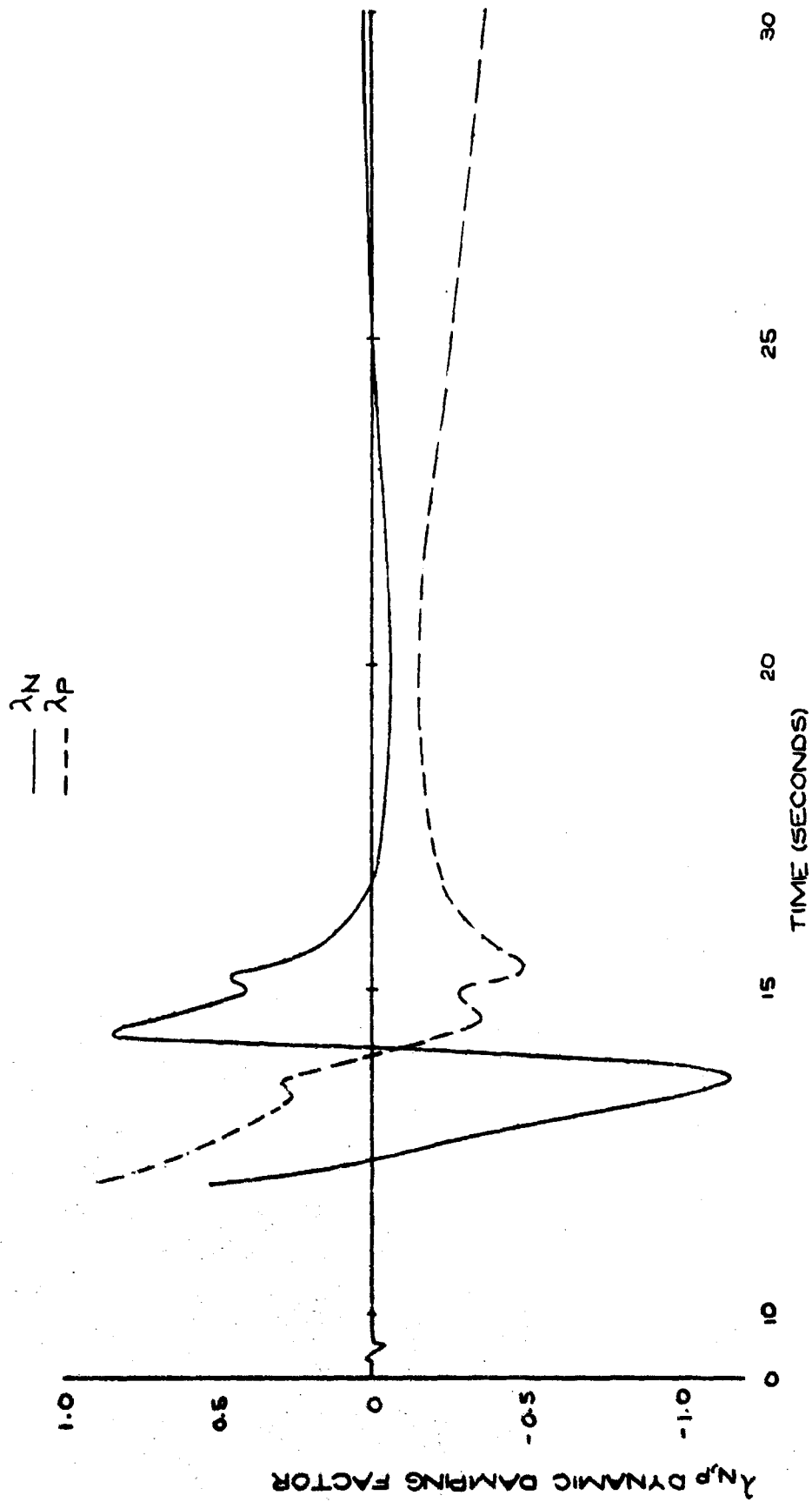


FIG. 39a DYNAMIC DAMPING FACTORS VERSUS
TIME FROM RELEASE FOR
SPLIT-SKIRT BOMB (739)

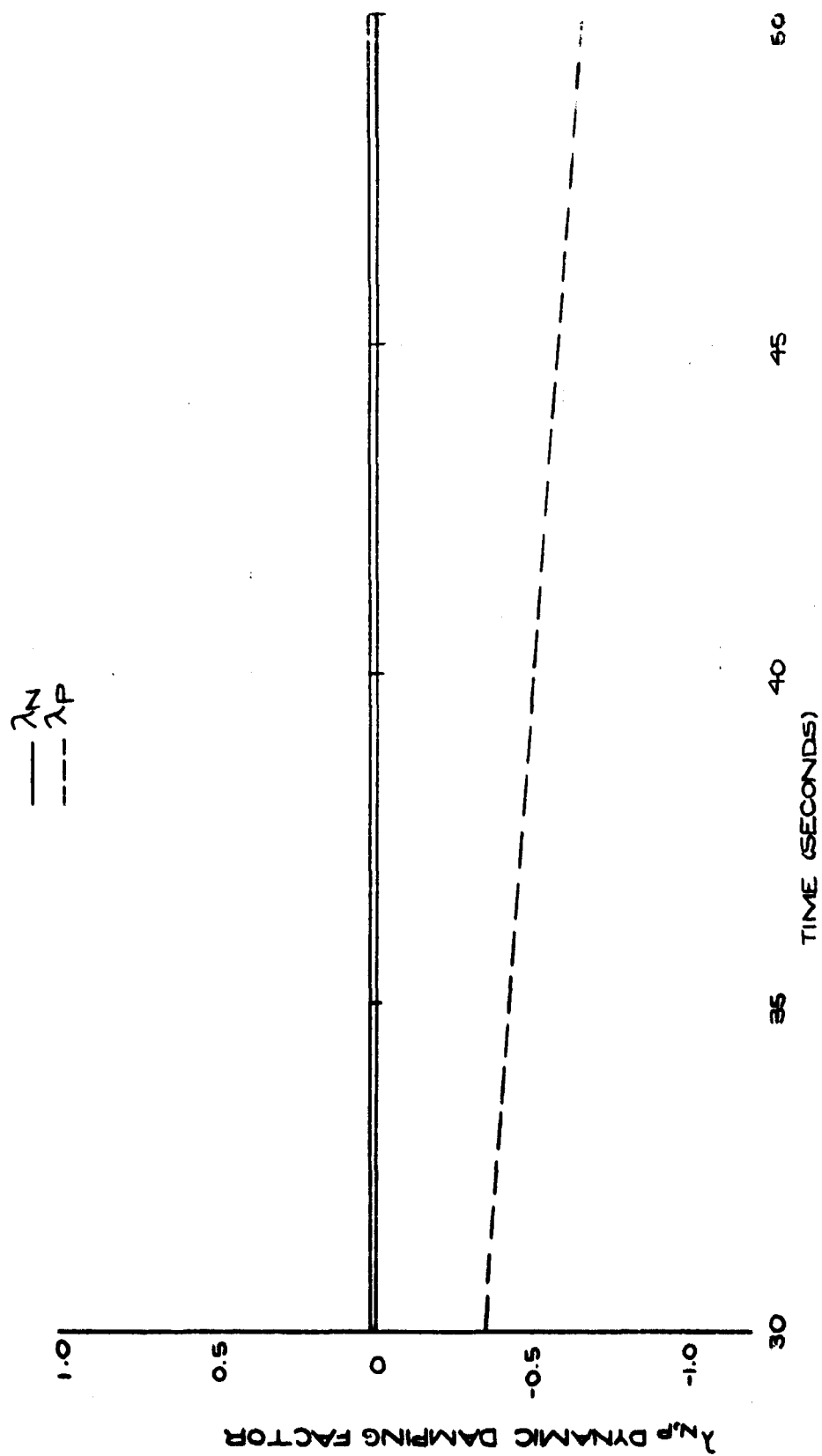


FIG 29 b DYNAMIC DAMPING FACTORS VERSUS
TIME FROM RELEASE FOR
SPLIT-SKIRT BOMB (739)

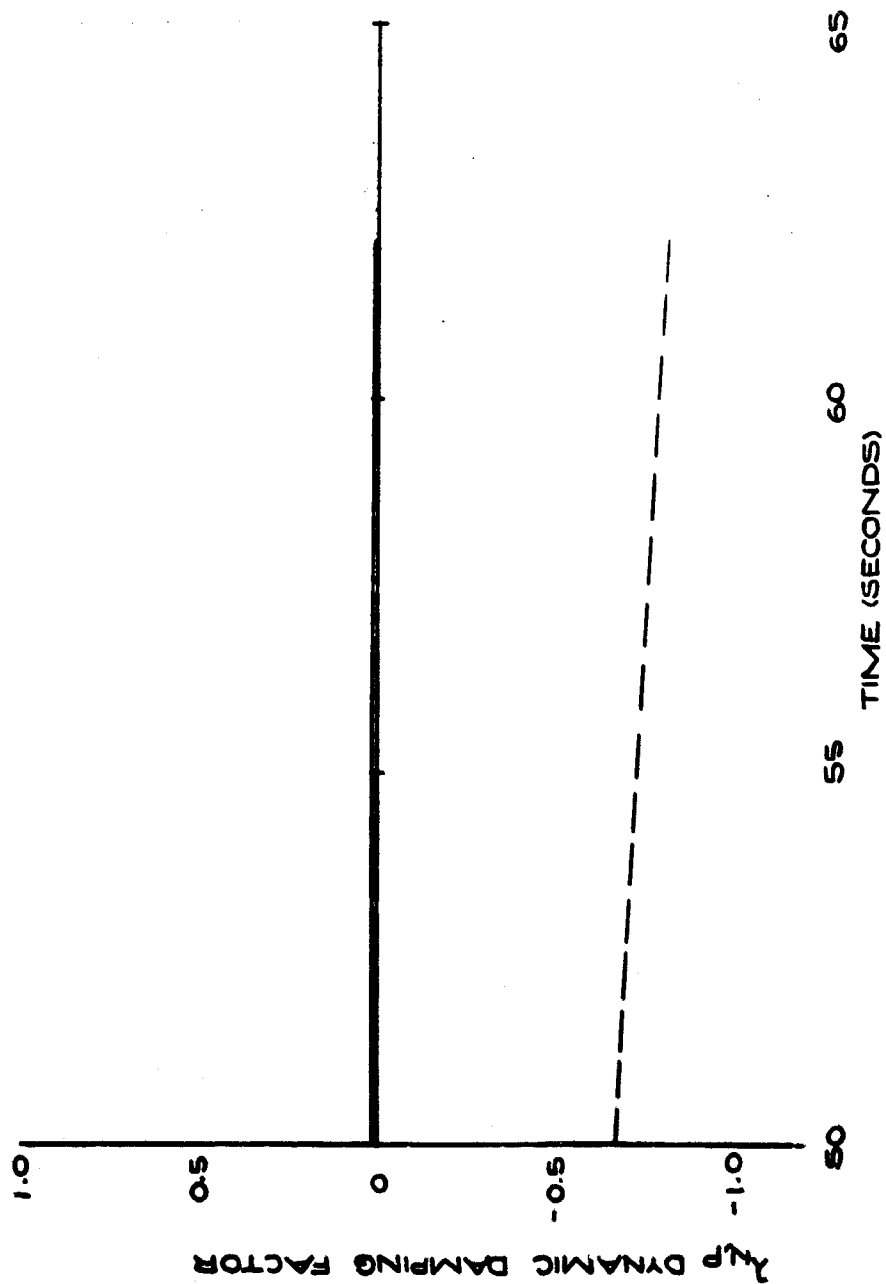


FIG. 39c DYNAMIC DAMPING FACTORS VERSUS
TIME FROM RELEASE FOR
SPLIT-SKIRT BOMB (739)

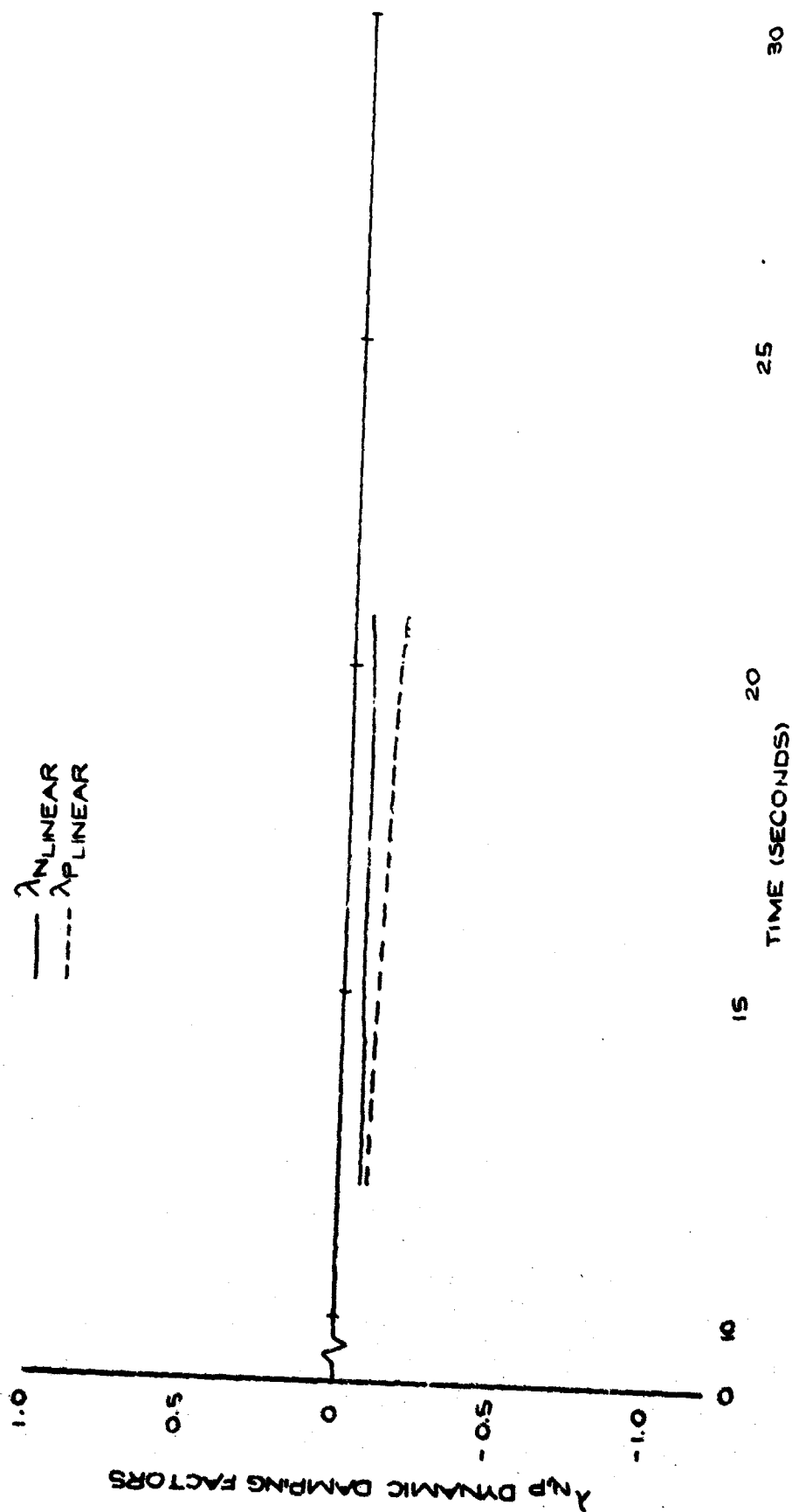


FIG. 40 DYNAMIC DAMPING FACTORS VERSUS
TIME FROM RELEASE FOR
SPLIT-SKIRT BOMB (739)

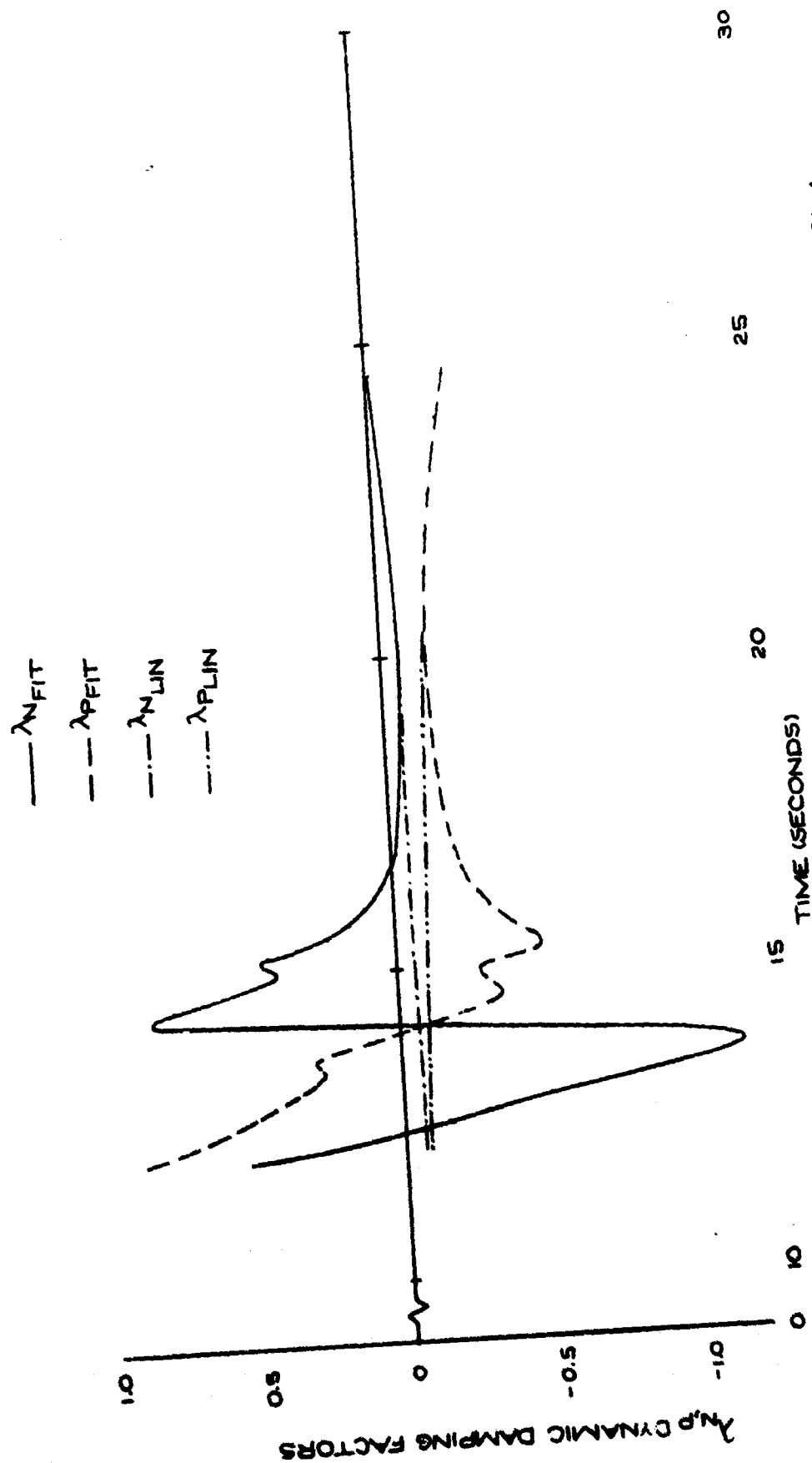


FIG 41 DYNAMIC DAMPING FACTORS VERSUS TIME FROM
RELEASE FOR SPLIT-SKIRT BOMB (739)

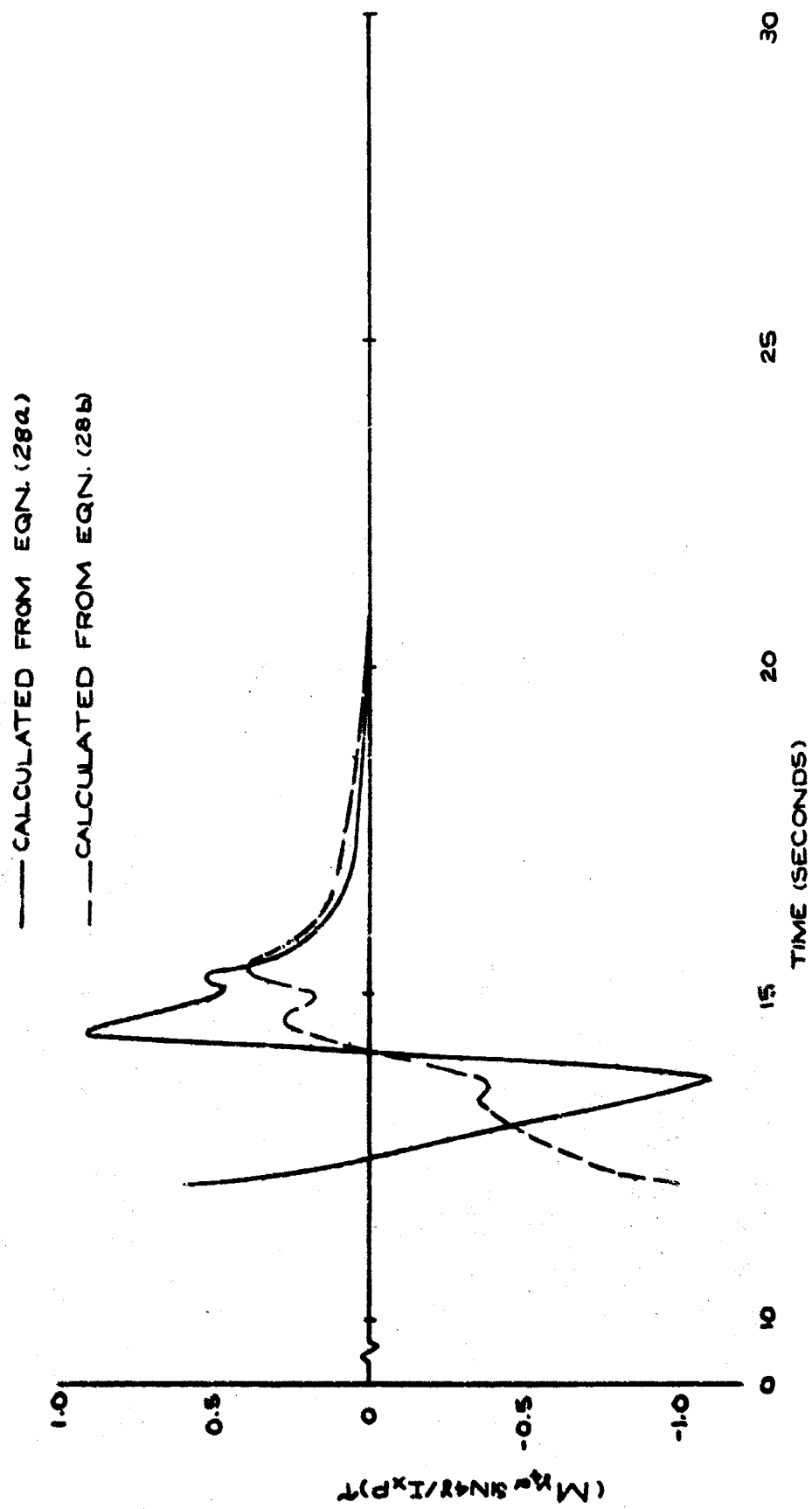


FIG. 42 INDUCED SIDE MOMENT TERM VERSUS TIME
 FROM RELEASE FOR SPLIT-SKIRT BOMB (739)

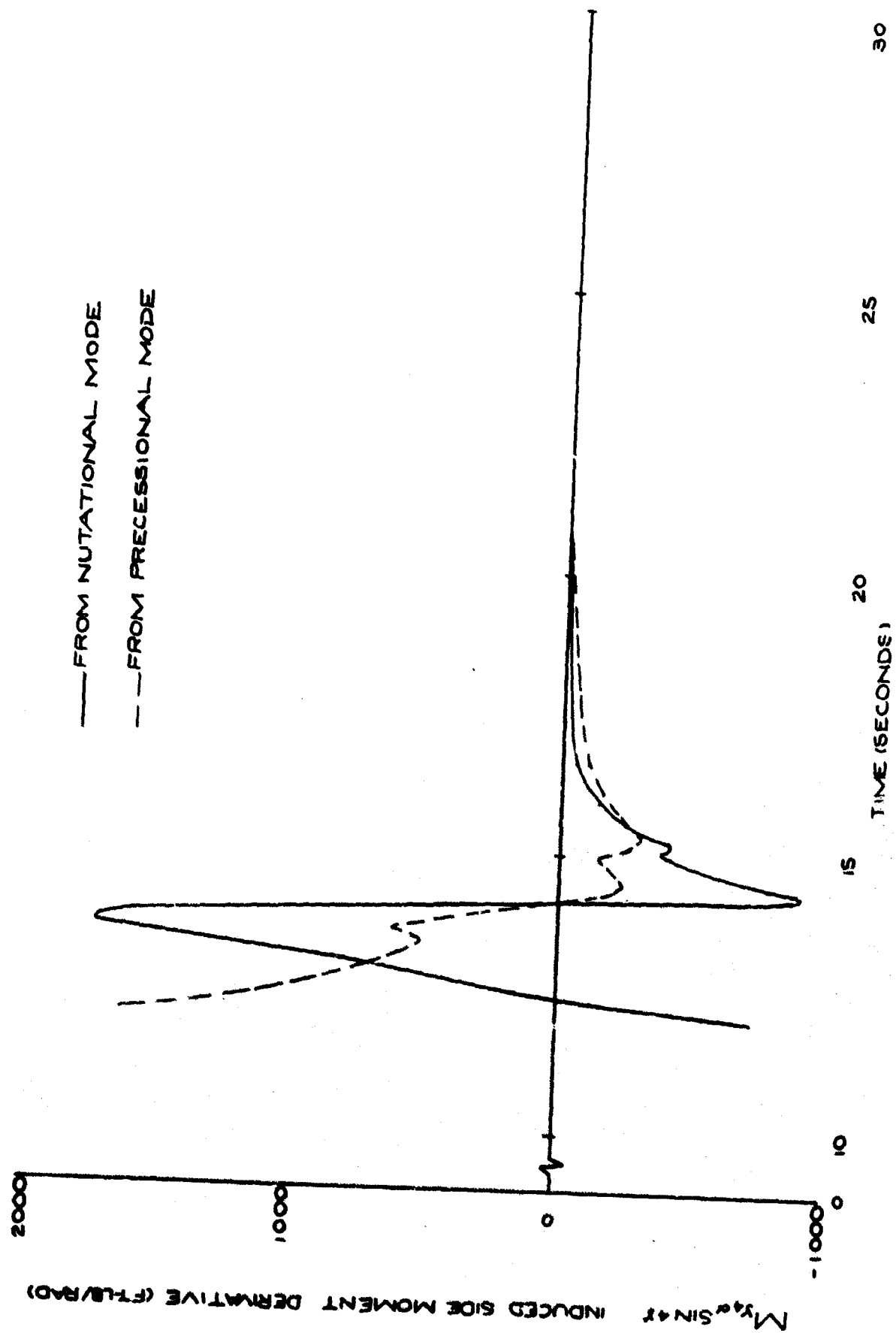


FIG. 43 INDUCED SIDE MOMENT DERIVATIVE VERSUS TIME
 FROM RELEASE FOR SPLIT-SKIRT BOMB (739)

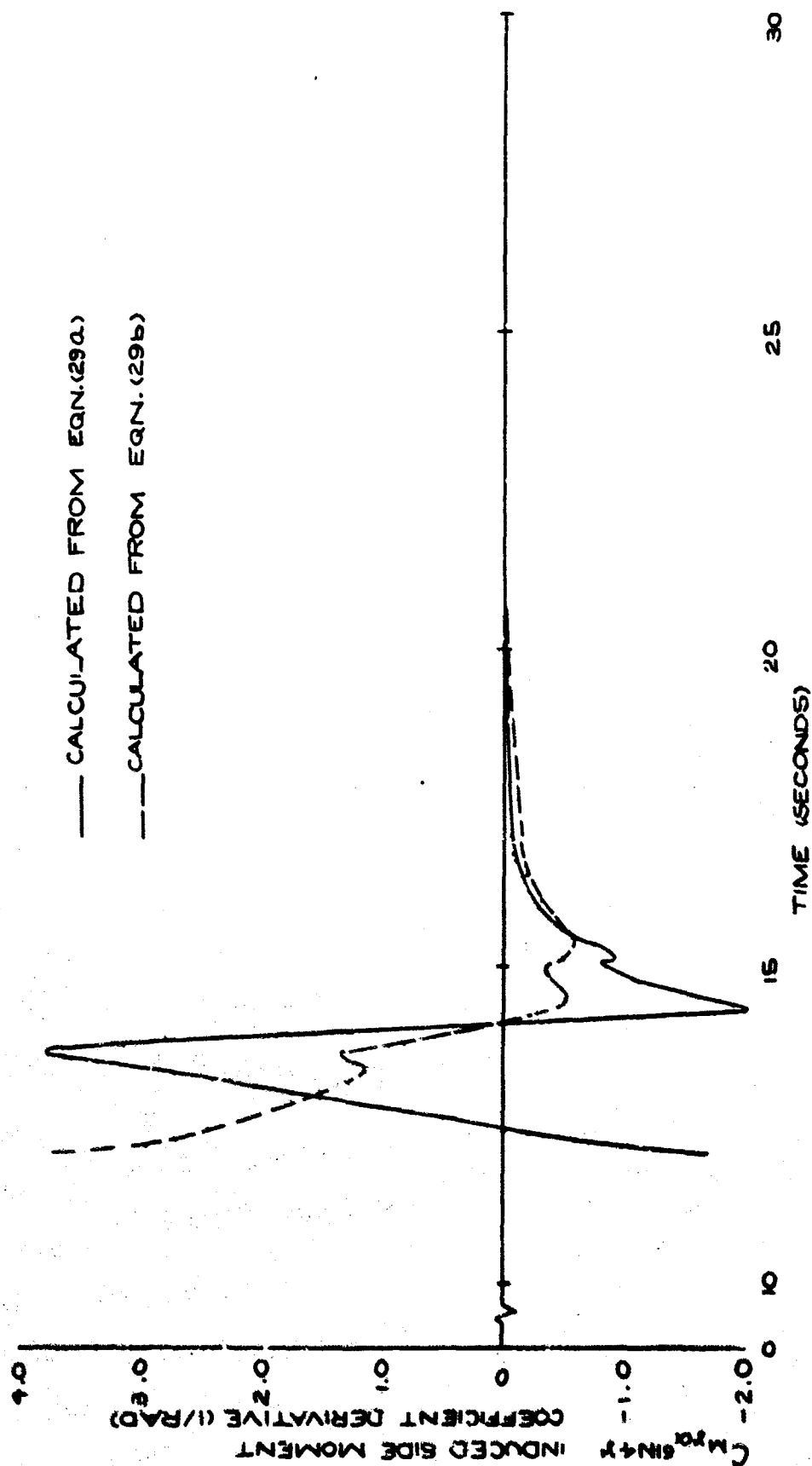


FIG. 44 INDUCED SIDE MOMENT COEFFICIENT DERIVATIVE
 VERSUS TIME FROM RELEASE FOR SPLIT-SKIRT BOMB (739)

reasons mentioned above, the average value is not felt to yield better results than the value obtained from the nutational mode. For completeness, however, the average value is presented in Fig. 45 as a function of time from release.

In order to investigate the induced side moment coefficient as a function of roll orientation, it was necessary to smooth out the oscillations in the roll orientation as a function of time from release curve, Fig. 32. The smoothed curve is shown in Fig. 45. Since γ , $C_{M_{\gamma}} \sin 4\gamma$, and $M_{\gamma} \sin 4\gamma$ are known as a function of time from release, cross-plotting yielded $C_{M_{\gamma}} \sin 4\gamma$ and $M_{\gamma} \sin 4\gamma$ as a function of γ as shown in Figs. 47 and 48. Again the most reliable result is felt to be that obtained from the nutational mode. It was noted that there is an obvious phase difference between the resulting curves and the theoretical curves. The theory predicts that the period be $\pi/2$ and that $C_{M_{\gamma}} \sin 4\gamma$ and $M_{\gamma} \sin 4\gamma$ have zero magnitude at 180° and 270° . Comparison with wind tunnel results¹⁶, however, shows that the period observed was also larger than $\pi/2$.

Non-Linearities in Stability Derivatives

For Round 739, Reynolds number, Mach number, and angle of attack were varying simultaneously. Due to non-linear effects, it was not possible, however, to determine the exact functional relationships of the stability derivative to these parameters without an analysis of numerous free flight rounds.

Angle of attack variations are large, from 7° to 28° , in the early portion of the flight while small variations, from 7° to 12° , occur during the last 40 seconds. Reynolds number also varied considerably, ranging from 13×10^6 at the beginning of the flight to 62×10^6 at the end. Mach number, on the other hand, experienced a relatively small variation, from 0.75 to 0.95. It should be noted, however, that a large portion of the flight was in critical range of Mach numbers, from 0.90 to 0.95. Since none of the free flight parameters may be assumed to be essentially constant, the difficulty of determination of relationships was not decreased.

Fig. 49 presents $C_{M_{\alpha}}$ as a function of angle of attack and Mach number. Substantial increases in magnitude can be seen to occur with increasing angle of attack. Also, $C_{M_{\alpha}}$ appears to be non-linear with respect to Mach number, even though the change in Mach number is small. It should be noted that since the fitting procedure obtains the stability parameter ω_{nd} from which $C_{M_{\alpha}}$ is calculated, by fitting over a prescribed number of cycles of data, the angles of attack used for this analysis are obtained by averaging the angle of attack over the number of cycles fitted. Referring to Figs. 30 and 33, it can be seen why the variations were observed in $C_{M_{\alpha}}$ as a function of time. $C_{M_{\alpha}}$ increased when angle of attack was increasing

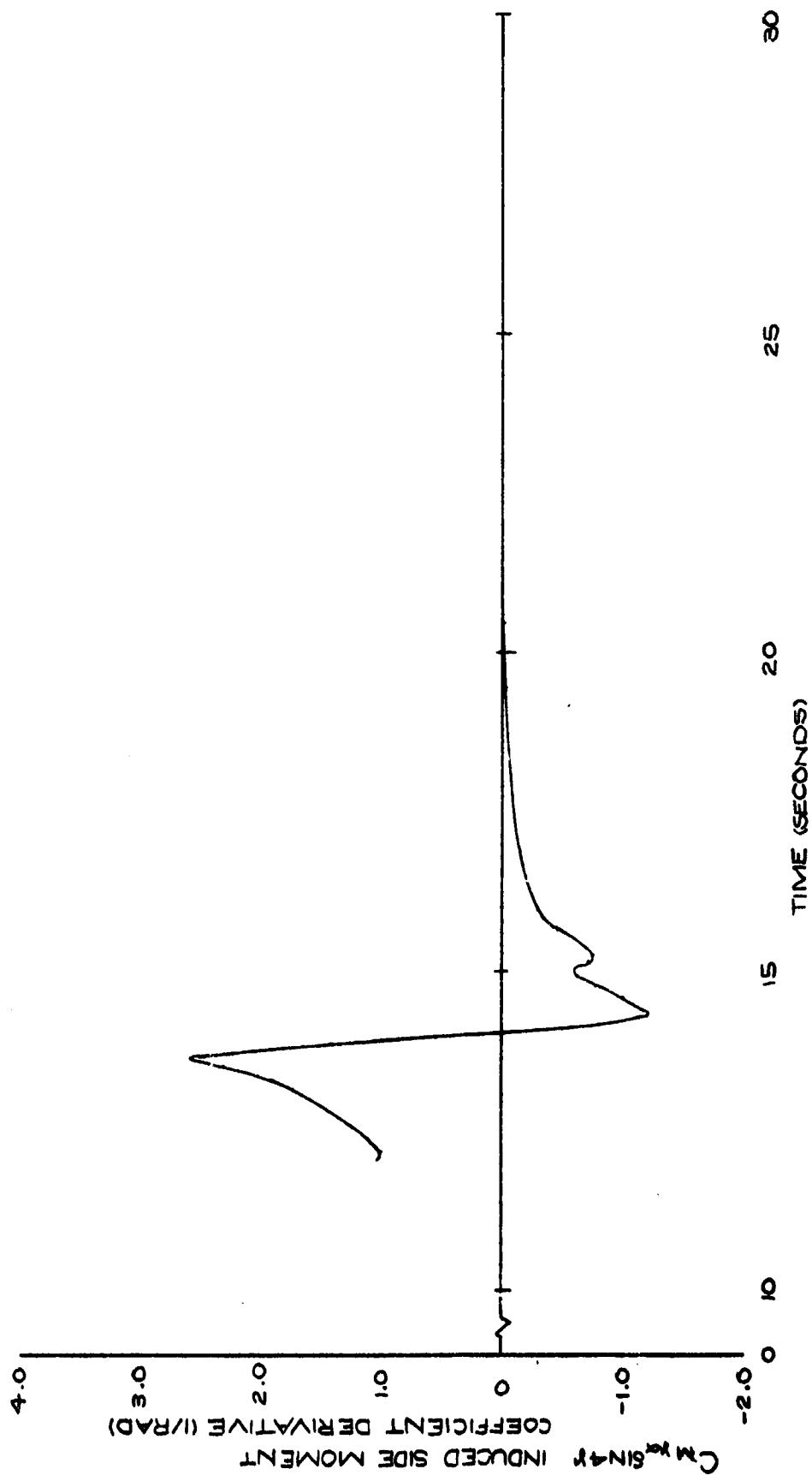


FIG. 45 INDUCED SIDE MOMENT COEFFICIENT DERIVATIVE
VERSUS TIME FROM RELEASE FOR SPLIT-SKIRT BOMB (739)

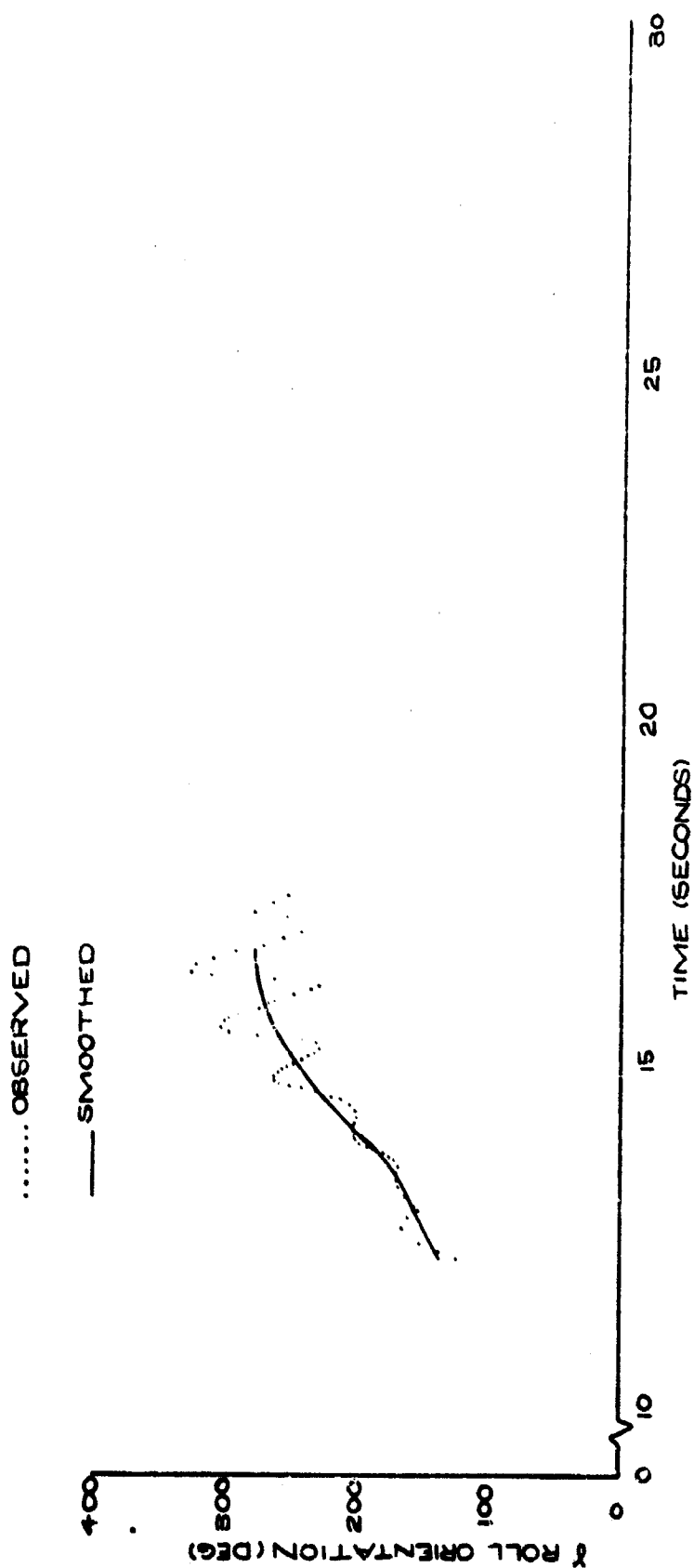


FIG 46 ROLL ORIENTATION ANGLE VERSUS
TIME FROM RELEASE FOR
SPLIT-SKIRT BOMB (739)

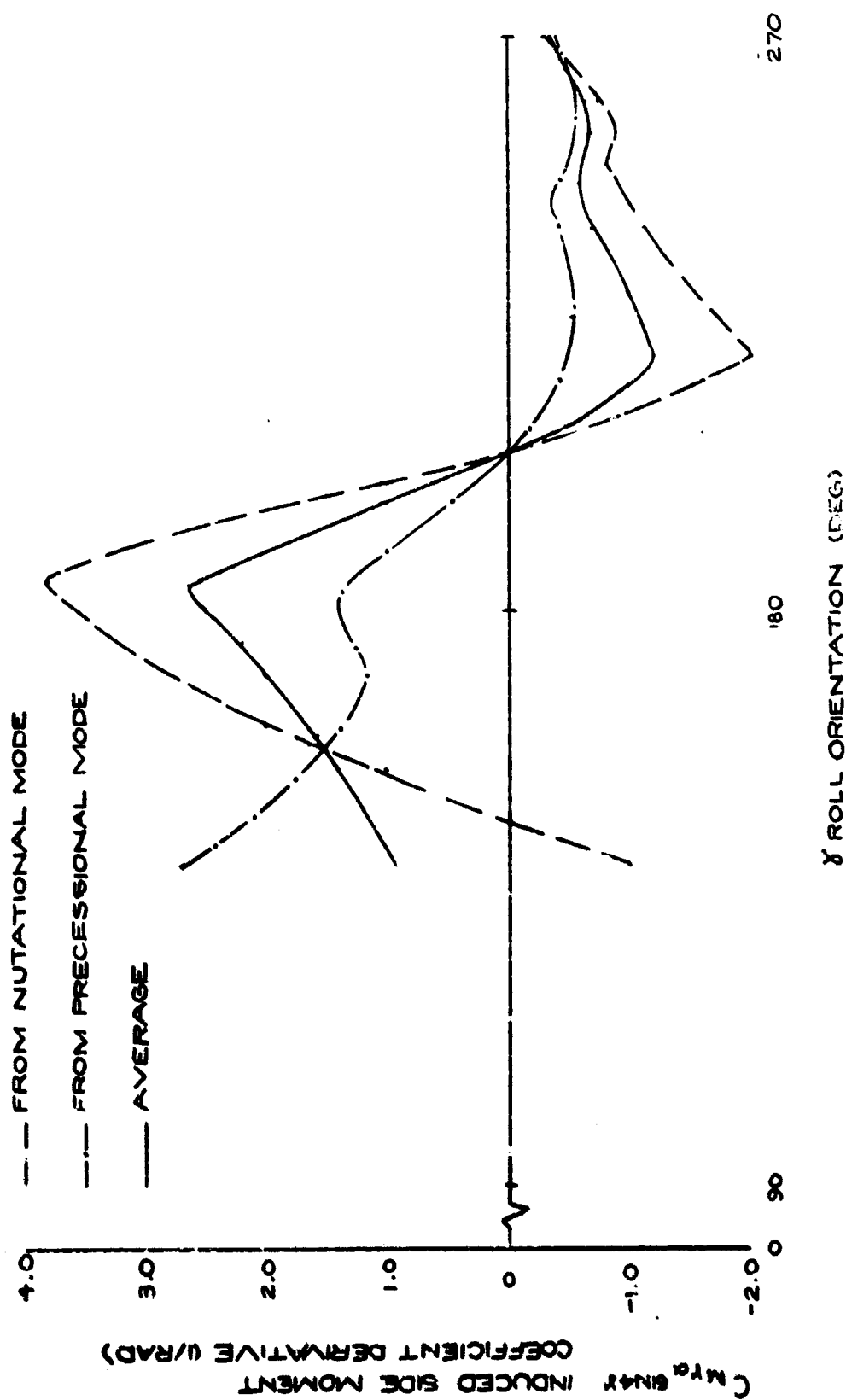


FIG. 47 INDUCED SIDE MOMENT COEFFICIENT DERIVATIVE VERSUS
ROLL ORIENTATION ANGLE FOR SPLIT-SKIRT BOMB (739)

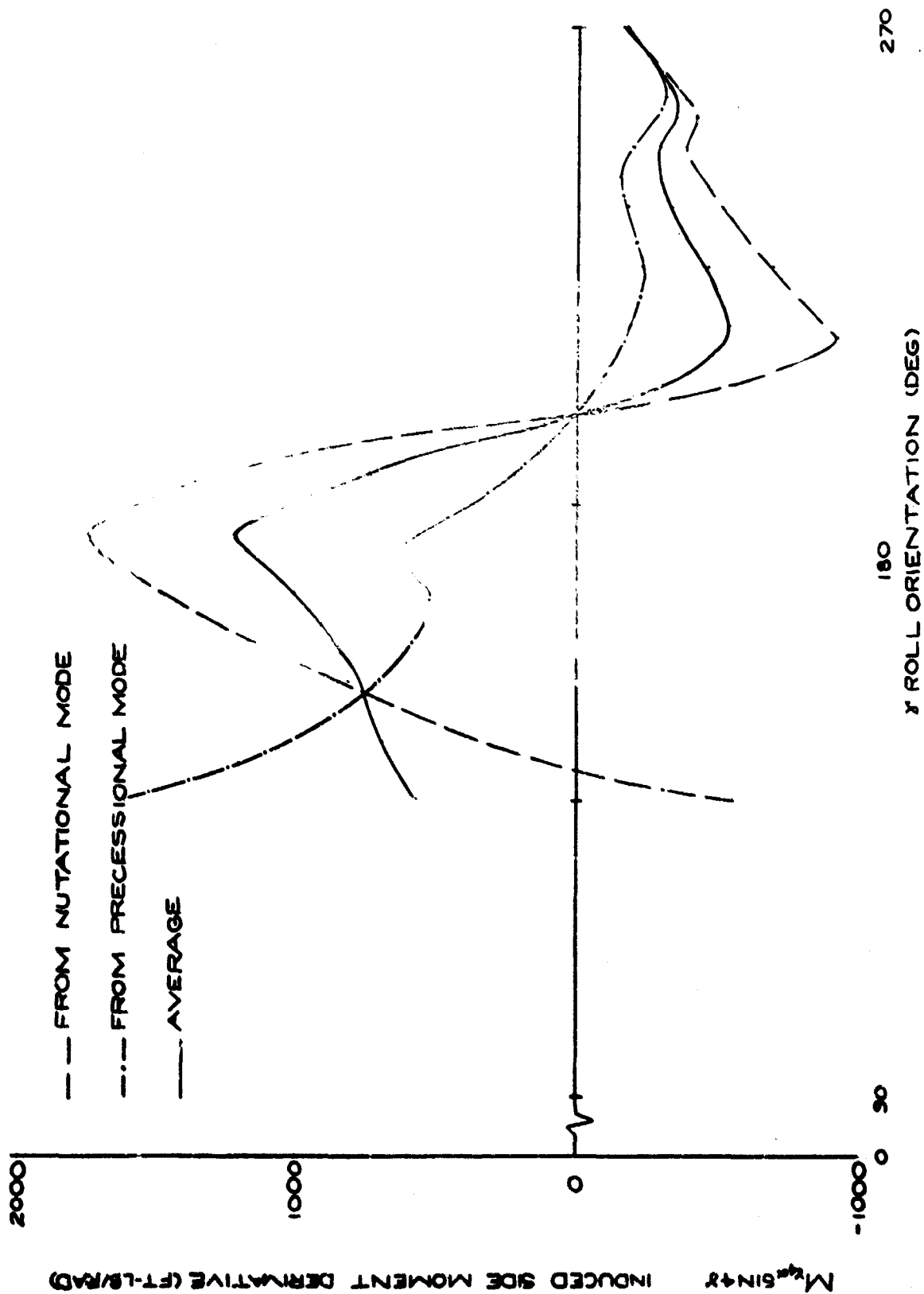


FIG. 48 INDUCED SIDE MOMENT DERIVATIVE VERSUS ROLL ORIENTATION ANGLE FOR SPLIT-SKIRT BOMB (739)

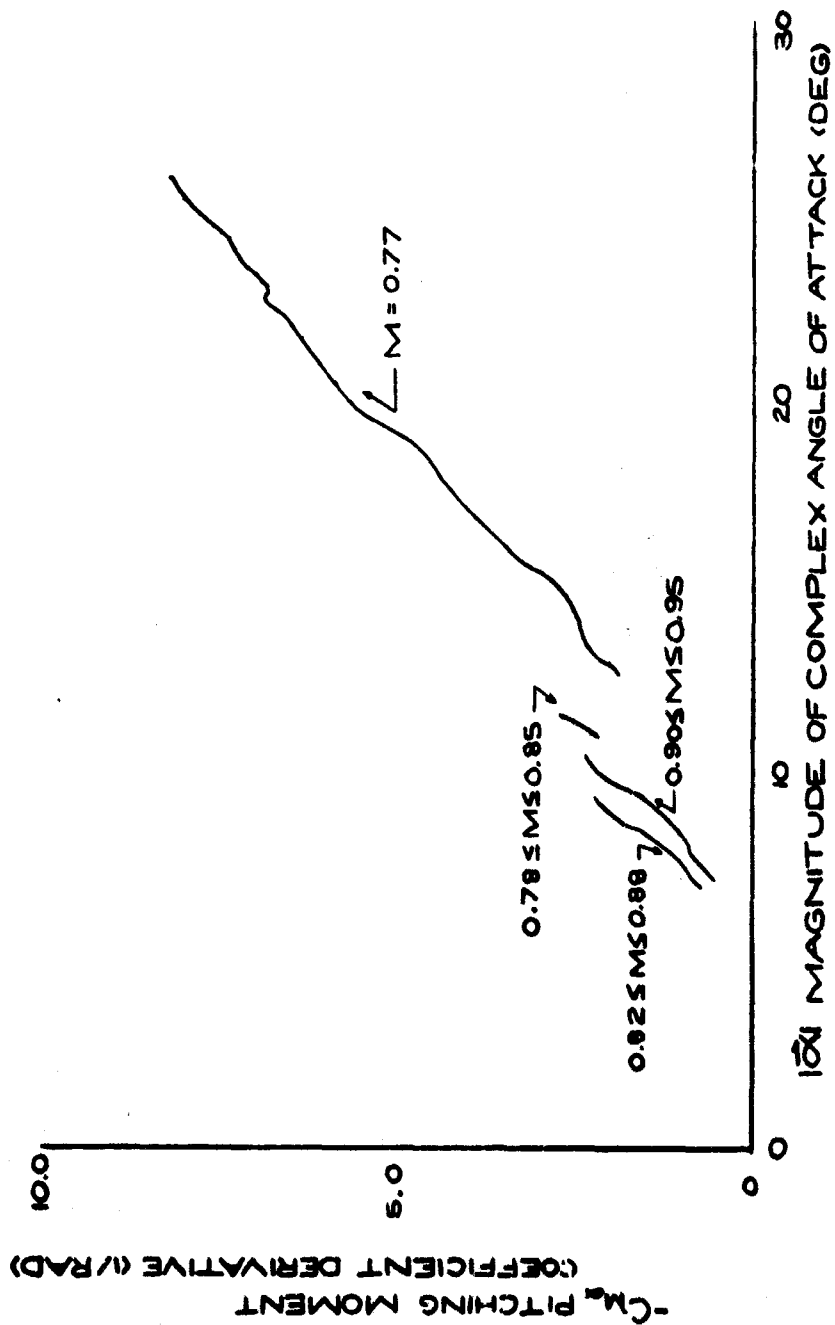


FIG. 49 PITCHING MOMENT COEFFICIENT DERIVATIVE
VERSUS MAGNITUDE OF COMPLEX ANGLE OF
ATTACK AND MACH NUMBER
FOR SPLIT-SKIRT BOMB (739)

and vice versa. An exact correlation between Figs. 30 and 33 cannot be made on the basis alone, however, due to the non-linearity of $C_{M\alpha}$ with Mach number. A curve presenting $C_{M\alpha}$ as a function of Mach number alone would not be representative due to the large variations of angle of attack over a small Mach number range. It should also be noted in Fig. 49 that Reynolds number effects are also present. Although one would expect the restoring moment to increase as Reynolds number increases due to the delayed separation, it is felt that, coupled with the fact that the boat-tail effect is slight and the magnitude of the Reynolds number is large, the variations in angle of attack and critical Mach number are more influential; thus, in the earlier phase of the flight, $C_{M\alpha}$ decreases with increasing Reynolds number.

Comparison of the free flight results with those from wind tunnel tests¹⁶ indicate the free flight results to be approximately one-half of the wind tunnel values. Table III shows typical comparative results. The wind tunnel results are presented in Appendix II. Reference 3 indicates that, when analyzing wind tunnel flow visualization results, asymmetric vortex pairs were observed. It was further mentioned that this type of vortex shedding is subject to scale effects in free flight. This scaling effect presents a possible explanation of the observed difference between free flight and experimental results.

It was not possible to compare $C_{M\alpha}$ at angles of attack higher than 12° due to the fact that C_M was non-linear with α at the higher angles of attack¹⁶ and thus $C_{M\alpha}$ could not be computed within the realm of the linear theory. It was possible, however, to compare C_M . This is feasible within the limits of the linear theory due to the fact that, in the fitting technique, it is assumed that the stability parameters, including $C_{M\alpha}$, are constant over each sectional fit. Hence, even though the angle of attack during the sectional fit may be large, C_M may be obtained, theoretically, by multiplying $C_{M\alpha}$ by the corresponding angle of attack, assuming zero trim. Fig. 50 shows these results obtained compared to the wind tunnel results. It should be noted that, in comparisons of both $C_{M\alpha}$ and C_M , the difference between free flight results and wind tunnel results increases with increasing Mach number. It is felt that the differences observed are due to possible effects of the critical Mach number region. In Fig. 50, at the lower Mach numbers the difference in C_M is as large as the higher Mach numbers, but this is primarily due to the fact that these lower Mach numbers are occurring at the higher angles of attack, where the linear theory assumption used to calculate C_M is not very good. But at the lower angles of attack, where this assumption is good, one would expect the difference to decrease. It does not, however, and it is felt that this is due to the Mach number becoming more critical. Finally, it should be noted that, although the magnitudes of the parameter are different, the general trends are the same.

TABLE III. COMPARISON OF FREE FLIGHT C_M TO WIND TUNNEL VALUES

<u>Mach Number</u>	<u>Angle of Attack (deg)</u>	<u>(1/rad) Free Flight</u>	<u>(1/rad) Wind Tunnel</u>	<u>% Difference</u>
0.80	11.4	-2.5	-4.52	44.2
0.90	10.5	-2.3	-4.45	47.7
0.95	9.4	-1.0	-2.66	62.5

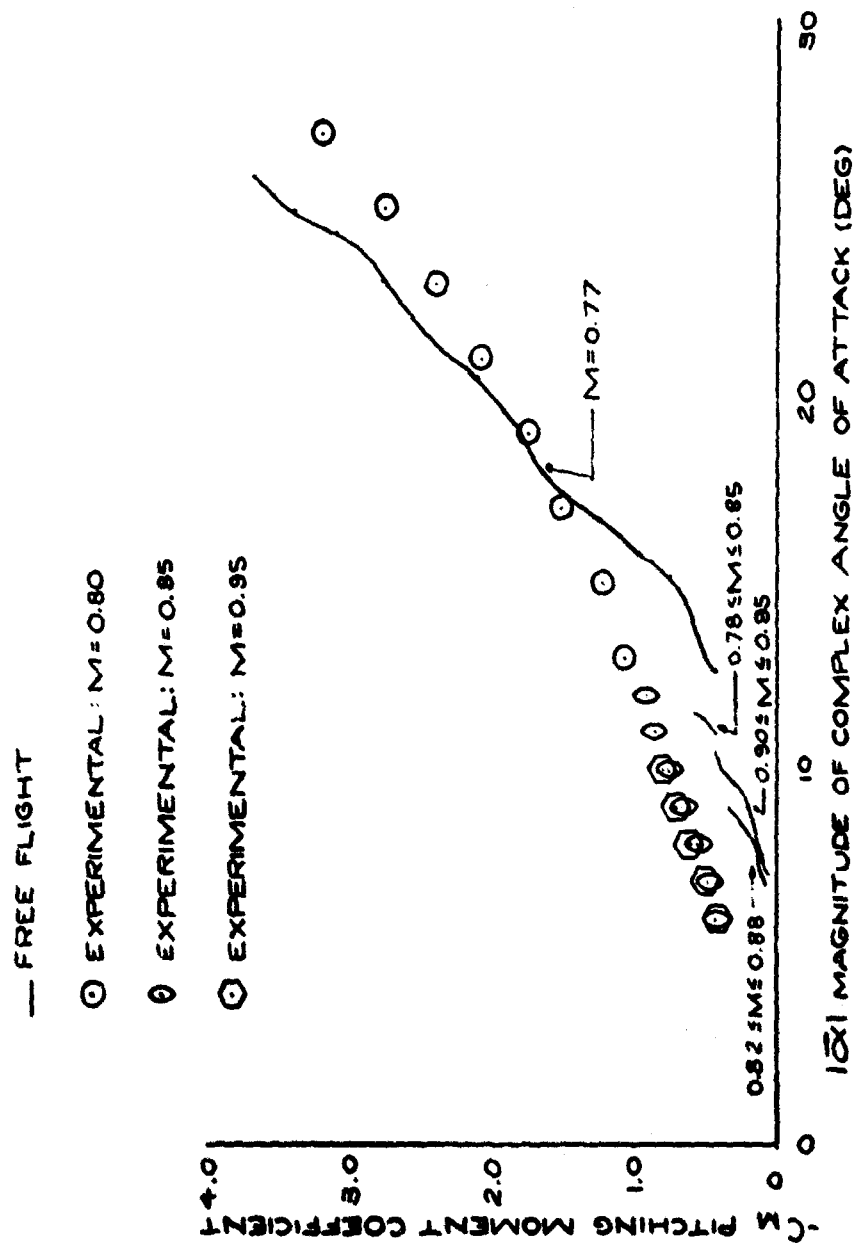


FIG. 50 PITCHING MOMENT COEFFICIENT VERSUS
MAGNITUDE OF COMPLEX ANGLE OF ATTACK
AND MACH NUMBER FOR SPLIT-SKIRT BOMB (739)

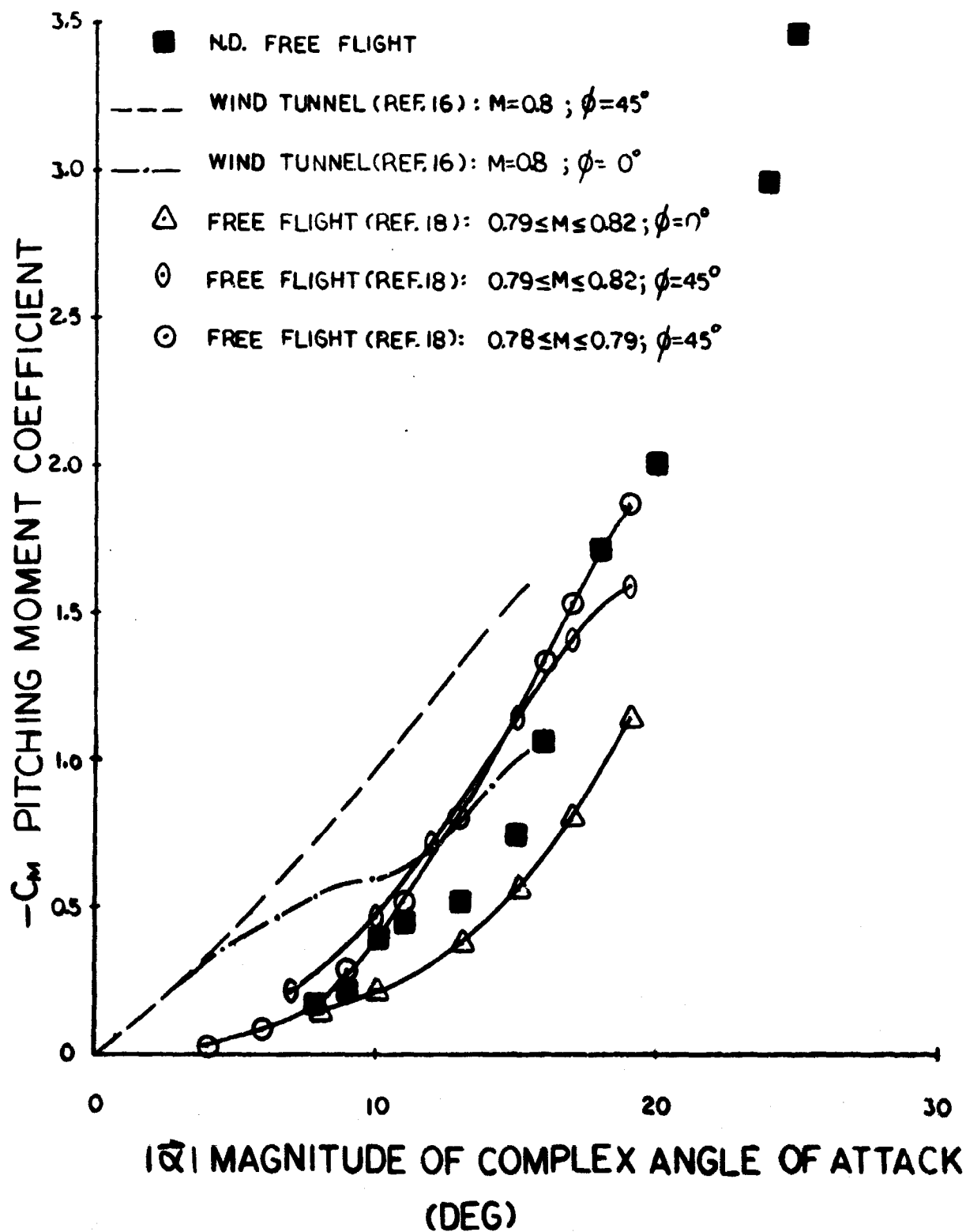


FIG 50A C_m VS $|\alpha|$ FOR SPLIT-SKIRT BOMB (739)

A comparison of the pitching moment coefficient with other free flight data was also available. The results of Reference 18 agreed very well with the results of this analysis. While the Unified Linear Theory does not include effects of roll orientation, it was expected that the results obtained would be averaged over roll orientation. Fig. 51 shows the free flight results of Reference 18 and of this analysis, and the experimental results of Reference 16. It is seen that the results of the Unified Linear Theory are approximately the average over the roll orientation of the results of Reference 18.

As discussed previously, the pitch damping moment coefficient derivative was able to be calculated for only a small segment of the flight due to the induced side moment effects and the damping out of the Precession Vector. The values calculated were essentially constant, and thus the extrapolated values were also equal to this constant value. Comparison with wind tunnel results was not possible due to the fact that the dynamic tests¹⁷ were made with a center of gravity position different from the free flight case. The free flight c.g. is 30.7% of the body length from the nose while the experimental c.g. is 40% of the body length from the nose. Since the tests were made at one c.g. position only, a transformation of the dynamic moment coefficient was not possible. Although comparison of the magnitudes was not valid, a comparison of the variation of $C_{m\dot{\alpha}} + C_{m\dot{\beta}}$ as a function of Mach number in the wind tunnel (see Appendix III) with that calculated from free flight data yielded both to be approximately constant. Thus, as mentioned previously, the assumption of extrapolating $C_{m\dot{\alpha}} + C_{m\dot{\beta}}$ as a constant equal the calculated amplitude was felt to be a valid one.

The Magnus moment coefficient derivative, $C_{m\dot{\beta}}$, yielded essentially constant results throughout the entire flight. Fig. 52 presents $C_{m\dot{\beta}}$ as a function of angle of attack and Mach number. As discussed previously, due to induced side moment effects, $C_{m\dot{\beta}}$ was assumed constant from 12.05 seconds to 20.75 seconds from release. As Fig. 49 shows, this time interval included a substantially large variation in angle of attack. Very slight variations were observed with Mach number; again, it is noted that the critical Mach number range, $0.90 \leq M \leq 0.95$, is characterized by the largest variation. The general continuity of the extrapolated values with the calculated values at the lower Mach numbers is felt to add assurance to the assumption made in the resonant portion of the flight. In accordance with the assumption used in the fitting procedure, $C_{m\dot{\beta}}$ may be calculated as a function of angle of attack, as presented in Fig. 53.

Although comparison of results for the induced side moment coefficient derivative was difficult, two interesting results were obtained. Results of wind tunnel tests¹⁶ on the split-skirt bomb yielded that, in general, the period of oscillation of the induced side moment coefficient is larger than $\pi/2$, as predicted theoretically. Free flight results indicate this same phenomena. Although free flight results from Reference 3 are with respect to cruciform finned bombs, the body profile is identical to the split-skirt

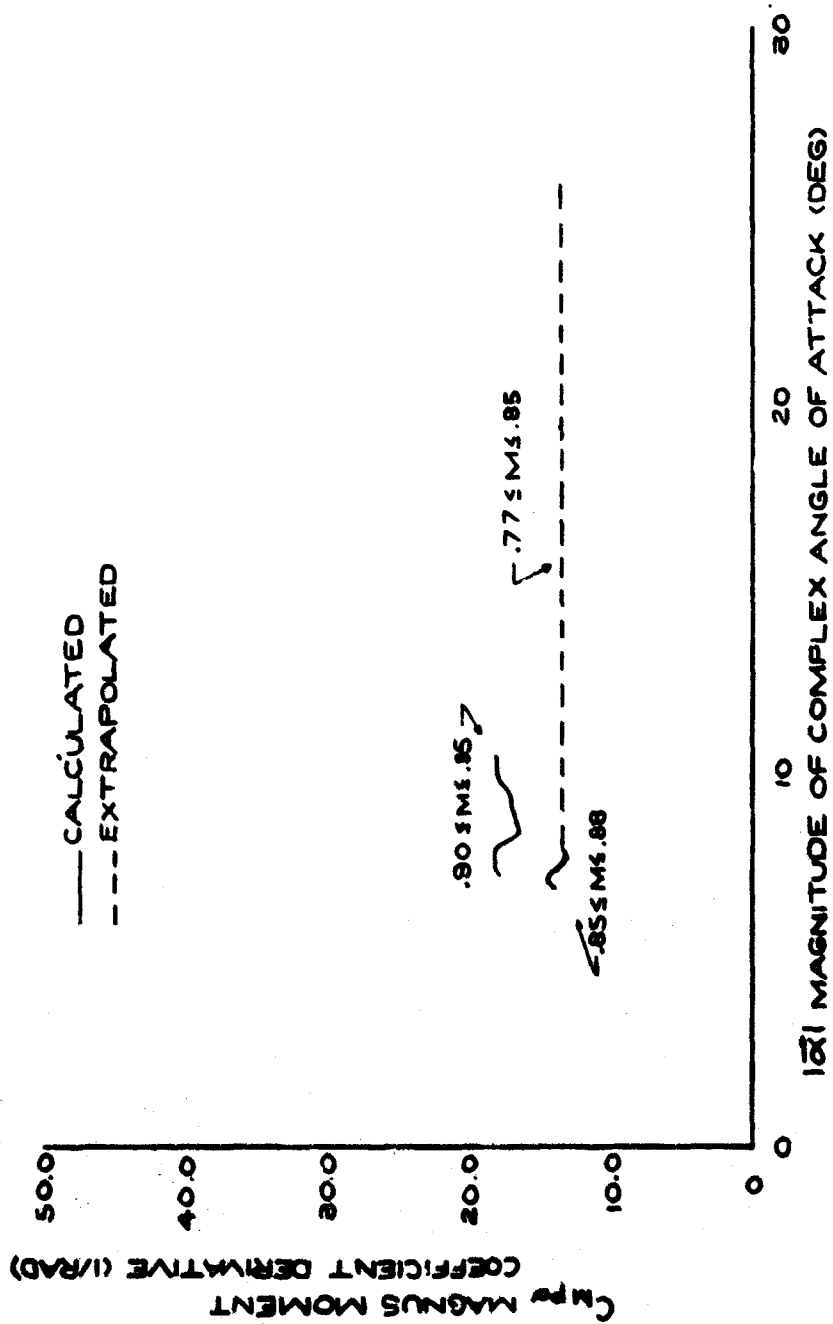


FIG. 51 MAGNUS MOMENT COEFFICIENT DERIVATIVE
VERSUS MAGNITUDE OF COMPLEX ANGLE OF ATTACK
AND MACH NUMBER FOR SPLIT-SKIRT BOMB (739)

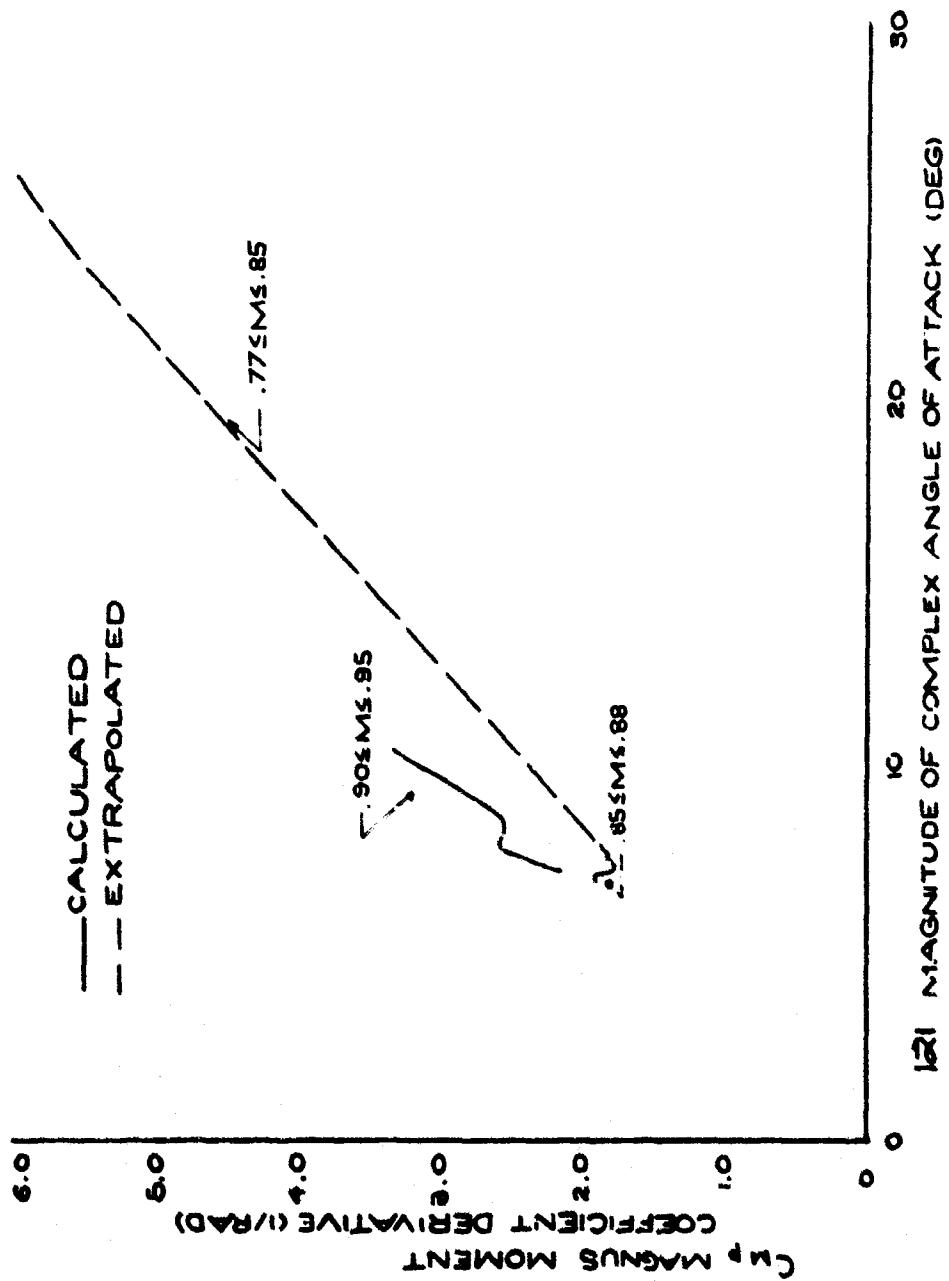


FIG. 53 MAGNUS MOMENT COEFFICIENT DERIVATIVE
VERSUS MAGNITUDE OF COMPLEX ANGLE OF ATTACK
AND MACH NUMBER FOR SPLIT-SKIRT BOMB (739)

bomb (739). These results indicate that the peak values for the induced side moment vary considerably with angle of attack, and in general, these values occur at roll orientation angles less than the theoretical values. Although, in the free flight results, constant angle of attack was not present, the peak value of the induced side moment coefficient was observed to occur at a smaller value of roll orientation angle than the theory predicts.

SECTION VI

CONCLUSIONS

Application of the Method of Differential Corrections to fit the Unified Linear Aeroballistic Theory to free flight angular orientation data has led to a determination of the aerodynamic moments influencing the dynamic stability of a split-skirt bomb. The data was fitted to within a maximum error of 7% of the magnitude of the motion. The aerodynamic coefficient derivatives which were determined included: pitching moment ($C_{m\dot{\alpha}}$), pitch damping moment ($C_{m\dot{\alpha}} + C_{m\dot{\alpha}}$), and Magnus moment ($C_{m\dot{\alpha}}$). In addition, an effort was made to determine the induced side moment coefficient derivative, $C_{m\dot{\alpha}} \sin \alpha$, by an extension of the linear theory. The last result, however, was questionable due to complications arising in the fitting technique. The analysis was carried out assuming no such complications although preliminary investigations are currently being carried out in this regard.

The stability analysis was made on the last 50 seconds of the 63-second flight. During this time, two instabilities were determined: Resonance and Magnus. Resonance occurred at approximately 14 seconds from release while Magnus effects were felt from 25 seconds to the end of the flight.

Magnus Instability

At 25 seconds from release the precessional mode damped out and the remainder of the flight was characterized by nutational undamping attributed to a positive Magnus moment. During this phase of the flight the motion was essentially circular, increasing in amplitude from 7° to approximately 12° .

It is important to realize that the cause of this instability does not lie in the destabilizing Magnus moment alone. From the Unified Linear Aeroballistic Theory, it is seen that the nutational mode does not necessarily undamp when a positive Magnus moment coefficient derivative is present. The Magnus term of the damping equation must be larger in magnitude than the pitch damping term in order that λ_n be positive. Each of these terms is composed of a combination of mass parameters, trajectory parameters, and aerodynamic coefficient derivatives.

Resonance Instability

At approximately 14 seconds from release, the bomb was at resonance. The magnitude of the complex angle of attack at this time was the largest experienced in the flight, 28° . An analysis of the rolling velocity and the roll orientation angle as a function of time showed that the bomb was trying to lock-in for approximately 6 seconds in the region of resonance. It was felt that this time period was sufficiently long to allow the induced side moment

to have a considerable effect on the magnitude of the complex angle of attack. Although the fitting procedure indicated the presence of an induced side moment at resonance, further investigations are currently being made to explore possible numerical problems at resonance. This results from a confusion of the Trim and Nutation arms at resonance. It was felt, however, that due to the length of the lock-in region, effects of the induced side moment surely were present. Hence, although the results presented may be magnified, the feeling is that the side moment is generally represented.

Comparison of the pitching moment coefficient was available with both wind tunnel and other free flight results. The wind tunnel results differed considerably from results of this analysis while the other free flight results compared favorably. It was felt that a possible explanation for the difference between free flight and wind tunnel results may be attributed to scaling effects of asymmetrical vortex shedding.

Thus, in conclusion it was demonstrated that the fitting technique developed at Notre Dame¹² accurately represented the angular oscillation data of a full scale bomb in free flight. From these fits, the pertinent aerodynamic stability coefficients affecting the dynamic stability of the bomb were accurately determined. The analysis indicated that the bomb experienced both Resonance and Magnus Instability. Thus, it was shown that, although the split-skirt tail configuration affords greater flexibility in retardation control and presents a more streamlined profile to the flow field than does the cruciform-finned configuration, it does not insure freedom from instabilities characteristic to the latter.

APPENDIX I

LOG DECREMENT TECHNIQUE APPLIED TO PRECESSION VECTOR

The magnitude of the Precession Vector may be expressed as a function of time as follows:

$$|\vec{K}_p| = |\vec{K}_p|_0 e^{\lambda_p(t-t_0)} \quad (\text{I-1})$$

where $|\vec{K}_p|_0$ is the initial magnitude at time t_0 . Taking the natural logarithm of Eq. (I-1) yields

$$\ln \left(\frac{|\vec{K}_p|}{|\vec{K}_p|_0} \right) = \lambda_p(t-t_0) \quad (\text{I-2})$$

which may be written

$$\lambda_p = \frac{\ln |\vec{K}_p| - \ln |\vec{K}_p|_0}{t - t_0} \quad (\text{I-3})$$

Thus, application of Eq. (I-3) at points along $\ln |\vec{K}_p|$ as a function of time from release, reinitializing at each point, yields λ_p as a function of time from release.

APPENDIX II

NOL STATIC WIND TUNNEL TEST RESULTS

Static wind tunnel test results¹¹ from the Naval Ordnance Laboratory (NOL), White Oak, were used to calculate the normal force coefficient derivative, C_{z_α} , as a function of Mach number.

Reference 1 presents the normal force coefficient, C_z , as a function of angle of attack and Mach number with roll orientation as a parameter. A least squares fit of the data up to an angle of attack of 12 degrees yielded C_{z_α} as a function of Mach number, with roll orientation as a parameter, within an accuracy of 1.0%. These results are shown in Fig. II-1. Fig. II-2 presents the same results averaged over roll orientation. It is these values which were used in the determination of the aerodynamic coefficient derivatives.

A similar procedure was used to obtain the pitching moment coefficient derivative, C_{M_α} , as a function of Mach number. These values were determined for the purpose of comparison with the free flight results. In the wind tunnel, the model was tested with its moment reference at the mid-point. Hence, for comparison, a transformation of the coefficient was necessary. The transformation equation used is as follows:

$$C_{M_\alpha}^* = C_{M_\alpha} + \frac{X_0}{d} C_{z_\alpha} \quad (\text{II-1})$$

where

- * refers to the new c.g. positions
- X_0 is the distance between the c.g. position
(positive direction is forward)
- d is maximum body diameter

Fig. II-3 presents C_{M_α} as a function of Mach number and moment reference (center of gravity) position. On a larger scale, Fig. II-4 C_{M_α} referred to the free flight center of gravity. It is these values which were used for comparison with free flight results.

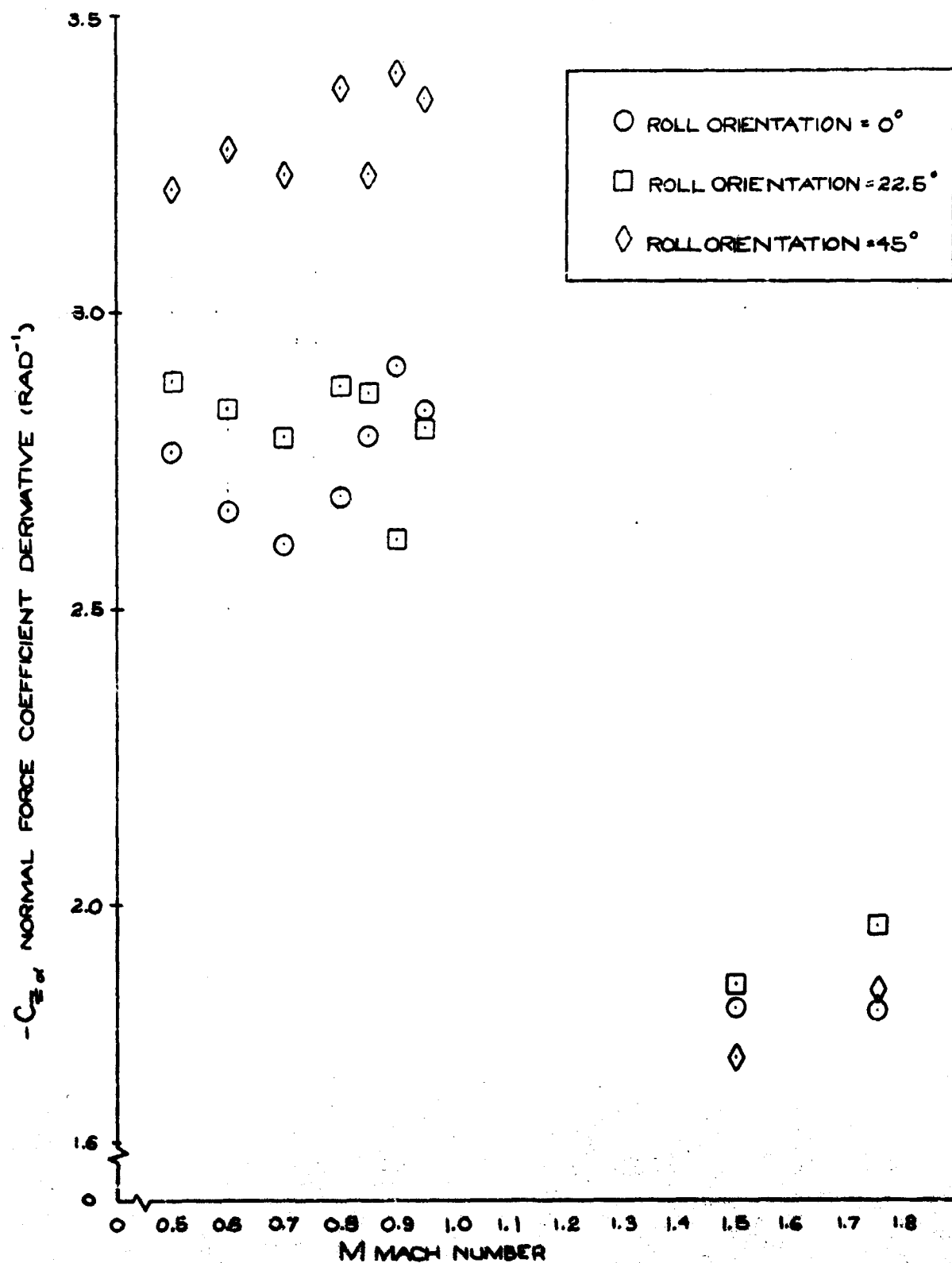


FIG.II-1 NORMAL FORCE COEFFICIENT
DERIVATIVE VERSUS MACH NUMBER
AND ROLL ORIENTATION
FOR SPLIT-SKIRT BOMB (739)

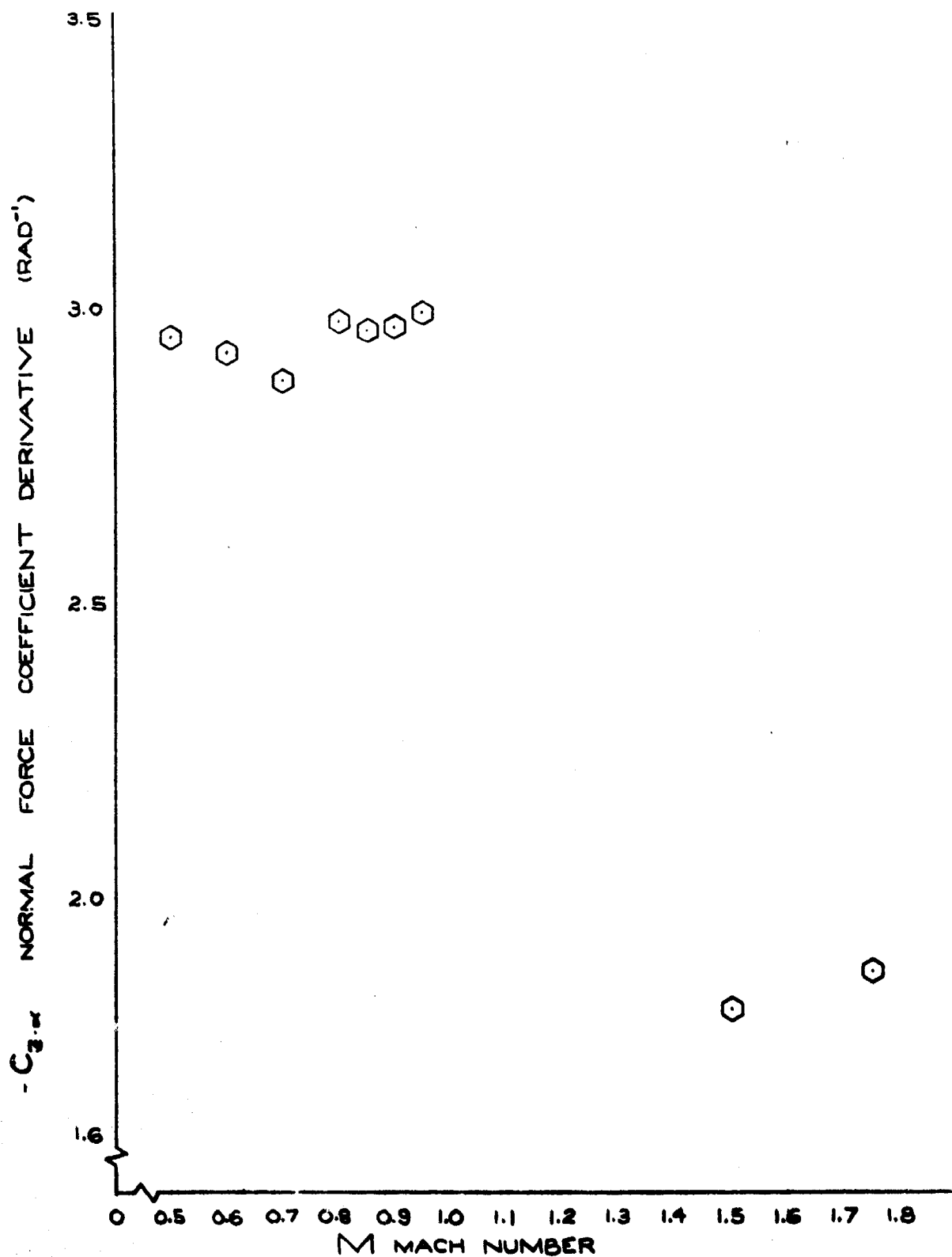


FIG. II-2 NORMAL FORCE COEFFICIENT
DERIVATIVE (AVERAGED OVER
ROLL ORIENTATION) VERSUS MACH
NUMBER FOR SPLIT-SKIRT BOMB (739)

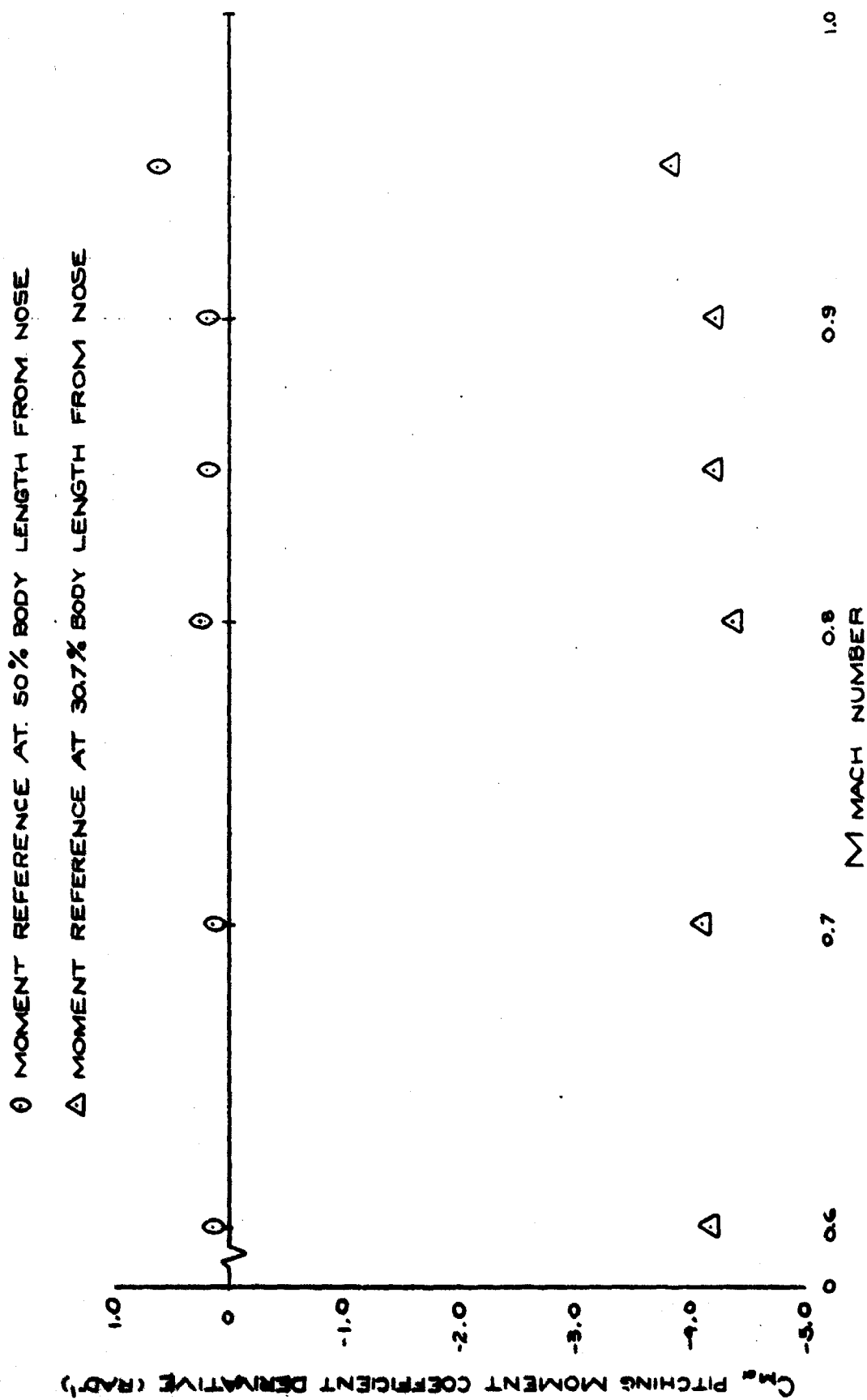


FIG II-3 PITCHING MOMENT COEFFICIENT DERIVATIVE
 (AVERAGED OVER ROLL ORIENTATION) VERSUS MACH
 NUMBER FOR SPLIT-SKIRT BOMB (739)

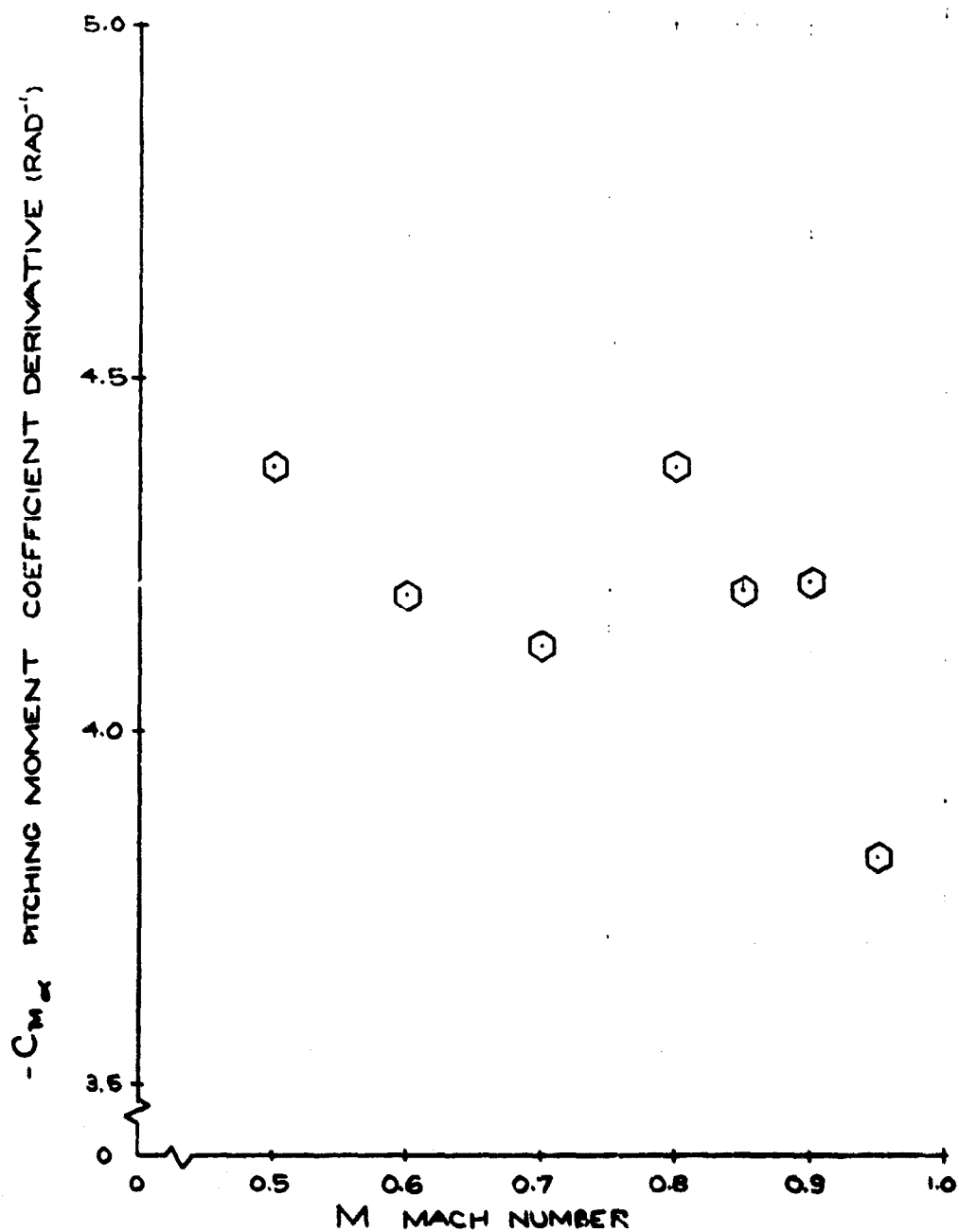


FIG II-4 PITCHING MOMENT
COEFFICIENT DERIVATIVE
(AVERAGED OVER ROLL
ORIENTATION) VERSUS MACH
NUMBER FOR SPLIT-SKIRT BOMB (739)

APPENDIX III

NOL DYNAMIC WIND TUNNEL TEST RESULTS

Dynamic wind tunnel tests¹² from the Naval Ordnance Laboratory (NOL), White Oak, yielded the pitch damping moment coefficient derivative as a function of Mach number and roll orientation.

The model was tested with the center of gravity located 40% of the body length from the nose. Since no other center of gravity positions were used, a transformation of c.g. positions was not possible. For completeness, however, $C_{M_q} + C_{M_{\dot{\alpha}}}$ as a function of Mach number and roll orientation is presented in Fig. III-1, while Fig. III-2 shows $C_{M_q} + C_{M_{\dot{\alpha}}}$, averaged over the roll orientation, as a function of Mach number.

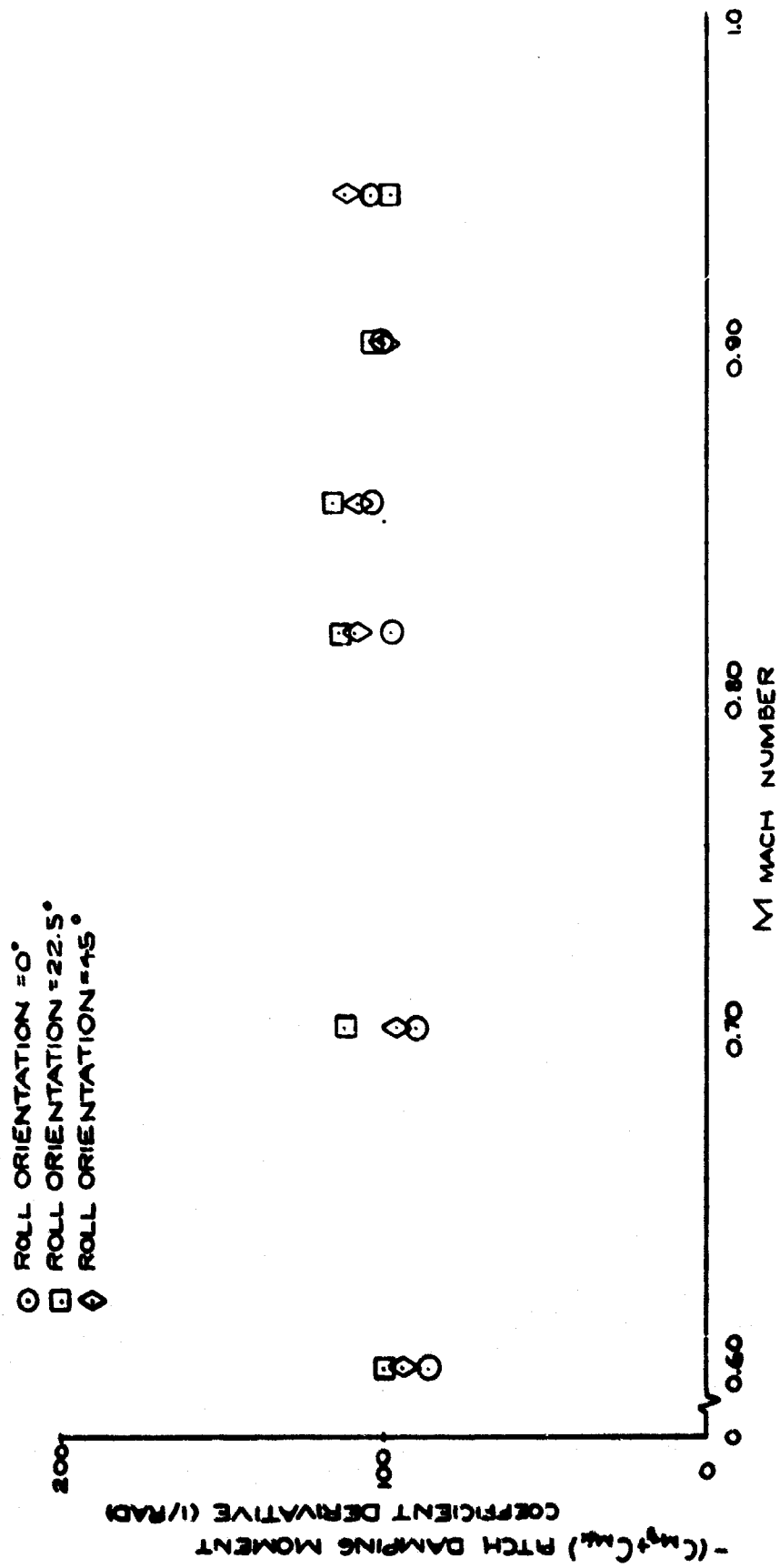


FIGURE I PITCH DAMPING MOMENT COEFFICIENT
DERIVATIVE VERSUS MACH NUMBER AND
ROLL ORIENTATION FOR SPLIT-SKIRT BOMB (739)

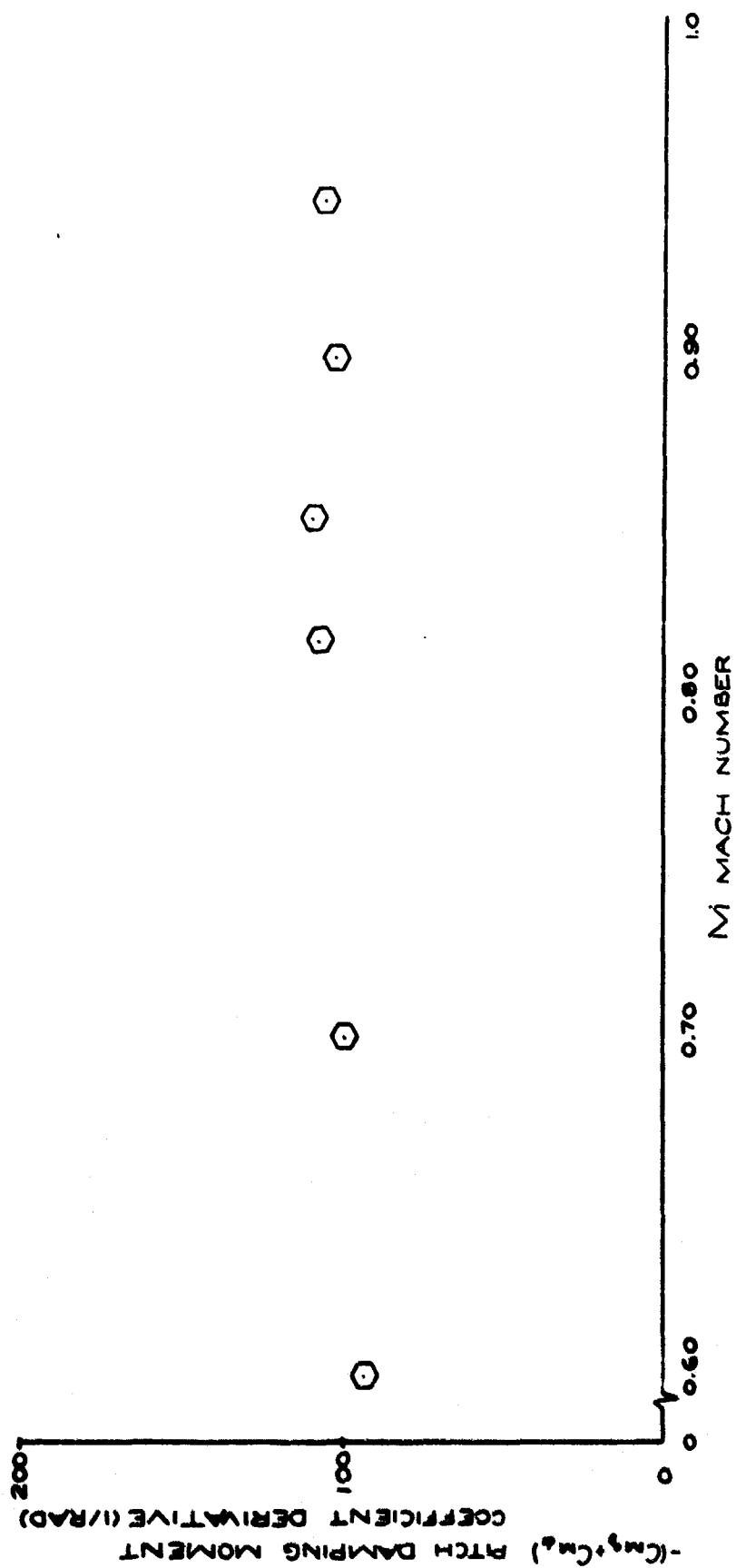


FIG. III - 2 PITCH DAMPING MOMENT COEFFICIENT
DERIVATIVE (AVERAGED OVER ROLL ORIENTATION)
VERSUS MACH NUMBER FOR SPLIT-SKIRT BOMB (739)

REFERENCES

1. Nicolaides, J.D., Eikenberry, R.S., Dynamic Wind Tunnel Testing Techniques, AIAA Aerodynamic Testing Conference, Los Angeles, California, Sept., 1966.
2. Nicolaides, J.D., Eikenberry, R.S., Ingram, C.W., The Determination of Aerodynamic Stability Coefficients from Sounding Rocket Flight Data, AIAA Sounding Rocket Vehicle Technology Specialist Conference, Williamsburg, Va., 1967.
3. Rhodes, J.W., Shannon, J.H.W., Results and Conclusions of the Joint R.A.E./W.R.E. Research Programme on the Flight Dynamics and Ballistic Consistency of Freely Falling Missiles; Part 1, Bombs Stabilized by Fixed Cruciform Fins, Department of Supply, Australian Defense Scientific Service, Weapons Research Establishment, HSA 20, 1965.
4. Australian Defense Scientific Service, Weapons Research Establishment, Salisbury, South Australia; Unpublished data on the Split-Skirt Bomb (739).
5. Goldstein, H., Classical Mechanics, Addison-Wesley Publishing Co., Inc., Reading, Mass., 1965.
6. Nicolaides, J.D., Missile Flight and Astrodynamics, Bureau of Weapons, Department of the Navy, TN 100A, 1959-1961.
7. Nicolaides, J.D., Two Non-Linear Problems in the Flight Dynamics of Modern Ballistic Missiles, IAS Report No. 59-17, January, 1959.
8. Nicolaides, J.D., An Hypothesis for Catastrophic Yaw, U.S. Navy Bureau of Ordnance, Technical Note 18, Sept., 1955.
9. Nicolaides, J.D., On the Free Flight Motion of Missiles Having Slight Configurational Asymmetries, BRL Rept. No. 858, 1953.
10. Nicolaides, J.D., A Review of Some Recent Progress in Understanding Catastrophic Yaw, N.A.T.O. AGARD Specialists Meeting, "The Fluid Dynamic Aspects of Ballistics," College Universitaire de Mulhouse, Mulhouse, France, Sept., 1966.
11. Nicolaides, J.D., Stumpfl, S.C., On Roll Lock-In In Unguided Rockets, Conference on Unguided Rocket Ballistics, University of Texas at El Paso, August, 1966.

12. Eikenberry, R.S., Wobble, A Computer Program to Analyze Missile Motion, Aero-Space Department Report (pending publication), University of Notre Dame, Notre Dame, Indiana.
13. Scarborough, J.B., Numerical Mathematical Analysis, 2nd Edition, Baltimore, Johns Jopkins University Press, 1950.
14. Neilsen, K.L., Methods in Numerical Analysis, The McMillan Company, New York, 1960.
15. Iberall, A.S., Attenuation of Oscillatory Pressures in Instrument Lines, U.S. Department of Commerce, National Bureau of Standards, Research Paper RP2115. Vol. 45, July, 1950.
16. Regan, F.J., Holmes, J.E., and Falusi, M.E., Static Wind Tunnel Tests of the M823 Research Stores with Split-Skirt Stabilizers, United States Naval Ordnance Laboratory, Department of the Navy, NOLTR 61-89, 1966.
17. Regan, F.J., Holmes, J.E., and Falusi, M.E., Pitch Damping Tests of the M823 Research Store with Cruciform and Split-Skirt Stabilizers, United States Naval Ordnance Laboratory, Department of the Navy, NOLTR 65-68, 1966.
18. Rhodes, C.W., Shannon, J.H.W., Weapons Research Establishment, Salisbury, South Australia, Free Flight Data Reduction for Pitching Moment Coefficient as a Function of Angle of Attack. (Unpublished)

13. ABSTRACT (continued)

the presence of an induced side moment at resonance. In this phase of the analysis, however, the numerical procedure used in fitting the data caused concern in that, at resonance, neither the Nutation Vector nor the Trim Vector are rotating (i.e. in body axes). Hence, it was felt that in fitting this portion of the data, the numerical procedure may not have been able to distinguish between the two.

UNCLASSIFIED

Security Classification

DOCUMENT CONTROL DATA - R & D

(Security classification of title, body of abstract and indexing annotation must be entered when the overall report is classified)

1. ORIGINATING ACTIVITY (Corporate author) Department of Aero-Space Engineering University of Notre Dame Notre Dame, Indiana		2a. REPORT SECURITY CLASSIFICATION UNCLASSIFIED	
		2b. GROUP	
3. REPORT TITLE AN INVESTIGATION OF THE DYNAMIC BEHAVIOR OF A SPLIT-SKIRT BOMB IN FREE FLIGHT			
4. DESCRIPTIVE NOTES (Type of report and inclusive dates) Final Report - June 1966 to June 1967			
5. AUTHOR(S) (First name, middle initial, last name) John D. Nicolaides Thomas A. Clare			
6. REPORT DATE August 1969	7a. TOTAL NO. OF PAGES 166	7b. NO. OF REFS 18	
8a. CONTRACT OR GRANT NO. AF 08(635)-5275 A. PROJECT NO.	8b. ORIGINATOR'S REPORT NUMBER(S)		
c.	8c. OTHER REPORT NO(S) (Any other numbers that may be assigned this report)		
d.	AFATL-TR-69-109		
10. DISTRIBUTION STATEMENT This document is subject to special export controls and each transmittal to foreign nationals may be made only with prior approval of the Air Force Armament Laboratory (ATRA), Eglin AFB, Florida 32542.			
11. SUPPLEMENTARY NOTES Available in DDC		12. SPONSORING MILITARY ACTIVITY Air Force Armament Laboratory Air Force Systems Command Eglin Air Force Base, Florida 32542	
13. ABSTRACT An analysis is presented of the full scale, free flight dynamic behavior of a tri-partite bomb of split-skirt and variable drag configuration. The angular data was obtained from internal instrumentation from the drop at the Woomera Test Range in Salisbury, Australia by the Australian Weapons Research Establishment. This test was part of a joint research program on instrumented bombs undertaken by the United Kingdom, Australia, Canada, and the United States. The analysis was carried out by the Department of Aero-Space Engineering, University of Notre Dame. The bomb was observed to experience Catastrophic Yaw in the early phase of the flight, while a Magnus instability was evident in the latter phase. An analysis of the last half of the flight data yielded an excellent determination of the aerodynamic stability coefficients, $C_{M_{\alpha}}$, $C_{M_q} + C_{M_{\dot{\alpha}}}$. The Unified Linear Aeroballistic Theory was found to represent the motion very well during the Magnus instability phase of the flight, thus yielding an accurate determination of the Magnus stability coefficient, $C_{M_{\dot{\alpha}}}$. An effort was also made to investigate the motion of the bomb as it passed through resonance. Roll lock-in was observed at this time coupled with a substantial increase in the magnitude of the complex angle of attack, thus indicating the possibility of induced side moment effects and Catastrophic Yaw. Fits of the Unified Linear Aeroballistic Theory to the data were successfully accomplished for this phase of the flight. An analysis of the motion yielded stability parameters which indicated			

DD FORM 1473

REPLACES DD FORM 1-73, 1 JAN 64, WHICH IS OBSOLETE FOR ARMY USE.

UNCLASSIFIED

Security Classification

UNCLASSIFIED

Security Classification

14.

KEY WORDS

LINK A

LINK B

LINK C

ROLE

WT

ROLE

WT

ROLE

WT

Dynamic Stability
Split-Skirt Bomb
Free Flight Data Analysis
Roll Lock-In;
Catastrophic Yaw
Magnus Instability
Unified Linear Aeroballistic Theory
"Wobble"

UNCLASSIFIED

Security Classification